Australian Government
Bureau of Meteorology

The Centre for Australian Weather and Climate Research
A partnership between CSIRO and the Bureau of Meteorology

CSIRO

Understanding the anthropogenic nature of the observed rainfall decline across south-eastern Australia

Bertrand Timbal... [et al.].

CAWCR Technical Report No. 026

July 2010

www.cawcr.gov.au

Understanding the anthropogenic nature of the observed rainfall decline across south-eastern Australia

Bertrand Timbal[1]…[et al.]

[1]*Centre for Australian Weather and Climate Research*
(A partnership between CSIRO and the Bureau of Meteorology)

CAWCR Technical Report No. 026

July 2010

ISSN: 1835-9884

National Library of Australia Cataloguing-in-Publication entry

Title: Understanding the anthropogenic nature of the observed rainfall decline across South Eastern Australia [electronic resource] / B. Timbal…[et al.].

ISBN: 9781921605901.

Series: CAWCR technical report; 26.

Notes: Includes bibliographical references and index.

Subjects: Rain and rainfall--Australia. Climatic changes--Australia.

Other Authors/Contributors: Timbal, B., Arblaster, J., Braganza, K.., Fernandez, E., Hendon, H., Murphy, B., Raupach, M., Rakich,C., Smith, I., Whan K. and Wheeler, M.

Dewey Number: 551.5772994

Enquiries should be addressed to:
Bertrand Timbal
Centre for Australian Weather and Climate Research:
A partnership between the Bureau of Meteorology and CSIRO
GPO Box 1289 Melbourne
Victoria 3001, Australia

b.timbal@bom.gov.au

Copyright and Disclaimer

FOREWORD

This report provides a single coherent compilation and synthesis of the research work undertaken in the Bureau of Meteorology (BoM) as part of the research provided to Theme 1 of the South Eastern Australia Climate Initiative during the three years of Phase 1 (SEACI-1) and the 6-month extension (SEACI-1P) of the program. Most of the work described in this report was originally published in several final project reports that can be accessed on the SEACI web site http://www.seaci.org which is hosted by the Murray-Darling Basin Authority (MDBA). This document also updates some early results.

The report was compiled by Bertrand Timbal (CAWCR-BoM) whom is the sole author of the conclusions presented herein. Several other researchers from the BoM (CAWCR and other branches) and other institutions have contributed to the research reported here:

- Bradley Murphy (CAWCR) did most of the research in Projects 1.1.1 and 1.1.2 and contributed to Project 1.3.1 (Chapters 2, 3 and 4);
- Elodie Fernandez (CAWCR) performed most of the calculations for Project 1.4.1, 1.5.1 and 1.2.1P (Chapters 5, 6 and 8);
- Karl Braganza (National Climate Centre, NCC), Harry Hendon (CAWCR) and Matt Wheeler (CAWCR) did the analysis related to the Southern Annular Mode presented in Project 1.1.2 (Chapter 3);
- Clinton Rakich (NSW regional office, BoM) did the analysis relating to the Gayndah-Deniliquin Index presented in Project 1.1.2 (Chapter 3);
- Julie Arblaster (National Center for Atmospheric Research, NCAR, USA and CAWCR-BoM) contributed to Project 1.5.1 (Chapter 6);
- Kirien Whan (Australian National University, ANU) performed the calculations used in Project 1.3.1P (Chapter 9);
- Michael Raupach (CSIRO) provided the surface hydrological variable used in Project 1.3.1P (Chapter 9); and
- Ian Smith (CSIRO) contributed additional research included in Project 1.1.1P and contributed to other parts of this document.

ACKNOWLEDGMENTS

The support of the funding agencies in SEACI is acknowledged. This report benefited from insightful and numerous comments made by Scott Power (BoM /CAWCR) and Rae Moran (VIC DSE). Finally, I would like to acknowledge Prof. Neville Nicholls, who was the BoM's main architect of the SEACI science plan before leaving for Monash University, leaving others to fill the blank pages. Without his vision, this report would not exist.

CONTENTS

LIST OF FIGURES

LIST OF TABLES

EXECUTIVE SUMMARY

This report summarises SEACI research conducted over the past four years. This substantial body of work has led to significant advances in our ability to characterize and explain the observed climate change experienced over south-east Australia (SEA) during the past decade. The research indicates that the current drought in SEA is very likely to be caused, in part, by anthropogenic changes in atmospheric greenhouse gases. The main results and conclusions are as follows.

The character of the current drought has been described in more detail than ever before. Many of the observed changes are very unusual:

- SEA (continental Australia south of 33.5°S and east of 135.5°S) has recorded the lowest thirteen-year rainfall period in the entire (1900-2009) historical record (-11.4%). The deficit is 45% larger than the previous driest thirteen-year period in the record (-7.8% during 1933-1945). Shorter low rainfall periods were observed in the past at the time of the Australian Federation and at the time of the WWII. However, the duration of the current drought is unprecedented.

- Across SEA, every year from 2001 received rainfall below the twentieth century (1900-1999) climatological average. The likelihood of observing such a long sequence of dry years by chance is less than 0.5%.

- The on-going drought is made up of a run of below average rainfall years with relatively low year-to-year variability, with no high rainfall years.

- The SEA rainfall deficit has been dominated by the autumn signal, which makes up 52% of the total decline during 1997-2009. The autumn rainfall decline began in the early 1970s. The 40-year duration of the autumn rainfall decline and the intensity of the autumn rainfall deficit (-25% during the last thirteen years) are both unprecedented in the historical record.

- A winter rainfall decline began in the early 1990s. A spring decline began in 2000. Both the spring and winter declines reinforced the pre-existing autumn rainfall decline. The relative size of the spring and winter declines became more prominent relative to the autumn decline in recent years. During 2006-2009 the largest deficit actually occurred in spring. The duration and the magnitude of the spring and winter deficits are within the range of earlier observed decadal to multi-decadal variability – in contrast to the autumn decline.

- SEA experienced significant warming during most of the last 50 years, which was generally consistent with the global warming of the planet at least for daily mean temperature. The diurnal temperature range has increased during the last twenty years: maximum day-time temperatures have risen across SEA by close to 1°C, while minimum night-time temperatures were either steady or declined (by up to 0.8°C in autumn, the season with the largest rainfall decline). This decline in daily minimum temperature is consistent with the observations of increased frost occurrences in some parts of SEA.

- Major rivers and dams have received inflows well below long-term averages and the decline in magnitude is at least 20% to 30% larger than the normally expected amplification of the rainfall signal in hydrological response. This larger than expected impact of the rainfall

decline seen across SEA has not been clearly established in this report but three likely causes were identified:

1) increased temperatures (very large for T_{max} as noted earlier), which are likely to have increased potential evaporation (evaporative demand) and thence contributed to lower soil moisture,

2) the importance of the autumn rainfall decline given that autumn is a key season for catchment saturation before winter and spring run-off and

3) the low inter-annual variability within the ongoing decline and the consequent lack of wet years to replenish the soil moisture store.

- Additional studies performed elsewhere within SEACI have led to improved quantification of these three contributions.

SEACI research has led to a much better understanding of the causes of the ongoing drought in SEA:

- The continental-scale pattern of the current drought closely resembles the pattern of rainfall change associated with changes in the Sub-Tropical Ridge Intensity (STR-I). This drought has occurred at the same time that rainfall has increased over much of northern Australia. This contrasts with the WWII drought, when most of the continent – not just southern Australia - experienced below average rainfall.

- Both the spatial and temporal signatures of the current drought across SEA are consistent with rainfall changes linked to a weakening of westerly winds across Southern Australia.

- The strengthening of the STR during 1997-2008 is estimated to account for 80% of the observed rainfall decline in the south-western part of Eastern Australia (SWEA). This contrasts with the WWII drought, when at most only one third of the rainfall decline could be attributed to the strengthening of the STR. The apparent southward shift of the STR does not appear to have had an additional effect on SWEA rainfall during the current drought.

- The current drought is clearly linked to global warming through the strengthening of the STR. Moreover, the WWII dry decade can be seen as the first dry decade of the 20th century in SEA that could be considered partially due to global warming through the intensification of the STR. However, based on IPCC findings, while most of the warming in the second part of the twentieth century is very likely to be anthropogenic, the warming during the first half of the century was mostly due to natural external forcing (i.e. solar variability).

- For the current drought, warming tropical SSTs have made no overall contribution to the rainfall decline since 1997. In contrast, during the WWII drought, tropical SSTs contributed to the rainfall decline, in conjunction with a strengthening of the STR. The contribution of tropical SSTs in SEA now and during the WWII drought is consistent with the Australia-wide rainfall anomalies during both periods and the known contributions of tropical modes of variability on the Australian continent: i.e. a continent that was generally dry during the WWII drought versus a continent that is currently dominated by wet anomalies.

There is a discernable impact of human activity on the SEA drought:

- The extent to which anthropogenic forcing has contributed to the current drought over SEA was investigated using a state-of-the-art coupled climate model and a sophisticated statistical downscaling method developed previously. The climate model was developed at the National Center for Atmospheric Research in the USA and is called the Community Climate System Model version 3 (CCSM3). The model was forced with natural forcing mechanisms (changes in solar insolation, and radiative changes caused by volcanic eruptions) and by anthropogenic forcing (increases in atmospheric greenhouse gas concentrations and changes in sulphate aerosols) over the entire 20th century. This enabled SEACI researchers to estimate the relative importance of both natural and anthropogenic forcing on observed climate change in SEA. Statistical downscaling helped improve the simulation of climatic variability.

- The climate model was best able to simulate the observed decline in rainfall and the intensification of the STR over SEA if *both* anthropogenic *and* natural external forcing was applied.

- The climate model produces an intensification of the STR at the end of the 20th century only when anthropogenic forcing is applied. There are no statistically significant long-term trends in the intensity of the STR in the simulations with natural forcing alone.

- In all simulations, the climate model exhibited lower than observed long-term trends in the STR (intensity and position) per degree of warming compared with the observations. This suggests that either the model is not as responsive to the external forcings as it should be or that a significant part of what has been observed is not in response to global warming. These two hypotheses have very different implications for future projections.

- The model forced with natural external forcing only has

    1) no increase in surface pressure in autumn-winter-spring as observed,

    2) no surface warming for either T_{min} or T_{max} all year around and

    3) small rainfall increases in these seasons. Thus natural forcing alone does not reproduce key characteristics of the observed changes.

- The disagreement between the model when forced with natural forcing only and the observed changes is robust in the sense that statistical downscaling did not reduce the disagreement. The observed rainfall decline in autumn is larger than one would expect from natural variability alone.

- The model forced with anthropogenic external forcing shows:

    1) an increase in surface pressure which resembles the observed strengthening of the STR,

    2) a significant increase in both T_{min} and T_{max} but

    3) only a weak rainfall decline, which is dominated by a decline in winter rather than in autumn. The statistical downscaling method was able to provide a more realistic rainfall series, with a large rainfall decline in autumn, a small decline in spring and very small decline in winter. The modelled rainfall decline in winter and spring is similar in magnitude to the observed ones; however it is happening in the model simulations about a decade earlier than in the observations.

- The largest autumn rainfall decline in the climate model occurs most frequently when both natural and anthropogenic external forcings are applied. However, the modelled, downscaled decline is approximately 50% smaller than the observed decline. Therefore, from this modelling perspective, the magnitude of the observed autumn rainfall decline is an unlikely occurrence even with anthropogenic forcing but beyond what internally generated natural variability and natural external forcings alone could produce.

- The downscaling of the model provides a more definitive attribution of the on-going surface warming across SEA for both T_{max} and T_{min} as the most recent trends in temperature are outside the 90% range of uncertainties obtained from the naturally forced ensemble. In contrast, the fully forced ensemble extended to 2008 using the A2 scenario matches the observed temperature trends very well.

1 Introduction and overview

The South Eastern Australian Climate Initiative (SEACI) began in 2006 and initially was planned as a three-year, $7.5 million research program aimed at investigating the causes and impacts of climate change and climate variability across south eastern Australia (SEA), including the Murray-Darling Basin (MDB). This region is one of the country's most valuable primary production areas. The MDB alone produces more than one-third of Australia's food supply and generates 40 per cent of the nation's agricultural income, with 70 per cent of Australian irrigation occurring in this region.

Phase 1 of the program (SEACI-1) started in January 2006 and ran to the end of 2008; it was further extended from January 2009 to June 2009 (SEACI-1P). SEACI-1 had three major research themes: better understanding of current climate and its drivers (Theme 1), improved long-term projections of climate change and its impacts on water resources (Theme 2), and improved seasonal forecasting (Theme 3). More details on the program can be found on the SEACI web site: http://www.seaci.org/.

The focus in Theme 1 was on the characterisation and attribution of current climate: including the assessment of the current state of knowledge about climate variability and its drivers over SEA. It was organised around a large number of projects carried out by the two research partners - the Commonwealth Scientific and Industrial Research Organisation (CSIRO) and the Bureau of Meteorology (BoM). Researchers from the CSIRO Marine and Atmospheric Research (CMAR) Division and the BoM participated in SEACI under the umbrella of the Centre for Australian Weather and Climate Research (CAWCR). Projects in Theme 1 involved:

- the review of previous studies of climate variability in the region;
- the analysis of site-specific meteorological records and the re-analysis data set with a view to detecting and quantifying any trends or shifts in climate;
- experimenting with global climate models to provide insight into the extent to which recent climatic trends and shifts can be attributed to various causal factors, including the enhanced greenhouse effect; and
- the development and validation of downscaling methodologies in order to provide local climate information in conjunction with research in Theme 2 (long-term projections) and Theme 3 (seasonal predictions).

The projects in Theme 1 were organised (Fig. 1) to maximise both the synergy within the Theme and the flow of information into the other two themes (future projections and seasonal predictions).

Figure 1 outlines the progress made during the course of the program starting from the basic undertaking in Project 1.1.1 but also the organisation of the research into different spatial scales:

- broad-scale - with a view to understanding the large-scale modes of variability which influence regional climate and how theses features are evolving with time;
- regional scale – at a scale of the SEA region of interest; and
- local scale - with a view to considering impacts at a scale relevant to climate impact studies.

Specific details of all the themes and the various projects are available on the SEACI web site.

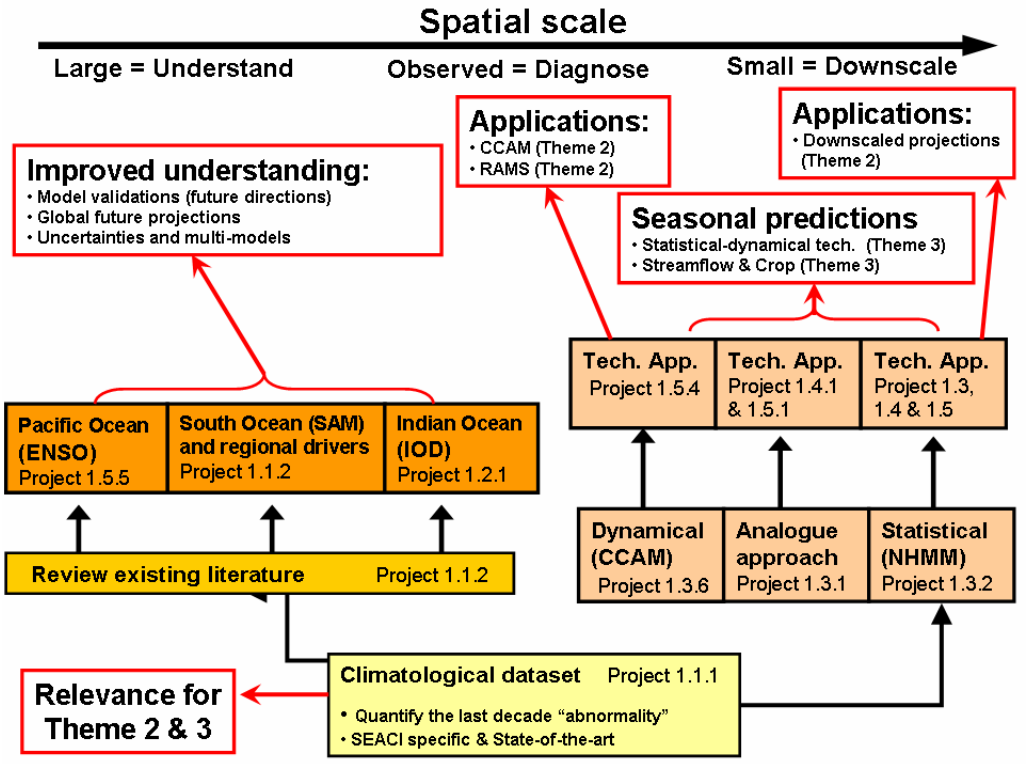

Fig. 1 *The organisation of the various projects in SEACI-1 Theme 1, their interactions and relevance to other themes in the program.*

In this report, the contribution from the BoM across SEACI-1 and SEACI-1P is summarised. Fig. 2 shows the logic of the work performed, the interactions between the various projects (reported here as chapters), its relevance to the overall Theme 1 research plan and the extension of the work during SEACI-1P.

The changes affecting SEA are described in Chapter 2. The contribution of several large-scale modes of variability to the ongoing changes in SEA climate is evaluated in Chapter 3. In chapters 4 to 6, we try to better understand the cause of the observed changes by using simulation of the 20th century climate with different external forcings. These chapters also describe the development (Chapter 4), evaluation (Chapter 5) and application (Chapter 6) the BoM statistical downscaling model (SDM). The BoM SDM allows us to enhance the signal to noise ratio, which is recognised as the biggest challenge when it comes to attributing changes at regional scales for highly variable rainfall (see p714 in Solomon et al. 2007). The following three chapters describe additional studies which were carried out during SEACI-1P:

- the evaluation of the relationship between global warming (GW) and the sub-tropical ridge (STR) in climate model simulations of the 20th century (Chapter 7);
- a comparison of the ongoing drought with the previous worst drought in the instrumental record before and during World War II, and a synthesis of the role of tropical modes of variability in both droughts (Chapter 8); and
- an analysis of the influence of the STR on the hydrological cycle diagnosed using the newly formed high resolution AWAP dataset (Chapter 9).

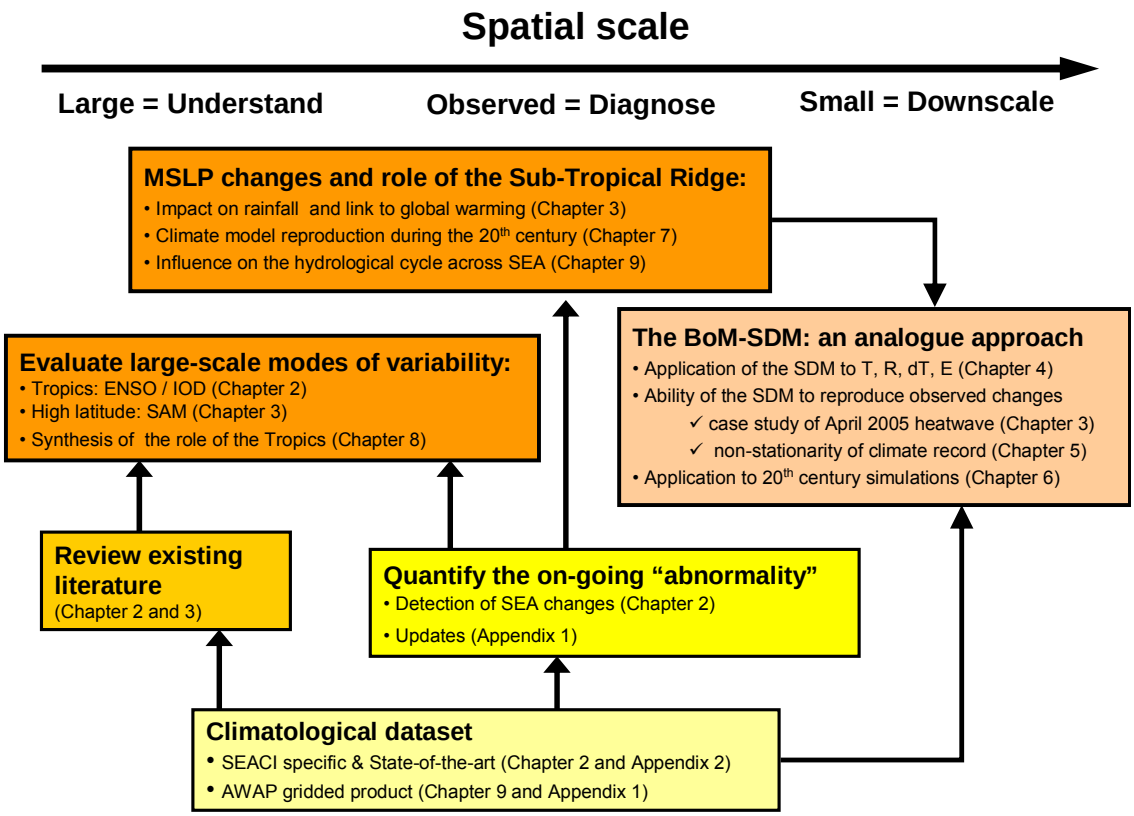

Fig. 2 *Details of the work performed in the BoM delivered as part of SEACI-1 and SEACI-1P programs that are summarised in this report.*

Chapter 10 has been included to update some earlier findings to the end of 2009 using the latest BoM dataset (i.e. AWAP). This chapter also includes additional information not reported earlier during SEACI-1 but presented at various SEACI meetings and that contributes to answer the original key scientific questions that were asked at the start of the SEACI-1 (see box below). The major findings are summarised against the key questions and a brief discussion of the outstanding scientific questions are discussed in Chapter 11, thus introducing the research proposed as part of the SEACI-2 science plan.

Key scientific questions targeted during SEACI in Theme 1

1) How has SEA climate changed?

2) What are the major drivers affecting historical and current climate in SEA?

3) What are the relationships between the drivers operating at different timescales and have these changed over time?

4) What are the causes of the dry conditions affecting parts of the study area over the last decade, and what is the prognosis?

5) What is the current climate baseline?

6) What criteria should be used to determine whether shifts in the baseline have occurred, or are likely to occur?

2 THE CHANGES IN SOUTH-EASTERN AUSTRALIAN CLIMATE

2.1 Introduction

At the beginning of the SEACI program, an up-to-date analysis of the climate of SEA was undertaken with a view to characterising climate variability and determining the nature of any change signal. To carefully quantify what changes had occurred and how unusual these changes have been in the context of the variability evident in previous decades and to ensure that the variability arose from genuine variability and not from changes in observation practise of instrumentation, the focus was on using the BoM high quality climate datasets. Variables examined were rainfall, maximum and minimum temperature, surface humidity, and pan evaporation at daily to decadal time scales. This was the first time that such a comprehensive analysis had been undertaken for SEA. In addition, the possibility of using additional stations to complement the spatial and temporal coverage of the high quality network was investigated and gaps in the spatial coverage of the observation networks for the variables listed above and their records were identified.

Using the datasets outlined above, the extent to which recent climatic trends depart from those of the past was assessed. In addition, the behaviour of the primary modes of climate variability affecting SEA such as the El Niño Southern Oscillation (ENSO) and the Southern Annular Mode (SAM) over the historical record was assessed and their relative contributions to observed long-term trends determined.

2.2 Assembling a climatological dataset for SEA

A database of surface meteorological variables relevant to the SEACI program was assembled. Variables are daily values for rainfall, daily extreme temperature (T_{max} and Tmin), dew point temperature (daily extreme: dT_{max}, dT_{min} and 10am local time value: dT10), relative humidity (derived from dT10) and pan-evaporation.

The spatial extent of the data to be retained was decided using the agreed SEACI domain. For each variable the cornerstone was the High Quality (HQ) network developed over the last ten years by the BoM, which is described in detail in the relevant literature (cited below), and is of the highest quality by international standards. Additional data from the BoM archive were sought in order to enhance the spatial coverage of the HQ networks. The focus was on stations with daily rainfall and temperature data extending back to 1958 still open today and with few missing data.

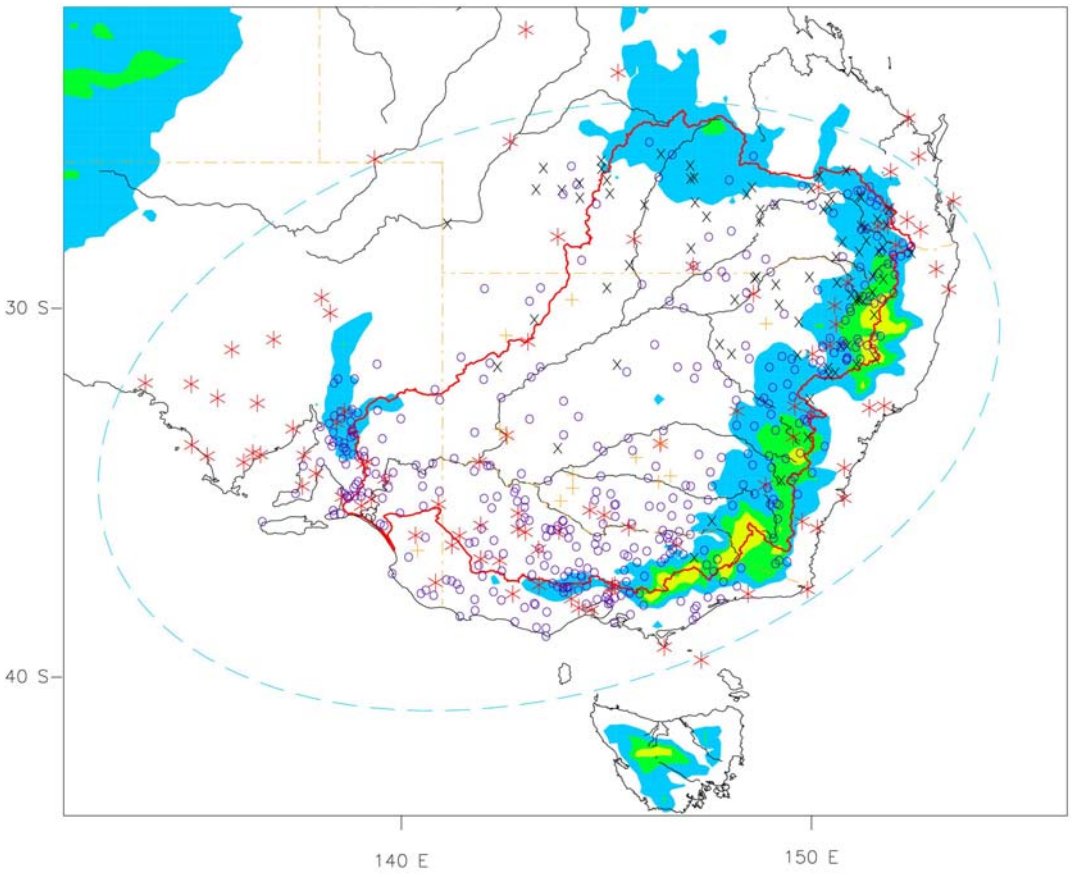

Fig. 3 *Location of the rainfall stations chosen for the SEACI program (symbols refer to data quality: red stars are HQ stations. The symbols 0, x and + refer to data quality flags 1, 2 and 3 – details in the Appendix).*

A total of 585 rainfall stations were chosen (Fig. 3), 95 of which are from the HQ rainfall network (Lavery et al. 1992 and 1997), updated in 2006, with some observations dating back to the late nineteenth century. Additional stations with less than five percent of missing data (and less than three percent since 1996) were chosen to provide a higher density network. In addition, data approaching these standards were extracted to fill spatial gaps in the coverage. In general, care has been taken to only select stations for which possible problems due to poor observing practices are less likely. A complete list of the station names, locations, and temporal coverage and data quality issues is provided in the Appendix.

For daily extremes of temperature (T_{max} and T_{min}), only 23 stations were added to the 62 HQ stations (Fig. 4). Daily HQ temperatures (Trewin 2001) have few observations dating back to the beginning of the twentieth century. Most start in the 1950s. Data for some additional locations were provided by merging neighbouring sites and hence have homogenisation issues. Others might have additional problems (site exposure or urban contamination).

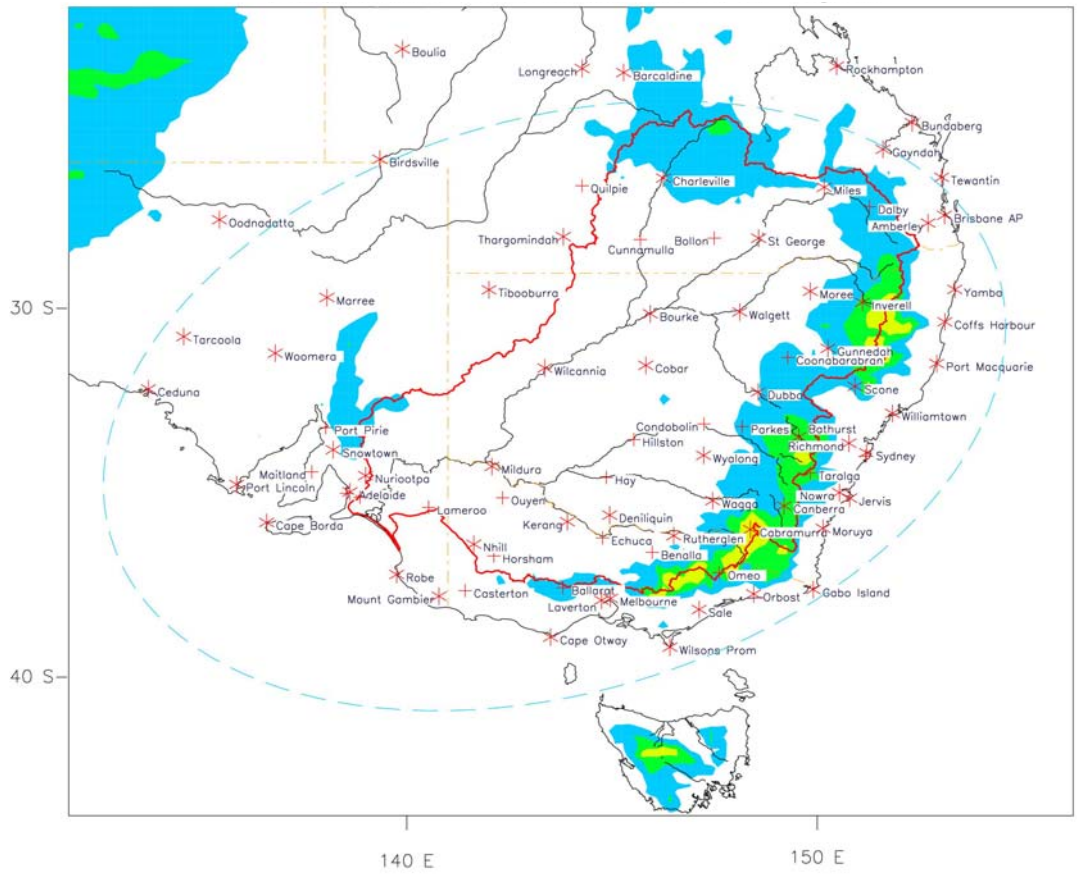

Fig. 4 *Location of the temperature stations chosen for the SEACI program (red stars indicates HQ stations, supplementary stations are shown with crosses).*

HQ dew point stations (Lucas et al. 2006) are only available from 1957 and only thirteen stations across the SEACI domain are available (Fig. 5). At each location, daily maximum, daily minimum, and 9am dew point temperatures are available. In addition 9am relative humidity has been calculated; however it is based on non-homogenised 9am air temperature at the same site and therefore is potentially problematic. *(NB: this issue was regarded as too important and not solvable and hence results on relative humidity are not reported)*. A complete list of the station names, locations and temporal coverage is provided in the Appendix.

Finally, monthly pan evaporation HQ station records have been recently assembled across Australia (Jovanovic et al. 2008) from 1975 to present. Nineteen stations are scattered across the SEACI domain (Fig. 6). The BoM pan-evaporation HQ dataset is a monthly dataset. We extended the quality control to daily values for the SEACI region, using monthly corrections for non-homogeneities at stations which required such correction. A complete list of the station names, locations and temporal coverage, as well as details of which stations required a daily homogenisation, is provided in the Appendix.

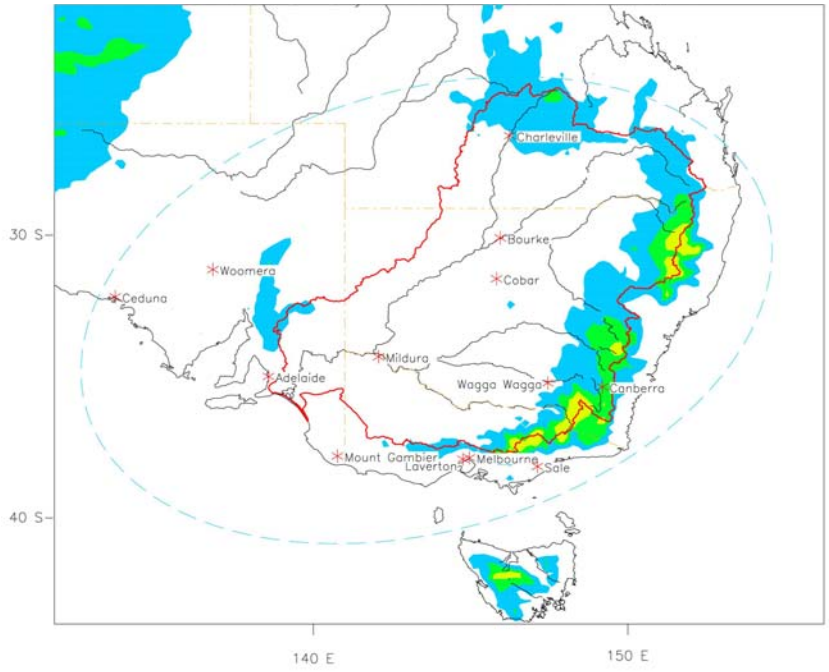

Fig. 5 *Location of the surface humidity stations chosen for the SEACI program.*

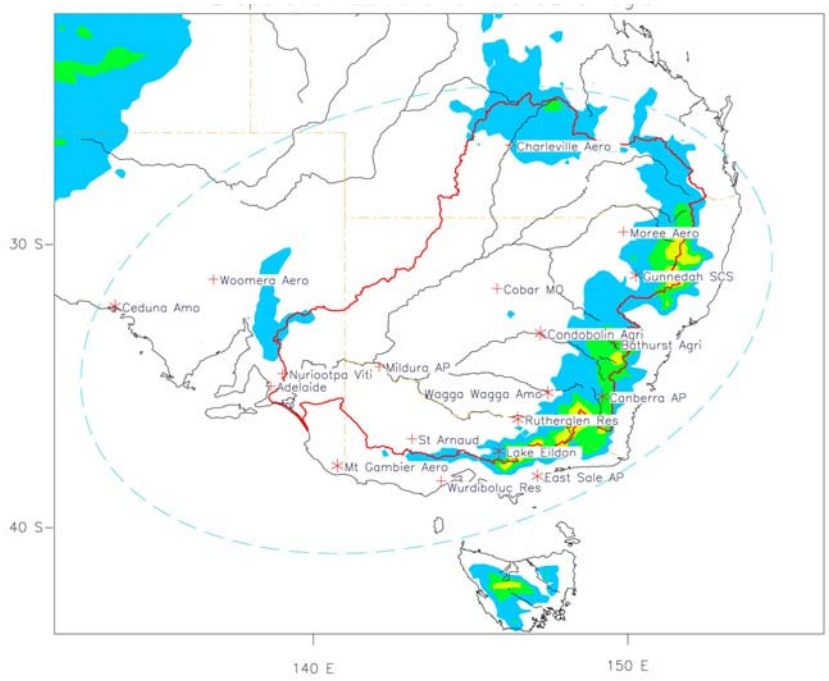

Fig. 6 *Location of the pan-evaporation stations chosen for the SEACI program. The + symbols indicate stations for which daily homogenisation was required.*

2.3 Characterisation of the climate of the last decade in SEA

The climate in SEA during last decade has been extremely dry (Trewin 2006). This dry decade has been characterised for the SEACI region using the dataset that has been assembled and additional gridded data from the National Climate Centre of the BoM have been used. The

recent climatic trend in SEA has been analysed and placed in the context of the long-term historical record.

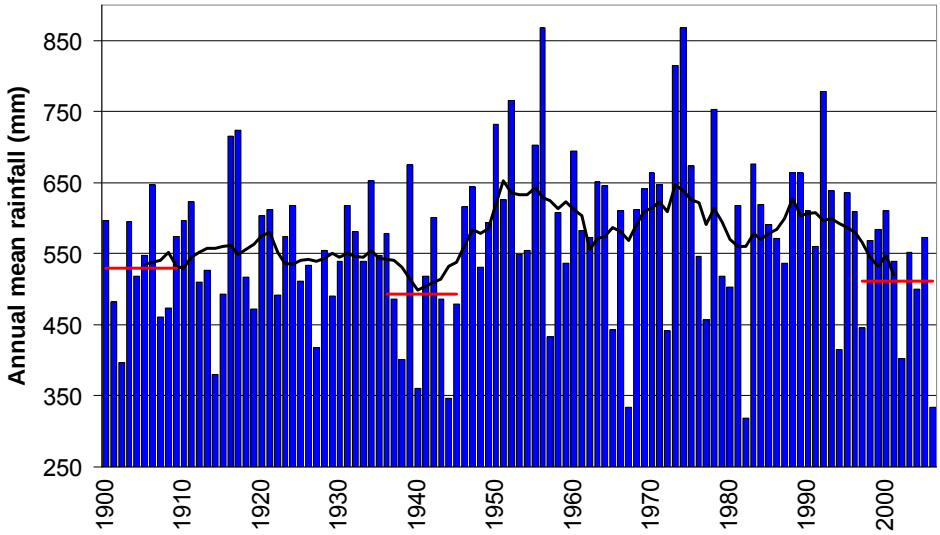

Fig. 7 *Mean annual rainfall over the south-eastern Australia region (mainland south of 33.5°S, east of 135.5°E) for each year from 1900 to 2006. Also shown are 10-year means for 1997-2006, 1900-1909 and 1936-1945 (thick, short horizontal lines) and the 11-year running mean (solid black). Units are mm.*

The original analysis of rainfall data showed that the dry conditions from 1996 to 2006 are not unprecedented in terms of annual rainfall: one drier ten-year was recorded for the region during the mid 1930s to mid 1940s (the WWII drought) and another decade around the turn of the century was nearly as dry (the so-called "Federation Drought" which commenced in the mid-late 1890s and lasted til around 1908) (Fig. 7).

Note that this statement made in 2007 needs to be updated. Firstly, it is worth noting that these results were obtained using the best available gridded rainfall product available from the National Climate Centre at the start of the SEACI project in 2006. By 2009, the older 1 degree gridded rainfall based on Barnes interpolation was replaced by the newer Australian Water Availability Project (AWAP), 5 km gridded rainfall database. This new dataset provides a better representation of the rainfall on topography such as along the Great Dividing Range (GDR) across SEA (Jones et al. 2009). Use of this data set resulted in larger decline in rainfall trends across most of SEA. Using the AWAP data, the decade from 1997-2006 was nearly as anomalously dry as the lowest decade on record from 1936 to 1945. In addition, the rainfall decline had continued and worsened across SEA after 2006 and became the longest dry spell on record based on analysis of both data sets – i.e. the previous 1° gridded rainfall (Timbal, 2009) and the new AWAP data. In fact, using the AWAP data set the deficit was even more pronounced. These updates to 2009 and using the latest AWAP data are discussed in more detail in Chapter 10.

The current drought has been exacerbated by three factors which make this recent climatic anomaly even more significant in terms of impacts than the two earlier decadal droughts. First, higher air temperatures due to ongoing global warming have been observed. Temperatures in the SEACI region have been increasing more rapidly since 1970. The last ten years have seen

warmer maximum temperatures across the SEACI region. Some regions (western Victoria and NSW) have been cooler at night and half of these reduced trends compare to the GW can be explained by drier conditions. Second, the last decade has been marked by very low interannual variability (the lowest on record) in rainfall. There has not been a single year well above the long-term average (2000 has been the wettest year and still was only about 6% above the long term average). The period saw a total lack of wet years to compensate for dry years. The third factor is that most of the trend in annual rainfall since 1991 (72%) is due to lower rainfall in autumn. This is an important season in which the wetting up of the soil profile prior to winter/spring rains often occurs (Murphy and Timbal 2008). The likelihood that the strong seasonal signal in the rainfall decline identified here caused the lower than expected runoff was subsequently evaluated by other scientists as part of SEACI. It was found all three contributors identified here are responsible for the unexpectedly severe declines in streamflow (Potter and Chiew 2009; Potter et al. 2010) which exceed the expected normal hydrological amplification of any rainfall decline (Chiew 2006).

2.4 Large-scale modes of variability and their relation to SEA

In order to characterise large-scale influences on the climate of SEA, a number of indices were computed for the modes illustrated in Fig. 8. SEA-means are defined as spatial averages of gridded data from the BoM's National Climate Centre over mainland Australia south of 33.5ºS and east of 135.5ºE. Rainfall data are available from 1900 to 2006, and temperature (T_{max} and T_{min}) from 1950 to 2006.

A series of indices were explored to analyse the impact of ENSO (Niño 3, Niño 4, Niño 3.4, and the SOI). All indices show similar behaviour and results are presented for Niño 4 (Western Pacific, 160°E-150°W and 5°N-5°W) constructed using Sea Surface Temperature (SST) anomalies from Smith and Reynolds (2004) reconstruction version 2. Similarly, indices were constructed using the same SST database to explore the role of the Indian Ocean. Its main mode of variability, the Indian Ocean Dipole (IOD), has been linked to rainfall in SEA (Meyer et al. 2007). An additional index is used for the Indonesia-Indian Equatorial Ocean (120°-130°E, 10°S-0°N) and another for the north-west shelf (NWS: 100°-130°E, 20°S-5°S). The focus here is on the eastern side of the IOD which is more likely to impact SEA rainfall. Only results for the NWS are presented as both indices yield similar results. An additional index built for the neighbouring Tasman Sea (NTS: 150°-160°E, 40°-30°S) SSTs was constructed. Finally, for the Southern Annular Mode (SAM), the Marshall (2003) index calculated from station pressure observations covering 1958-2005 was used.

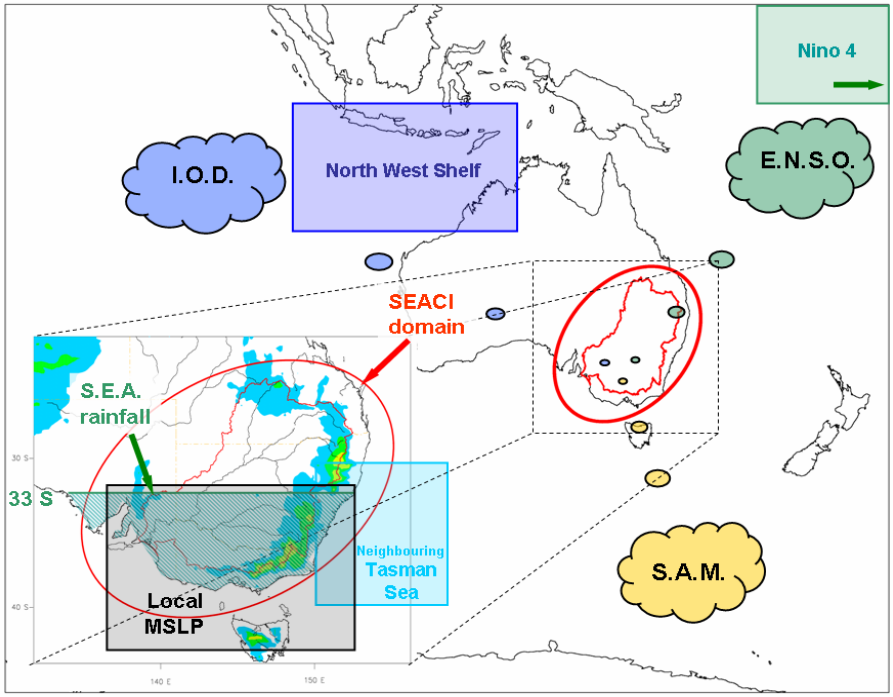

Fig. 8 *Schematic of the SEACI region and the large-scale influences affecting the climate of the region (see subsequent text for details on the various area-averages used).*

Many of the influences of the climate indices on SEA come about through modulations of the atmospheric circulation. This was quantified by computing a Mean Sea Level Pressure (MSLP) index for SEA (from 140°E to 150°E and from 33°S to 40°S) using gridded HadSLP2 data with 5° resolution from 1850 to 2004 (Allan and Ansell 2006). In order to remove this indirect influence we have calculated a time series of SEA rainfall (Rain) and have regressed this time series of rainfall on the MSLP time series. The rainfall residual time series (R-f (P)) is therefore uncorrelated with SEA MSLP.

The significance of the correlations obtained was assessed using the method described by Power et al. (1998). The method takes into account the autocorrelations of the time series and the consequent reduction in the effective degrees of freedom. Generally the autocorrelations at 1 month lag were very small for most indices. Only for the SST-based indices were they greater than 0.1. So the impact of these autocorrelations was minimal. When we talk of significant correlations we mean that the correlations are deemed to be significantly different from zero at the 90% significance level (in bold in Table 1) or very significantly different at the 99% significance level (in red in Table 1).

Table 1 *Correlation coefficient between SEA mean Tmax, Tmin, Rainfall and a rainfall residual (with the linear relationship to Mean Sea Level Pressure removed) and a range of climate indices for the four calendar seasons. The climate indices are discussed in the text. Note: red figures indicate significance above the 99% level and bold figures above the 90% level.*

Autumn	T_{max}	T_{min}	Rain	R-f(P)
MSLP	**0.40**	**-0.24**	**-0.29**	
Niño4	0.16	**-0.26**	-0.16	-0.06
NWS	**0.28**	0.11	0.07	**0.19**
SAM	-0.06	-0.02	-0.02	0.09
NTS	**0.32**	**0.49**	**0.25**	**0.27**

Winter	T_{max}	T_{min}	Rain	R-f(P)
MSLP	**0.54**	**-0.44**	**-0.74**	
Niño4	0.19	-0.16	**-0.20**	-0.06
NWS	0.08	**0.41**	**0.30**	**0.32**
SAM	-0.01	**-0.31**	**-0.27**	0.17
NTS	**0.39**	**0.30**	0.07	**0.22**

Spring	T_{max}	T_{min}	Rain	R-f(P)
MSLP	**0.46**	**0.29**	**-0.39**	
Niño4	**0.33**	-0.11	**-0.37**	**-0.28**
NWS	0.00	**0.34**	**0.26**	**0.19**
SAM	-0.20	**0.28**	**0.31**	**0.47**
NTS	**0.40**	**0.60**	0.16	**0.22**

Summer	T_{max}	T_{min}	Rain	R-f(P)
MSLP	0.14	**0.34**	0.14	
Niño4	0.11	-0.07	**-0.18**	**-0.23**
NWS	**0.24**	0.19	-0.09	-0.13
SAM	0.02	**0.30**	**0.31**	**0.27**
NTS	**0.43**	**0.55**	**0.19**	**0.19**

The main findings are:

1. Local MSLP has the greatest influence of all indices except in summer when it is mostly negligible (except for T_{min}). Local MSLP is associated with reduced rainfall. This association is strongest during winter when rainfall variability is linked to the frequency and intensity of low pressure systems and fronts. Increased MSLP is also associated with an increase in T_{max}. The influence on minimum temperature is more complex and reverses sign between the autumn/winter half of the year, when high MSLP is associated with clear skies and colder night-time temperatures, and spring/summer half of the year when the relationship becomes positive due to the influence of T_{max} (Power *et al.* 1998).

2. ENSO-related correlations are at their strongest in spring and generally highest for rainfall and T_{max}. The correlation with largest magnitude is only -0.39 between Niño 3.4 and SEA-mean rainfall in spring but it reaches 0.50 with the SOI, explaining 25% of the variance. This confirms that SEA is not the Australian region most affected by ENSO (Nicholls 1989). The strong relationship with rainfall in spring is strongly reduced when the influence of local MSLP is removed, thus confirming that the influence of ENSO on SEA rainfall occurs through large-scale circulation changes.

3. Indian Ocean SSTs are related to rainfall and T_{min} in winter and spring, but are stronger in winter. Interestingly the relationship with rainfall is only reduced slightly in spring when the influence of local MSLP is removed. In winter and autumn the strength of the relationship increases and becomes significant with the MSLP influence removed. This suggests that the influence of the warm SSTs along the north-west coast of Australia is felt in SEA by mechanisms other than circulation changes, *e.g.* moisture fluxes.

4. The Southern Annular Mode (SAM) index correlates significantly with SEA rainfall in all seasons except autumn. The SAM modulates SEA rainfall in winter where the negative correlation indicates that the southward contraction of storm track leads to less rain. The

opposite is true in spring and summer where there is more rain with associated with increase easterly flow (Hendon *et al.* 2007). The signature for T_{min} is similar. There is no influence of SAM on T_{max}. When the effect of MSLP is removed the correlation between the SAM and SEA rainfall in winter changes sign, and in spring it is much stronger. This suggests that the direct influence of SAM on SEA rainfall is stronger due to some changes in the advection of moist airflow but is reduced by the concomitant impact on regional MSLP.

5. The strongest apparent influence of neighbouring Tasman Sea SSTs is seen on temperature: T_{max} in winter and T_{min} in spring-summer-autumn. The only significant correlation with rainfall is in autumn (0.25). When the impact of MSLP is removed, the relationship with rainfall is strengthened, becoming significant in all seasons, though remaining modest.

From these relationships between SEA climate and large-scale indices, it is hard to explain the step change of rainfall in SEA that has occurred in autumn. This is because none of the climate indices have a strong relationship in that season and the only significant ones (the neighbouring Tasman Sea with rainfall, and NWS with rainfall residual) are unlikely to explain the rainfall decline since both indices have been trending upward and should have been associated with an increase of rainfall not a decrease. At this stage, it appears that the rainfall decline can only be explained as part of a response to an increase in local MSLP. The causes of the MSLP increase will be discussed later in this report.

2.5 Regional contrast

So far we have considered SEA as one homogenous region. In reality, there are contrasts in the climate variability and the cause of variability in different parts of SEA. In order to investigate this further, we look at rainfall in four areas included within the SEACI domain (dashed blue ellipse in Fig. 3) matching the subregions considered by Drosdowsky and Chambers (2001). We calculated the average monthly-mean rainfall for two high quality stations in each region that capture the variability of rainfall. High quality rainfall stations were used. Maps of the correlation coefficients between these time series and the monthly gridded HQ rainfall data over the period 1948-2005 are shown in Fig. 9 where area where the correlations explain more than 20% of the total variance are shaded.

The defined regions match very well four of the patterns (rotated EOFs) from Drosdowsky and Chambers (2001): number 1 (Fig. 9, top left) based on rainfall at Peak Hill and Bingara), number 2 (Fig. 9, top right) based on rainfall at Murray-Bridge and Orroroo), number 5 (Fig. 9) bottom left, based on rainfall at Meredith and Yan-Yean) and number 8 (Fig. 9, bottom right) based on rainfall at Thargomindah and White Cliffs). The four patterns generally do not overlap and cover most of the SEACI region. The mean monthly rainfall of each pair of stations was averaged to give a time series of a regional rainfall index. Some interesting regional features emerge (Table 2).

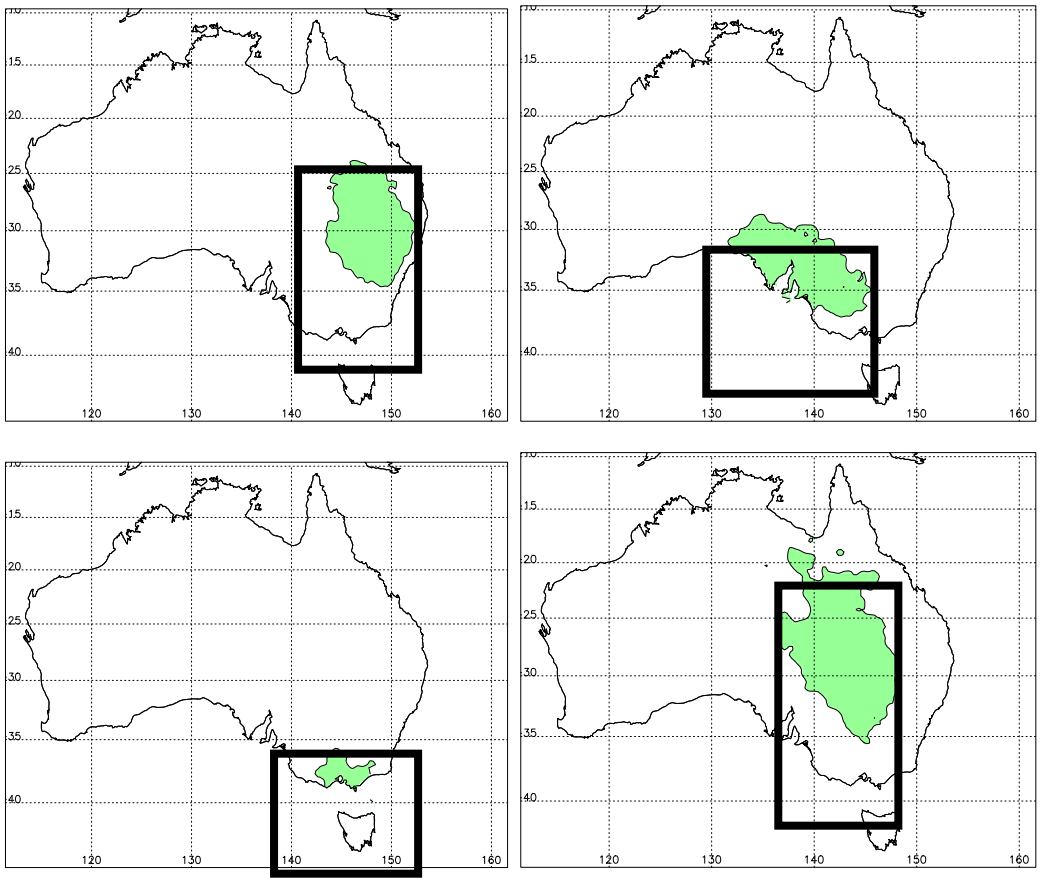

Fig. 9 *Four rainfall patterns covering SEA (see text for details on their calculation) and referred to in the following analysis as: Eastern (top left), North-West Cloud Band (NWCB) (top right), Victoria (bottom left), Central (bottom right).*

Table 2 *Correlation coefficients between rainfalls for four regions in the SEACI domain and a range of climate indices for the four calendar seasons. Red figures indicate significance above the 99% level and bold figures above the 90% level.*

Autumn	NWCB	Victoria	Eastern	Central
MSLP	**-0.43**	**-0.39**	**-0.26**	**-0.36**
Niño 4	**-0.35**	**-0.30**	-0.16	**-0.37**
NWS	0.04	-0.19	0.08	-0.16
SAM	0.04	-0.01	-0.01	0.05
NTS	0.18	0.08	0.21	0.21

Spring	NWCB	Victoria	Eastern	Central
MSLP	**-0.28**	**-0.33**	-0.06	**-0.25**
Niño 4	-0.14	**-0.45**	**-0.46**	**-0.43**
NWS	0.07	0.05	0.20	0.16
SAM	0.18	0.13	**0.33**	**0.29**
NTS	0.04	-0.17	**0.31**	**0.24**

Winter	NWCB	Victoria	Eastern	Central
MSLP	**-0.68**	**-0.45**	**-0.31**	**-0.33**
Niño 4	0.05	-0.15	**-0.46**	**-0.29**
NWS	**0.35**	0.09	**0.27**	**0.34**
SAM	-0.13	**-0.30**	0.14	0.13
NTS	0.15	-0.12	0.19	**0.29**

Summer	NWCB	Victoria	Eastern	Central
MSLP	0.03	0.14	-0.17	-0.09
Niño 4	0.03	-0.04	-0.15	**-0.33**
NWS	-0.06	-0.11	0.00	-0.18
SAM	0.17	0.16	0.22	**0.29**
NTS	0.09	0.08	**0.39**	0.18

As for rainfall across SEA, the relationship with local MSLP (using MSLP in the rectangular boxes depicted in Fig. 9 to define each rainfall sub-region) was removed from the rainfall series and compared with the four major climate indices for all seasons except summer when the rainfall-MSLP relationship is non-existent (Table 3).

Table 3 *Correlation coefficients between the rainfall residual (i.e. with the relationship to Mean Sea Level Pressure removed) for four regions in the SEACI area and four climate indices for autumn, winter and spring. Note: red figures indicate significance above the 99% level and bold figures above the 90% level.*

Autumn	NWCB	Victoria	Eastern	Central
Niño 4	-0.17	-0.21	-0.02	-0.19
NWS	**0.26**	0.00	0.24	-0.02
SAM	0.19	0.14	0.08	0.16
NTS	0.13	0.08	0.21	0.16

Winter	NWCB	Victoria	Eastern	Central
Niño 4	**0.31**	-0.05	**-0.39**	**-0.24**
NWS	**0.26**	0.02	0.23	**0.27**
SAM	**0.28**	-0.05	**0.33**	**0.33**
NTS	**0.28**	-0.04	**0.25**	**0.28**

Spring	NWCB	Victoria	Eastern	Central
Niño 4	-0.02	**-0.34**	**-0.44**	**-0.29**
NWS	-0.02	0.00	0.17	0.10
SAM	0.25	**0.30**	**0.35**	**0.34**
NTS	0.13	0.08	0.21	0.16

The important regional variations which add information to the previous analysis of the entire SEA spatial averages are:

- The relationship between local MSLP and rainfall is strongest in the Victoria and NWCB regions (particularly in winter).

- The influence of Niño4 SSTs on the rainfall is strong in Eastern and Central regions but disappears further west in winter. In autumn the picture is rather different, with stronger correlations away from the Eastern region. While the relationship with rainfall in the eastern regions in winter remains significant once the influence of local MSLP is removed, it is not so in autumn with the western regions. This suggests two different mechanisms for the influence of Niño4 on the SEACI domain: a direct influence for the north-eastern part of the domain in winter (possibly due to moisture fluxes) and an indirect influence for the south-western part of the domain in autumn (due to circulation changes diagnosed from the relationship with MSLP).

- The influence of the IOD is weak everywhere in autumn but moderate in winter outside the Southern region. However, once the relationship with local MSLP is removed (increasing correlations in autumn by about 0.2 and decreasing them in winter by about 0.1) the influence is very similar in both seasons (apart from the Central region). The seasonal differences appear to be due to circulation changes (as diagnosed by the relationship with MSLP) which differ in both seasons.

- The negative influence of SAM in winter is limited to the south-west of the domain and changes sign further north (in agreement with Hendon et al. 2007). As per the SEA average, correlations increase everywhere in magnitude once the MSLP influence is removed. No significant correlations are seen in autumn.

- The apparent influence of the NTS is felt mostly outside the MSLP influence and is moderate in winter everywhere apart from the Southern region. In autumn, the relationship between NTS and rainfall residual is similar than with raw rainfall but it is not significant everywhere.

2.6 Conclusions

As part of this program, datasets of daily values of rainfall, temperature, humidity and pan-evaporation are now available for stations in the entire SEACI region. The dataset combines stations of the highest possible quality with additional stations when necessary to enhance spatial coverage.

An analysis of long-term rainfall trends and variability, based on this dataset, shows that most of SEA south of 33.5°S received rainfall during 1997-2006 that is in the lowest 10% of historical totals on record. Only one previous 10-year period had average rainfall over SEA less than the 1997-2006 average *(NB: this is not the case once the data are updated to 2009 and the AWAP rainfall is used)*. Most of the rainfall decline in SEA has come in the autumn season (up to 72% when considering the decline since 1991 to 2006). Year-to-year variations in annual rainfalls over SEA were also very low. Furthermore, the recent dry period has been compounded by an underlying warming trend.

SEA rainfall variability is closely linked to changes in SEA MSLP in all seasons except summer. MSLP has been trending toward higher values. Over the entire SEA region the step change in autumn rainfall does not appear to be clearly related to a single mode of large-scale variability; correlations with indices representing the various modes of variability are usually weak to moderate. These influences of the modes vary from one sub-region to another. E.g. significant negative correlations with Niño4 SSTs are apparent in autumn for the south-western and central part of the domain.

As an aside, these results are consistent with the pattern of the rainfall decline in SEA since 1996 observed to peak in the south-west of the region (Trewin 2006). It suggests the possibility that the warming of the tropical central Pacific (Niño4 region), which is not necessarily related to a trend in ENSO but simply to the global warming of the ocean, together with the rises of MSLP above SEA, have contributed to the autumn rainfall decline. No attempt is made here to explain the causes of the MSLP increase. But it is reasonable to suggest in light of these results that the interplay between these modes of variability and the local MSLP are important in explaining the regional rainfall decline.

Summary

- Datasets consisting of station data of daily values of rainfall, temperature, humidity and pan- evaporation are now available for the entire SEACI region. The dataset combines stations of the highest possible quality with additional stations when necessary to enhance spatial coverage.

- Based on this dataset, most of SEA south of 33°S received rainfall during 1997-2006 in the lowest 10% on record. Only one previous 10-year period (1936-1945) received average rainfall over SEA that is less than the 1997-2006 average.

- Using the latest BoM high resolution gridded rainfall dataset and updating the analysis to the end of 2009, the period 1997-2009 received the lowest 13-year average annual rainfall in the historical record by a large margin (512 mm or -11.5% relative to the long-term average from 1900 to 2009). The previous lowest 13 year average was 536 mm from 1933 to 1945 and corresponds to only a 7.4% decline [Details in Chapter 10].

- Most of the rainfall decline in SEA during the recent period has come in the autumn season. In addition, year-to-year variations in annual mean rainfalls over SEA have been very low. The recent dry period has been compounded by an underlying warming trend (up to 0.7°C in the last 50 years).

- SEA rainfall variability and change is closely linked to change in MSLP. MSLP has been trending toward higher values and that relates well with the rainfall decline in all seasons except summer.

- No single large-scale mode of variability explains the rainfall decline, but several have an impact on the regional climate. The combination of the most relevant factors differs from one part of the SEACI domain to another.

3 ATTRIBUTION OF THE OBSERVED CLIMATE CHANGES TO LARGE-SCALE MODES OF VARIABILITY

NB: in this chapter, data are used up to 2006, rainfall and other climate data are not calculated on the AWAP data but on the previous BoM gridded product on a 0.25° grid and anomalies are calculated using the WMO reference period: 1961-1990

3.1 Introduction

In the previous chapter we provided a simple analysis of the role of key large-scale modes of variability performed earlier. In addition, as part of a review of the existing scientific literature on the climate of SEA, we saw that rainfall variability and change is closely linked to variability and change in MSLP. In this chapter, we will examine MSLP and rainfall changes in more detail by:

- investigating the causes of the changes of MSLP across southern Australia and its role in relation to the rainfall decline in SEA;
- compare recent observed changes in climate to the variability associated with the SAM and evaluate the likelihood that the SAM has contributed to the observed rainfall decline directly or through its influence on local MSLP;
- investigate the role of MSLP changes in explaining recent heat waves, using the April 2005 Murray-Darling Basin wide heat wave as a case study.

3.2 Improved detection

The specifics of the rainfall decline across the south-east of Australia in the period 1997-2006 were described in Chapter 2. Key results emerging from this in-depth analysis are that although the rainfall decline up to 2006 is not unprecedented in the historical record, some associated changes have been. This is illustrated in Table 4.

Table 4 *Mean and standard deviation for total rainfall, autumn (March-April-May) rainfall, annual temperature and Murray River modelled inflow for three periods: 1997-2006, 1936-1945 and 1961-1990.*

Period vs. Variables	**1997-2006**		**1936-1945**		**1961-1990**	
	Mean	**Std**	**Mean**	**Std**	**Mean**	**Std**
Total Rain (mm)	511	90	494	106	595	120
Autumn Rain (mm)	98	32	116	36	149	51
T_{max} (ºC)	20.4	0.27	19.7	0.47	19.9	0.48
Murray Inflow (GL)	4872	2722	5855	4406	9437	5541

By comparing a series of numbers (Table 4) for the dry decade (1997-2006) and the driest decade on record (1936 to 1945), it can be seen that the Murray inflow was well below long-term averages (as expected from the hydrological response to rainfall decline – Chiew (2006)). But the decline in inflows is about 20% to 30% larger in the recent decade compared to the previous dry one, than the rainfall decline.

Three reasons for this "*amplification"* of the streamflow response were proposed:

(1) About 60% (using the Barnes gridded rainfall across SEA, and the WMO reference period) of the rainfall decline is concentrated in autumn (67% in the five month period from March to July); this precedes the period (winter/spring) typically associated with the largest runoff during the year. During the previous dry decade the autumn decline was less than one third of the total rainfall decline.
(2) The year-to-year variability (measured by the standard deviation in each period) has been lower during the decade 1997-2006 than the previous driest decade (1936-1945). There has been an absence of years with rainfall markedly in excess of the long-term average which is likely to have exacerbated the impact on streamflows.
(3) The ongoing warming may have increased the evaporation and reduced the amount of water available for run-off in parts of SEA. Maximum day-time temperatures during the 1997-2006 period were about 0.7 ºC higher. This is a very significant warming (about 1.5 times the standard deviation over the long-term means).

The contribution of these three factors was subsequently quantified by SEACI researchers (Potter and Chiew 2009 and Potter et al. 2010).

The autumn rainfall decline averaged across SEA is somewhat misleading and a better understanding of the regional pattern of the decline across SEA is captured by considering how the full annual cycle of rainfall has been affected in different parts of the SEACI region. In the southern part of SEA, most of the rainfall occurs during the cold months from the autumn to spring. There the largest decline (in absolute terms) is in late autumn to early winter as rainfall in early autumn is typically negligible. In contrast, in the northern part of SEA where more rainfall falls during the warmer months, the decline is most noticeable in summer to autumn (C. Rakich and P. Wiles, personal communication).

A convenient way to separate the two regions is to use the location of the Sub-Tropical Ridge (STR). The STR has a marked annual cycle; during autumn it varies rapidly between a mean summer position of 38ºS and a mean winter location of 31ºS and sits around 35ºS (Drosdowsky 2005). We have used the position and intensity of the STR as calculated by Drosdowsky (2005) in our analyses: a meridional profile of MSLP is averaged using monthly MSLP values between 147.5 and 152.5ºE and interpolated to a fine 0.5º latitudinal resolution using a cubic spline; the absolute maximum pressure of this profile is assumed to be the position of the STR.

As shown in the previous chapter, remote large-scale modes of variability have limited influence on the local rainfall whereas most of the rainfall decline can be related directly to regional MSLP trends.

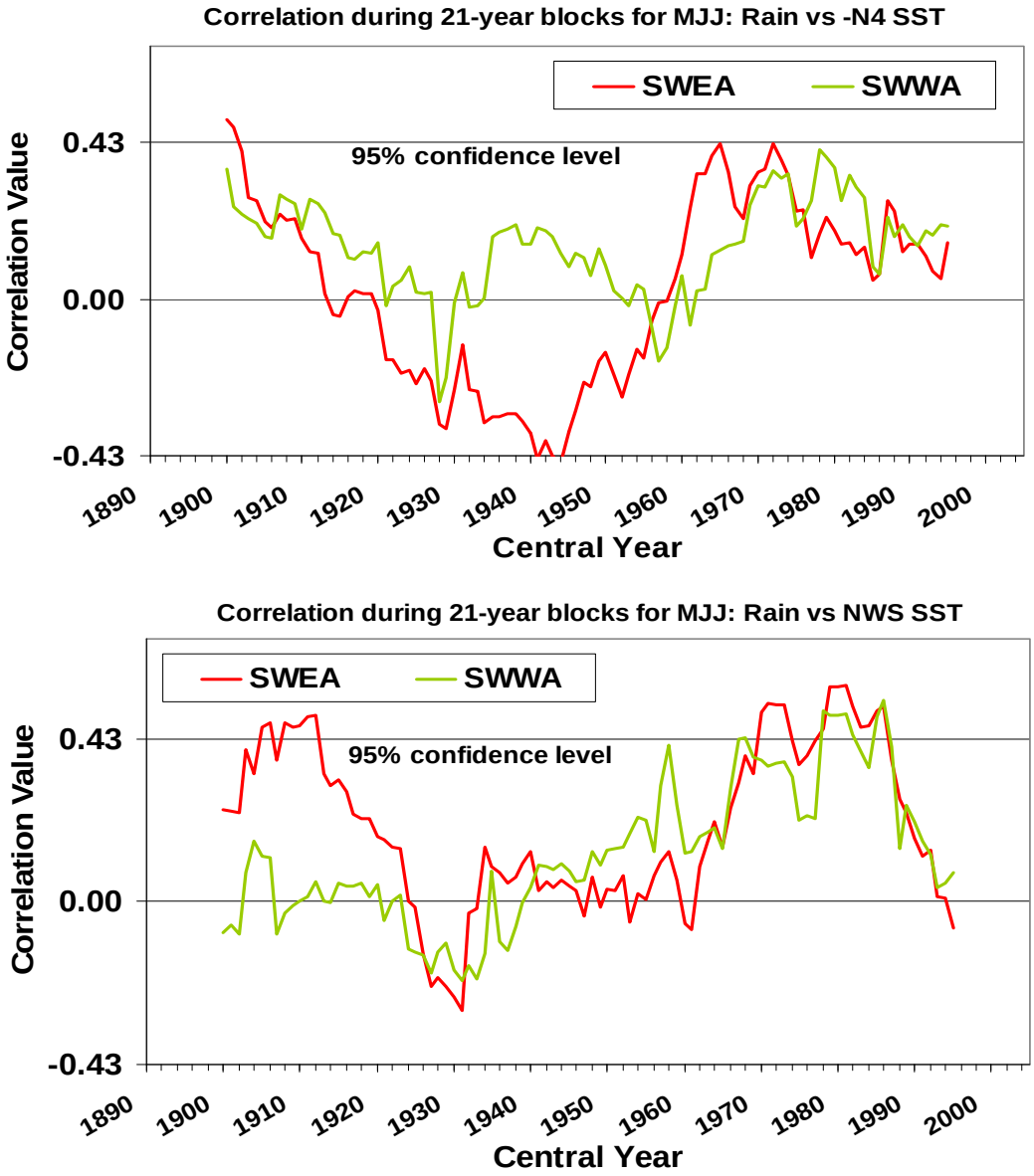

Fig. 10 *Correlation between the May-June-July rainfalls in SWEA (red lines) or in SWWA (green lines) and Sea Surface Temperatures at lag 0, averaged in the North-West Shelf (NWS) box (shown in Figure 8) and in Niño 4 box (note the use of a reverse sign for N4 SST). Correlations are calculated for 21 year periods, and the correlation value is placed at the central year (correlations significant at the 95% significance level are used on Y-axis).*

As a consequence of the findings listed above and coming from Chapter 2, the focus here is on rainfall trends studied separately between the South-West of Eastern Australia (SWEA) and a large area on the other side of the STR (the exact definition of the SWEA is depicted in the Fig. 17 in Chapter 4). The focus on autumn was tuned to early winter in SWEA and warm season rainfall further north. Amongst the large-scale modes of variability, only the role of the SAM was investigated further as it appears that the strength of the teleconnections between tropical SSTs in both the Pacific (linked to ENSO) and the Indian Ocean (linked to IOD) and the rainfall in SEA is relatively weak overall and these relationships tend to vary with time and in the case of SWEA have been declining in the last 20 years (Fig. 10). Correlations over 21-year periods

are hardly ever significant (the 95% confidence level is indicated on Fig. 10) and hence the changes in strength of the relationship may be totally random. However, the consistency between the two sources of tropical forcings of inter-annual variability (Nino4 and NWS) and the responses for two climate regions SWEA and the South-West of Western Australia (SWWA) suggest an apparent de-coupling between tropical modes of variability and southern Australia rainfall regions. *(N.B: it was shown outside the SEACI program that SWWA and SWEA are two climatic regions showing many similarities (Hope et al. 2009)).*

This finding suggests that the rainfall decline in most of SEA (at least in the southern winter-rainfall dominated area) is unlikely to be explained by the time-evolution of these tropical modes of variability as, if anything, their influence on the local rainfall is rather small and diminishing in the last two decades. It was also noted that in SWEA the ongoing rainfall trend is consistent with future projections (Timbal and Jones 2008) for which there is a general agreement amongst models which has been linked to a general agreement on future trends for SAM amongst the models (Miller et al. 2006).

3.3 Past trends in the SAM and their influence on rainfall and MSLP

SAM describes a naturally occurring oscillation in pressure that represents an exchange of air mass between the mid-latitudes of the southern hemisphere and the southern polar region. The high-phase of SAM is characterised by higher than normal pressure over the southern mid-latitudes and lower than normal pressure over Antarctica. Conversely, the low-phase of SAM is characterised by lower than normal pressure over the mid-latitudes and higher than normal pressures over the pole.

The importance of the SAM on Australian temperature and rainfall has been documented (Hendon et al. 2007). We conducted the same analysis for the SEACI domain using the high resolution AWAP gridded rainfall (Fig. 11). This analysis reveals that rainfall on and south of the Great Dividing Range across Victoria is more related to SAM than previously thought. This is better captured with a finer gridded rainfall data. This could be an important result as this mountainous area is a high rainfall area and is important in generating runoff for most of the eastern part of Victoria. Comparison of the monthly and seasonal interactions shows that the SAM-rainfall relationship is much more robust on seasonal timescales. Month to month relations are less statistically reliable due to the small number of days in each phase and do not confirm a possible role in SAM in explaining the month to month variability in rainfall decline: large in April, May and July but not in June (Murphy and Timbal 2008).

The seasonal relationships calculated by Hendon et al. (2007) were adapted to match the key seasons for SWEA: early winter (May-Jun-July), when observed rainfall has declined and the SAM index is trending upward and late winter (August-September-October), when rainfall has not declined and SAM is not trending upward. It was found that a rainfall decline of 5% in MJJ could be attributed to the SAM trend using the Marshall (2003) SAM index from 1959 onward. This is well below the observed decline in this region of about 11% at this time of the year. In ASO, there is hardly any rainfall decline attributable to SAM (below 1%) since the index has hardly any trend since 1959. Taken at face value, these estimates indicate that almost 50% of the total decline in rainfall in MJJ could be attributable to the SAM increase in MJJ. However

closer inspection of the timing of SAM changes, and rainfall changes, indicate that the relationship is perhaps more complex. While the SAM increased during the 1960s and 1970s, the rainfall decline has occurred only since the mid-1990s.

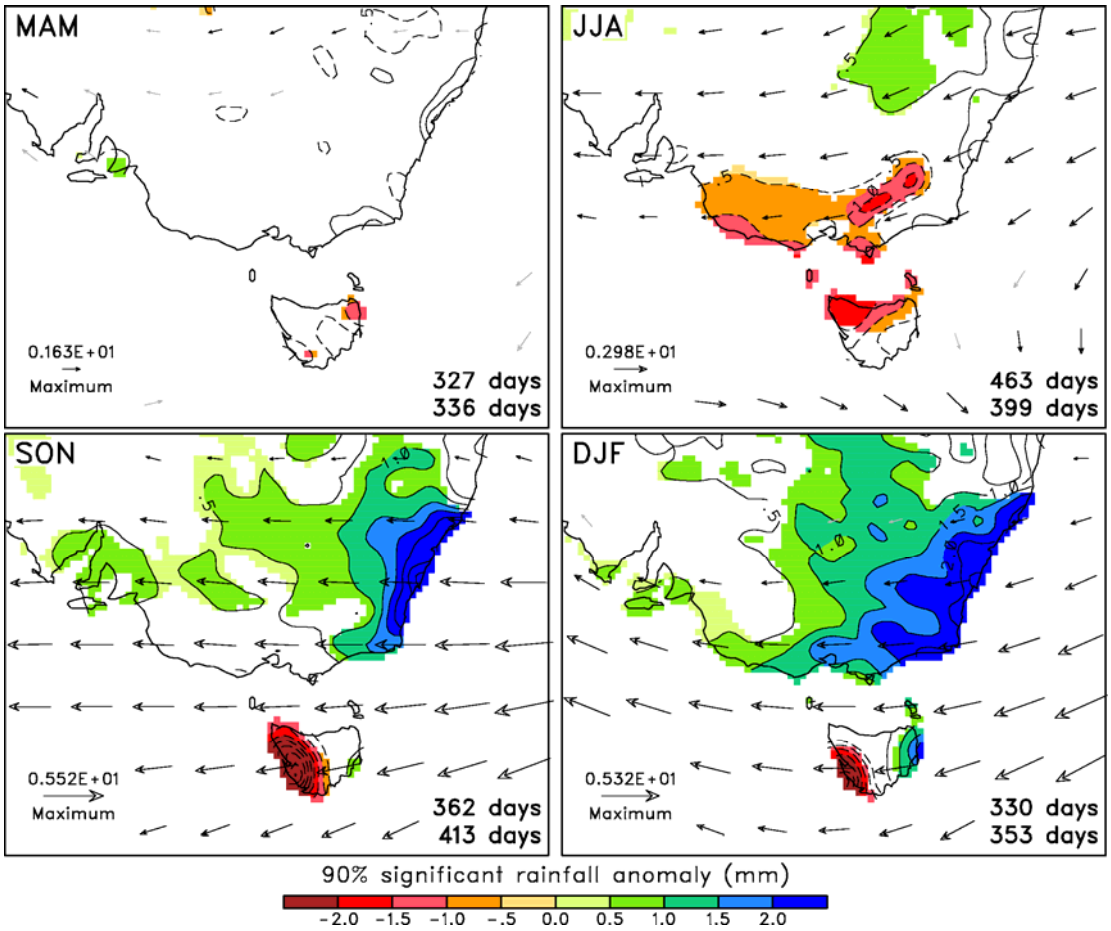

Fig. 11 *Composite daily rainfall (contours and shading) and 850 hPa winds (maximum vector shown in lower left corner of each panel) for high minus low polarity of the SAM index for MAM (top left), JJA (top right), SON (bottom left and DJF (bottom right), using daily data (1979 to 2005). Significant differences at the 90% level are shaded. The number of days in the high and low index polarity of the SAM is listed in each panel.*

The work of Hendon et al. (2007) was also adapted for MSLP. It shows that, for all seasons, increasing SAM is associated with increasing pressure over SEA, with the largest signal in the observations occurring in MJJ. Using the Marshall SAM index, the observed trend in the SAM index can be translated into a MSLP rise of 0.5 hPa in the vicinity of SEA. This is a significant amount corresponding to up to one third of the observed MSLP increase in MJJ. As for rainfall, there is a timing issue as most of the MSLP increase above the eastern part of Australia has happened since the 1970s (Timbal and Hope 2008).

3.4 Future trends in the SAM and their influence on rainfall and MSLP

Climate models are very consistent in predicting that global warming will lead to a more permanent high-phase of the Southern Annular Mode. Models are also very consistent in projecting a winter-time rainfall reduction affecting southern Australia, including SWEA. The Hendon et al. (2007) analysis was adapted and applied to a series of climate simulations with the CSIRO Mk3.5 global climate model:

- a 2000-year control simulation (i.e. no external forcings such as greenhouse gas increases). This was used to obtain the statistical significance of the results under 'natural' climate variability;
- a simulation of the 20th century with all known external natural and anthropogenic forcings; and
- a projection for the 21st century forced with anthropogenic forcings according to the SRES A2 emission scenario.

Figure 12 provides a global perspective for the contribution of SAM to rainfall in the Southern Hemisphere from the CSIRO model. This is the pattern of rainfall changes one would expect from an increasingly positive SAM index. The model appears to perform very well since the results are consistent with the observations across Australia - in particular, the rainfall reductions in the south-east of the continent, as well as the south-west. This change is most likely associated with increases in local pressure, and a southerly shift in the storm systems that bring wintertime rainfall to these regions.

Table 5 *Trend in SAM expressed as units of standard deviation from observations and for future climate model projections. The trends are expressed as 30 year trends using 11 year low pass filtered data. Projections indicate a tendency toward a high-phase in the months May through to August.*

Season	Observed 1971-2006	CSIRO GCM 1971-2000	CSIRO GCM 2001-2030
DJF	0.81	0.61	-0.11
MAM	1.92	-0.06	0.13
MJJ	**1.71**	**0.41**	**0.79**
JJA	1.51	0.74	1.03
SON	0.20	0.22	0.00

Trends in the SAM are analysed for various 30-year periods from all CSIRO simulations and compared to the observations (Table 5). In order for all the SAM indices to be comparable we used a MSLP based index as is the case with the Marshall index. The SAM index estimated from NCEP reanalysis of surface pressure shows larger positive changes in winter and spring than the Marshall index. In comparison the CSIRO model underestimates the observed trends during the 20th century. The future projected trends for the 21st century are very comparable to the modelled trends for the 20th century.

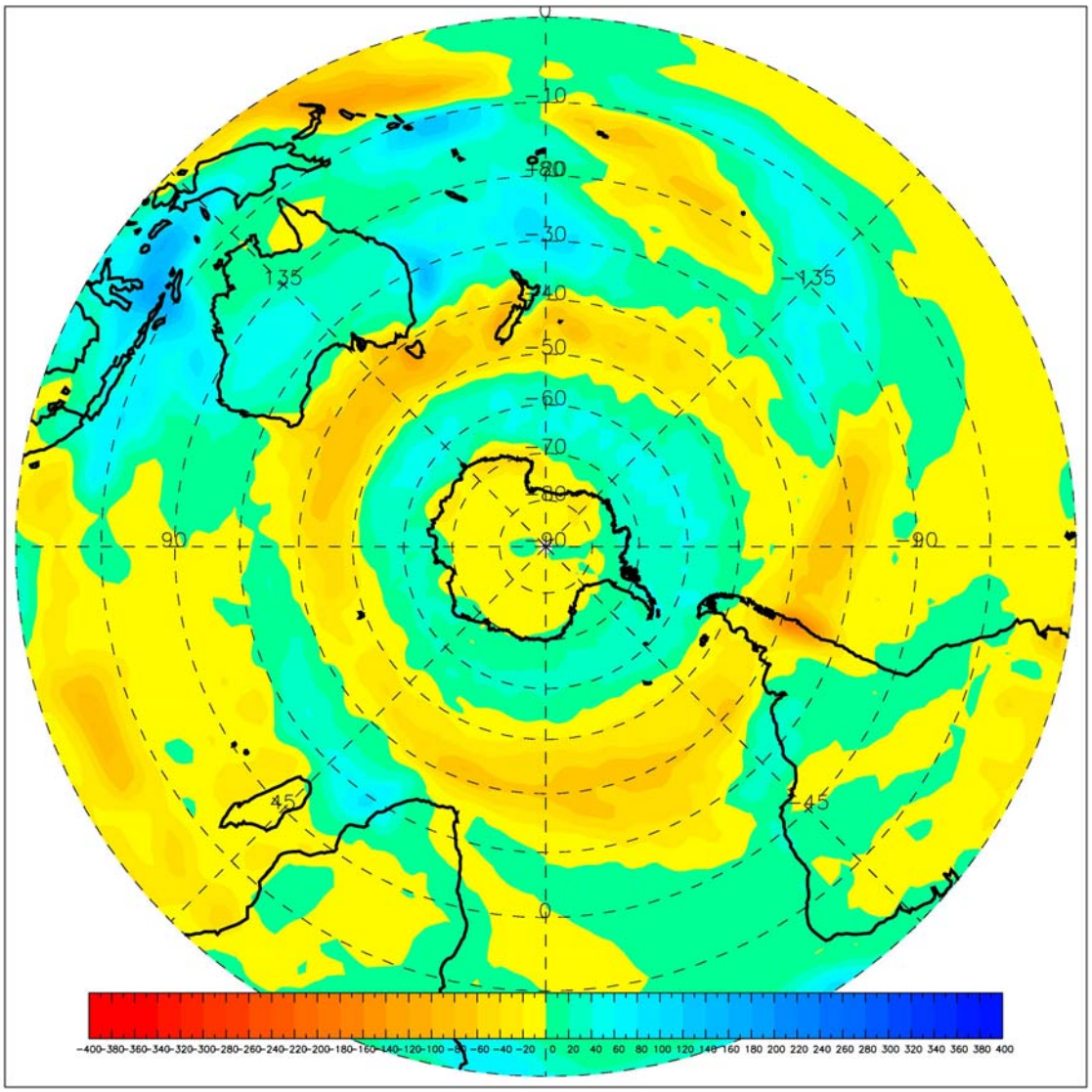

Fig. 12 *Mean composite rainfall difference for seasonal (MJJ) SAM high-low phase events using the CSIRO model. Negative values indicate a net rainfall reduction for that region associated with high-phase SAM. South west Western Australia and south eastern Australia are regions associated with reduced rainfall during high phase SAM.*

The model SAM signal is then translated into a rainfall signal using Hendon et al. (2007) to project SAM related rainfall and pressure changes in a future, warmer world and these estimates are compared with the total rainfall and pressure projections in the future climate scenario. The rainfall changes for the south-east of the continent expected from future changes in SAM using the CSIRO model are quite sizeable for both 30-year periods: 2031-2060 and 2061-2090 relative to pre-industrial climate (Table 6). The underlying SAM-rainfall relationship for SEA is calculated from the model by considering multiple 30 year samples from the 2000 year control simulation. Similarly, uncertainty in the underlying SAM-rainfall relationship is calculated from the distribution of 30 year samples. The SAM related rainfall change accounts for around 60% (2031-2060) and 30% (2061-2090) of the total predicted trend in MJJ rainfall in the CSIRO climate change projections.

Similarly, the SAM-pressure signal accounts for between 60% and 95% of future MJJ and JJA pressure changes (Table 7). For the periods 2031-2060 and 2061-2090, for autumn and winter months, the SAM-related changes in pressure account for a much higher proportion of total pressure changes in the CSIRO climate projections when compared to rainfall. A caveat to this result is that SAM-related changes account for much more of the total pressure changes in the model compared to the observed for the 20th century, and so the model might be overestimating the impact of SAM on MSLP and rainfall.

Table 6 *Future projected changes in rainfall (mm) due to changes in the Southern Annular Mode under global warming (SRESA2) emissions scenario. The GCM SAM-Forced rainfall amounts represent the implied change in rainfall due to future SAM.*

	2031-2060		2061-2090	
	SAM-Forced Rainfall Trend	% of total projected rainfall trend	SAM-Forced Rainfall Trend	% of total projected rainfall trend
DJF	0.91	-4.39	0.89	-3.35
MAM	2.15	-21.89	2.36	-12.12
MJJ	-7.47	62.67	-9.45	30.89
JJA	-6.43	38.28	-9.25	28.61
ASO	0.06	-1.16	0.21	-0.62
SON	1.17	-51.99	3.17	-10.23

Table 7 *Future projected changes in pressure (hPa) due to changes in the Southern Annular Mode under global warming (SRES A2) emissions scenario. The GCM SAM-Forced rainfall amounts represent the implied change in rainfall due to future SAM.*

	2031-2060		2061-2090	
	SAM-Forced Pressure Trend	% of total projected Pressure trend	SAM-Forced Pressure Trend	% of total projected Pressure trend
DJF	4.48	31.97	4.38	-10.69
MAM	40.26	71.90	44.21	42.51
MJJ	115.00	68.86	145.55	65.27
JJA	96.00	94.12	138.00	91.39
ASO	19.42	-176.51	64.22	91.74
SON	15.48	110.55	41.88	62.51

In general, the SAM-pressure correlations are more robust than those for rainfall. This result perhaps reflects the fact that rainfall has a much higher level of variability or climate noise compared with pressure. In particular, the signal to noise ratio of the SAM-pressure relationship in the long control simulation is much higher than that for the SAM-rainfall relationship. Changes in pressure associated with SAM may therefore be a more robust way to characterise future SAM related climate change for southern Australia.

3.5 The influence of the sub-tropical ridge on south-east Australian rainfall

Previous analyses of the influence of the STR on SWEA rainfall revealed that up to 80% of the MJJ rainfall decline could be related to the strengthening of the STR since the 1970s. It is worth noting that the timing of the increase of the STR intensity corresponds better to the timing of the rainfall decline than the SAM related rainfall decline mentioned earlier (SAM had a positive trend but in the 1960s and 1970s, a period when no rainfall decline was observed). Furthermore, during that earlier period the STR intensity was relatively low compared to the previous dry decades of the 1940s and that might have offset the expected SAM related decline.

We are now extending the analysis of the role of STR across the entire SEA region and not the SWEA only and across the months for which the rainfall decline is largest: from March to July (compare to MJJ previously). Across SEA, rainfall in March-April-May-June-July (MAMJJ) decreased from a mean of 262mm.year^{-1} from 1950 to 1980 to a mean of 201mm.year^{-1} since 1997 (a 23% decline). The MAMJJ decline represents 57% of the annual decline (note that this percentage is lower than when the reference period is 1961-1990). Although the relationship between MSLP and rainfall is strongest in winter, it remains significant in autumn and overall quite high over the entire MAMJJ period (Table 8).

Table 8 *Pearson correlation between MSLP or the intensity of the sub-tropical ridge (STR-I) and the rainfall averaged across the SEA region for several periods: autumn (March to May), March to July and early winter (May to July). The bold correlation is used to infer a rainfall reduction linked to the STR intensification across SEA.*

	SEA rainfall		
	MAM	MAMJJ	MJJ
MSLP	-0.29	-0.53	-0.68
STR-I	-0.42	**-0.59**	-0.70

Correlations with the STR intensity are higher than with MSLP, and in MAMJJ the relationship explains up to 35% of the inter-annual rainfall variability (Fig. 13).

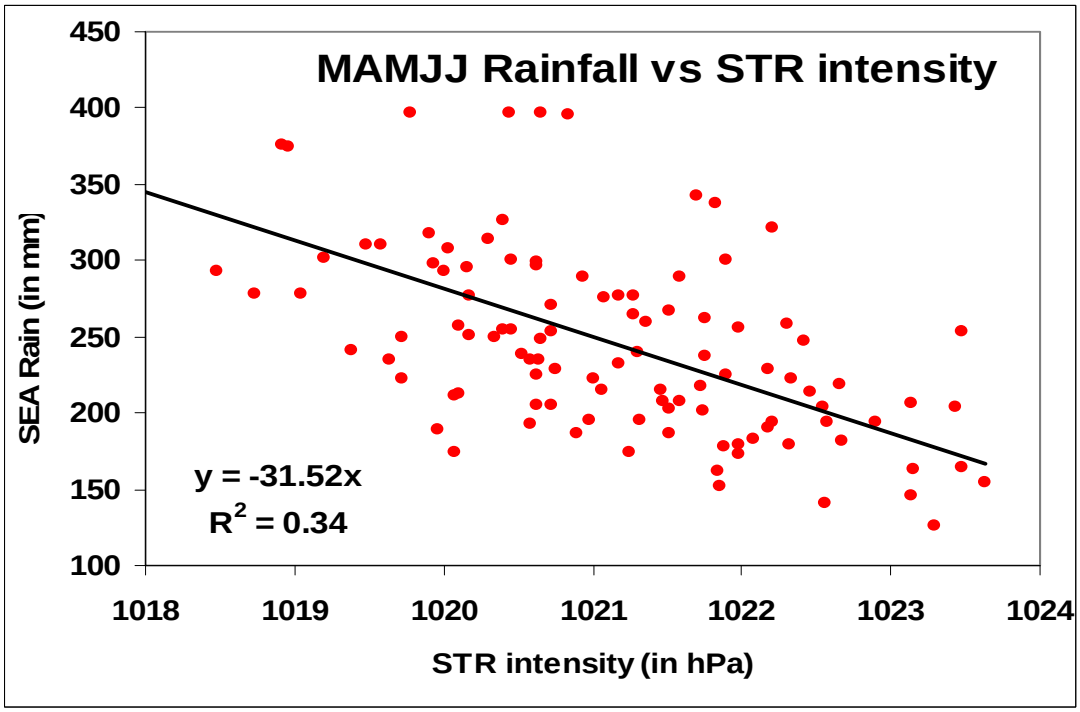

Fig. 13 *Relationship between SEA March-April-May-June-July rainfall and the sub-tropical ridge (STR) intensity during the same five months. The slope of the linear relationship and the amount of explained variance (r^2) is shown in the lower left corner.*

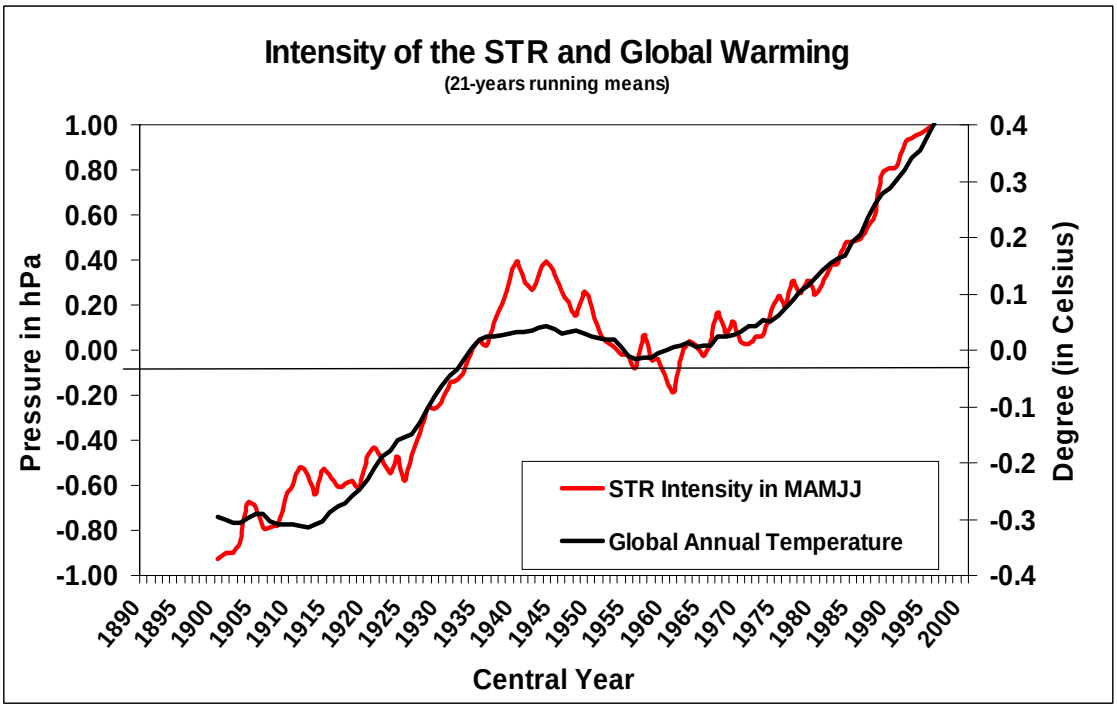

Fig. 14 *Long-term (21-year running mean) evolution of the Sub-Tropical Ridge (STR) March-April-May-June-July mean intensity (anomalies in hPa shown on the left-hand Y-axis) compared with the global annual surface temperature (data are from the Climate Research Unit in the UK; anomalies were calculated as per the STR curve and are in Degree Celsius shown on the right-hand Y-axis).*

The long-term evolution of the intensity of the STR in MAMJJ was compared to the average surface temperature of the globe (data from the Climatic Research Unit, University of East Anglia, UK). For both variables, 21-year running annual means were calculated (Fig. 14) centred on the 20th century (to have a mean of zero on the graph) and using different Y-axes (on the left for the STR and on the right for global temperature). The long-term co-evolution of both variables is remarkable. The previous high values of the STR correspond to the 1940s to 1950s when the global temperature reaches a maximum before decreasing until the 1960s and then rising again after the 1970s as does the global temperature. Using the slope of the relationship (-31.5 mm.hPa^{-1}) it is possible to translate the intensification of the STR from the low values between 1950 and 1980 to the record high since 1997 into a rainfall signal equivalent to 43mm.year^{-1}. This amounts to 70% of the observed decline. This amount is comparable, albeit lower than that calculated for the similar role of the STR in the MJJ rainfall decline in SWEA where up to 80% of the observed decline can be linked to the STR intensification. It shows that although the role of STR intensification is strongest in the south-west of the SEACI domain, where winter rainfall dominates, it can be felt across the entire domain.

3.6 North of the sub-tropical ridge: the influence of MSLP gradient on rainfall

In addition to diagnosing the influence of the STR on rainfall and the influence of the SAM, south of the STR a further analysis has been conducted examining the relationship between rainfall in the northern part of SEA and large-scale forcing using a newly developed MSLP index: the Gayndah-Deniliquin Index or GDI (Rakich et al. 2008). This index represents the variability in the trade wind flow over eastern Australia bringing moisture inland from the surrounding Tasman Sea, and relates particularly well with warm season (summer and autumn) rainfall (correlation of 0.76) in NSW (Fig. 15). This index exhibits large decadal variability corresponding to abrupt changes in rainfall over vast areas of the eastern Australian continent where warm season rainfall dominates.

An analysis of the relative contributions of each pole of the index (Fig. 16) reveals that until 1946, the MSLP variations at the two locations were roughly synchronized, leading to a relatively stable GDI. In contrast, during the late 1940s and early 1950s, a strong rise in Deniliquin MSLP combined with a fall in MSLP at Gayndah resulted in a rapid rise in the GDI at the time when most of SEA started to experience its wettest 30-year period on record. Since the 1970s, MSLP at the northern pole (Gayndah) has been rising, slowly regaining levels seen prior to 1947. The recent sharp decline in the GDI has resulted from this continued rise of summer MSLP at Gayndah, combined with a sudden decline of summer MSLP at Deniliquin since 2000, at a time where the on-going drought which was already well underway in SWEA started to extend to the rest of eastern Australia.

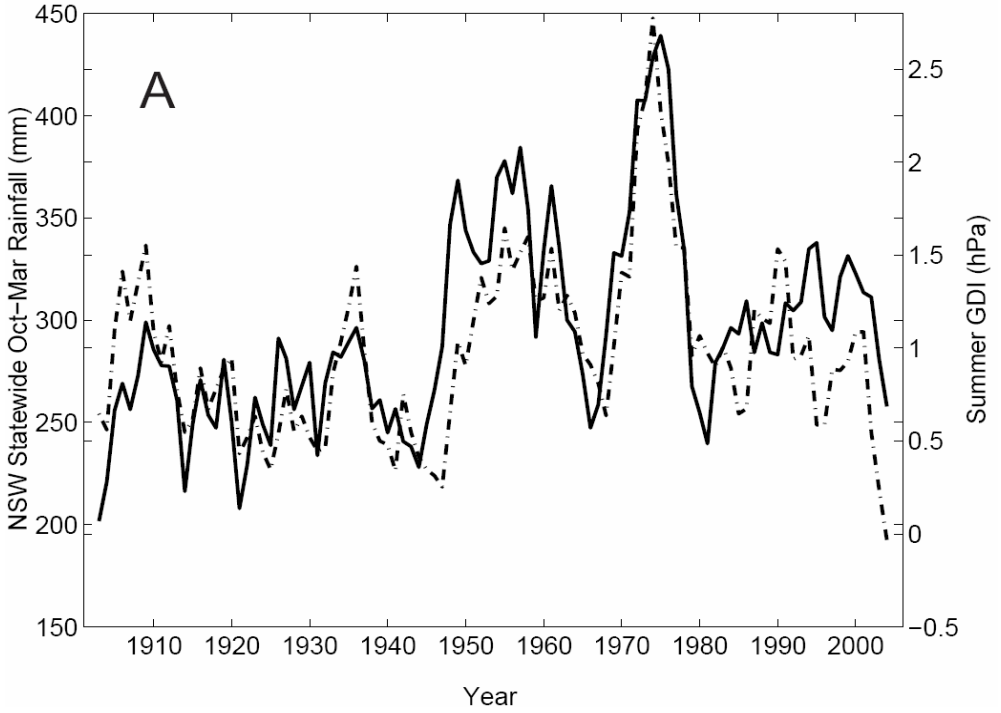

Fig. 15 *Five-year moving averages of both the warm season (Oct-Mar) NSW state-wide average rainfall (solid line) and the summer GDI (dashed line).*

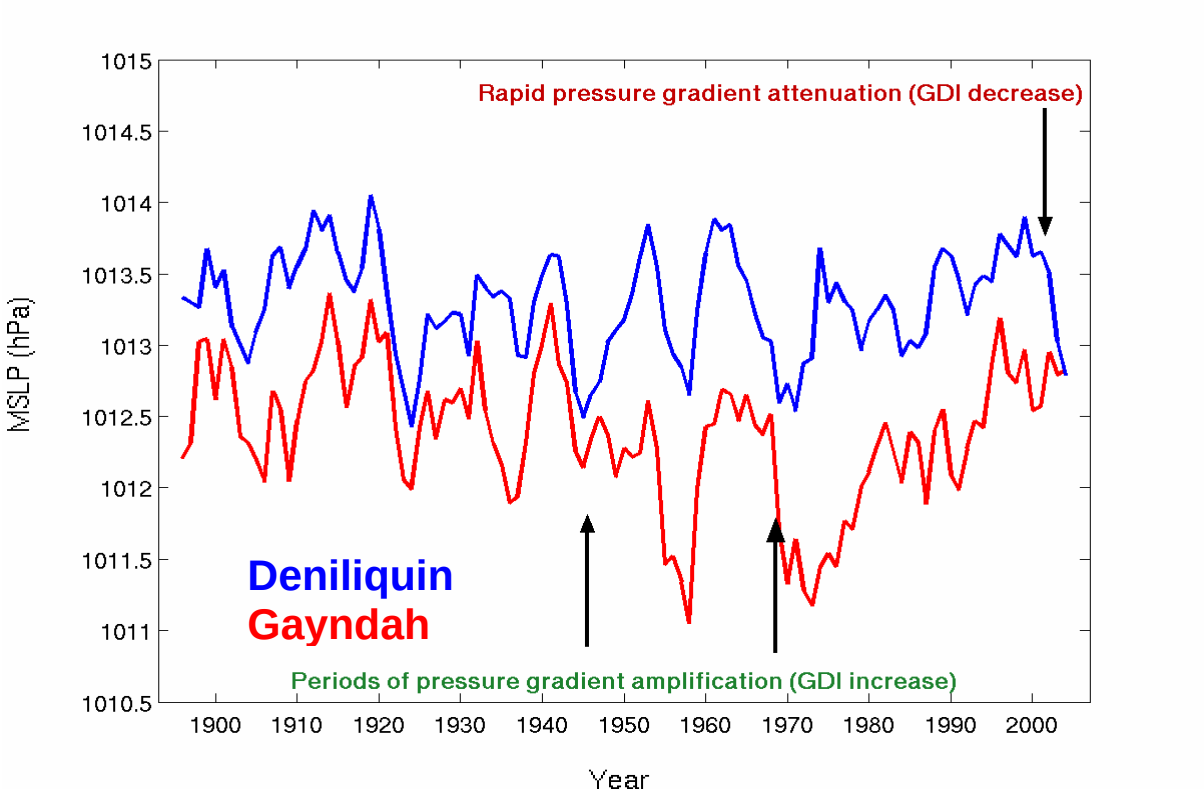

Fig. 16 *Five-year moving averages of summer (DJF) MSLP at Gayndah, QLD (red line) and Deniliquin, NSW (blue line) showing periods of rapid pressure gradient amplification (e.g. late-1940s and late-1960s) and rapid pressure gradient attenuation (e.g. mid-1960s and 2000-2006).*

The GDI was found to be complementary to the ENSO in summer and autumn, when the south-easterly trade winds affect eastern Australia and the SOI-rainfall relationship is at its weakest. It was also found that the relationship between the GDI and the SOI is asymmetric as is the ENSO-rainfall relationship: an asymmetry between positive and negative phases (see Power et al. 2006 in the case of ENSO). This generates inter-decadal variability in the strength of the relationship between GDI and the SOI during El Niño-dominated and La Niña-dominated epochs (see Power et al. 1999 in the case of ENSO). Similarly the GDI-rainfall relationship exhibits multi-decadal variability in strength. This suggests that although complementary, the relationship between the GDI and warm season rainfall over eastern Australia is not independent of ENSO.

3.7 Can the heat wave of April 2005 be attributed to global warming?

It is difficult to attribute a single extreme event to climate change. On the other hand, change in the frequency of particular extreme events can sometimes be attributed successfully. In the case of high temperatures and heat waves, a number of records have been established in the last decade or so and there has been some attempt to attribute the increase in the frequency of record to global warming. In this study, we investigated the causes of the heat wave experienced in April 2005. On a national scale, April 2005 saw the most extreme temperature anomalies ever recorded for Australia (NCC, 2005). The Australian mean temperature was 2.58°C above the 1961-90 average, nearly 1°C above the previous April record (1.73°C in 2002), and well above the largest anomaly previously recorded for any month (2.32°C in June 1996). Averaged across the MDB, the anomaly was spectacular: 4°C which is almost 1.5°C above the previous record in 2002.

The BoM Statistical Downscaling Model (SDM) (Timbal and McAvaney 2001) was used to examine the role of day-to-day meteorological conditions in producing the extreme temperatures across the MDB. The large-scale mean sea level pressure (MSLP) and temperature at 850 hPa (T_{850}) were used to see whether the heat wave can be explained by natural variability in atmospheric circulation or whether global warming is a major contributor. The SDM takes analogues from a "pool" of MSLP and/or T_{850} fields from 1958-2004 to reproduce the situation in April 2005.

As a starting point, the ability of the SDM to reproduce the inter-annual variability in observed temperatures and trends over the entire 1958 to 2004 period was evaluated. The T_{850} predictor was able to reproduce much of the year-to-year variations in surface maximum temperatures and had more skill than the MSLP predictor. Skill generally improved when the two predictors were used together. It was found that changes in MSLP patterns in April should actually have resulted in cooling temperature anomaly at MDB stations, whereas the T_{850} patterns produced no trend when averaged across MDB stations. However, combining both large-scale circulation (MSLP) and temperature (T_{850}) produces a positive, but weaker than observed, temperature change. This result is difficult to interpret; it suggests that part of the surface temperature change across the Basin can be accounted for by changes in synoptic situations combined with warmer air aloft, thus emphasising the importance of mid-tropospheric warming in explaining the surface changes. However, the absence of any trend when MSLP is used as a single

predictor clearly demonstrates that the ongoing warming across the basin cannot be explained by changes in synoptic situations.

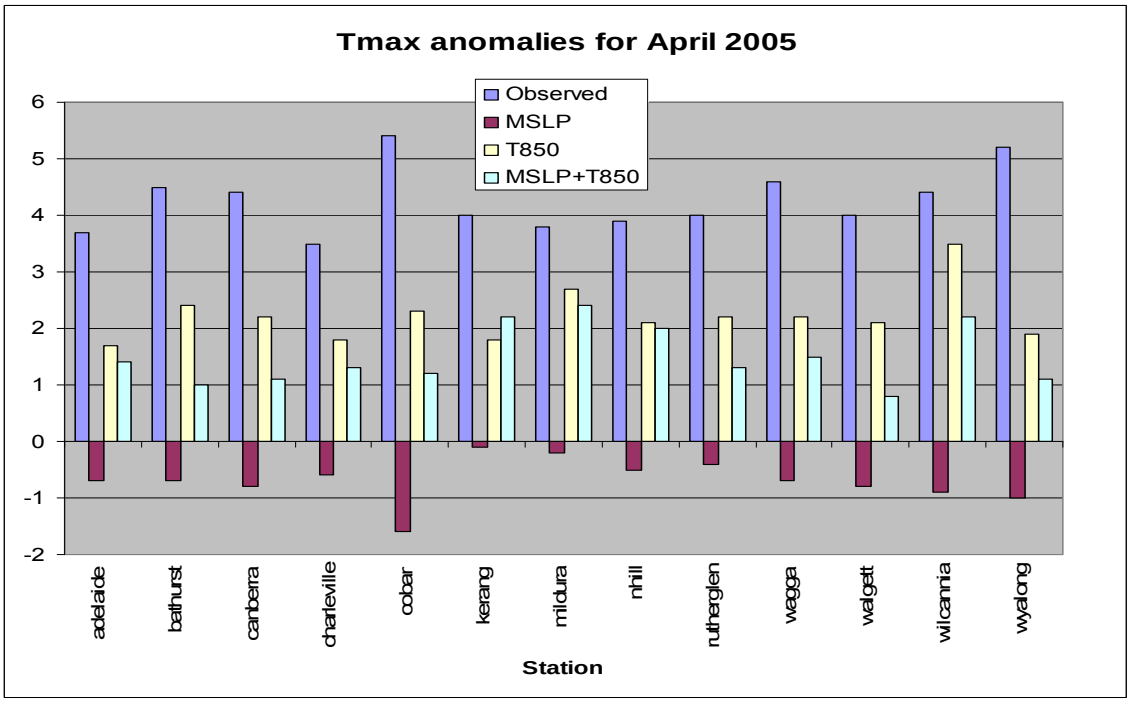

Fig. 17 *Mean maximum temperature anomalies for April 2005 observed and as simulated by downscaling model with MSLP, T_{850} and MSLP/T_{850} as predictors.*

We then applied the SDM in a cross-validated mode to try to reproduce the heat wave of April 2005. The T_{850} patterns reproduce about half of the observed hot anomaly in April 2005 across the MDB while MSLP reproduces very weak and generally negative anomalies (Fig. 17). When the two predictors are combined, the anomalies are in most cases smaller. The results show that the April 2005 heat wave cannot be accounted for by anomalous synoptic situations (i.e. it was not due to a series of anomalous meteorological situations). On the contrary, the warming of the troposphere appears critical and explains about half of the observed surface heat wave, thus clearly indicating that the observed April 2005 heat wave was not possible without on-going warming of the mid troposphere.

SUMMARY

- 60% of the total decline in SEA rainfall is due to the autumn decline. There are however regional contrasts to this. For example in the south of the SEACI domain, the decline is a combination of declines in autumn to early winter but in the north it is a combination of a summer to autumn decline. In the south, the decline started in the early 1990s but it is only apparent since 2000 in the north. The two areas can be broadly separated by the location of the Sub-Tropical Ridge (STR).
- The modes of variability generated in tropical oceans (ENSO and IOD) are unlikely to have contributed to the rainfall decline as, if anything, their influence on the local rainfall is rather small and has been diminishing during the last the two decades.
- In the south-western part of eastern Australia (SWEA), when the Southern Annular Mode (SAM) is in a positive phase this has a negative impact on rainfall during the six month period from May to October, which is when most of the total rainfall is encountered. In autumn as a whole, the SAM influence on rainfall in SEA is negligible, as the negative influence in May is cancelled out by the positive influence in summer extending to March.
- The SAM index has been trending upward over most of the second half of the 20th century. There is a positive trend in the 1980s and 1990s across summer and autumn but it does not translate into a rainfall decline. Arguably, the positive trend in SAM index extends to early winter (May to July) when the series is extended back in time to the 1960s and 1970s; this trend could have resulted in a rainfall decline of about 5% in those decades, but did not.
- The SAM-rainfall relationship is mostly captured by the local MSLP-rainfall relationship. The main control of MSLP over southern Australia is the intensity and location of the STR. The intensity of the STR has been trending upward since the 1970s and this can be translated into a rainfall decline of about 70% of the observed decline in autumn to early winter from March to July.
- The intensity of the STR also peaked in the 1940s at the time of the previous dry decade in SEA. During the 20th century the long-term evolution of the intensity of the STR follows the curve of the global temperature of the planet. This relationship indicates a high likelihood that the current rainfall deficit is linked to global warming, through the intensification of the STR.
- On the northern side of the STR, the rainfall relates well to a north-south MSLP gradient along the east coast called the Gayndah-Deniliquin Index (GDI). This index suggests a combination of long-term trends and decadal variability as the most likely explanation for the current rainfall deficit.
- Weather patterns diagnosed from MSLP do not explain the heat wave observed in April 2005, while the long term lower tropospheric warming trend appears as an important contribution. However, it does not appear to be the only explanation.

4 OPTIMISING AN ANALOGUE DOWNSCALING TECHNIQUE TO RELATE OBSERVED SURFACE CHANGES TO LARGE-SCALE PREDICTORS

4.1 Introduction

Following on the work done on describing the observed surface climate change (Chapter 2) and understanding the large-scale changes which explain the local changes (Chapters 2 & 3), the focus here is to set up a statistical downscaling technique to relate these large-scale changes to local variations of the climate across SEA. To do so, the Bureau of Meteorology's (BoM) existing SDM is expanded to include humidity variables (dew point temperature and pan evaporation) in addition to proven datasets (rainfall and daily temperature extremes). A series of large-scale predictors is tested and the spatial variation of skill across south-eastern Australia is assessed for all calendar seasons for the suitable stations data described earlier and using identified coherent climatic regions across SEA.

4.2 Expanding the existing downscaling model to humidity dataset

The BoM has developed a SDM using the idea of meteorological analogues (Timbal and McAvaney 2001). This is one example of a more general type of SDM based on weather classification methods in which predictands are chosen by matching previous (i.e. analogous situations) to the current weather-state. The method was originally designed for weather forecasting applications but was abandoned due to its limited success and lack of suitable analogues for systems with large degrees of freedom. The popularity of the method has recently increased with the availability of longer time-series datasets following the completion of the reanalysis project and the recognition that the size of the search space must be suitably restricted when identifying analogues. Even so, the analogue method still performs poorly when the pool of training observations is limited and/or the number of classifying predictors is large. The Bureau SDM was first developed for daily temperature extremes (T_{min} and T_{max}) across the Murray-Darling Basin (MDB) (Timbal and McAvaney 2001). It was then extended to rainfall occurrences (Timbal et al. 2003) and amount (Timbal 2004).

As part of this SEACI project, the BoM existing downscaling technique has being tested for new surface variables to complement previous work done on rainfall and temperature. These new surface variables are the most recent addition to the Bureau's High Quality (HQ) climatological networks. Dew point stations were homogenised (Lucas 2006) and are available in the HQ dataset from 1957 to 2003. 13 stations across the SEACI domain were considered. At each location, daily maximum, daily minimum, and 9am dew point temperatures are available, but the optimisation of the SDM was applied only to daily extreme dew point temperature. Pan evaporation HQ stations have been also been assembled across Australia (Jovanovic et al. 2008) from 1975 to 2003. 24 stations are scattered across the SEACI domain. The Bureau pan-evaporation HQ dataset is a monthly dataset; the quality control was extended to daily values across the SEACI region, using monthly corrections for non-homogeneities at stations which required such correction (described in Chapter 2). The application of a SDM to these moisture

variables is a very novel research area as there are currently very few examples in the literature of fitting a statistical downscaling model to surface moisture variables (Huth 2005 for a case study for dew point across the Czech Republic) and none as extensive as our study.

Overall, applying a single technique across a large region such as the SEACI domain and across a large range of predictands is a very large undertaking. This extensive work (a total of 72 individual SDMs were optimised: 3 regions * 4 seasons * 6 predictands) was possible due to the relative simplicity of the analogue downscaling method chosen. Despite its simplicity, this method has been shown to compare well with more advanced techniques (Zorita and von Storch 1999). The simplicity, flexibility and robustness of the technique enabled us to use a single technique across a range of variables and several climatic regions.

4.3 Choice of coherent climatic regions

In order to apply the BoM SDM to the SEACI domain, surface observations were gathered into three distinct *climate entities* (Fig. 17), approximating the regions identified previously by Drosdowsky (1993):

(1) the South-West of Eastern Australia (SWEA): southwest of a line roughly from Melbourne to the south of the Flinders' ranges and following the end of the Great Dividing Range (GDR) over Western Victoria;

(2) the southern half of the Murray-Darling Basin (SMD): south of 30ºS in the north, limited in the west by SWEA and in the east by the GDR; and

(3) the South-East Coast (SEC): a coastal band east of the GDR from Wilson's Promontory in Victoria in the south all the way along the New South Wales coast up to the Hunter valley in the north.

That methodology was chosen to be consistent with the development of the BoM SDM to obtain an Australian wide downscaling tool and hence differs from the previous regions (Chapter 2) which were based on the Drosdowsky and Chambers (2001) rotated EOFs.

The number of surface predictands available in each climatic region is summarised in Table 9. Although only a small part of the Australian continent is covered by these three climatic regions, together they cover a large proportion of the number of HQ observation sites across Australia (between 30% for dew point temperature and 54% for rainfall. This is because population centres are scattered across the region, which has led to a relatively dense network of observations especially for rainfall (Table 9).

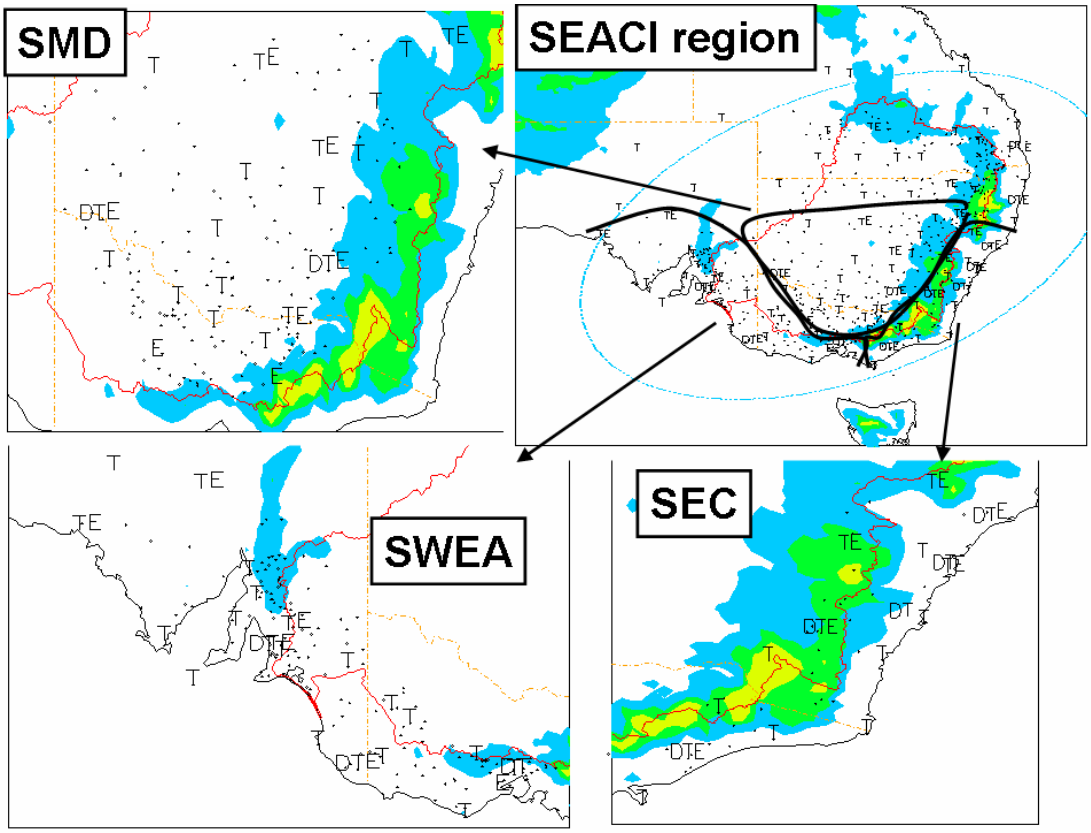

Fig. 18 *Location of the station data chosen for the SEACI program (upper right map) and for the three climatic entities used to optimise the statistical downscaling model: the Southern Murray-Darling Basin (SMD), the South-West of Eastern Australia (SWEA) and the South-East Coast (SEC). Different symbols are used for different surface predictands: D for dewpoint temperature, E for pan-Evaporation, T for temperature and the small points are rainfall stations.*

Table 9 *Number of stations considered in each climatic region for the four types of predictand*

Predictands		SWEA	SMD	SEC
Temperature (T_{max} & T_{min})		22	18	16
Rainfall	**HQ network**	31	24	11
	additional stations	133	137	30
Pan-Evaporation		6	8	6
Dew point (dT_{max} & dT_{min})		3	2	5

A large number of stations were added to the HQ network for rainfall (separate entry in Table 9) while for temperature, only a handful number were added (included with the HQ number in Table 9). Details were provided in Chapter 2. Overall, not all the SEACI relevant stations identified in Chapter 2 (and shown in the top right of Fig. 18) are included in one of the three regions as the original stations cover a wider geographical area than the three climatic entities (inserts in Fig. 18).

4.4 Optimization of the predictors

The choice of the optimum combination of predictors constitutes the first step in the optimisation of the individual SDMs. The predictors considered were chosen on the basis of previous experience while developing the BoM SDM (Timbal and McAvaney 2001; Timbal et al. 2003; Timbal 2004), and evidence in the literature from other studies in similar areas. The optimum combination of predictors varies across regions, seasons and predictands (Table 10).

Table 10 *Optimum combination of predictors for each calendar season and the six predictands in three regions: SWEA, SEC and SMD. The predictors are defined as follows: MSLP is the Mean Sea Level Pressure; T_{max} and T_{min} are the surface min and max temperature; PRCP is the total rainfall; Q is the specific humidity; R is the relative humidity; T is the temperature; U and V are the zonal and meridional wind components; and subscript numbers indicate the atmospheric level for the variable in hPa.*

Variable	Season	SWEA	SEC	SMDB
Maximum Temperature **T_{max}**	Summer	MSLP & T_{850}	MSLP & T_{max}	MSLP & T_{max}
	Autumn	MSLP & T_{max}	MSLP & T_{max}	MSLP & T_{max}
	Winter	MSLP & T_{850} & T_{max} & U_{850}	MSLP & T_{max}	MSLP & T_{850} & T_{max} & U_{850}
	Spring	MSLP & T_{850}	MSLP & T_{850} & T_{max} & U_{850}	MSLP & T_{850} & U_{850}
Minimum Temperature **T_{min}**	Summer	MSLP & T_{850}	MSLP & T_{850} & Q_{850}	T_{850} & Q_{850}
	Autumn	MSLP & T_{850} & Q_{850}	MSLP & T_{850} & Q_{850}	T_{850} & Q_{850}
	Winter	MSLP & T_{850} & Q_{850}	MSLP & T_{850} & T_{min} & U_{850}	MSLP & T_{850} & Q_{850}
	Spring	MSLP & T_{850} & Q_{850}	MSLP & T_{850} & Q_{850}	MSLP & T_{850} & Q_{850}
Rainfall **PRCP**	Summer	MSLP & PRCP & T_{850}	MSLP & T_{max} & Q_{850} & U_{850}	MSLP & PRCP & V_{850}
	Autumn	MSLP & T_{max} & Q_{850} & U_{850}	MSLP & PRCP & Q_{850} & U_{850}	MSLP & PRCP & V_{850}
	Winter	MSLP & PRCP & V_{850}	MSLP & PRCP & U_{850}	MSLP & PRCP & V_{850}
	Spring	MSLP & PRCP	MSLP & PRCP & Q_{850} & U_{850}	MSLP & PRCP & V_{850}
Maximum dew-point Temperature **dT_{max}**	Summer	MSLP & Q_{925}	MSLP & Q_{925} & T_{min}	MSLP & Q_{850} & T_{min} & V_{850}
	Autumn	MSLP & Q_{925} & T_{min} & V_{850}	MSLP & Q_{925} & T_{min}	MSLP & Q_{850} & T_{min} & V_{850}
	Winter	MSLP & Q_{925} & T_{min}	MSLP & Q_{925} & T_{min}	T_{min}
	Spring	MSLP & Q_{925} & T_{min}	MSLP & Q_{925} & T_{min}	MSLP & Q_{850}
Minimum dew-point Temperature **dT_{min}**	Summer	MSLP & Q_{925} & T_{min}	MSLP & Q_{925} & T_{min}	MSLP & Q_{850} & T_{850}
	Autumn	MSLP & Q_{925} & T_{min}	MSLP & Q_{925} & T_{min}	MSLP & Q_{850} & T_{min} & U_{850}
	Winter	MSLP & Q_{925} & T_{min}	MSLP & Q_{925} & T_{min}	MSLP & Q_{850} & T_{min} & V_{850}
	Spring	MSLP & Q_{925} & T_{min}	MSLP & Q_{925} & T_{min}	MSLP & Q_{850} & T_{850}
Pan-Evaporation **P-Evap**	Summer	T_{max} & R_{925}	T_{max} & R_{925}	T_{max} & R_{850}
	Autumn	T_{max} & R_{925}	T_{max} & R_{925}	T_{max} & R_{850}
	Winter	T_{max} & R_{925}	MSLP & T_{max} & R_{925}	T_{max} & R_{925}
	Spring	T_{max} & R_{925}	T_{max} & R_{925} & U_{850}	T_{max} & R_{850}

The optimum number of predictors is often three, apart from pan evaporation where most frequently only two predictors are used, and rainfall where four predictors are often required. The need for a larger number of predictors for rainfall shows that it is a difficult predictand to capture from large-scale analogues. Some general patterns emerge from the optimum combinations of predictors:

- MSLP is the most frequently chosen predictor. It is used for all individual SDMs in the case of rainfall, T_{max} and dT_{min} but is picked up far less often for pan evaporation. This feature suggests that MSLP is a critical predictor for a synoptically-driven techniques such as the analogue approach used here.
- Thermal predictors are very important, especially for T_{max} and T_{min}. In general, T_{850} is the most important thermal predictor, although T_{min} is more important for dT_{min} and dT_{max}; thermal predictors rarely matter for rainfall.
- Moisture variables are also important predictors across all predictands with the notable exception of T_{max}. Specific humidity is almost always picked up apart to predict pan evaporation for which relative humidity leads to more skill. Model rainfall is often part of the optimised predictor's combination for downscaling rainfall.
- Some measure of the air flow (either the zonal or meridional component of the wind) is often added to the optimised combination. It is an additional predictor to the de-facto combination of synoptic-thermal-moisture predictors. Airflow is most useful for rainfall and then T_{max}, and least useful for dew-point temperature and pan evaporation. The zonal (east-west) component is more frequently used than the meridional (north-south) component.

The second step in the optimisation of individual SDMs was to set up some critical parameters of the analogue model. The SDM includes a large number of tuneable parameters; however previous studies have shown that only three parameters are critical and therefore only these three where systematically explored:

1. The size of the geographical domain used for the predictors (latitude and longitude): in general two domain sizes were tested with the sizes being region dependent,
2. The calendar window from which analogues are found. Three periods were tested: 15, 30 and 60 days prior to or after the date for which an analogue is searched for.
3. The way the daily anomalies are calculated: using either three monthly means or a single seasonal average.

Once these two steps were completed, the optimised SDMs were validated and their skills were systematically evaluated.

4.5 Skill of the SDM

The skill of the SDMs was evaluated using a fully cross-validated approach to avoid spurious or artificial skill. The model was first optimised on one half of the existing dataset and then applied to the other half. The length of these halves varies for each predictand according to the length of the available record. When applied to the validation part of the dataset, analogues are identified in the development half of the dataset to ensure full cross-validation. Hence, if the climate has recorded a mean shift during the two periods, the method has to be able to reproduce that shift, thus adding confidence in the ability of the technique to reproduce non-stationarity in the climate system now and in the future. Simulating change in the historical record is useful for detection and attribution while modelling future changes provides regional station level projections. In this chapter, the evaluation of the SDMs focused on the ability of the technique to reproduce the main characteristics of the observed series and whether it is

doing it for the right reasons. The ability of the method to reproduce observed changes is described in the next chapter.

A range of metrics was used to evaluate the SDMs. First, the ability of the technique to reproduce the observed probability distribution functions (PDFs) was evaluated by looking at the first two moments of the PDFs: the mean and the variance. This assesses the ability of the technique to reproduce the observed shape of the PDFs as defined by the first two moments of the series. It is also important to ensure that the technique is skilful in reproducing day-to-day variability driven by large-scale synoptic changes. This is because a random choice of analogue would reproduce perfectly the observed mean and variance but have no skill in reproducing the sequence of the variability in time. To check this, the Pearson correlation coefficients between daily observed and reconstructed series was calculated for each region, each season and for each predictand. An average across all observations available in each region is provided. The Root-Mean-Square error (RMSE) was also used to complement the evaluation of the skill of the SDMs to reproduce the amplitude of the day-to-day variability.

4.5.1 Temperature

In the case of daily extreme temperature, the development period is 1958 to 1982 and the validation period is 1983 to 2006 (i.e. analogues to reproduce 1983 to 2006 are picked up from 1958 to 1982, a notably cooler period in many instances). The reproduction of the mean values for both predictands (Fig. 19) is very accurate. In each graph, points correspond to a single location for a single season with the observed mean value on the x-axis and the reconstructed mean along the y-axis. The number of points in each graph is equal to the total number of stations in one of the three climate regions times four seasons (224 in the case of temperature). Results for the mean are close to perfect match (especially for T_{max}). Perfect agreement arises if the modelled and observed values are equal and therefore fall on the diagonal shown. Deviations from the diagonal indicate errors. There is no evidence that the SDMs have more difficulty at reproducing mean observed values at either hand of the spectrum (large or small values).

Results are also shown for the reproduction of the standard deviation (Fig. 19). There is a tendency to underestimate the observed variance as points are aligned below the diagonal for most cases. This is particularly true in summer for T_{max} but obvious across all seasons for T_{min}. Averaged across all stations the reduction of variance ranges from 11.8% in winter to 0% in spring for T_{max} and 11.8% in winter and 5.3% in summer for T_{min}.

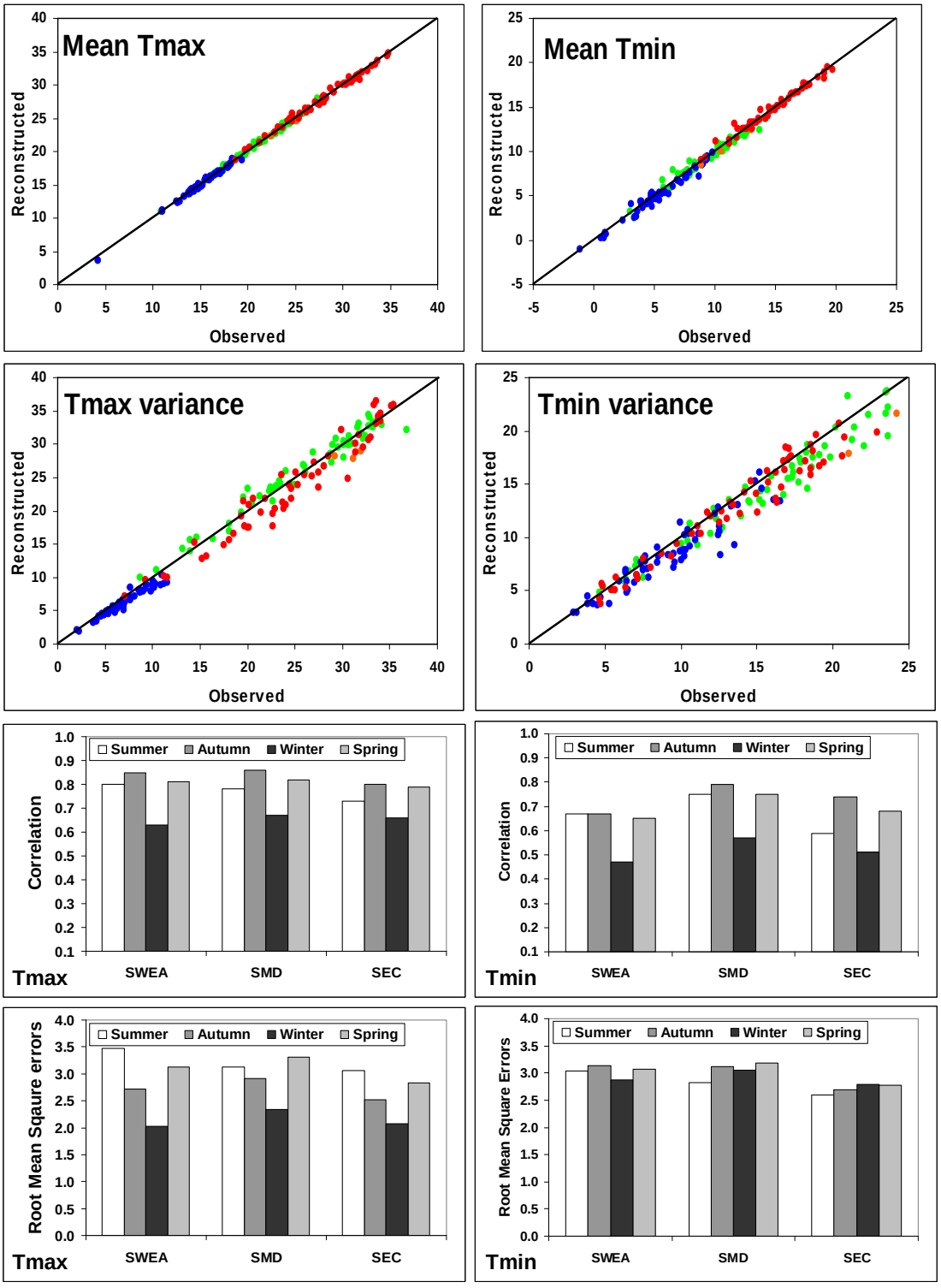

Fig. 19 *Scatter plot of the reconstructed versus observed mean (top row) and variance (second row) and correlations (third row) and RMSEs (fourth row) between the two series for T_{max} (left) and T_{min} (right). On the scatter plots, there is one point per station and per season, the colour-code refers to season: winter (blue), spring (green), summer (red) and autumn (orange). The diagonal is the line of perfect fit. Correlations and RMSEs are averaged across all stations per region (name on X-axis) and specified by season (coloured bars). Units for mean, variance and RMSE are °C.*

This variance underestimation is relatively small with the analogue approach (which does not require any linear assumption) compared to many other techniques (especially linear techniques). Nevertheless, it remains an issue for all statistical downscaling techniques (von Storch 1999). For temperature, as daily values are not far from being normally distributed, therefore the underestimation of the variance does not have a flow-on effect on the reproduction of the mean (which is unbiased as noted earlier).

The ability of the SDM to skilfully reproduce day-to-day variability (i.e. the ability to reproduce the right PDFs for the right reasons) appears very strong based on correlations for both T_{max} and T_{min}. There is a marked seasonal cycle in correlation coefficients: lower values are observed in winter and highest values during autumn and spring. However in most instances, in particular for T_{max}, lowest RMSEs occur in winter. Therefore the lower correlation does not imply less skill but rather indicates a season where day-to-day variability is smaller and hence harder to capture. In autumn and spring the high correlation values are partly due to the large day-to-day variability that occurs in these transient seasons. In the case of T_{min}, the additional skill as measured by correlation is not obvious as RMSEs are fairly similar across all seasons and hence the lower correlations in winter suggest that the model is less skilful. Overall, no particular region stands out as a climatic entity where the SDM skill in reproducing day-to-day variability is consistently lower or higher across all seasons. This result vindicates the use of the model over the entire SEA, where the climate is, by and large, driven by synoptic disturbances.

4.5.2 Rainfall

Similar graphs were generated for rainfall (Fig. 20). The development period is 1958 to 1982 and the validation period is 1983 to 2006. The reproduction of the first two moments of the series (mean and variance) is less successful than for temperature (left plots in the first two rows of Fig. 19). The underestimation of the variance is much larger, ranging from 27% in autumn to 45% in summer. The consequence of the reduction of variance, in the case of rainfall, can be seen on the reproduction of the mean: points are located further from the diagonal. This fact indicates a bias toward drier values in the reconstructed series. In the case of rainfall, the reproduction of the mean depends on the ability of the technique to reproduce the observed variance, as rainfall is not normally distributed. For this reason, a correction factor to adjust the reconstructed rainfall series (to enhance the variance and improve the reproduction of the mean) was introduced in earlier applications of the analogue approach to rainfall series in Western Australia (Timbal et al. 2006).

The rationale for the correction applied is that the analogue reconstructed rainfall is affected by the size of the pool of analogues which becomes smaller in the case of rare large rainfall events. Therefore, the error in finding the best matching analogue increases and the chances are that the best analogue found would describe more frequent but less intense rainfall events, thus underestimating the rainfall in the reconstructed series. It is assumed that the size of the pool depends on the ratio of rain days over dry days and that is valid across the range of climates encountered in SEA as was the case in WA.

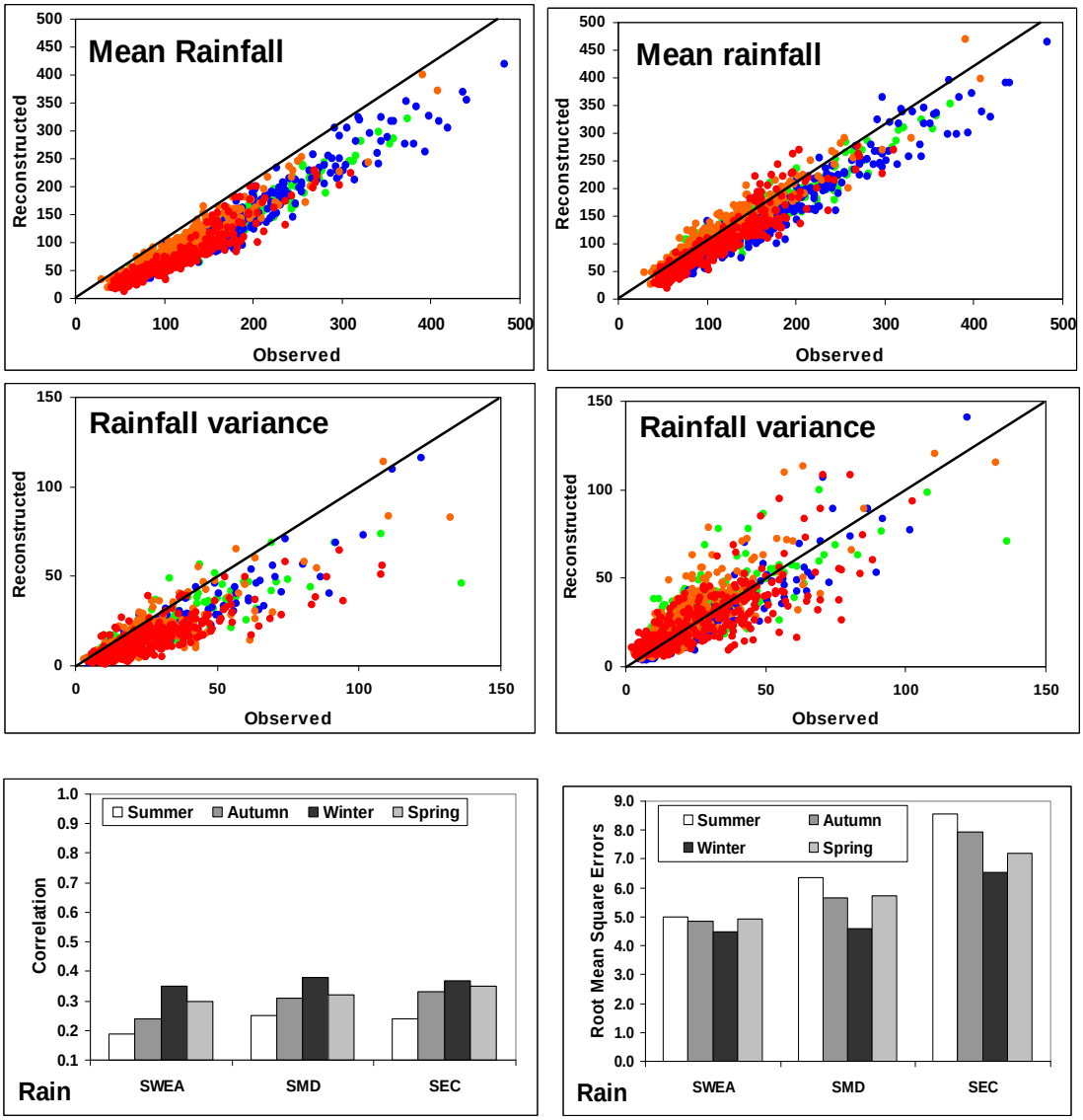

Fig. 20 *As per Fig. 19 but for rainfall. The additional two scatter plots of the reconstructed versus observed mean and variance (in the right column) are for rainfall with an inflation factor applied to the reconstructed series (see main text for details). Units are mm.*

It was decided that the very simple factor as used in Western Australia should be applied without further adjustment to limit some of the danger linked to artificially inflating the variance when using downscaling techniques (von Storch 1999). The following single factor was used:

$$C_{factor} = 1. + a \times \left[\frac{N_{dry}}{N_{wet}} \right]^{b} \quad \text{And} \quad C_{factor} \leq c$$

Where N_{dry} and N_{wet} are the numbers of dry and wet (> 0.3mm) days observed for the season at an individual location and a=0.1, b=1 and c=1.5. The numbers of dry and wet days are station and season dependent. They are calculated on the basis of the available observations from which analogues are drawn and are therefore independent of the series being reconstructed.

These ratios are equally applicable when developing the downscaling model (and evaluating the impact of the inflation factor) or when downscaling climate simulations. The constant a, b and c are not station or season dependent and where not particularly tuned for SEA but used based on the prior optimisation for the WA study.

The impact of the inflation factor is clear (right plots in the first two rows of Fig. 19). It has dramatically reduced the variance bias and leads to an un-biased reproduction of the mean (as was the case for temperature) and an un-biased reproduction of the variance, bettering the ability of the model to reproduce temperature variability. However, the average error of the reconstructed versus observed series is unchanged from the non-inflated series and remains larger than for temperature.

For rainfall, correlations between observations and reconstructions are far lower than for temperature. However, as a very large sample considered (about 2000 days) all these correlations are significant at the 95% level or higher. Correlations peak in winter (up to 0.3 to 0.4) and are particularly low for summer and autumn in the case of SWEA. These low correlations are accompanied by high RMSEs. The largest errors are seen in summer and the smallest in winter. These results confirm that the SDMs are more skilful for rainfall during winter.

4.5.3 Dew-point temperature

In this sub-section, the skill of the model is evaluated for the newly formed high-quality dataset, starting with dew-point temperature (Lucas 2006): daily maximum (dT_{max}) and daily minimum (dT_{min}). In the case of daily extreme dew-point temperature, the development period is 1958 to 1982 and the validation period is 1983 to 2003. Unfortunately, the high quality dataset only extends to 2003 at this stage.

Results (Fig. 21) are very similar to results for temperature. The SDMs are able to reproduce the mean of the observed series very accurately (with slightly larger errors for dT_{min}). An underestimation of the variance is again visible, ranging between 11.6% in summer and 4.4% in autumn for dT_{max}, and between 16.7% in winter and 7.7% in spring for dT_{min}. As for temperature, daily values of dew-point temperature are not far from being normally distributed, and hence the underestimation of the variance does not cause a problem with reproducing the mean.

Correlations between reconstructed and daily series for dT_{max} have a lot in common with results for temperature, albeit with correlation coefficients being lower overall. Lowest correlation coefficients occur during winter. However RMSEs are low at this time. Highest correlation coefficients occur during autumn and spring and largest RMSEs tend to be in summer. Results for dT_{min} are very similar across all seasons and regions. The exception is SMD during the spring and summer when RMSEs are much larger and correlations coefficients are rather low, suggesting that the model is less skilful during the warmer seasons in this region.

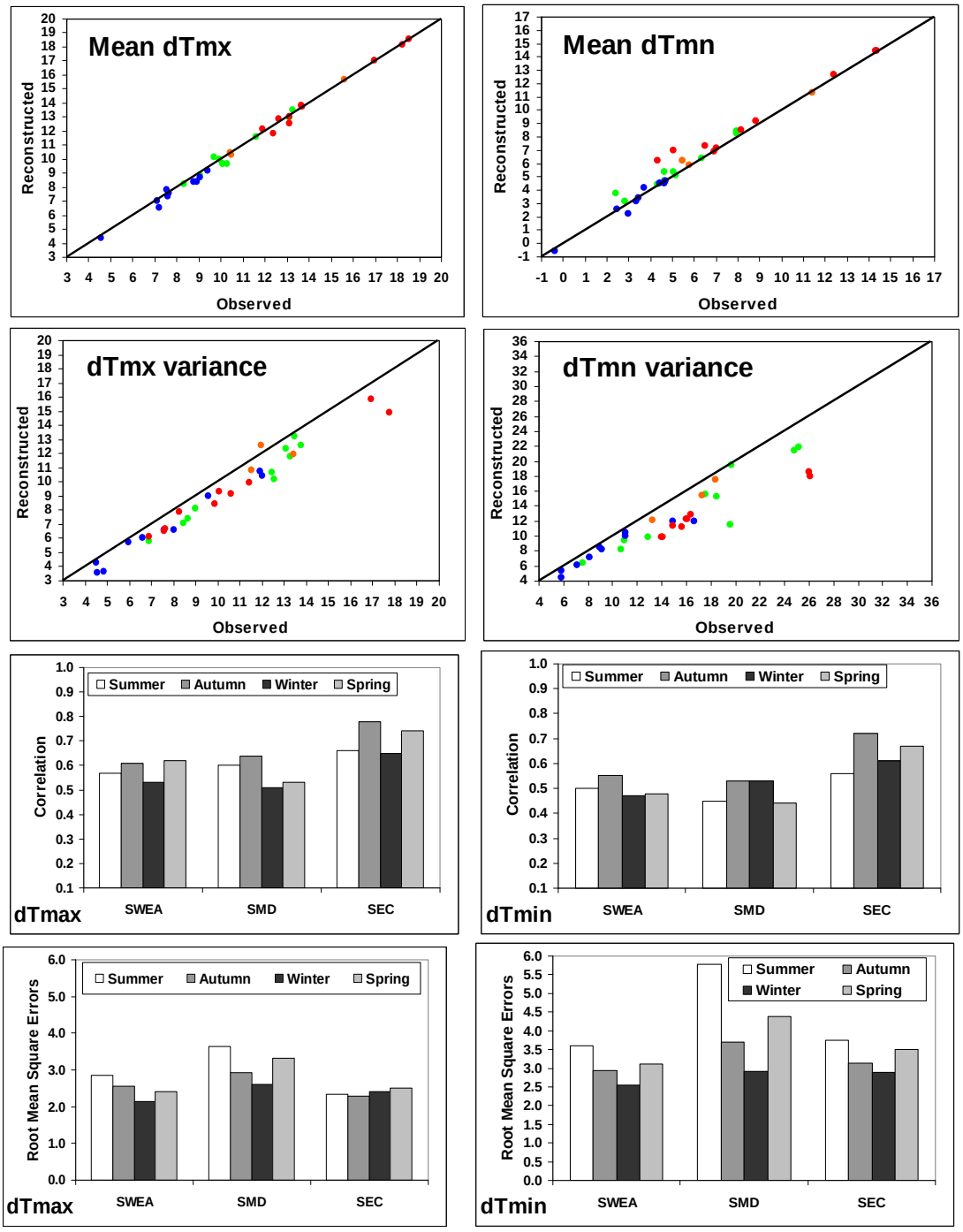

Fig. 21 *As per Fig. 19 but for daily maximum dew point temperature (left) and daily minimum dew point temperature (right). Units for mean, variance and RMSE are ºC.*

4.5.4 Pan-evaporation

The pan-evaporation high quality dataset spans the shorter period from 1975 to 2003 (Jovanovic et al. 2008). The development period is chosen to be 1975 to 1988 and the validation period is 1989 to 2003. Again the high quality dataset has not been updated past that point.

As for the other variables, the mean of the reconstructed series is very accurate although some errors of up to 1 mm day^{-1} are noticeable during spring and summer. Errors in the variance can be quite large, up to 3 mm day^{-1} in some instances, but there is a slightly smaller reduction in the variance. The mean variance bias ranges between 13.7% in winter and 1.6% in spring (Fig. 22).

The skill of the SDMs in reproducing day-to-day variability varies a lot from one season to another according to the correlation: it is high for the transition seasons and low in both winter (especially in SMD and SWEA) and summer (especially in SEC). However the very small RMSEs suggest that the low correlations in winter are partly due to very small day-to-day variability. In contrast, low correlation coefficients and high RMSEs in summer suggest that the SDMs have less skill in this season.

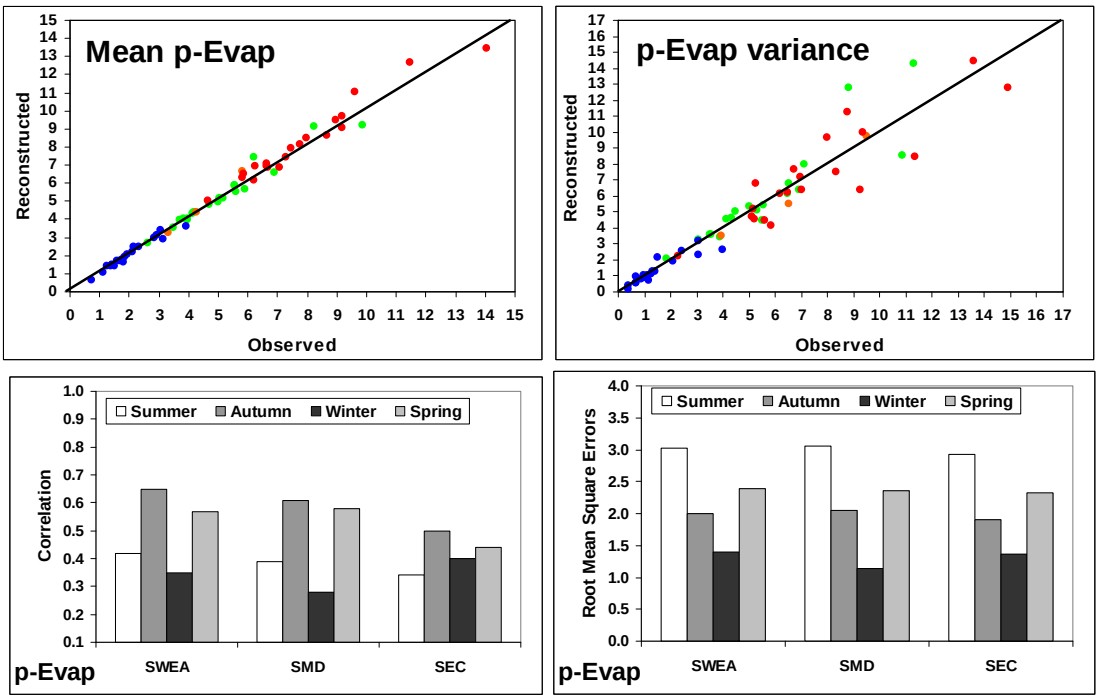

Fig. 22 As per Fig. 19 but for pan-evaporation. Units for mean, variance and RMSE are mm day^{-1}.

4.6 Conclusions

The evaluation of the skill of the SDMs shows that:

- The results are fairly consistent across the three regions, thus confirming that the analogue approach is equally suitable across mid-latitude temperate climate;
- The reproduction of the mean of the observed series (in a fully cross-validated sense) is very accurate with the exception of rainfall;
- For all variables, the reconstructed series under-estimates the observed variance. This underestimation varies from one predictand to another and is largest for rainfall;
- As rainfall tends to have a daily PDF which departs from the normal distribution and is usually skewed toward large rainfall events, the reduced variance leads to a dry bias. This dry bias can be reduced with a very simple and robust inflation factor;
- The variance reduction issues and subsequent dry bias can be addressed using a very simple (i.e. a single parametric coefficient applicable to all stations and all seasons) and robust (i.e. it only depends on the pool of observed rainfall occurrences and hence is applicable to the downscaling of climate models) inflation factor;
- Greatest skill tends to be achieved for most variables during the "transition seasons" autumn and spring;
- Correlations between observed and reconstructed data in winter are often low but this is often because the day-to-day variability in winter is low rather than because the model is less skilful; and
- All variables apart from daily temperature extremes are less accurately reproduced by the SDM (low correlation and high RMSEs) in summer.

SUMMARY

- This project has seen the development and validation of a downscaling method based on the idea of meteorological analogues for the entire SEACI region and for all existing high quality climate surface data: rainfall, temperature, dew-point temperature and pan-evaporation.

- The SEACI domain was divided into three climate entities: the Southern part of the Murray-Darling basin; the South-East Coast (east of the SMD, on the coastal side of the Great Dividing Range); and the South-West coast of Eastern Australia (west of the SMD). Rainfall variability tends to be coherent within each subregion.

- Individual SDMs were optimised for each region, each calendar season and each predictand: a total of 72 SDMs (3 regions * 4 seasons * 6 predictands) were created.

- The optimisation consisted of two steps: the selection of the best combination of predictors (step 1) and then setting up other critical parameters of the SDM (step 2).

- The skill of the SDMs is similar across the three regions, the four seasons and the six predictands. The results confirm that the analogue approach is a suitable downscaling method for mid-latitude temperate climate.

- The ability of the SDMs to reproduce the observed PDFs of the surface predictands was assessed by checking mean and variance of the station data. The mean of the observed series is very well reproduced with the exception of rainfall. The reconstructed series tend to under-estimate the observed variance. This underestimation varies from one predictand to another and is largest for rainfall.

- In the case of rainfall, because the daily PDFs are not near normally distributed the reduced variance leads to a dry bias which can be reduced through use of a very simple and robust inflation factor.

- The skill of the SDMs was assessed by looking at their ability to reproduce day-to-day variability. The best performance for most variables occurs during the "transition seasons" autumn and spring. Correlations in winter are often low but with low RMSEs (i.e. not less skill). In contrast, for all variables except daily temperature extremes, the model tends to have less skill (low correlation and high RMSEs) in summer.

5 ABILITY OF THE STATISTICAL DOWNSCALING TECHNIQUE TO REPRODUCE OBSERVED CHANGES

5.1 Introduction

Having been optimised (described in Chapter 4), the BoM SDM is used to study the relationship between observed local changes and large-scale changes during the 2nd half of the 20th century. In particular, the individual role of the predictors selected earlier in explaining the observed climatic trends (warming trend and drying trend) of the last decade is to be investigated. The final analysis in this chapter is critical in ensuring that the SDM is applicable to climate model simulations of the 20th century (i.e. is likely to increase the regional climate change signal by relating regional changes to large-scale changes) in order to conduct attribution studies. To do so, the optimised SDM is applied to the NNR from 1958 to 2006 in order to investigate the large-scale predictors which relate to the observed changes. The technique is applied separately to rainfall, daily temperature extreme (max and min) and humidity datasets (dew point temperature max and min and pan-evaporation). The seasonality of the changes is investigated with a focus on the autumn to early winter rainfall decline. The SEACI relevant datasets assembled earlier are used and separated into sub-regions according to the climate entities defined in previous chapter.

5.2 Update on the methodology and preliminary comments

The original project scope was broadened and some additional analyses were performed:

- Following on from the evaluation of the performance of the individual SDMs in 3 SEACI sub domains (Chapter 4), the objective was to go one step further and analyse the ability of the SDMs to capture observed long-term trends. This validation is important in ensuring that the large-scale predictors are capturing the forcing that explains local trends. It is a pre-requisite step before applying the technique to simulations of the 20th century to investigate the possible attribution of observed trends to external forcings (Chapter 6).

- Linear trends were fitted to observed data and compared with similar trends from reconstructed series based on the optimised SDMs applied to the entire length of the available record (from 1958 to 2006) whenever possible. However, due to data limitations, trends for pan-evaporation are calculated from 1975 to 2003 and from 1958 to 2003 for dew point temperature. As discussed earlier (Chapter 2), the technique underestimates day to day variability with a flow-on effect on the ability to reproduce inter-annual variability which, in turn, affects linear trends. This shortcoming is dealt with by using “normalised” trends: linear trends calculated at any location for the analogue reconstructed series are divided by the percentage of the inter-annual variability observed at the local station captured by the SDMs. In this report, normalised trends are discussed unless otherwise stated.

- The focus of this chapter has been on the observed rainfall decline. Results have been restricted to two of the three regions for which the BoM SDM was optimised for in Chapter 4: SWEA and SMD. The third region (SEC) was not used principally because of earlier results showing that ongoing trends, in particular for rainfall, are different between the

eastern coastal eastern Australia and the inland areas (Chapter 3 and Rakich et al. 2008). SMD and SWEA cover most of the SEACI region (apart from eastern Gippsland) and completely encompass the area of significant rainfall decline across SEA (Murphy and Timbal 2008).

- The purpose of a SDM is to provide local information. The usefulness of such a method greatly depends on the spatial coverage of available observations. The level of detail contained in the report reflects this and depends on the number of stations available for each variable: 324 rainfall stations were used and the ability of the technique to reproduce local rainfall trends is reported in greater detail; 41 temperature stations were used, which enables us to evaluate of spatial structures; for pan-evaporation (14 stations) and dew-point temperature (5 stations) only regional averages are discussed.

- Beyond the ability of the technique to reproduce observed trends, a further validation was done by splitting the record into earlier (wetter and cooler) and later (dryer and warmer) periods. This fully cross-validated test, although not essential to applying the technique to simulation of the 20th century, is critical before the technique can be used for future projections.

- The SDM produces daily values and hence full PDFs can be calculated. This provides opportunity to investigate extreme values. Recently, late and damaging frosts in SEA have raised widespread interest in frost occurrences. This perceived increase in frost occurrences is somewhat contradictory to the ongoing global warming. Although not part of the original project, it was decided to analyse our results further to evaluate the ability of the technique to reproduce local frost occurrences and investigate these observed frost trends in the face of on-going GW.

5.3 Reproduction of drying trends across SEA

The ability of the SDM to reproduce observed rainfall is first assessed from a regional perspective by looking at seasonal averages across all stations (Table 11) in the two climate entities: the South-West of Eastern Australia (SWEA) and the Southern Murray Darling Basin (SMD). The largest signal, the autumn rainfall decline, is well reproduced (80% in SWEA and 60% in SMD using normalised trends and 100% in SWEA and 75% in SMD without normalisation). It is worth noting that the normalisation of the trends does not improve the results. This indicates that the inflation factor used for rainfall to reduce the underestimation of variance (Timbal et al. 2008; 2009) is effective and there is no additional gain in normalising trends.

Table 11 *Summary statistics for each calendar season of the rainfall linear trends computed from 1958 to 2006 and averaged across all stations in two regions (SMD and SWEA): observed (left two columns), reproduced by the analogue models (columns 3 and 4) and then normalised by the*

amount of interannual variability reproduced by the analogue model (columns 6 and 7). The spatial correlations across the 324 stations (SMD and SWEA combined) are shown in columns 5 and 8 (bold values are statistically significant at the 95% level). Trends are in mm day^{-1} per century.

mm/day^{-1} per century	Observation		Analogue			Analogue normalised		
	SMD	SWEA	SMD	SWEA	r	SMD	SWEA	r
Summer	-0.30	0.13	-0.55	0.60	**0.55**	-0.42	0.58	**0.57**
Autumn	-1.13	-1.06	-0.80	-1.03	**0.17**	-0.69	-0.85	**0.37**
Winter	0.33	0.28	0.38	0.43	**0.37**	0.33	0.63	**0.40**
Spring	-0.20	0.02	-0.18	0.25	**0.21**	-0.22	0.36	**0.25**

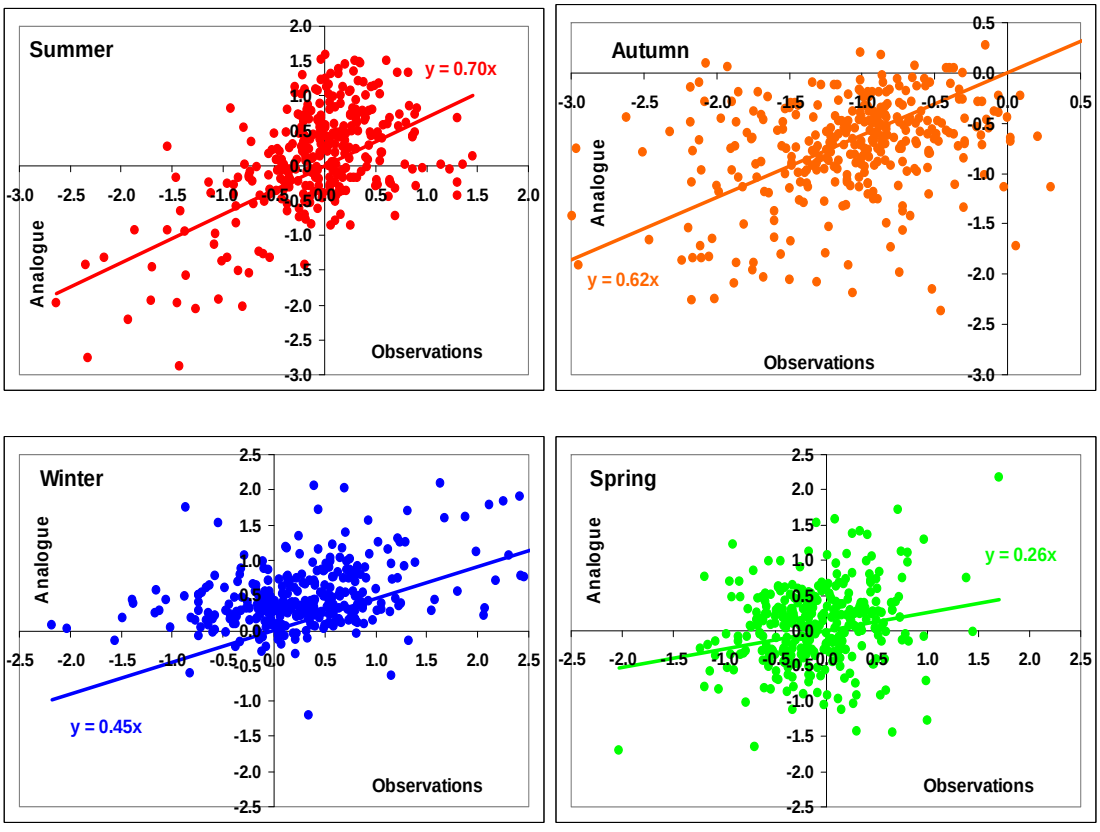

Fig. 23 *Reproduction of the observed rainfall trends (in mm day^{-1} per century) using 324 rainfall stations across the SEACI regions SMD and SWEA (a season per plot). Each point has for the x-coordinate the observed linear trends computed between 1958 and 2006 and the normalised trend for the analogue reconstructed series as y-coordinate. Linear best fits are fitted through the origin (0, 0) and their slopes are shown on each graph.*

The SDM captures both the negative trends in summer and spring in SMD and the positive trends in the SWEA during the same season. Local trends are reproduced with some skill:

spatial correlation between linear trends calculated on the observed and reconstructed series, after normalisation, varies between 0.25 and 0.57 which are significant at the 95% level. Scatter diagrams showing observed vs. analogue linear trends at the 324 SEACI stations are presented in Fig. 23. The slope of the line of best fit is high in summer (0.70) and autumn (0.62) (a value of 1 would be a perfect match), but low in winter (0.45) and spring (0.26) when most analogue reconstructed series show modest positive rainfall trends between 0 and 1 mm day^{-1}/century, while the trends in the observations vary greatly between -1.5 and 1.5 mm day^{-1}/century.

The analysis of SDMs using a single predictor (Fig. 24) shows that in 7 out of 8 cases, MSLP alone produces linear trends which encompass the observed trends based on six SDMs sampling the uncertainties of the statistical linkage. The mean of the six SDMs usually provides a trend of the right sign and of a magnitude comparable to the observations.

Linear trends produced by the optimised SDMs are not a simple addition of the linear trends produced by individual predictors due to existing relationships between large-scale atmospheric variables. But, providing that the large-scale forcings are complementary (such as a combination of synoptic, moisture and thermal variables), then the optimised model will combine the influence of each individual predictor.

In this light, it is worth noting that moisture variables (principally Q_{850}) exhibit small linear trends of the right sign which, combined with the MSLP influence, are likely to provide a better match to the observations: e.g. the negative trends in autumn are likely to enhance the negative trends produced with MSLP, and the small positive trends in summer are likely to reduce the negative trend produced by the synoptic (captured by MSLP) changes.

In some instances, wind components are used in the optimum combination of predictors (predictors used in optimised SDMs are highlighted by red boxes in Fig. 24) and generate trends which are likely to provide a better match to the observations.

The ability to reproduce observed trends is one component of the statistics used to evaluate and optimise the SDM. It is worth emphasising that it is not the most important aspect evaluated: the optimised combination of predictors relies mostly on analysis of the day-to-day skill and the ability to reproduce the main moment of the series (Timbal et al. 2009a; 2009b). The choice of optimised combinations of predictors was not influenced by this analysis: i.e. the best combination of predictors was not chosen to ensure the best possible reproduction of the observed trends. This is an independent test whose only purpose is to shed light on the large-scale changes which help explain ongoing trends.

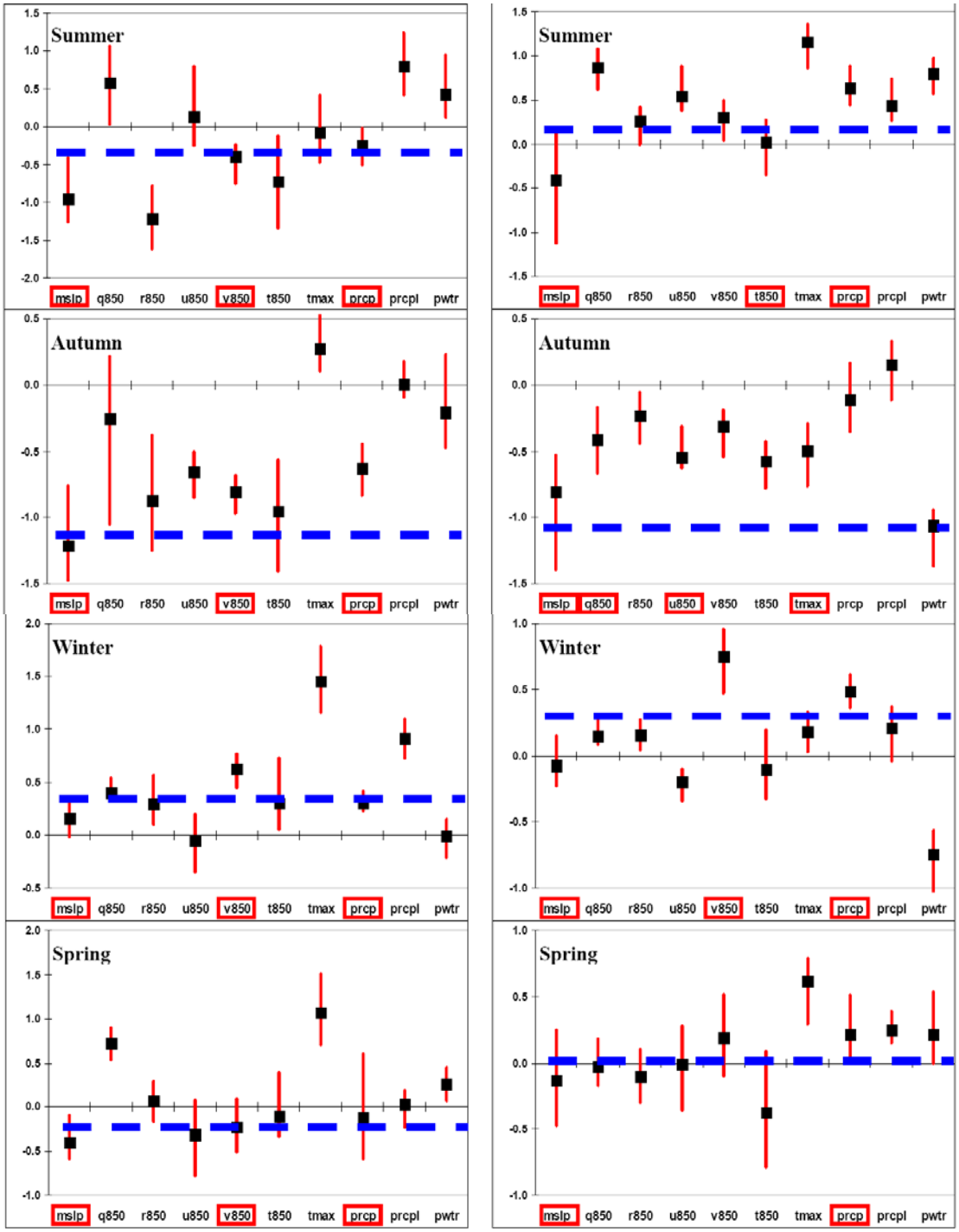

Fig. 24 *1958 to 2006 Linear trends averaged across all rainfall stations in SMD (left) and SWEA (right) for the four seasons (summer to spring from top to bottom) fitted on analogue reconstructed series based on a single predictor (predictors included in the optimum combinations are indicated by red squares. Black squares show the mean of 6 SDMs, while the red bars show the full range; magnitudes of the observed trends are indicated by dashed blue lines.*

5.4 Reproduction of the warming trends

The ability of the SDM to reproduce observed warming is first assessed from a regional perspective looking at seasonal averages across all stations in SWEA and SMD for both T_{max} (Table 12, upper) and T_{min} (Table 12, lower). Contrary to rainfall, the underestimation of warming trends due to the underestimation of the variance (there is no correction factor for temperature) is very clear. The normalisation (right columns) of the trends (factoring in the underestimation of the inter-annual variability) eliminates the systematic biases, as differences between trends from the observations and the reconstructed series are either positive (6 cases) or negative (10 cases) across the two predictands, two regions and four seasons. Some warming trends are still largely underestimated: T_{max} in summer in both regions and in autumn in SWEA for both T_{max} and T_{min}. In contrast, the analogue reconstructed series are warming too strongly in spring for T_{max} in both regions and in winter and spring for T_{min} in SMD.

Table 12 *Summary statistics of the reproduction of the observed trends for T_{max} (upper) and T_{min} (lower) as per Table 11; units are in ºC per century.*

ºC per century	**Observation**		**Analogue**			**Analogue normalised**		
	SMD	SWEA	SMD	SWEA	r	SMD	SWEA	r
Summer	2.16	1.51	0.57	0.77	**0.45**	1.07	1.16	**0.48**
Autumn	1.65	1.48	0.76	0.07	0.21	1.42	0.08	0.20
Winter	1.57	1.58	1.12	0.72	0.23	2.30	1.34	0.29
Spring	1.81	1.73	1.24	1.49	**0.39**	2.86	2.35	**0.47**

ºC per century	**Observations**		**Analogues**			**Analogue normalised**		
	SMD	SWEA	SMD	SWEA	r	SMD	SWEA	r
Summer	1.27	1.20	0.69	0.60	**0.49**	1.19	1.15	**0.57**
Autumn	-0.61	0.06	-0.36	-0.55	**0.47**	-0.73	-0.99	**0.61**
Winter	0.32	1.44	0.90	0.56	**0.35**	1.90	1.45	0.30
Spring	0.46	1.20	0.90	0.55	0.29	1.59	1.02	**0.36**

The ability of the technique to capture local features of the temperature trends is assessed by the correlations between linear trends for the observed and analogue reconstructed local series (41 in total). Correlations are in most instances significant at the 95% level (shown as bold figures in Table 12) but low: from 0.20 for T_{max} in autumn to 0.61 for T_{min} in autumn. Across all the stations and all the seasons the slope of the line of best fit between the observed and reconstructed data is reasonable: 0.75 for T_{max} (Fig. 25, upper) but only 0.49 for T_{min} (Fig. 25,

lower). However, season by season (as can be seen from the colour code), the scatter of points is relatively "flat" suggesting that very little of the station-to-station differences in warming trends is being captured. This is particularly true for T_{max} as measured by the spatial correlations in Table 12.

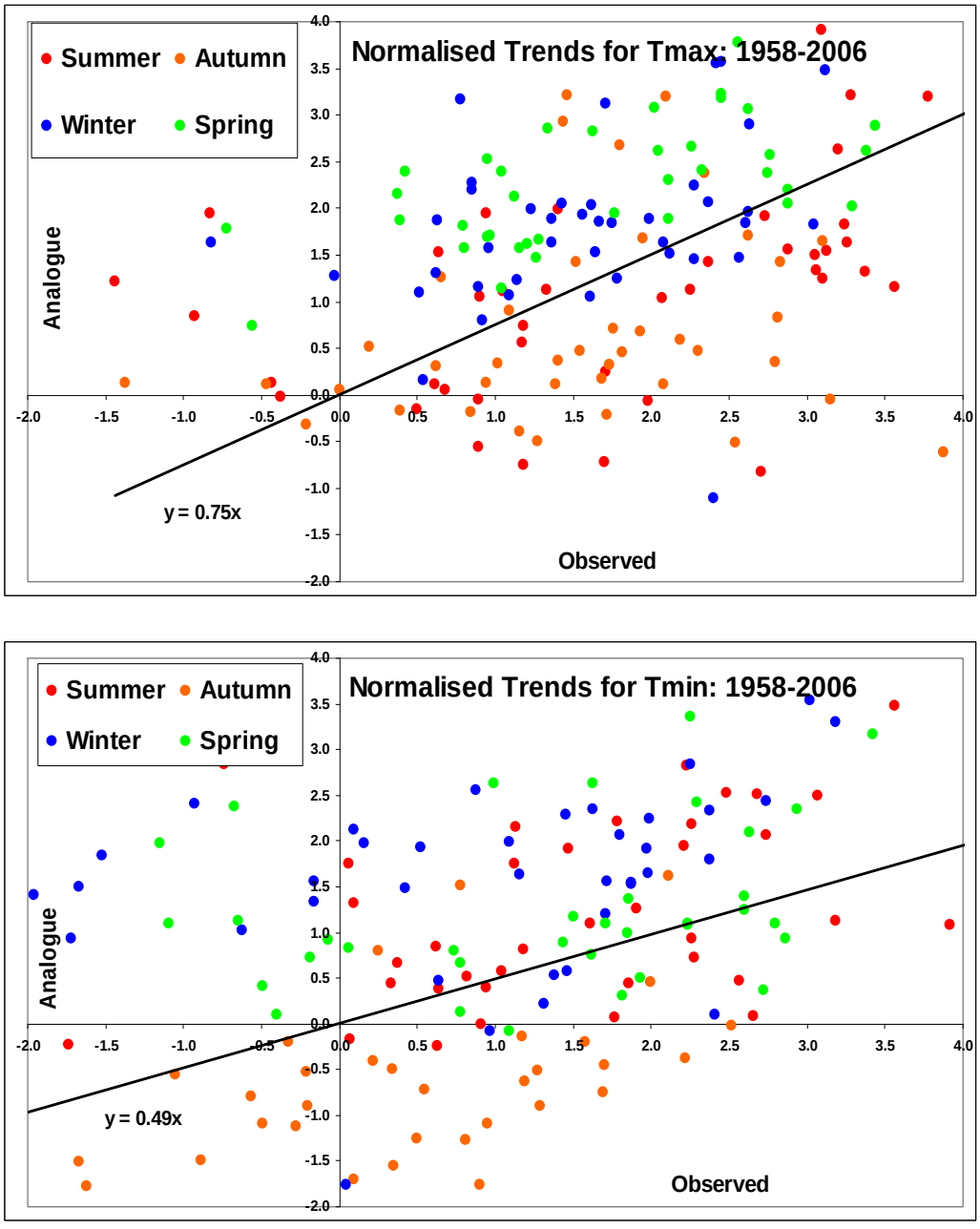

Fig. 25 *Reproduction of the observed trends for T_{max} (upper) and T_{min} (lower) for the 41 temperature stations across the SEACI regions (SMD and SWEA combined); the four calendar seasons are shown on a single graph using colour codes. Each point has for the x-coordinate the observed linear trends computed between 1958 and 2006 and the normalised trend for the analogue reconstructed series as the y-coordinate. Linear best fits fitted through the origin (0, 0) across all data points (4 seasons together) and their slopes are shown on the graph.*

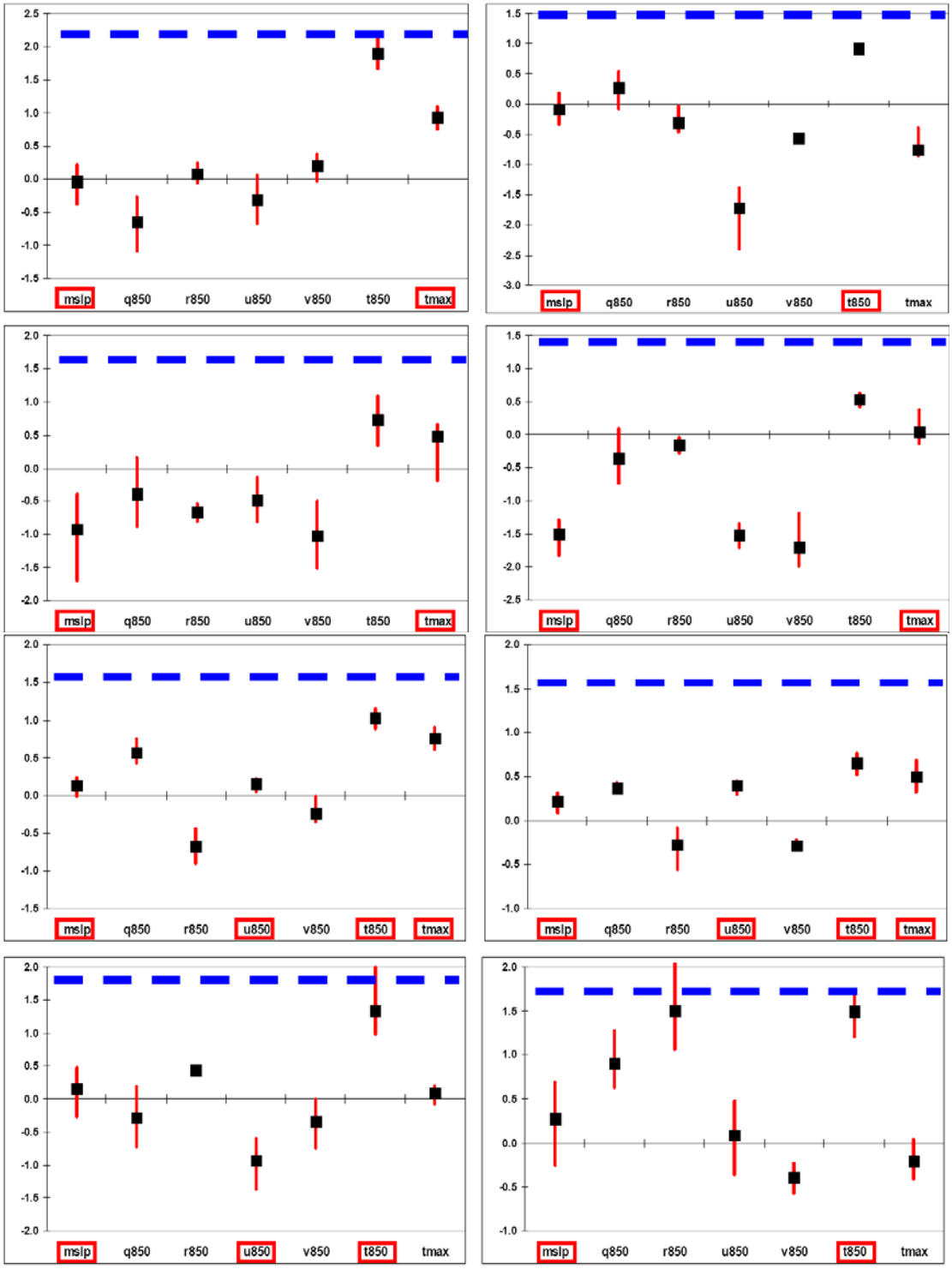

Fig. 26 *As per Fig. 24 but for T_{max} (left column for SMD and right column for SWEA, summer to spring from top to bottom).*

The analysis of SDMs using a single predictor shows that, in most instances, tropospheric warming (T_{850}) provides the largest warming trends of any single predictor and, in 6 instances (Figs 26 and 27), matches the observed trends. In contrast, MSLP, as a predictor, hardly suggests any warming trends and in some cases (mostly in autumn for both region and both T_{max}

and T_{min}) points toward large cooling trends. Additional predictors such as Q_{850} for T_{min} are also likely to contribute to the trends from the analogue model using the optimum combination of predictors.

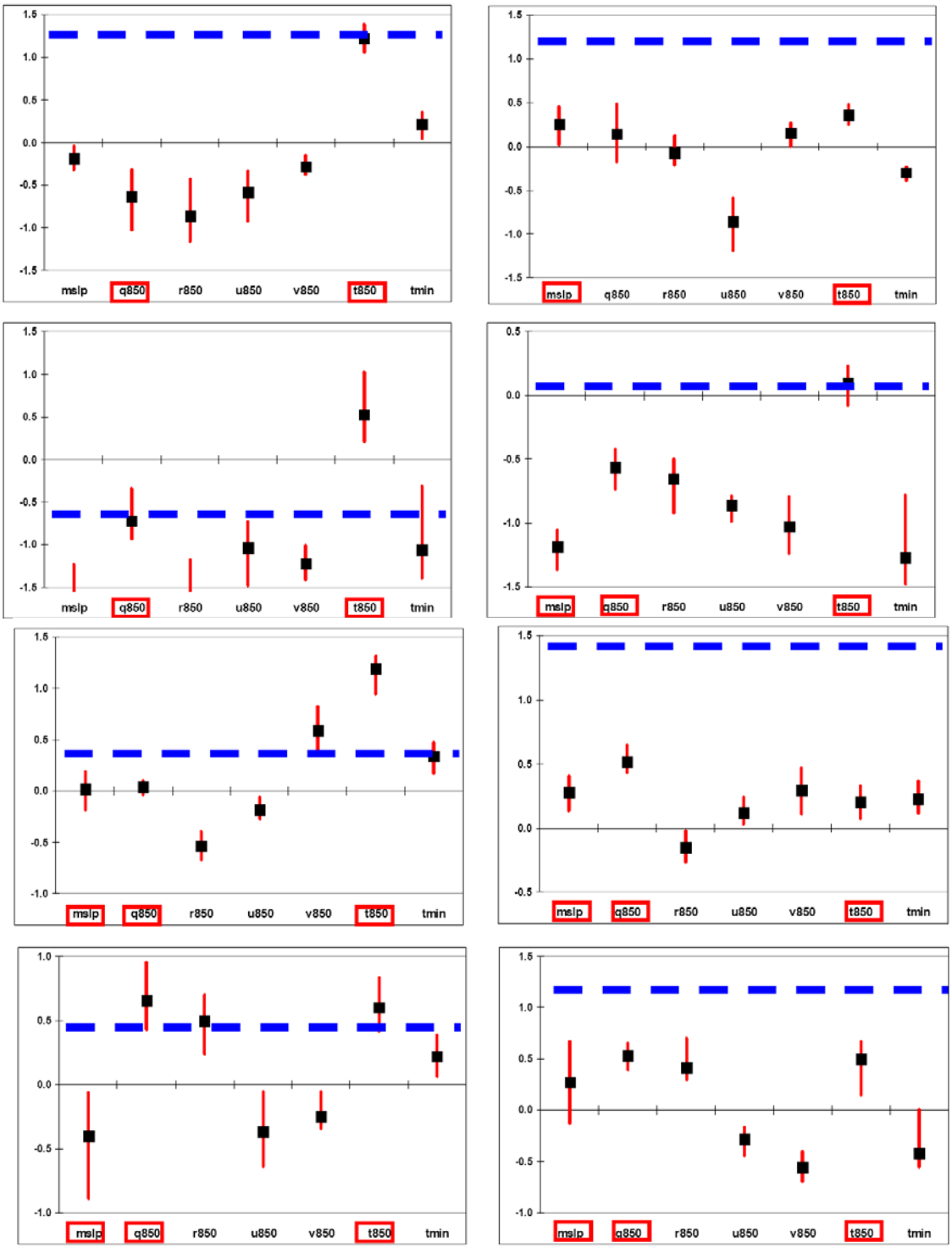

Fig. 27 *As per Fig. 24 but for T_{min} (left column for SMD and right column for SWEA, summer to spring from top to bottom).*

5.5 Reproduction of trends for the additional variables

The ability of the SDM to reproduce observed trends for additional variables relevant to the surface water balance is assessed on a regional basis. Seasonal averages across all stations in SWEA and SMD are accumulated into regional average for pan-evaporation (Table 13, upper), dew-point maximum (DT_{max}, Table 13, middle) and minimum (DT_{min}, Table 13, lower) temperatures.

Table 13 *Summary statistics of the reproduction of the observed trends from 1958 to 2003 for pan-evaporation (upper, units are in mm day^{-1} per century) dew-point maximum (middle) and minimum (lower) temperature as per Table 11 (units are in ºC per century).*

mm day^{-1} per century	**Observation**		**Analogue**		**Analogue normalised**	
	SMD	SWEA	SMD	SWEA	SMD	SWEA
Summer	-3.48	-1.56	-1.41	-0.64	-4.73	-1.69
Autumn	-1.60	-0.98	-0.08	-0.55	-0.20	-1.29
Winter	-0.57	-0.14	0.19	0.00	0.40	0.00
Spring	-1.17	-1.16	-0.35	-0.61	-1.35	-1.67

ºC per century	**Observation**		**Analogue**		**Analogue normalised**	
	SMD	SWEA	SMD	SWEA	SMD	SWEA
Summer	-1.17	1.18	-0.68	0.42	-1.17	0.97
Autumn	-0.92	1.46	-0.59	0.49	-1.25	1.04
Winter	0.88	1.52	0.07	0.42	0.24	0.88
Spring	0.38	1.14	0.55	0.30	1.51	0.60

ºC per century	**Observation**		**Analogue**		**Analogue normalised**	
	SMD	SWEA	SMD	SWEA	SMD	SWEA
Summer	-6.67	-0.12	-0.92	-0.05	-2.99	-0.10
Autumn	-2.14	0.77	-0.40	-0.04	-0.84	-0.07
Winter	0.81	0.76	0.21	0.23	0.86	0.44
Spring	-3.07	-0.54	-0.08	-0.06	-0.39	-0.15

The underestimation of observed trends is very large and strongly relates to the underestimation of the variance as it did for temperature (there is no correction factor for these variables). The normalisation of the trends (factoring in the underestimation of the inter-annual variability) eliminates the systematic biases and results in trends either larger or smaller than observed.

In all cases except in winter in the SMD, the sign of the predictand trends is captured by the technique. The magnitude in most instances is within +/- 30% of the observed values but with

some notable exceptions: pan-evaporation in autumn and winter in SMD and in spring in SWEA, DT_{min} in autumn and spring in both regions and DT_{max} in winter in SMD.

5.6 Reproduction of non-stationarities in the climate record

In this section, we examine the ability of the technique to reproduce a shift in the climate. The magnitude of the changes between the latter part of the climate observational record in SEA and the earlier part (column ΔO in Table 14) are comparable to future climate change projections and hence makes this exercise meaningful as a validation of the suitability of the SDM for climate change applications. This is particularly true for rainfall, where the magnitude of the rainfall decline in autumn (-30% across the 324 stations in SWEA and SMD) is as large as any future projections. In contrast, temperature changes (mostly warming apart for T_{min} in autumn) range between 0.15ºC and 0.54ºC and are an order of magnitude smaller than future projections by 2050.

Results for rainfall are not "normalised" but they are normalised for temperature (i.e. the ΔT calculated from the analogue series is divided by the amount of inter-annual variability reproduced in the 1991-2006 period).

Table 14 *Summary statistics for three surface predictands (T_{max}, T_{min} and Rainfall) of the ability of the technique to reproduce the observed changes between 1991-2006 and 1958-1990. Values are averages across all available stations in SWEA and SMD combined (41 for temperature and 324 for rainfall, in ºC for temperature and percentage for rainfall) and calculated for the observations (ΔO) and for the fully cross validated analogue reconstructed values for 1991-2006 (ΔA_{XV}). Spatial correlations between the observed and analogue reconstructed Δ at each station are indicated in a third column (correlation in bold are significant at the 95% level). Analogue reconstructed temperatures are "normalised" but rainfall is not.*

	Summer			**Autumn**			**Winter**			**Spring**		
	ΔO	ΔA_{xv}	r	ΔO	ΔA_{xv}	r	ΔO	ΔA_{xv}	r	ΔO	ΔA_{xv}	r
T_{max}	0.40º	0.41º	0.27	0.27º	-0.16º	**0.34**	0.54º	0.48º	0.23	0.31º	0.68º	**0.35**
T_{min}	0.30º	0.24º	0.21	-0.48º	-0.60º	**0.55**	0.25º	0.01º	**0.31**	0.15º	-0.12º	0.18
Rain	11.6%	7.3%	-0.04	-30.7%	-21%	**0.55**	1.2%	-10.6%	**0.24**	5.1%	-8.6%	**0.21**

Overall, the results for this cross-validated exercise should be analysed and compared to the results discussed earlier regarding the ability of the SDMs to reproduce the observed trends over the entire period (not cross-validated). In general, the ability of the SDM to reproduce the observed changes (spatial correlation in Table 14, slope of the line of best-fit in Fig. 28 and Fig. 29) resemble those obtained earlier and only show a slight reduction in the overall performance of the SDM. Noteworthy, is the SDM reproduction of the dryer recent period: the rainfall reduction in autumn is underestimated (70% of the observed change is reproduced, which is comparable to the ability of the SDM to reproduce the trends); however, a decline in winter and spring is produced by the analogue reconstruction which is not apparent in the observed series.

The reproduction of the observed ΔT is satisfactory apart for T_{max} in autumn and T_{min} in spring where the sign is wrong, albeit with very small values. The slope of the line of best-fit (Fig. 29) is similar for T_{min} (0.55 compared to 0.49 for the trends: Fig. 29 vs. Fig. 25) but reduces for T_{max} (0.41 instead of 0.75: Fig. 29 vs. Fig. 25).

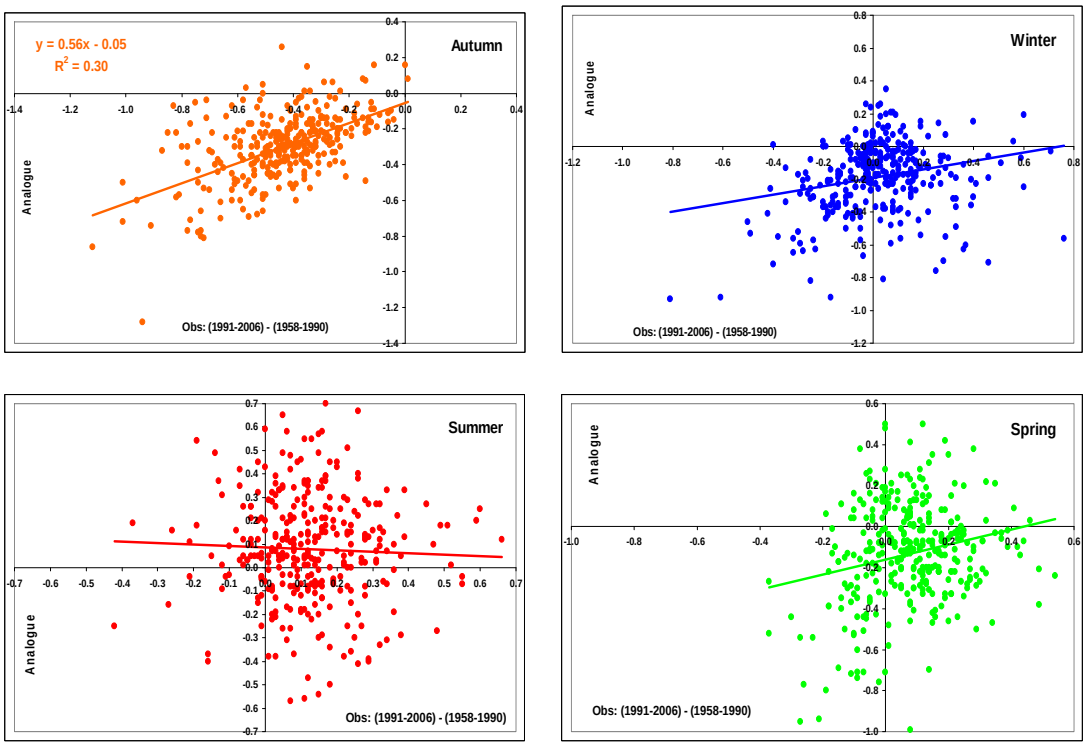

Fig. 28 *Cross validated reproduction of the observed changes since 1990 for rainfall for the 324 rainfall stations across the SEACI regions (SMD and SWEA) and for the four calendar seasons. Each point has for x-coordinate the ΔR_{obs} (i.e. the 1991-2006 mean minus the 1958-1990 mean) from observations and the similar quantity from the analogue reconstructed as a y-coordinate. The 1991-2006 mean is fully cross-validated as it uses analogues from the 1958 to 1990 period. Linear best fits are shown on each graph.*

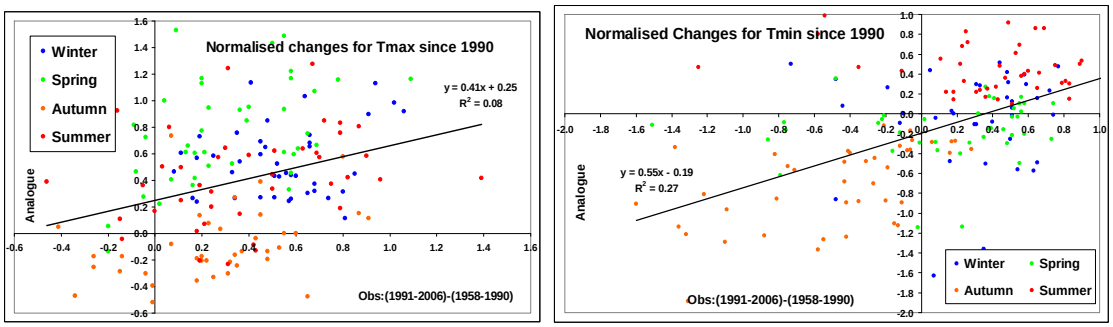

Fig. 29 *As per Fig. 28 but for T_{max} (left) and T_{min} (right) for the 41 temperature stations across the SEACI region and for the four calendar seasons in one plot.*

5.7 Using the Bureau of Meteorology SDM to understand trends in frost occurrences

In this section we investigate the nature of frost occurrences across SEA and the observed variability and trends. The climatological analysis was performed on a subset of the 56 stations identified in SEA. Stations with missing years after 1958 and coastal stations with very few frost occurrences (FO) were removed. In total, 23 stations were used. 905 FO per year are observed across the chosen network (Fig. 30), with two thirds of these frosts occurring during the winter months (JJA). The inter-annual variability is large (STD = 184 frost occurrences per year) and linked to the El Niño Southern Oscillation (ENSO). The correlation with the SOI is -0.38 (-0.36 in JJA). Peaks of FO during El Niño years are clearly visible along the historical record (red circles in Fig. 30). This is consistent with the known impact of ENSO on SEA climate: lower rainfall, higher maximum temperature and lower minimum temperature (Power et al. 1998) and hence higher FO (Murphy and Timbal 2008). Frost number increase during El Niño years because there tends to be a higher number of high pressure systems over the SEA which favour dry conditions, clear skies and cool nights. This is best diagnosed by looking at the relationship between the Sub-Tropical Ridge intensity (STR-I) as diagnosed by Drosdowsky (2005). The STR over SEA reaches its northern-most location in winter (30ºS) and shifts south in spring (31ºS) and autumn (34ºS). The relationship between STR-I and FO is stronger than the relationship between the SOI and FO: r=0.41 all year around and r=0.59 in JJA (both significant at the 99% level). In autumn the relationship is weaker (r=0.37), it is insignificant in spring (r=0.09).

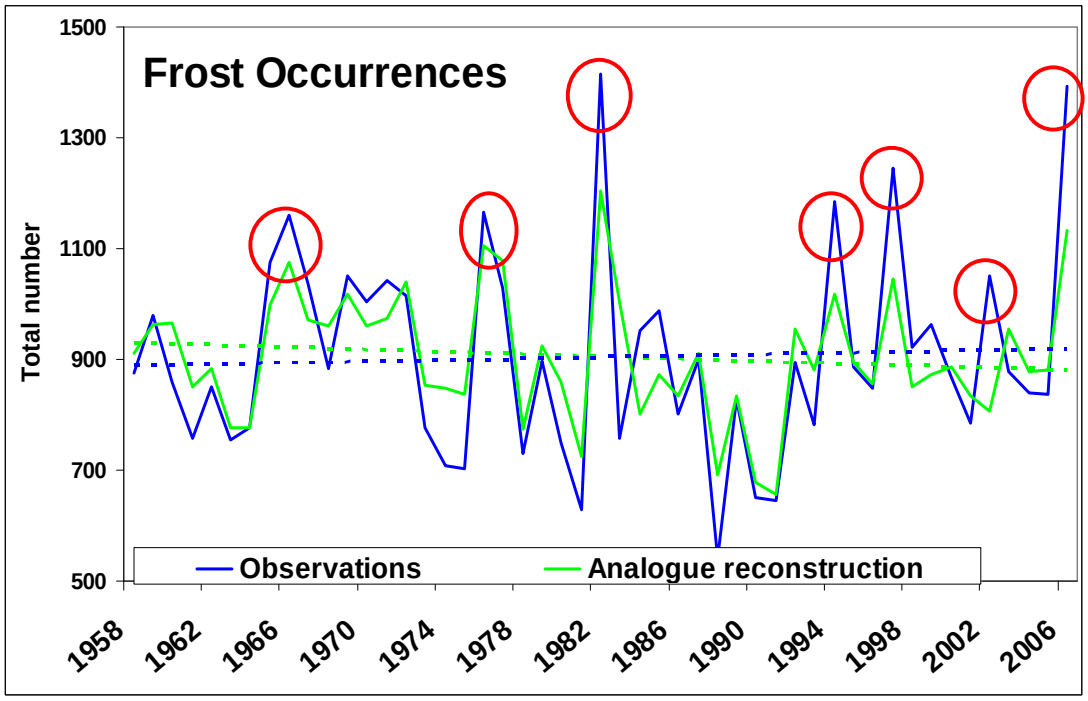

Fig. 30 *Interannual variability of the total number of observed frost occurrences (minimum temperature below 2ºC) all year round across 23 stations in SEA (blue lines) and for the analogue reconstructed series (green lines). Linear trends are shown as dashed lines. Major El Niño events during the period are indicated with red circles: 1965-66, 1977-78, 1982, 1994, 1997, 2002 and 2006.*

The long-term trend in frost occurrence across SEA is small and insignificant: +31 occurrences over 50 years across all stations limited to the transition seasons: +12 in autumn and +25 in spring and a very small decline in winter. These small spatial averages hide important geographical features: there are a near equal number of stations with positive (7) or negative (8) large (and statistically significant at the 95% level) trends. Stations with decreasing FO tend to be located in western Victoria and South Australia (Mount Baker, Mount Gambier, Lameroo, Ouyen and Mildura), while stations with large positive trends are located further east (Horsham, Ballarat, Echuca, Rutherglen, Sale and Orbost). Stations at higher elevations in the Great Dividing Range (Omeo, Canberra) experience reduced FO.

Table 15 *1958 to 2006 linear trends for frost occurrences (FO in total number of days across SEA per 50 years) and T_{min} (in ºC per century) in autumn, winter and spring from observations and analogue reconstructed series using as predictors: MSLP, MSLP combined with T_{850} and with the full optimised analogue model.*

	Observation		**MSLP only**		**MSLP & T_{850}**		**Optimised analogue**	
	F. O.	$<T_{min}>$	F. O.	$<T_{min}>$	F. O.	$<T_{min}>$	F. O.	$<T_{min}>$
Autumn	+12.0	-0.48	+21.2	-0.62	-5.7	+0.0	+3.6	-0.32
Winter	-6.7	+0.16	+11.5	+0.02	-43.5	+0.27	-55.5	+0.34
Spring	+25.1	-0.04	-0.5	-0.06	-21.5	+0.28	+4.3	+0.17

Overall the SMD reproduces the total number of FO across SEA exactly (905 cases per year), the inter-annual variability is well captured (r=0.82) but underestimated (STD=117 simulated versus 184 observed). The long-term trend of analogue reconstructed frost occurrences is small and insignificant as observed but with the opposite signs (Fig. 31). Details on the seasonality of the trends (positive in the transition seasons, negative in winter) are well captured by the analogue reconstruction (Table 15, right columns) but with a bias toward more negative trends. Analysis of the month-by-month trends (Fig. 31) to explain that behaviour shows that is largely due to a large error for the month of August when a strong increase in FO is hardly captured by the analogue reconstruction.

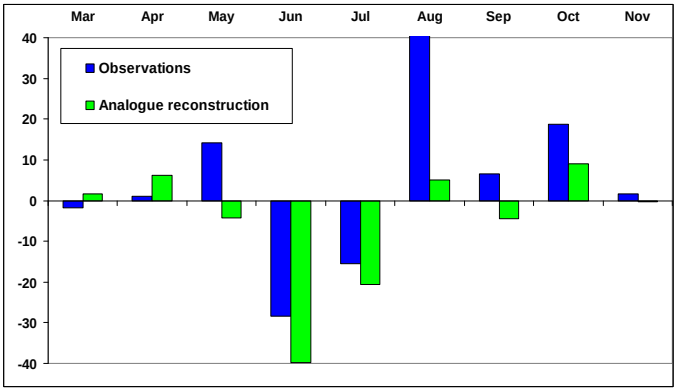

Fig. 31 *Month by month linear trends from 1958 to 2006 for frost occurrences (minimum temperature below 2ºC) averaged across 23 temperature stations in SEA.*

The large-scale forcing of the FO trends was investigated by comparing the analogue reconstructed series with SDMs using: 1) only MSLP, 2) MSLP combined with T_{850} and 3) the optimised SDMs where a moisture variable is always added and sometimes a wind field. MSLP is a critical predictor in capturing the FO trends (Table 15). It is interesting that while MSLP has limited value in capturing temperature trends overall, it is important for T_{min} and, in particular, for getting the negative trends of FO in autumn. In particular the inclusion of MSLP generates larger than observed negative trend for T_{min} and a larger than observed positive trend for FO. This is consistent with earlier results (shown in the second row of Fig. 27) and shown to be even more important for the lower tail of the distribution (i.e. frost occurrences).

Once the thermal predictor is added, the surface warming is stronger than observed, as is the reduction in FO. Finally, with an additional moisture variable added, trends get closer to the observed values for both T_{min} and FO. Besides the importance of using a combination of predictors to best capture the observed trends (arguably MSLP alone performed better than the optimised SDM), the added skill for the more complex SDM is shown by looking at its ability to reproduce local trends as measured by the correlation coefficients between observations and the analogue reconstructed series for the 23 locations (Table 16). Correlation coefficients are always higher with the optimised model (very much so when compared to the SDM using MSLP only) and, apart from FO in autumn, is always statistically significant at the 95% level.

Table 16 *Spatial correlation (based on 23 stations across SEA) between linear 1958 to 2006 trends for the observed series (frost occurrences and T_{min}) and analogue reconstructed series using as predictors: MSLP, MSLP combined with T_{850} and with the full optimised analogue model.*

r	**MSLP only**		**MSLP & T_{850}**		**Optimised analogue**	
	F. O.	$<T_{min}>$	F. O.	$<T_{min}>$	F. O.	$<T_{min}>$
Autumn	0.07	0.08	0.03	0.28	0.16	**0.40**
Winter	0.01	0.25	**0.50**	**0.60**	**0.64**	**0.64**
Spring	-0.38	-0.21	-0.06	0.01	**0.62**	**0.39**

Overall, local trends in FO and minimum temperature are result from a combination of the ongoing regional warming (captured by T_{850}), limited by circulation changes (captured by MSLP) leading to a surface cooling in autumn and an increase in FO, and complemented by associated moisture changes (drying in autumn which reinforced the FO increase, not so in winter). Based on the evidence presented here, it is hard to claim that circulation changes explain the local trends for T_{min} during the autumn-winter-spring part of the year since the seasonality and magnitude of the trends appears to be more complex and involve global temperature increases and local moisture changes. This is consistent with earlier findings that circulation changes could not explain the recent extreme heat wave of April 2005 (Timbal et al. 2007; Chapter 3 of this report).

5.8 Conclusions

This project completes the evaluation of the BoM SDM for 6 surface predictands across the entire SEACI region. The technique is able to reproduce local PDFs and skilfully capture day-to-day and inter-annual variability (Chapter 4). The technique reproduces many features of the observed climatic trends across the regions. It was demonstrated to be a suitable tool to apply to climate simulations. This justifies the application of the technique to 20th century climate in order to improve our ability attribute the observed changes to known external forcings compared to the simple use of climate model direct outputs. This will be the focus of the next chapter.

In addition, a better understanding of the large-scale changes responsible for the observed local changes has been gained and documented. Finally, the BoM SDM appears able to reproduce observed specific climate shifts during the last 50 years across SEA. This finding, combined with the availability of downscaled climate change projections Australia-wide for six different predictands based on the latest crop of IPCC-AR4 models (Timbal et al. 2009), makes it a very suitable tool to generate local climate change projections across the SEACI domain.

SUMMARY

- The BoM SDM reproduces 60 to 80% of the observed rainfall decline in autumn. In other seasons, local rainfall trends, either positive or negative, are generally well reproduced in terms of magnitude and spatial structures.

- Observed temperature trends (always positive with the exception of T_{min} in autumn) are well captured. The spatial structure of temperature trends is relatively well reproduced but the magnitude is consistently underestimated. Most of this underestimation is due to the reduced interannual variability of the reconstructed series and can be dealt with by "normalising" the trends (i.e. factoring in the underestimation of the inter-annual variability).

- Mean Sea Level Pressure (MSLP) is the most important single predictor in explaining rainfall trends. However, when large rainfall trends are observed, MSLP alone is not sufficient and additional predictors (in particular moisture variables such as specific humidity at 850 hPa) ensure that use of the optimised combinations of predictors provide results that better match the observed trends.

- MSLP, as a single predictor, explains very little of the observed temperature trends. Tropospheric temperature (at 850 hPa) is often the most important predictor in explaining local warming but tends in some cases to produce larger trends than observed (e.g. T_{min} in autumn). In these instances, the optimum combination (which includes a moisture variable) leads to more realistic trends, thus confirming the role that the drying in the South-East of Australia has had on some temperature trends.

- Overall, the ability of the SDM to reproduce non-stationarities in the climate record (a fully cross-validated test) is only slightly less than the ability to reproduce observed trends (this test is not cross validated).

- The increase of frost occurrences has been documented. It is limited to the central and eastern parts of inland SEA at low elevation and to the start and end of the frost seasons. Although the optimised SDMs are capable of reproducing some aspects of the long-term trends for frost occurrences, it is less skilful than for the mean T_{min}. This suggests that the importance of highly localised effects is not captured by the downscaling technique. The observed frost increases are due to a combination of synoptic trends (particularly important in autumn) and moisture changes.

6 A FORMAL ATTRIBUTION OF THE OBSERVED CLIMATE CHANGES ACROSS SOUTH-EASTERN AUSTRALIA

6.1 Introduction

Following on from the evaluation of the BoM SDM ability to reproduce observed local trends, the SDM has been applied to coupled climate model simulations of the 20th century forced with several external forcings to evaluate the ability of climate models to capture the large-scale changes which drive the observed regional changes. The purpose is to draw conclusions about the extent to which the observed climate change is formally attributable to particular external forcings, either natural or anthropogenic.

To do so, the BoM SDM has been applied to ensembles of simulations using different external forcings: natural only, anthropogenic only and natural and anthropogenic combined; each ensemble had five members. The climate model used is the Community Climate System Model version 3 (CCSM3), developed by NCAR in the U.S.A. First, the ability of the climate model to reproduce the large-scale changes is assessed as well as the dependence of the model responses to the external forcing. Then, the possibility of attributing observed changes to external forcing is considered.

Update on methodology and optimisation of the SDM (Chapters 4 and 5), the National Climate Atmospheric Research (NCAR) laboratory was approached to obtain the most up to date set of data for analysis. In the past, a series of ensembles from the Parallel Climate Model (PCM) were used to perform a similar attribution of the rainfall decline in the Southwest of Western Australia (Timbal et al. 2006; Timbal and Arblaster 2006). One of the issues faced during that work was that not all the predictors needed were available from the NCAR archived results. Recently, similar externally forced ensembles of simulations were performed with a newer climate model: the Community Climate System Model version 3 (CCSM3, Collins et al. 2006). While the limitations regarding the list of predictors we wanted to use remain, it was thought preferable to source this new set of data from the model currently being developed by NCAR. Overall, the framework used by NCAR to perform these simulations is very well suited to this formal attribution study. The model is run with well defined external forcings separated in two groups:

1. anthropogenic - which includes greenhouse gases, aerosols and stratospheric ozone;
2. natural – which includes variations of the solar constant and volcanic eruptions; and
3. both natural and anthropogenic forcings combined (Meehl et al. 2006).

Each ensemble consists of five simulations with slightly different initial conditions (starting around 1850) enabling an estimation of the uncertainty of the climate signals. All 20th century simulations were run until the end of 1999.

In this chapter, the ability of each ensemble to reproduce observed climatic trends for both temperature and rainfall in SEA is evaluated. Direct Model Output (DMO) is used as well as

results from the statistical downscaling of the three climate model ensembles using the BoM SDM adapted to the surface climate data selected for the SEACI program (Chapters 2 and 4). The ability of the SDM to reproduce ongoing climatic trends was assessed in Chapter 5. Results are shown for two climate entities: SWEA and SMD.

Table 17 *Optimum and modified combinations of predictors, for 4 calendar seasons, the 3 predictands in 2 regions: SWEA and SMD. The predictors are: MSLP is the Mean Sea Level Pressure; T_{max} and T_{min} are the surface min and max temperature; PRCP is the total rainfall; Q is the specific humidity; R is the relative humidity; T is the temperature; U and V are the zonal and meridional wind components; and subscript numbers indicate the atmospheric level for the variable in hPa. Predictors which had to be modified are indicated with bold font.*

Season		SWEA		SMDB	
		Optimum	**Modified**	**Optimum**	**Modified**
T_{max}	DJF	MSLP & T_{850}	MSLP & T_{850}	MSLP & **T_{max}**	MSLP & **T_{850}**
	MAM	MSLP & **T_{max}**	MSLP & **T_{850}**	MSLP & **T_{max}**	MSLP & **T_{850}**
	JJA	MSLP & T_{850} & **T_{max}** & U_{850}	MSLP & T_{850} & U_{850}	MSLP & T_{850} & **T_{max}** & U_{850}	MSLP & T_{850} & U_{850}
	SON	MSLP & T_{850}	MSLP & T_{850}	MSLP & T_{850} & U_{850}	MSLP & T_{850} & U_{850}
T_{min}	DJF	MSLP & T_{850}	MSLP & T_{850}	T_{850} & **Q_{850}**	T_{850} & **PRCP**
	MAM	MSLP & T_{850} & **Q_{850}**	MSLP & T_{850} & **PRCP**	T_{850} & **Q_{850}**	T_{850} & **PRCP**
	JJA	MSLP & T_{850} & **Q_{850}**	MSLP & T_{850} & **PRCP**	MSLP & T_{850} & **Q_{850}**	MSLP & T_{850} & **PRCP**
	SON	MSLP & T_{850} & **Q_{850}**	MSLP & T_{850} & **PRCP**	MSLP & T_{850} & **Q_{850}**	MSLP & T_{850} & **PRCP**
Prec	DJF	MSLP & PRCP & T_{850}	MSLP & PRCP & T_{850}	MSLP & PRCP & V_{850}	MSLP & PRCP & V_{850}
	MAM	MSLP & **T_{max}** & **Q_{850}** & U_{850}	MSLP & **T_{850}** & **PRCP** & U_{850}	MSLP & PRCP & V_{850}	MSLP & PRCP & V_{850}
	JJA	MSLP & PRCP & V_{850}	MSLP & PRCP & V_{850}	MSLP & PRCP & V_{850}	MSLP & PRCP & V_{850}
	SON	MSLP & PRCP	MSLP & PRCP	MSLP & PRCP & V_{850}	MSLP & PRCP & V_{850}

The optimum combination of predictors for each SDM had to be modified to match the existing dataset available in the CCSM3 archive stored at the NCAR, USA (Table 17). In particular Q_{850} was not available and was, in general, replaced by model precipitation. In addition T_{max} and T_{min} were not archived for the all forcing simulations and hence could not be used for all cases. To prevent mismatches in the application of the SDM to CCSM3 simulations, both T_{max} and T_{min} were replaced by T_{850} whenever needed. In the case of rainfall, the only modification required affects the downscaling for SWEA in autumn, when Q_{850} is replaced by PRCP. As a single predictor, PRCP produced a smaller rainfall trend (Fig. 24). T_{max} was replaced by T_{850} which was producing similar trends. Overall the modified SDM is expected to reproduce only slightly less of the rainfall trends because the single most important predictor is MSLP which was used as predictor in all SDMs (Fig. 24). In the few instances where T_{max} had to be replaced by T_{850}, it is not expected to downgrade the results of the downscaling for T_{max}, as in most instances, T_{850}

as a single predictor was producing a larger temperature trend than observed. Similarly for T_{min}, the change from T_{850} to T_{min} is not anticipated to significantly impact on the SDM's ability to reproduce observed changes.

6.2 Analysis of large-scale predictor in the 20th century simulations

The large-scale changes simulated by CCSM3 during the 20th century were investigated by looking at differences between the last 30 years (1970 to 1999) and the earlier part of the 20th century (1900 to 1969). Linear trends were also investigated but were found to be noisier and harder to interpret. Therefore, in this chapter, only maps of differences between the two periods are shown. Earlier research during SEACI demonstrates that the rainfall decline in SEA is linked to the build up of MSLP above southern Australia (Chapter 3). The rise in MSLP above southern Australia is well documented (Timbal and Hope 2008) and, since it is one of the most important large-scale predictors used in the statistical downscaling of rainfall, T_{max} and T_{min} across SEA, it is appropriate to analyse how the CCSM3 modelled MSLP response to external forcings (Figs 32 to 35).

The natural ensemble displays anomalies in the latter period of the 20th century which are small (mostly below 0.2 hPa) and which, if anything, tend to be negative in summer and winter over SEA. In autumn and spring, anomalies are slightly positive (about 0.1 hPa) over SEA. Overall there is no large-scale build-up of MSLP around Australia in the CCSM3 mean ensemble forced with natural external forcings.

In contrast, the ensemble mean in the case of anthropogenic forcings exhibits a clear and consistent build up of MSLP above southern Australia in all 4 seasons. This feature resembles future projections of MSLP due to increases in greenhouse gases (Fig. 10.9 p 767, in the IPCC 4th assessment, Solomon et al. 2007). The structure of the MSLP increase is mostly zonal with largest values south of the continent (up to 1 hPa at 45º to 50ºS). Above SEA, the largest signal is in winter (+0.4 to 0.6 hPa) and spring (0.2 to 0.5 hPa) and is weaker in summer and autumn (0 to 0.2 hPa).

Finally, the ensemble forced by natural *and* anthropogenic forcings combined, displays very similar patterns to the anthropogenic ensemble. This indicates that anthropogenic forcings are the most important driver of the simulated differences in the late 20th century. Above SEA, the signal is larger for the combined forcings than for anthropogenic forcings alone in winter (up to 0.8 hPa higher) and autumn, similar in summer and weaker in spring. The small differences (i.e. a larger signal in autumn, a smaller signal in spring) make the fully forced ensemble the best match to the observed MSLP changes in HadSLP2 data (Allan and Anselm 2006; Timbal and Hope 2008).

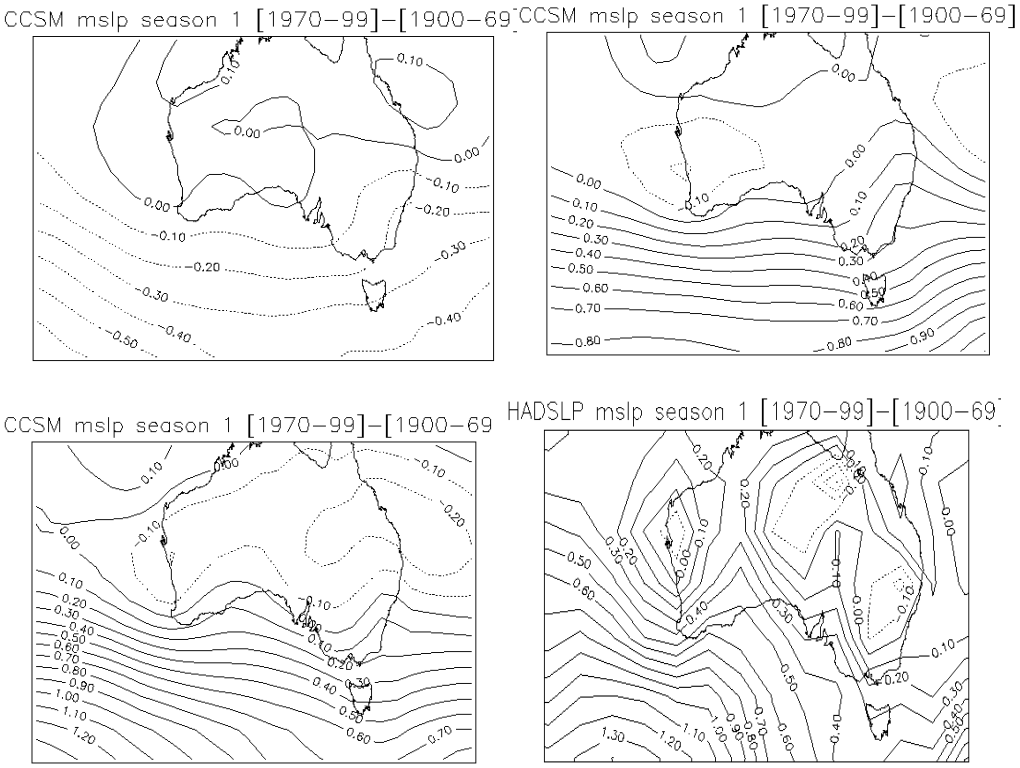

Fig. 32 *Maps of differences of summer MSLP (in hPa) between 1970-1999 and 1900-1969, for the natural (top left), anthropogenic (top right), and all forcings (bottom left) ensemble means and for the HadSLP2 dataset (bottom right).*

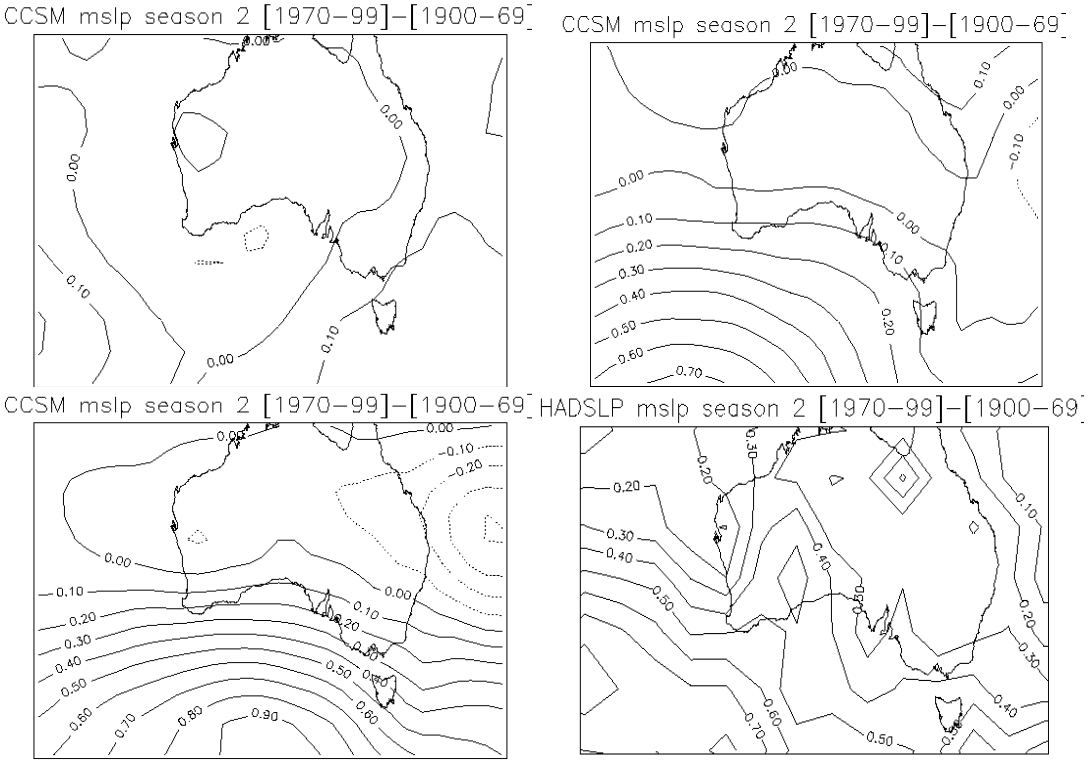

Fig. 33 *As per Fig. 32 but for autumn.*

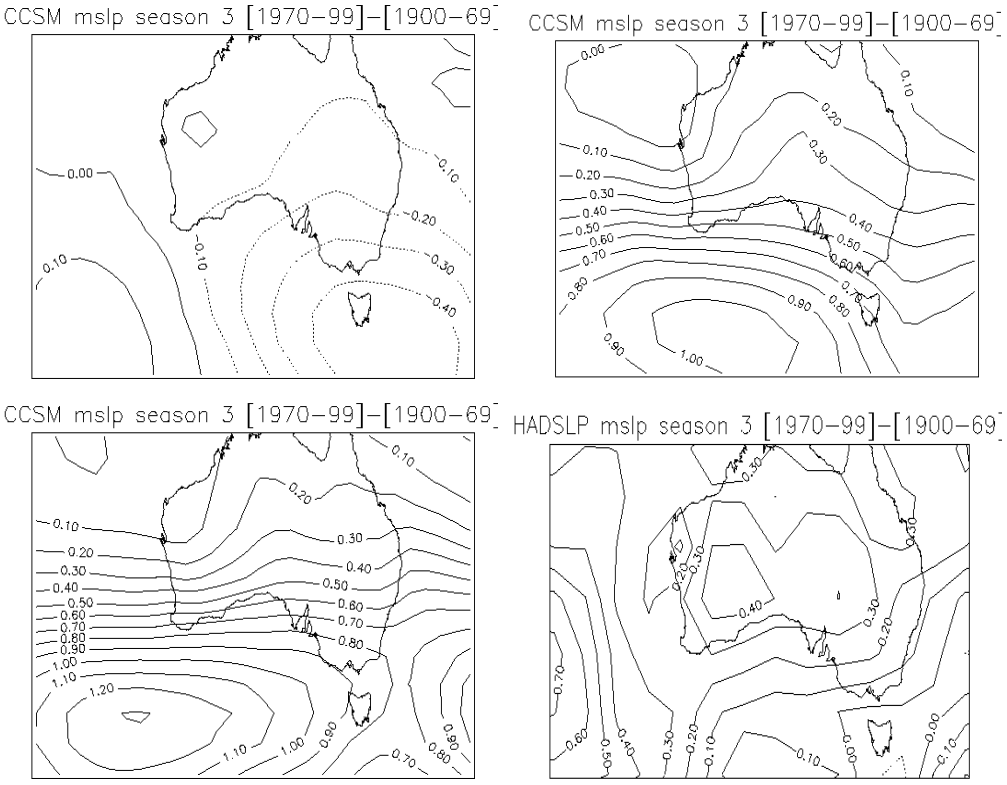

Fig. 34 *As per Fig. 32 but for winter.*

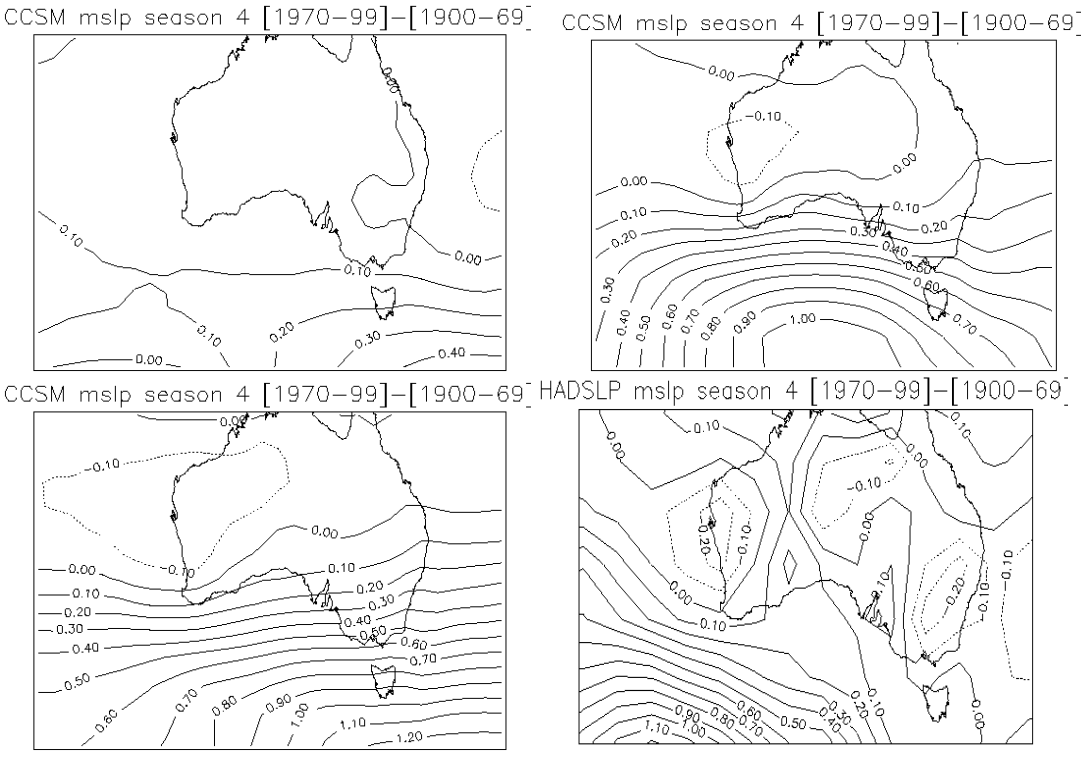

Fig. 35 *As per Fig. 32 but for spring.*

In addition to the MSLP response to external forcings, the DMO for rainfall was also evaluated. This is important for two reasons: 1) to evaluate the possibility of attributing the observed rainfall decline directly without using the BoM SDM and 2) to understand the downscaled rainfall response in the modified version of the BoM SDM, given that the DMO rainfall is the second most important predictor in the SDM after MSLP.

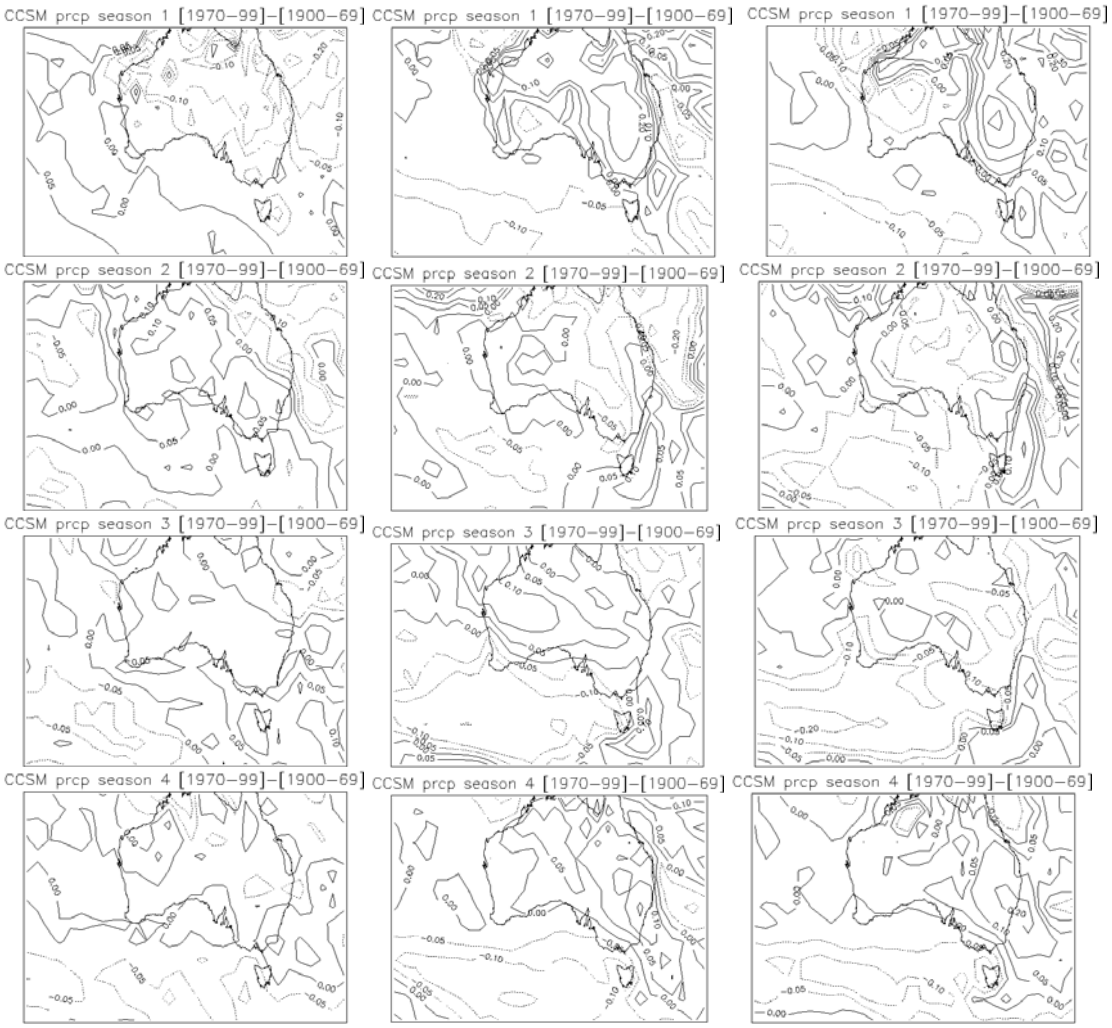

Fig. 36 *Maps of differences in rainfall (mm day^{-1}) between 1970-1999 and 1900-1969, for the natural (left), anthropogenic (middle), and all forcings (right column) ensemble means. Each row shows a season: summer, autumn, winter and spring from top to bottom.*

Overall, the rainfall difference maps (Fig. 36) have much greater finer-scale spatial structure. The differences are harder to interpret than the MSLP difference maps. The mean of the natural ensemble suggests a decline in summer rainfall across the Australian continent which is greatest in the north but also evident across SEA. In autumn and winter the model suggests a small increase in precipitation. The response in the anthropogenic ensemble is rather different: an increase in summer rainfall, a decrease during autumn over a large part of eastern Australia, including SEA, as well as a decrease confined to southern Australia (SWWA and SWEA), two regions which have been identified as having linked rainfall variability (Hope et al. 2009).

Finally, as per MSLP, the full forcing ensemble is more closely aligned with the anthropogenic ensemble than the natural one. For the full forcing ensemble, the autumn rainfall decline is now shifted more toward central Australia (and hence is less realistic for SEA), while the winter rainfall decline is more widespread (and hence more realistic).

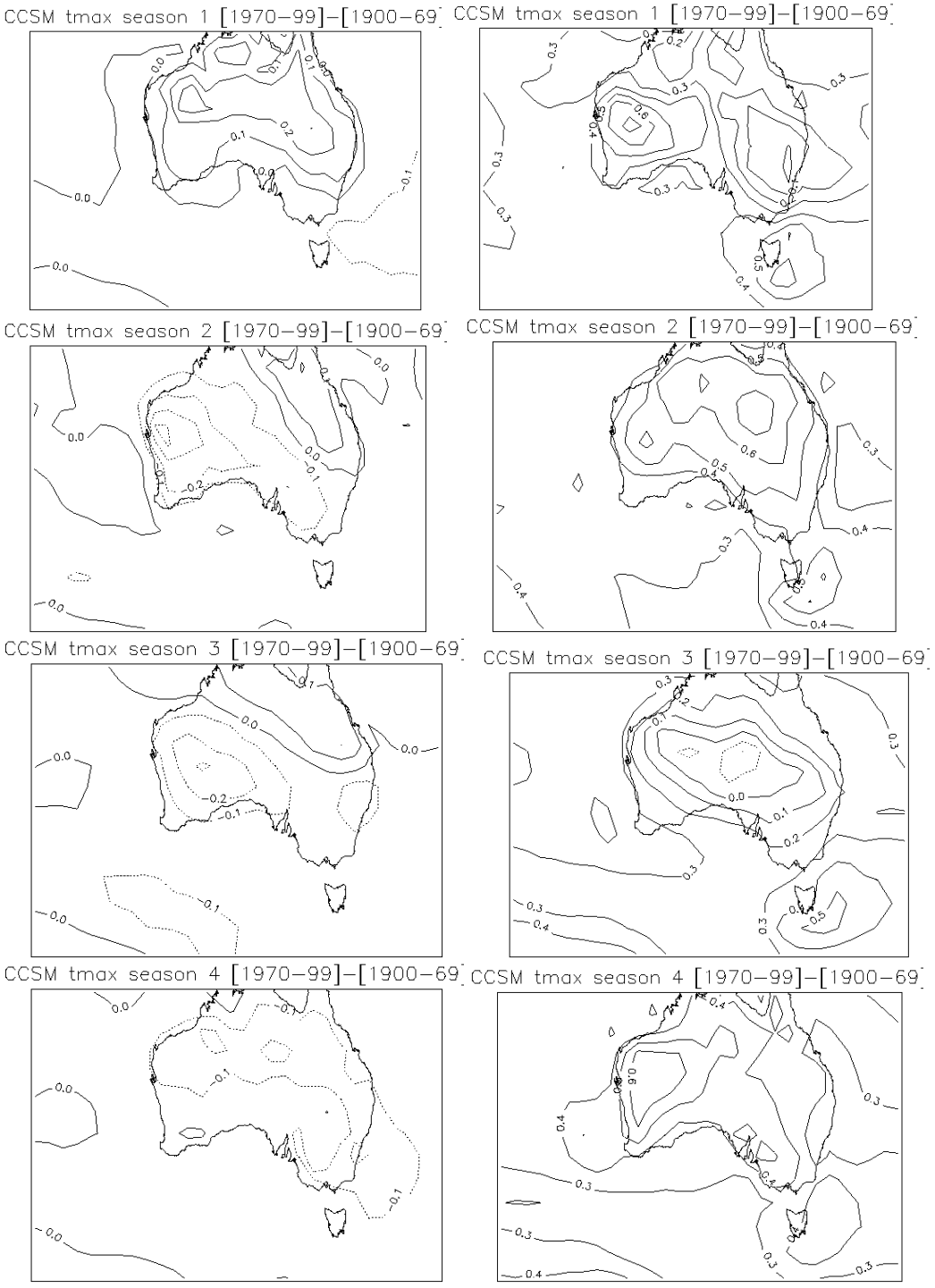

Fig. 37 *As per Fig. 36 but for maximum Temperature (T_{max}) in °C. The natural (left) and anthropogenic (right) ensembles are shown.*

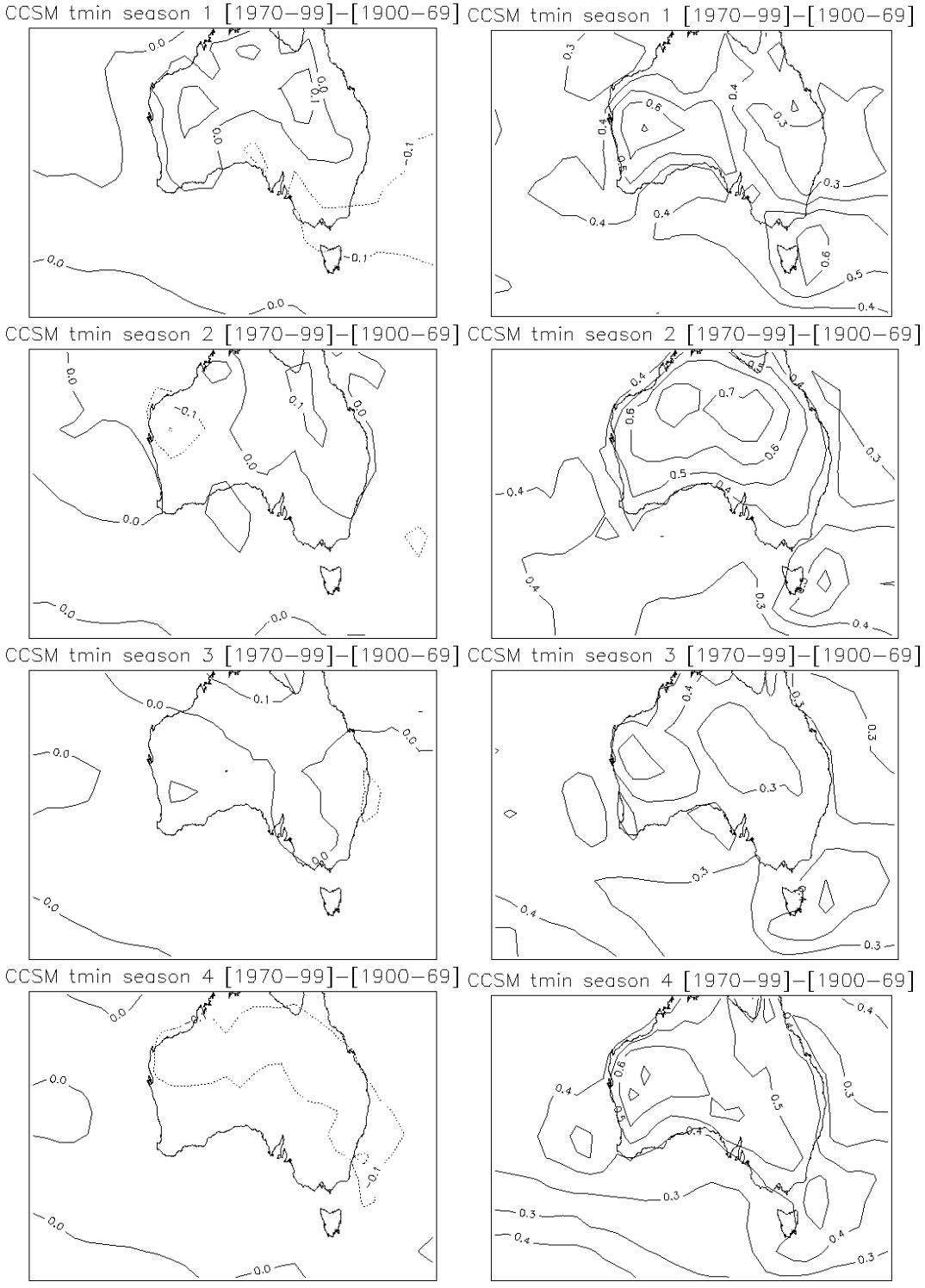

Fig. 38 *As per Fig. 37 but for minimum Temperature (T_{min}) in ºC.*

The other two surface variables investigated are T_{max} (Fig. 37) and T_{min} (Fig. 38). As with rainfall, temperature is an important predictor in the statistical downscaling of the CCSM3 ensembles. As noted earlier, T_{max} and T_{min} are not available for the all forcings ensemble but, since a clear contrast is visible between the natural ensemble and the anthropogenic ensemble,

and the results obtained earlier, for MSLP and rainfall, very strongly suggest that the ensemble mean response in the all forcing simulations is close to the anthropogenic only ensemble mean. Overall, with natural forcings only, there is hardly any warming across the Australian continent in either T_{max} or T_{min}. The only case with a warming above 0.2ºC is T_{max} in summer. In all other cases there is either no signal or a small cooling. In contrast, the mean of the ensemble forced with anthropogenic forcings displays a consistent (across all ensemble members) warming. The structure and amplitude varies from season to season. Across SEA, it ranges from 0.2 to 0.4ºC and is strongest in autumn and spring for both T_{max} and T_{min}. In general the model produces a stronger warming for T_{min} than T_{max}.

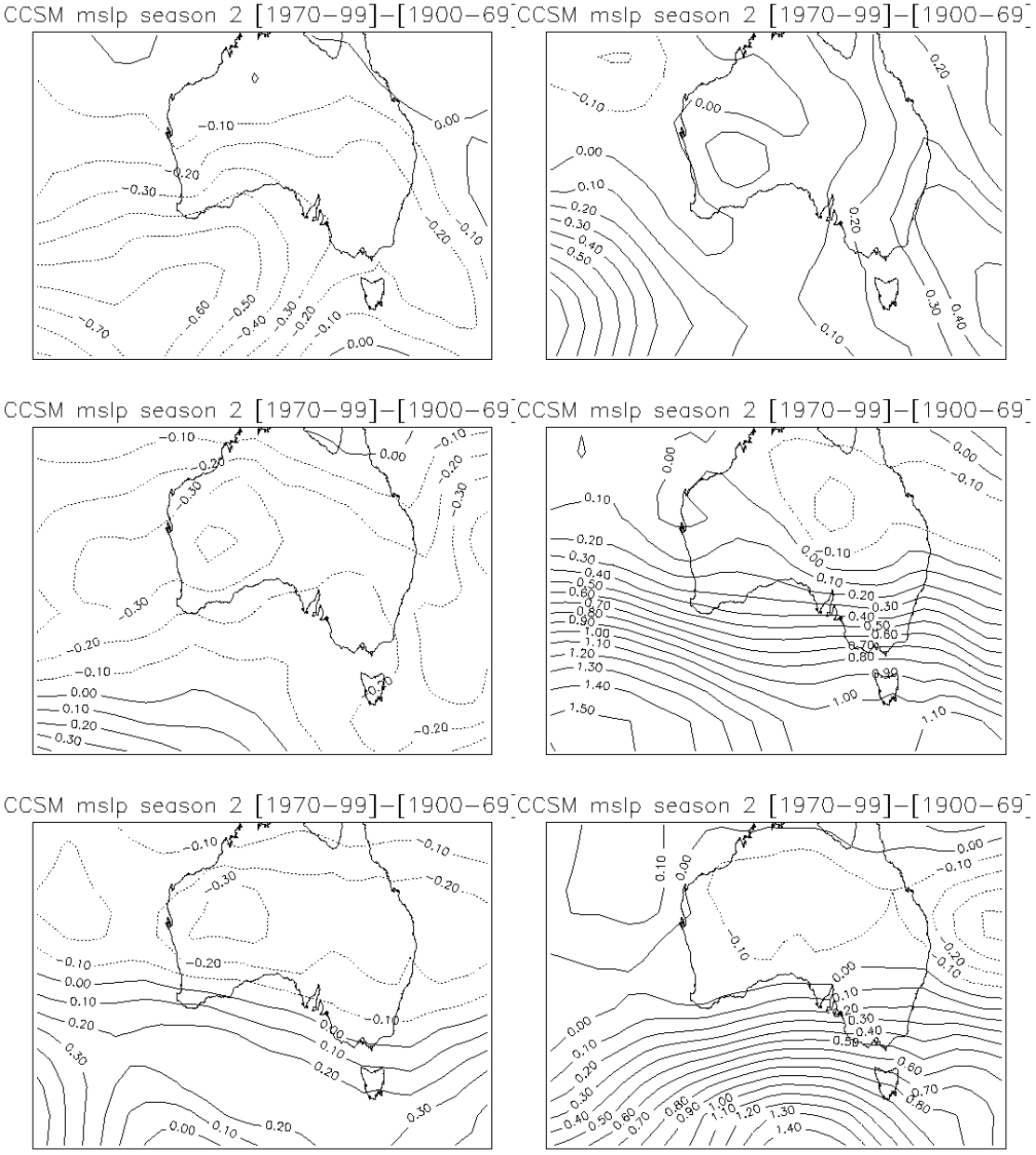

Fig. 39 *Maps of differences of autumn MSLP (in hPa) between 1970-1999 and 1900-1969, for individual simulations from the natural (top), anthropogenic (middle) and all forcings (lower) ensembles. The left column illustrates the lowest MSLP increase above southern Australia in each ensemble; the right column illustrates the largest MSLP increase.*

In order to assess the consistency of the signal in each ensemble, it is necessary to examine the changes evident in each of the 5 ensemble members. This is illustrated by showing MSLP changes in autumn in Fig. 39 for two very contrasted simulations for each ensemble. As expected, the internally generated natural variability in each ensemble member gives rise to differences in the changes evident in each ensemble. This internally generated variability masks the common externally forced response we are trying to identify. The spread is quite large compared to the changes evident in the ensemble means.

For the natural ensemble, MSLP is either declining by up to 0.2 hPa across SEA or increasing by the same amount. For the two other ensembles (anthropogenic and full forcings), all simulations exhibit a MSLP increase which is mostly zonal, with the largest values further south. However, the magnitude of the increase is quite different and leads to very different MSLP anomalies over SEA ranging from slightly negative (-0.1 to -0.2 hPa) to strongly positive (ranging from 0.3 to 0.7 hPa across SEA) in the case of the anthropogenic forcing. In the simulations for anthropogenic and natural forcings combined, the uncertainties of the response resemble those of the anthropogenic ensemble but are smaller. A similar analysis was conducted for the surface variables (rainfall, temperature). As expected, due to the noisy nature of rainfall 9compared to MSLP), the uncertainties in all three ensembles are very large and there is overlap between the ensembles (not shown). In contrast, for both T_{max} and T_{min}, individual simulations from the two ensembles show a more consistent signal, suggesting a significant difference between the two ensembles.

In order to better assess the significance of the changes simulated by each ensemble and to compare them with observed changes. Results were averaged across SEA and are shown over the century. Fig. 40 shows how well the model has captured the observed variability of MSLP over a large domain around SEA (between 120º and 160ºE and 20º and 50ºS: this is a larger domain than for SEA rainfall as MSLP has more spatial coherence) during the 20th century. The black solid line depicts the observational estimate based on HadSLP2 dataset (Allan and Anselm 2006). It is a 20-year running average from 1900 to 2008 with the century mean removed. The blue lines represent the 75% confidence interval for the same value from the natural ensemble. The confidence interval was estimated using:

$$\mu \pm 1.96 \times [1 + (1/\sqrt{\mathrm{N}})] * \sigma \quad \text{where}$$

μ is the ensemble mean of the 20-year running average of the natural ensemble, and

σ is estimated using seasonal means from the 5 simulations over the same 20 years.

The same confidence interval is shown for the anthropogenic (red lines) and full forcing ensembles (green lines), one panel per calendar season. All 20th century simulations were run until 1999 and, hence, the centred 20 year running mean stops in 1990. The last value given for example in 1990 corresponds to the 20-year average over 1980-1999. Because the fully forced simulations were used by NCAR as the starting point for the 21st century future projections using IPCC emission scenarios, we used the first 10 years of the simulations forced with the A2 scenario, which is very close to the observed emissions from 2000 to 2008 to extend the full forcings ensemble to 2008.

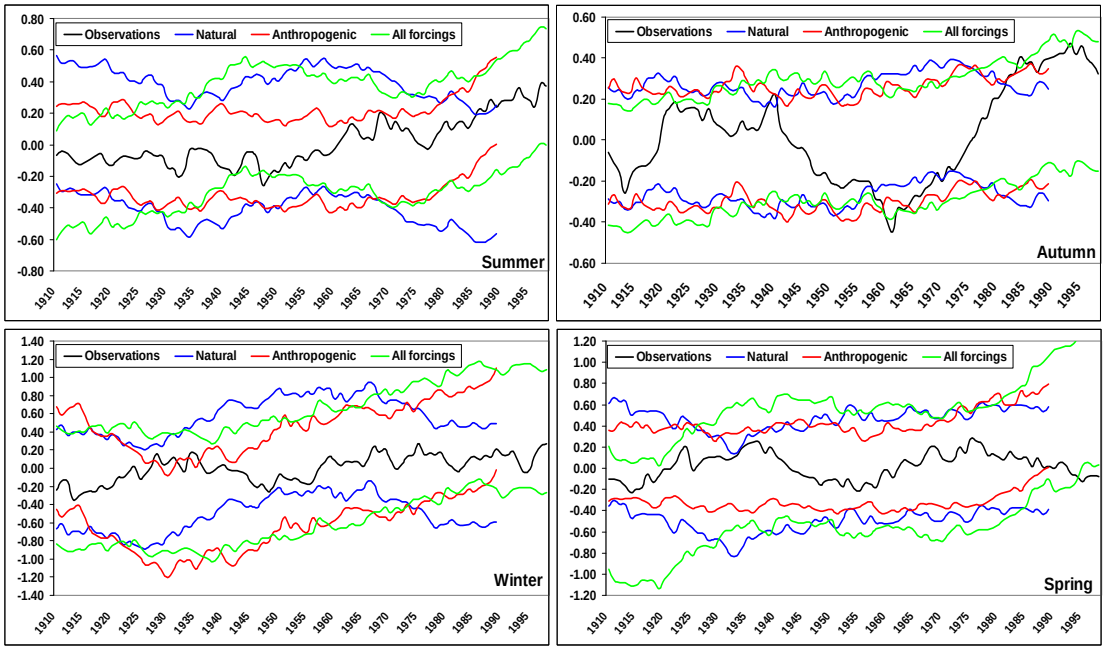

Fig. 40 *20-year running average from 1900 of observed MSLP anomalies from the 20th century climatology (in hPa) across SEA (black line, until 2008); estimates of the uncertainty range from the natural (blue), anthropogenic (red) and full forcings (green) ensemble at the 75% confidence level (see main text for details on the calculations); the full forcings ensemble is extended to 2008 using A2 emission scenario.*

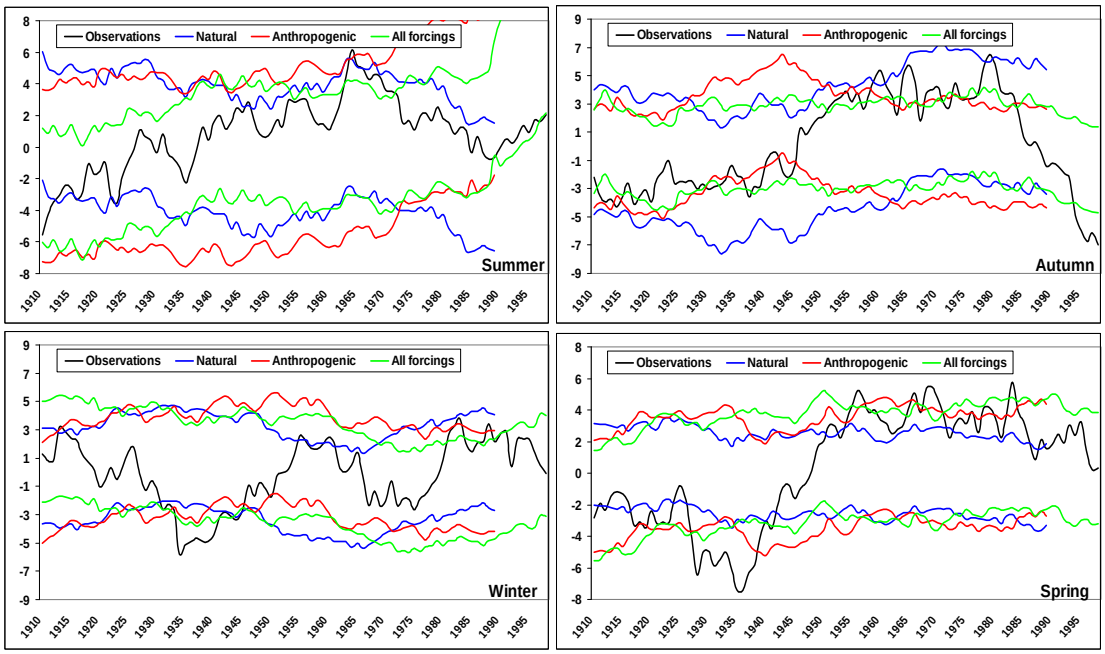

Fig. 41 *As per Fig. 40 but for precipitation (in mm).*

Similar results are depicted for rainfall (Fig. 41), where rainfall is averaged over the Australian mainland south of 33.5ºS and east of 135.5ºE (our definition of SEA) and compared with the BoM National Climate Centre (NCC) 0.25º gridded rainfall from the same region. Fig. 42 and

Fig. 43 show the same results for T_{max} and T_{min}, for which seasonal means of the observations over SEA are only available from 1950.

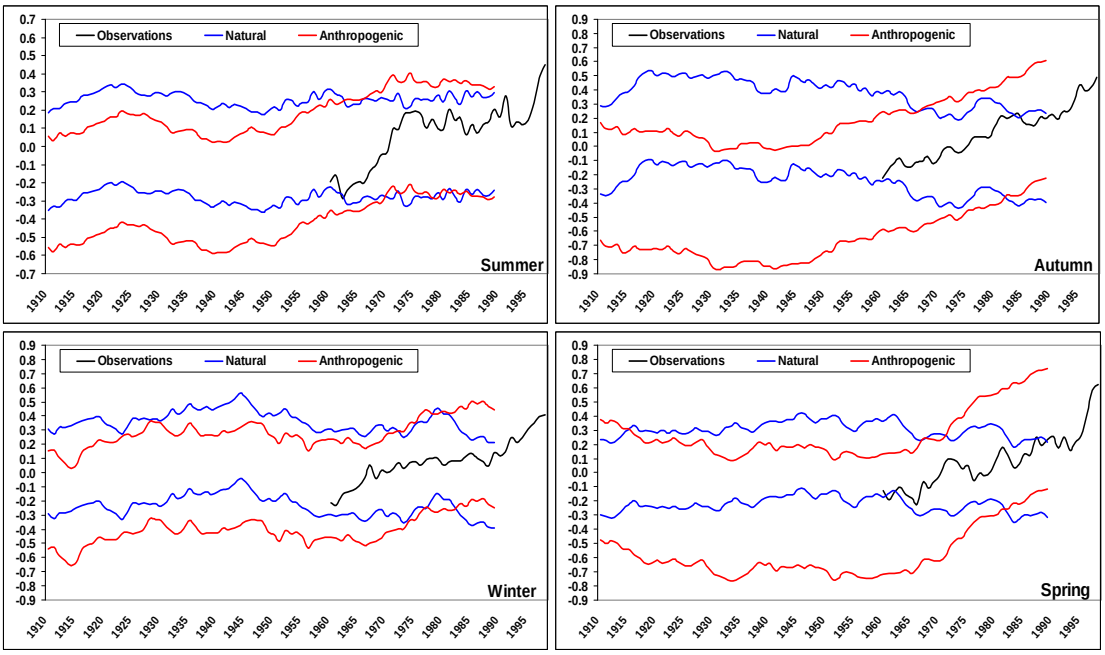

Fig. 42 *As per Fig. 40 but for T_{max} (in °C). No data are available for the full forcings ensemble.*

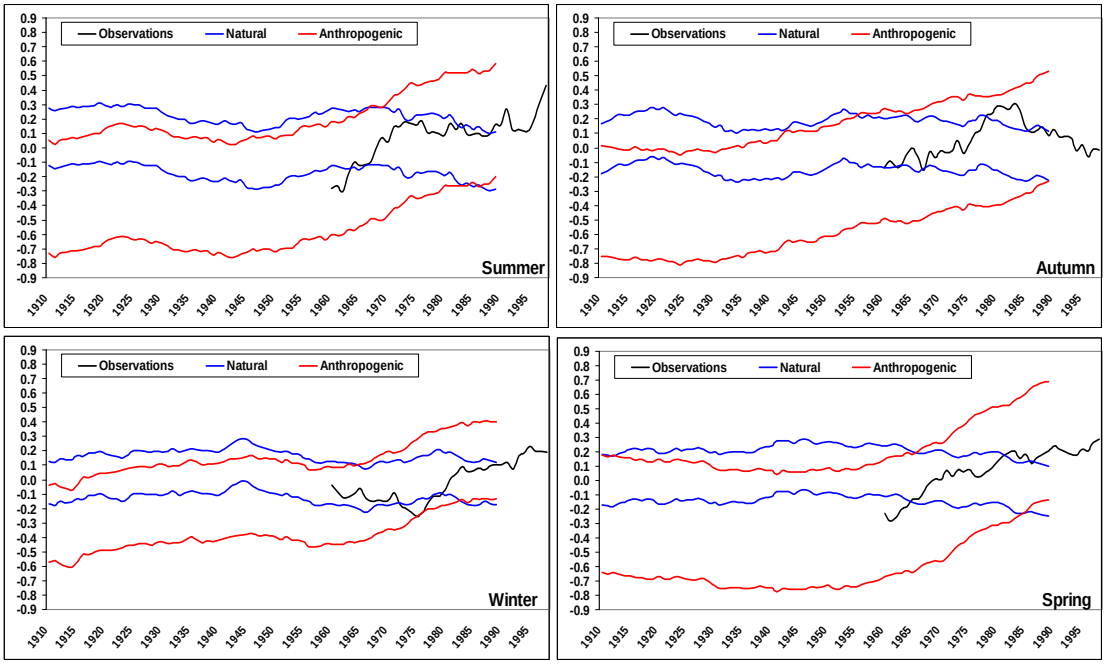

Fig. 43 *As per Fig. 40 but for T_{min} (in °C).*

For MSLP, no observed values appear as being outside the range of uncertainties of any particular ensemble. Even the most dramatic observed feature, the rise of MSLP in autumn from the 1960s to 2008, is mostly within the uncertainty range of all three ensembles. The lowest

value in the 1960s was slightly outside the range of all three ensembles and the most recent highest value on record appears to be outside the range of the natural ensemble, but within the 75% limit of the anthropogenic forcings and within the range of the full forcings ensemble. This confirms that the MSLP increase in autumn is best captured by the full forcings ensemble. However, the natural forcings ensemble cannot be totally discounted as it is expected that observations from time to time (25% over a century) would simply by chance fall outside a 75% confidence interval. The MSLP increase in summer is also more consistent with the full forcings ensemble. The anthropogenic forcings gives a stronger rise in the last 20 years than the observations. The natural forcings ensemble suggests declining values of MSLP. In winter and spring the observed MSLP variability over SEA is consistent with any of the three ensembles.

Not surprisingly for rainfall, a highly variable field, the observed time series in Fig. 41 often reaches the 75% limit in all the ensembles. In particular the very high rainfall observed during the 1960s to 1980s appears to be just at the upper limit of all three ensembles (most noticeably in spring). The recent low values in autumn as well as the low values in the 1930s and 1904s in winter and spring are beyond the 75% uncertainty level of all three ensembles. During the middle of the century, no particular ensemble appears to be lower than the other one. For the recent decline in autumn, the anthropogenic forcings and, more importantly, the full forcings ensemble (extended into the beginning of the 21st century using scenario A2) suggests a significant rainfall decline, albeit not as large as the decline that has been observed.

For surface temperature no attempt was made to extend results beyond the end of the 20th century as only natural and anthropogenic ensembles were available. In almost all cases, by the end of the century, the overlap between the two ensembles is reduced because the anthropogenic ensemble starts to track significantly higher values. However, by the end of the 20th century, none of the observed temperature anomalies across SEA are outside the 75% range of any ensemble. All black curves are getting close to the upper limit of the natural ensemble (most notably for T_{min}) and it is likely that the recent rapid rise at the beginning of the 21st century for T_{max} would push the limit of the natural ensemble if the simulation was continued during the last decade. But in the absence of the values for the early part of the 21st century, it is not possible to definitely attribute the observed trends of the late 20th century to external forcings as it is still consistent with the internally generated natural variability in any of the externally forced ensembles.

Following on the analysis of the CCSM3 DMOs, we will now look at the results of the statistical downscaling of the same three ensembles of simulations.

6.3 Reproduction of the drying trends across SEA using the SDM

The BoM SDM was applied to daily output from the five simulations of the three different ensembles with the CCSM3 model using the modified version of the optimised SDM to deal with the data limitations discussed earlier (Table 17). In order to assess the ability of the downscaled model simulations to reproduce the observed rainfall trends, linear trends were calculated over two periods 1980-1999 and 1960-1999 and averaged across the 324 rainfall stations used in the two climate entities, SWEA (Table 18) and SMD (Table 19), and for all four calendar seasons. Although 20 years is a short period to calculate reliable linear trends, it is

made necessary by the relatively short period of time since the start of the observed rainfall decline.

Table 18 *Averages across the 164 SWEA rainfall stations of the 20 and 40-years linear trends (in mm day^{-1} per century) fitted to the observations (left column) and to the downscaled reconstructed series, for each calendar season and each CCSM3 ensemble: with natural external forcings, anthropogenic external forcings and all forcings combined. The full range (min and max) for each ensemble is based on 6 SDMs applied to 5 simulations per ensemble (30 cases).*

		Obs	Natural forcings			Anthropogenic forcings			All forcings combined		
			average	min	max	average	min	max	average	min	max
DJF	**60-99**	0.05	-0.10	-0.57	0.59	0.09	-0.37	0.75	0.27	-0.31	0.73
	80-99	2.74	0.79	-0.56	2.22	-0.51	-2.21	1.84	0.18	-3.01	1.76
MAM	**60-99**	-1.23	-0.11	-0.94	0.61	-0.38	-1.34	0.40	-0.61	-1.16	0.11
	80-99	-2.64	-0.05	-2.20	1.55	-0.84	-3.60	0.57	-1.25	-4.43	0.39
JJA	**60-99**	0.63	0.44	-0.62	1.76	-0.36	-0.98	0.14	-0.15	-0.83	0.39
	80-99	-1.55	0.93	-0.97	5.01	0.23	-1.56	1.70	-0.20	-2.05	1.76
SON	**60-99**	0.49	0.08	-0.37	0.65	-0.13	-0.82	0.45	-0.06	-0.78	0.73
	80-99	1.93	1.26	-0.52	3.27	-0.15	-2.43	2.39	-0.72	-2.82	0.40

Table 19 *As per table 18 but for the 160 stations in SMD.*

		Obs	Natural forcings			Anthropogenic forcings			All forcings combined		
			average	min	max	average	min	max	average	min	max
DJF	**60-99**	-0.09	-0.20	-1.31	1.38	0.09	-0.78	1.25	0.38	-0.10	0.98
	80-99	2.23	0.65	-2.23	3.95	-2.03	-4.35	0.62	1.35	-1.67	3.70
MAM	**60-99**	-0.55	0.10	-0.85	1.21	-0.25	-1.02	0.58	-0.29	-0.91	0.61
	80-99	-1.61	1.01	-2.33	4.02	-0.39	-3.76	2.75	-0.82	-3.90	1.85
JJA	**60-99**	0.73	0.36	-0.71	1.84	-0.02	-0.52	0.56	-0.36	-0.99	0.47
	80-99	-0.71	0.78	-1.01	2.28	0.23	-3.29	2.67	-0.27	-2.99	3.61
SON	**60-99**	0.28	0.10	-0.93	0.95	0.02	-1.50	1.11	0.06	-0.86	1.01
	80-99	3.83	1.15	-0.79	3.93	-0.10	-3.32	2.84	-1.31	-3.61	0.20

The ranges of linear trends are provided for each ensemble and both periods as well as the ensemble mean. Histograms of the linear trends are also presented (Fig. 44). The histograms comprised 30 cases for each ensemble: five simulations time six different SDMs. The different SDMs are obtained by perturbation of three parameters of the SDM. The histograms show the linear trends for the shorter periods. Despite the higher uncertainties, they better capture the magnitude of the recent rainfall decline across SEA which is only apparent in most seasons and regions in the trends calculated since 1980 and not in the trends since 1960.

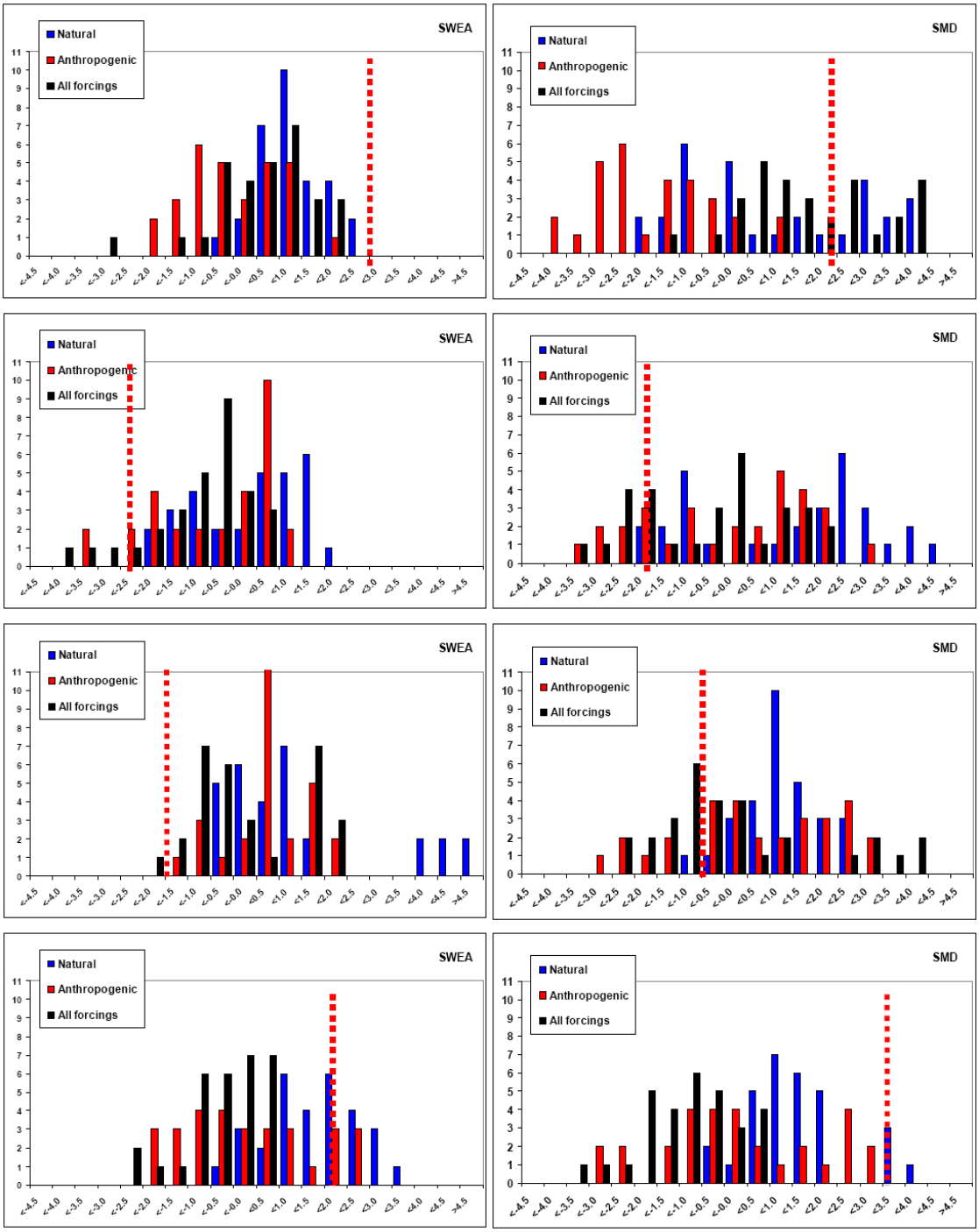

Fig. 44 *Histograms (number of cases) of the linear 1980-1999 rainfall trends (in mm day^{-1} per century) obtained from the downscaling of CCSM3 ensembles (with natural, anthropogenic and combined external forcings) for SWEA (left) and SMD (right) and the four calendar seasons (summer to spring from top to bottom). Observed trends are shown as dashed red line.*

It is worth noting that although the rainfall decline across SEA is generally observed since 1996 (Timbal and Murphy 2008), at which time there was a noticeable step change in the rainfall series (and more particularly in streamflows), it is clear from the observed rainfall curve shown earlier (Fig. 41) that in autumn, winter and spring, rainfall across SEA has been declining since

the early 1980s. Starting from a higher than normal base at the end of the very wet 1960s and 1970s, the average rainfall has only fallen below the long-term average since the mid 1990s. In terms of linear trends, negative linear trends are consistently obtained for any period since 1980.

The most significant feature affecting SEA climate is the autumn rainfall decline which is larger in SWEA than in SMD. A key finding is that the observed autumn rainfall decline is outside the range of linear trends from the statistical downscaling of the natural ensemble. Taken at face value this mean that the observed decline in autumn rainfall is unlikely to be caused by naturally forced or naturally internally generated variability alone.

On the other hand, the observed autumn rainfall time series is not outside the range for the other two ensembles, although the negative mean trends in both ensembles are smaller than the observed value. The histogram illustrates the magnitude of uncertainties for all three ensembles. The tail of the distribution encompasses the observed value for the anthropogenic and full forcing ensembles. In SMD where the observed trend is slightly less, the spread amongst ensembles even larger and the observed value is not outside the range obtained from the downscaling of the natural ensemble members. But again, only the anthropogenic and full forcings ensembles have mean negative trends in SWEA, and the full forcing ensemble is the closest to the observed trend.

In winter in both SWEA and SMD, results are very similar to those of autumn, with the natural ensemble suggesting a rainfall increase and the full forcings ensemble providing the simulation closest to observed. The observed trends lie within the range of all 3 ensembles.

In spring, all three ensembles are very consistent with the winter signal: a rainfall increase with the natural ensemble, a small decrease with the anthropogenic forcing and a larger decrease in the full forcing ensemble. However, no rainfall decrease has been observed in spring during 1980-1999. It is only in the latest decades that spring rainfall in SEA has started to decline: in SWEA the linear trend for the observations from 1980-2008 is -0.19 mm day^{-1} per century, accelerating during 1990-2008 to -3.39 mm day^{-1} per century.

Finally, the observed rainfall increase in summer is better captured by the natural and the full forcings ensembles and less by the anthropogenic forcings ensemble (i.e. in SMD, the observed trend is outside the uncertainty range of the anthropogenic ensemble).

6.4 Reproduction of warming trends across SEA using the SDM

The BoM SDM was also applied to generate daily temperatures at 41 locations across SEA. The optimised SDM was adapted to deal with data availability from the CCSM3 archive (Table 17). As per rainfall, linear trends were calculated on the reconstructed series for 1960-1999 and 1980-1999, and averaged over SWEA and SMD. Results for T_{max} are presented in Table 20 and 21 and for T_{min} in Table 22 and 23.

Table 20 *As per table18 but for T_{max} based on 22 SWEA stations (in ºC per century).*

		Obs.	Natural forcings			Anthropogenic forcings			All forcings combined		
			average	min	max	average	min	max	average	min	max
DJF	**60-99**	0.94	-0.40	-1.76	0.50	0.58	-0.72	1.49	0.91	-0.33	2.29
	80-99	-0.92	0.41	-1.12	2.66	0.00	-3.51	2.84	-0.55	-2.16	0.96
MAM	**60-99**	1.46	-0.36	-1.51	0.98	0.80	-0.59	2.91	1.56	0.30	3.86
	80-99	-3.10	-0.40	-4.46	4.85	1.53	-1.29	5.28	0.76	-1.96	4.14
JJA	**60-99**	1.50	0.02	-0.63	0.83	0.46	-0.64	1.40	0.89	0.12	1.40
	80-99	1.84	-0.43	-2.32	0.60	-0.01	-1.83	1.85	0.19	-0.99	1.51
SON	**60-99**	0.99	-0.37	-1.97	0.87	1.73	0.21	3.38	1.19	-0.40	2.61
	80-99	-2.81	-0.54	-3.21	2.12	1.19	-0.82	3.70	1.49	-2.08	7.42

Table 21 *As per table 20 but for T_{max} based on 19 SMD stations (in ºC per century).*

		Obs.	Natural forcings			Anthropogenic forcings			All forcings combined		
			average	min	max	average	min	max	average	min	max
DJF	**60-99**	1.66	-0.34	-1.09	1.38	-0.02	-0.83	1.17	1.00	-1.00	1.83
	80-99	-3.52	-1.46	-4.73	0.33	0.05	-2.92	2.79	-0.31	-1.69	1.13
MAM	**60-99**	1.47	-0.25	-1.91	1.48	1.04	-0.49	3.67	1.53	-0.29	3.92
	80-99	-2.05	-1.07	-4.58	4.83	1.25	-2.23	4.57	0.41	-2.71	4.57
JJA	**60-99**	1.11	-0.01	-1.04	1.08	0.85	-0.47	2.30	1.38	0.29	2.44
	80-99	3.13	-0.61	-3.00	0.71	0.21	-3.45	3.13	0.34	-2.33	3.21
SON	**60-99**	0.23	-0.67	-2.25	0.87	2.13	0.77	3.60	1.04	-1.45	2.12
	80-99	-5.64	-1.19	-2.35	0.18	0.85	-1.21	4.87	1.54	-3.21	6.45

Table 22 *As per table 20 but for T_{min} in SWEA (in ºC per century).*

		Obs.	Natural forcings			Anthropogenic forcings			All forcings combined		
			average	min	max	average	min	max	average	min	max
DJF	**60-99**	0.55	-0.25	-1.15	0.48	0.65	0.05	1.52	0.67	-0.53	1.34
	80-99	1.40	0.31	-0.79	1.54	0.83	-1.83	3.71	0.12	-0.92	2.04
MAM	**60-99**	0.26	-0.06	-0.65	0.81	0.44	-0.65	1.04	0.59	-0.60	1.51
	80-99	-4.70	-0.07	-1.61	1.42	0.76	-1.29	2.06	-0.14	-2.34	3.02
JJA	**60-99**	1.44	0.38	-0.55	1.07	0.27	-1.07	0.99	0.59	0.17	1.41
	80-99	1.18	0.54	-0.98	2.60	0.42	-1.13	2.47	0.50	-0.68	1.89
SON	**60-99**	1.20	-0.30	-1.78	0.95	0.72	0.15	1.36	0.50	-0.36	1.30
	80-99	-1.02	-0.40	-2.68	1.58	0.45	-0.55	1.45	0.57	-1.06	3.80

Table 23 *As per table 20 but for Tmin in SMD (in ºC per century).*

		Obs.	Natural forcings			Anthropogenic forcings			All forcings combined		
			average	min	max	average	min	max	average	min	max
DJF	**60-99**	1.02	-0.38	-1.22	0.90	0.20	-1.02	1.37	0.86	-0.48	1.84
	80-99	1.01	-0.92	-2.68	2.37	-0.89	-4.45	1.08	-0.23	-2.34	2.54
MAM	**60-99**	0.12	0.24	-1.35	1.25	0.48	-0.85	1.31	1.34	-0.38	3.62
	80-99	-6.34	0.24	-2.27	3.63	1.36	-0.72	3.53	-0.04	-5.09	4.29
JJA	**60-99**	0.90	0.60	-0.56	1.36	0.41	-0.94	1.57	0.68	-0.29	1.38
	80-99	1.01	1.13	-1.86	4.73	0.53	-1.09	2.07	0.65	-1.65	2.16
SON	**60-99**	0.59	-0.19	-1.35	0.62	1.30	0.32	2.03	0.74	-0.42	1.86
	80-99	-0.35	0.22	-1.54	3.34	0.09	-1.26	1.70	0.56	-1.76	4.41

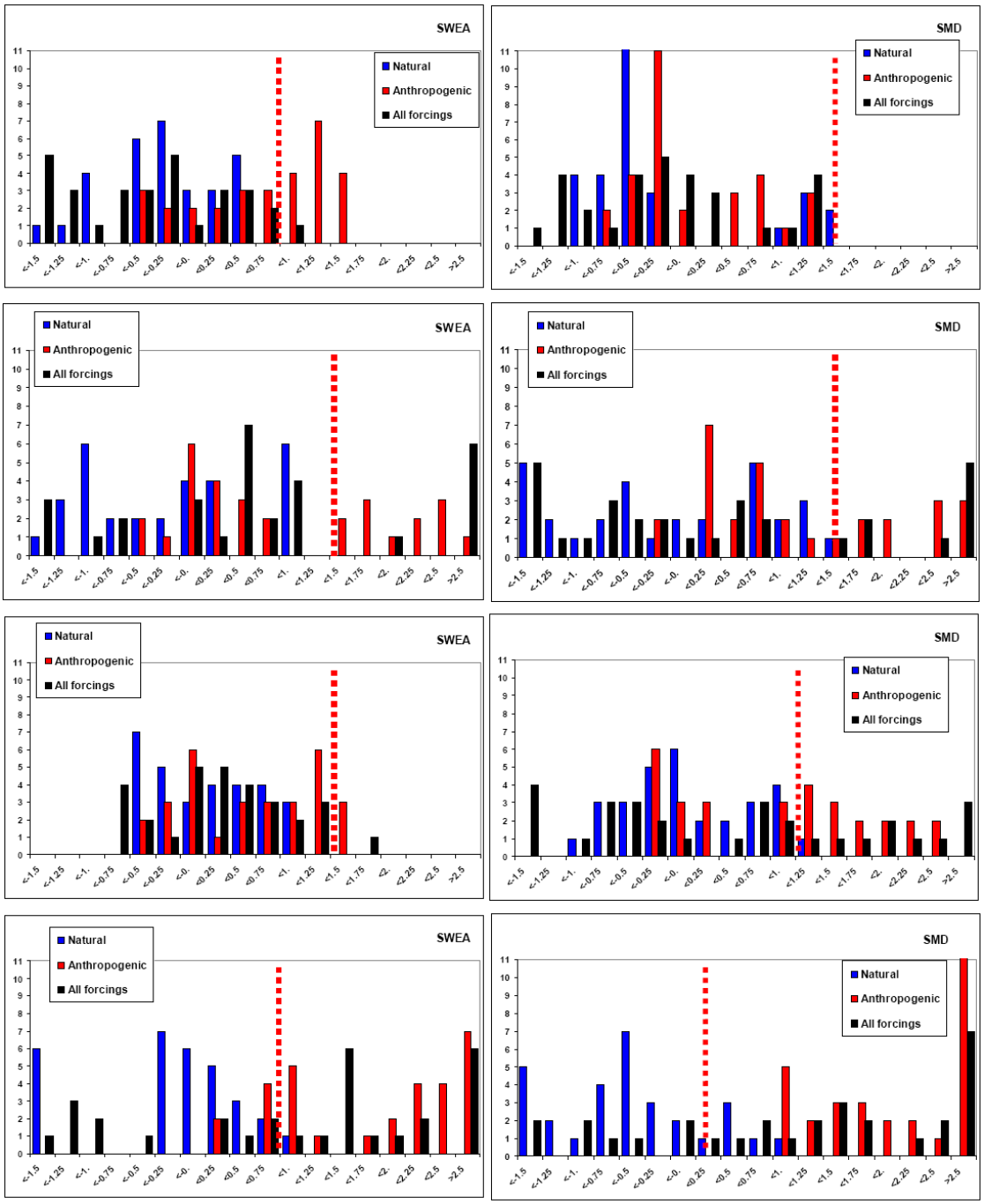

Fig. 45 *As per Fig. 44 but for the 1960-1999 T_{max} trends (in ºC per century).*

In contrast to rainfall, the ongoing warming is seen in the observational record from earlier on. As a consequence, as the longer term trends are more stable, we will focus on the linear trends calculated from 1960 to 1999. Accordingly the histograms of the trends calculated from the 30 cases for each ensemble are shown for this 40 year period (Figures 45 and 46).

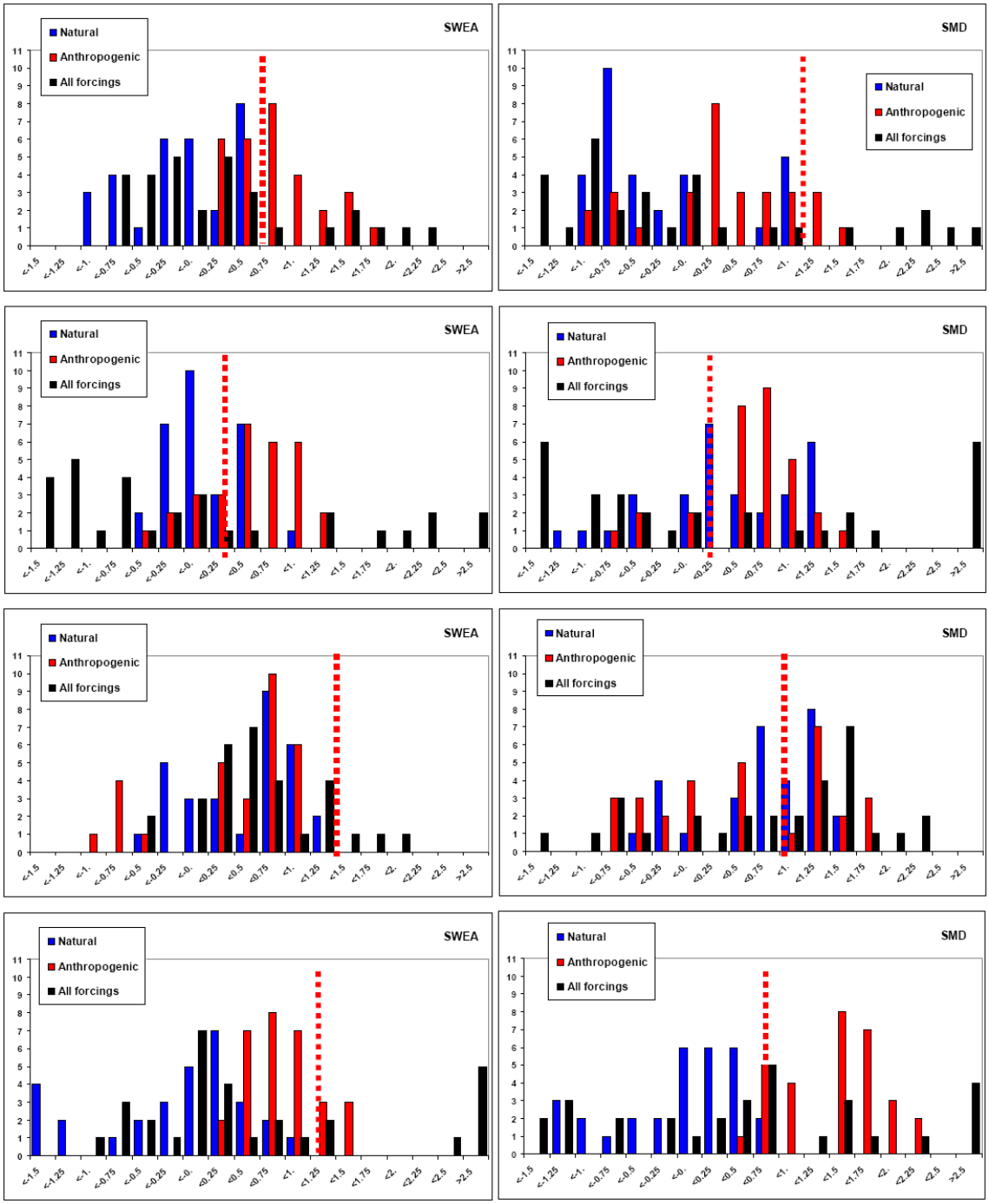

Fig. 46 *As per Fig. 44 but for T_{min}.*

Downscaled results are presented in Figures 44 and 45. They are very consistent with DMO. In general, the observed trends are outside the range of variability evident in the natural ensemble. This is the case for T_{min} in summer in both regions and in winter and spring in SWEA. It is also true for T_{max} in both regions in summer and winter, and in autumn and spring in SWEA.

In stark contrast to the natural ensemble, the observed trends are almost always within the range of variability in the downscaled full forcings ensemble. In all cases, the best match between observed and downscaled is obtained from the full forcings ensemble. The mean of this

ensemble is closer to the observed values than any other ensemble mean in all cases for T_{max} and in most cases for T_{min} (although there are a few instances where the mean from the anthropogenic ensemble is closer to the observed value). The observed value is nearly always within the range of uncertainties obtained from the downscaling of the full forcing ensemble (the sole exception is winter in SWEA).

It is therefore very clear that natural forcings alone are not able to explain the observed warming across SEA. And while anthropogenic forcings alone provides good estimates, the full forcings provide the best match.

Since all ensembles can be compared using the downscaling results, it was found interesting to redo the century long evolutions of the uncertainties of each ensemble (shown for DMOs in Fig. 42 to 43) using the downscaled stations results averaged across the entire SEA (Fig. 47 to 48).

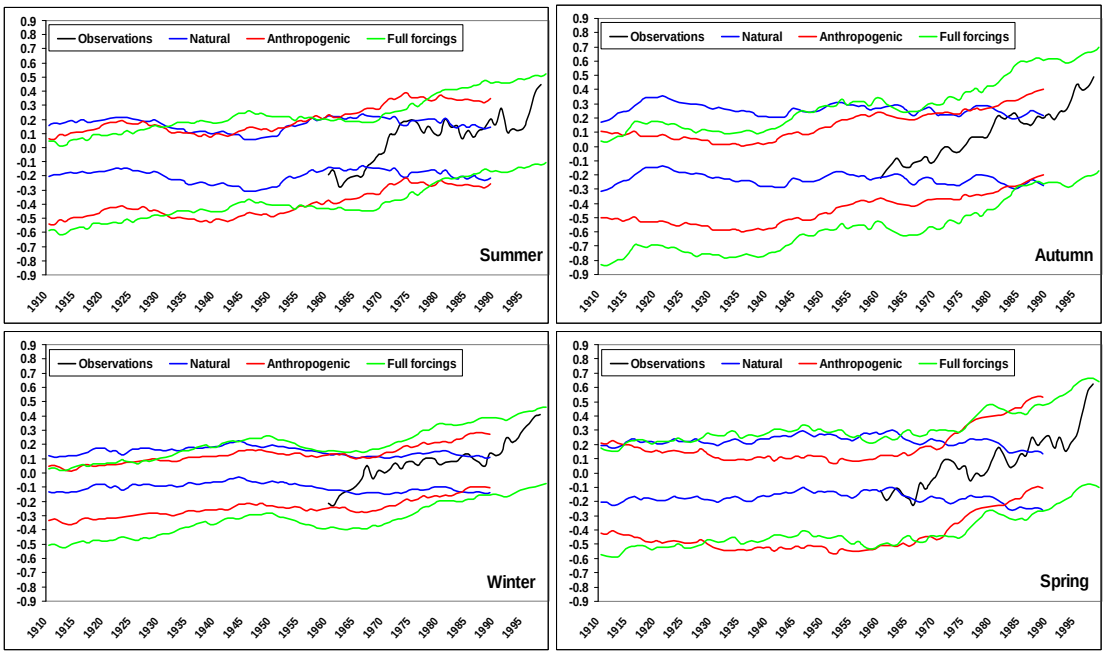

Fig. 47 *As per Fig. 42 but for downscaled T_{max} series (in °C). The ensemble uncertainty range is based on the 90 percentile instead of the 75 percentile as in Fig. 41.*

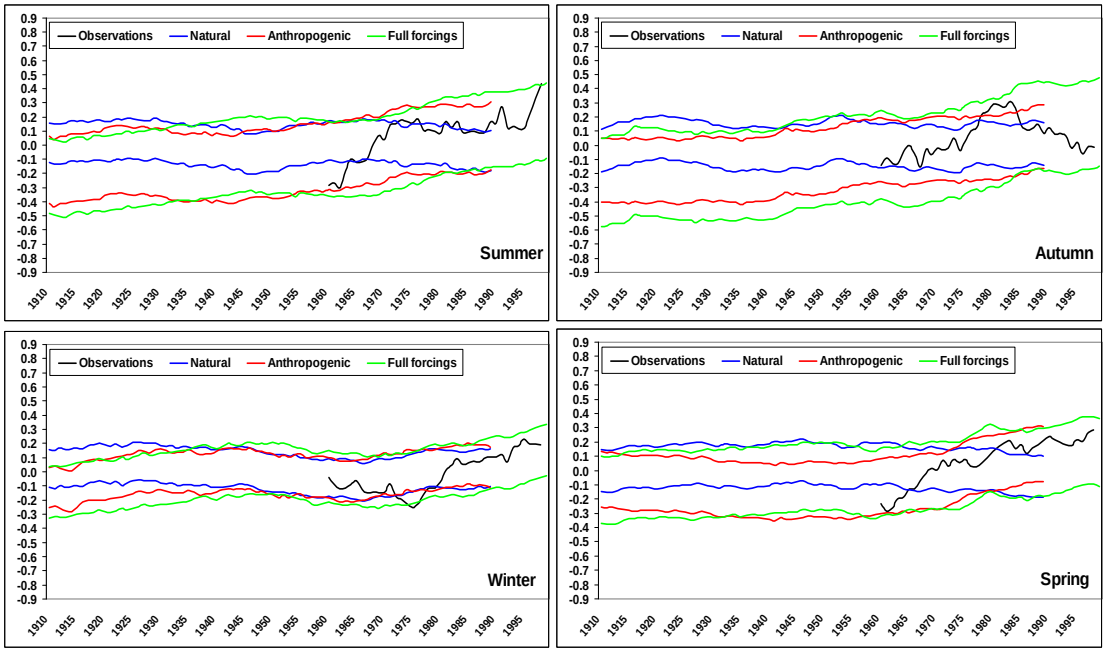

Fig. 48 *As per Fig. 47 but for T_{min}.*

For temperature, the new graphs show the improvement resulting from using statistical downscaling versus DMOs. The statistical downscaling of the CCSM3 ensemble provides a narrower band of uncertainty than does DMOs. This allows us to use the 90% confidence interval instead of 75% in Fig. 47 and 48.

The fact that the observations in the most recent decade are often sitting at the edge of the natural ensemble uncertainty range (upper blue line) provides further evidence that the most recent warming observed across SEA is not consistent with natural forcings alone. In addition, we were able to obtain downscaled values for the full forcings ensemble and its continuation into the early 21st century using the A2 emissions scenario (green lines). Even during the first decade of the 21st century, the downscaling of the CCSM3 model forced with full forcings tracks the observations very well, including the recent acceleration of warming for T_{max} due to the ongoing drought, as well as the T_{min} reduction in autumn which is also contributed to by the rainfall anomaly in that season.

The overall picture for rainfall (not shown) is not much different. In autumn, the current rainfall decline is clearly now within the range of the full forcings ensemble but stretches the bounds of uncertainties of the other two ensembles.

6.5 Conclusions

The application of the BoM SDM to simulations of the 20th century with the NCAR CCSM3 climate model externally forced with natural and anthropogenic forcings has permitted a full attribution study of the observed surface climate changes (temperature and rainfall) across SEA.

The application of the SDM provides additional information to the DMO, and in some instances provides a clearer picture. For example it allows ruling out as extremely unlikely (i.e. not capture with the ensemble sample size available) natural forcings as a possible explanation for some of the observed trends, namely:

1. most of the observed surface warming; and
2. the large autumn rainfall decline across SWEA.

Overall, the large-scale changes important to an understanding of the observed changes in SEA climate are better represented by the CCSM3 model when a full set of forcing (combining natural and anthropogenic forcings) is used.

In many instances, most of the changes (trends or differences) are already captured using anthropogenic forcings alone, therefore suggesting that anthropogenic forcings are the most important to reproduced observed climate trends. But a more realistic behaviour is observed when both anthropogenic and natural forcings are applied simultaneously. This is consistent with the general understanding that combining both types of forcings provides the most realistic on-going external forcings of the climate system.

SUMMARY

The analysis of the direct model outputs (DMOs) from the CCSM3 climate model series of ensembles shows that:

- The model forced with natural external forcings only shows: 1) no build up of surface pressure in autumn-winter-spring as observed; 2) small rainfall increases in these seasons; and 3) no surface warming for either T_{min} or T_{max} in any season

- The model forced with anthropogenic external forcing shows: 1) a build up of surface pressure which resembles the observed strengthening of the STR; 2) a significant surface warming for both T_{min} and $T_{max;}$ but 3) only a weak rainfall decline that occurs mostly in winter rather than in autumn.

Downscaling of the CCSM3 ensembles using the BoM SDM leads to the following valuable, additional conclusions:

- The recent observed rainfall decline in autumn is outside the range of variability (at least in parts of the SEACI domain) evident in the naturally forced ensemble.

- The mean response from the naturally forced ensemble pointed toward significant rainfall increases in autumn, winter and spring across SEA and therefore does not match the observations.

- In contrast, the two ensembles forced with anthropogenic forcings alone, and with anthropogenic forcings combined with natural forcings, point toward rainfall declines in the last 20 years: large in autumn and spring and small in winter.

- The largest rainfall decline is most often obtained from the ensemble combining both natural and anthropogenic external forcings (rather than anthropogenic forcings alone). The model rainfall decline is smaller (only about 50%) than the largest observed declines in autumn but comparable to observed values in the other seasons.

- The downscaling of CCSM3 provides a more definitive attribution of the ongoing surface warming across SEA for both T_{max} and T_{min}. The most recent temperature values are outside the 90% range of uncertainty obtained from the naturally forced ensemble. In contrast, the fully forced ensemble extended to 2008 using the A2 scenario matches the observed temperature trends very well.

In summary, the downscaled results indicate that the observed decline is much more likely to occur when anthropogenic forcing is applied than without.

7 REPRODUCTION OF THE SUB-TROPICAL RIDGE IN 20TH CENTURY CCM3 SIMULATIONS

Following on from the demonstration of the ability of the CCSM3 model to reproduce realistic changes of the climate system during the 20th century provided anthropogenic forcings are used (Chapter 6), it was decided to investigate if the key mechanism of the STR intensification identified earlier (Chapter 3) is being reproduced by the CCM3. To do so, the Drosdowsky (2005) methodology is used to diagnose trends in both the STR intensity and position in the different ensembles of simulations of the 20th century forced with natural, anthropogenic forcings and the combination of both.

7.1 Adapting the methodology to the CCSM3 simulations

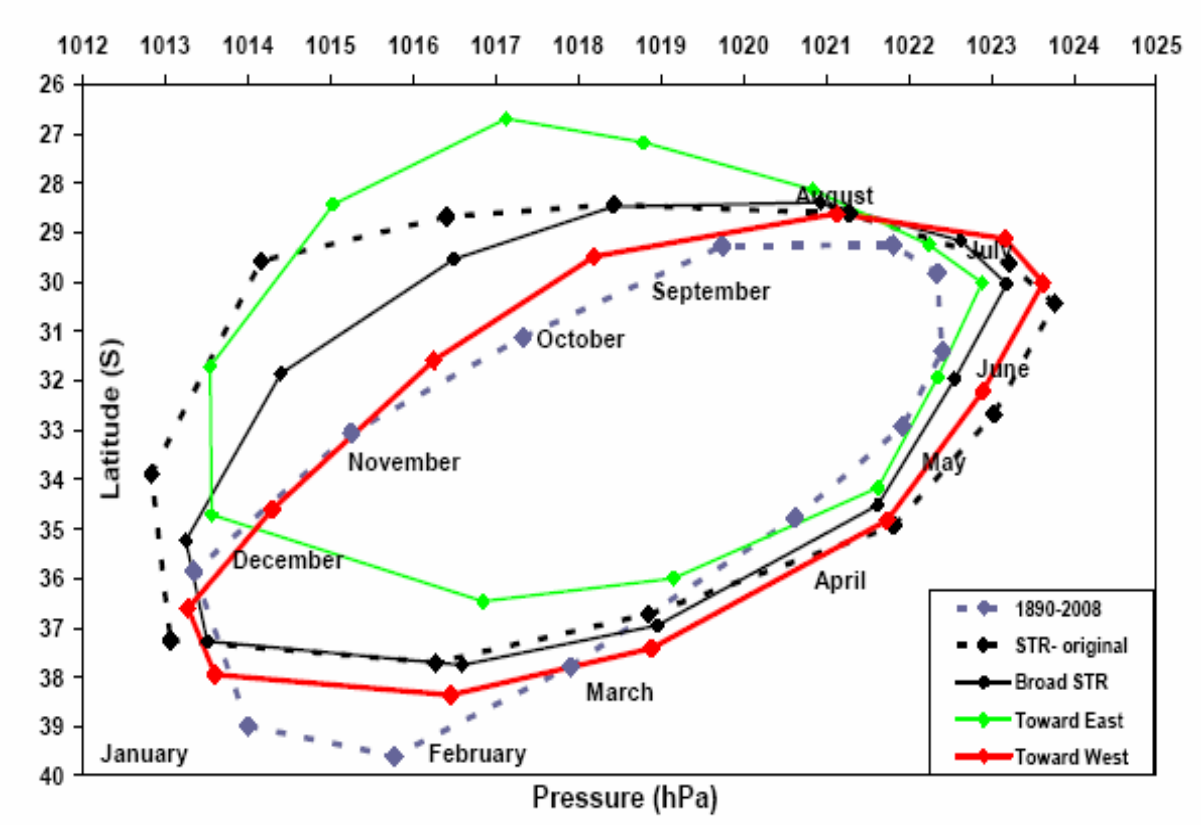

Fig. 49 *Annual cycle of the sub-tropical ridge intensity (X-axis) and position (Y-axis) from the observations (dashed grey line) and diagnosed from a CCSM3 simulation of the 20th century using different longitude bands (see text for details).*

The ability of the CCSM3 to reproduce a realistic STR in the vicinity of Australia was assessed using the methodology used by Drosdowsky (2005) to calculate observed STR position and intensity. One difference is that monthly values of observed MSLP used by Drosdowsky were on a 1 by 1º grid, while the CCSM3 has a resolution of 1.4 by 1.4º. Monthly values of MSLP were first averaged over a longitude band from 145 to 150ºE (i.e. 4 longitudes for CCSM3).

In order to provide a close match to Drosdowsky (2005), the location of the STR was defined as the latitude of the maximum pressure between 44ºS and 10ºS (42.7ºS and 10.5ºS in the case of the CCSM3); and the intensity of the STR was defined by the value of this maximum. Diagnosed this way, the annual cycle of the STR position and intensity in the CCSM3 model was relatively poor (Fig. 49); in particular the ridge was diagnosed up to 4º too far north in spring. In order to provide a better reproduction of the annual cycle, the STR was subsequently diagnosed using a broader band of longitude (between 139.2 to 154.7ºE). Finally, two additional longitude bands were tried: one further east (green curve: 146.2 to 154.7ºE) and one further west (red curve: 137.8 to 149.1ºE). The most accurate reproduction of the observed STR annual cycle (intensity and position) was found with the latter (i.e. the further west) option.

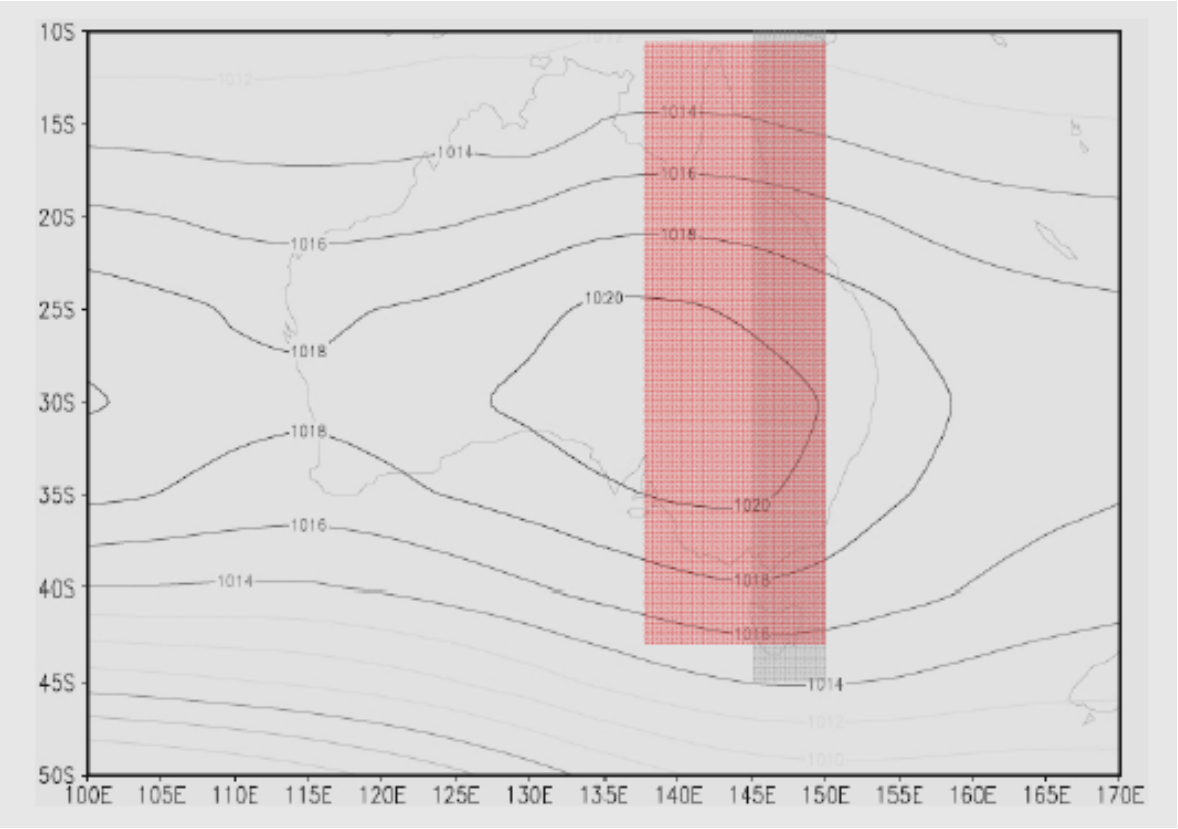

Fig. 50 *Geographical area used to diagnose the STR in the observations (grey band) and in the CCSM3 simulations (red band) overlaid above the long-term 1850 to 2004 mean of MJJ MSLP from the HadSLP2 dataset around the Australian continent.*

All year round, monthly modelled values are, on average, within 0.8º and 0.9 hPa of the observed values. While the simulation is very good, it is not perfect: the intensity of the modelled STR is too large from April to July (largest error is 1.2 hPa in June) and the position of the modelled STR is not as far south as observed (by about 1 to 1.2º) in January and February. Overall, while keeping these errors in mind, the ability of the model to produce a STR similar in location, intensity and with the right annual cycle was found to be suitable, providing the STR is diagnosed on a broader longitude band than for the observations (Fig. 50). The larger band further west better encompasses the actual location of the observed maximum

pressure during the peak of the STR intensity in May-June-July, which is centred on the Australian continent and it also overlaps better with the SEACI area of interest. It is also worth noting that the choice to use a narrow band along the eastern seaboard was driven in part by the availability and reliability of long climatic record of MSLP (Drosdowsky, pers. comm.). This is a concern that we do not have with model data.

7.2 Decadal STR trends in CCSM3 simulations

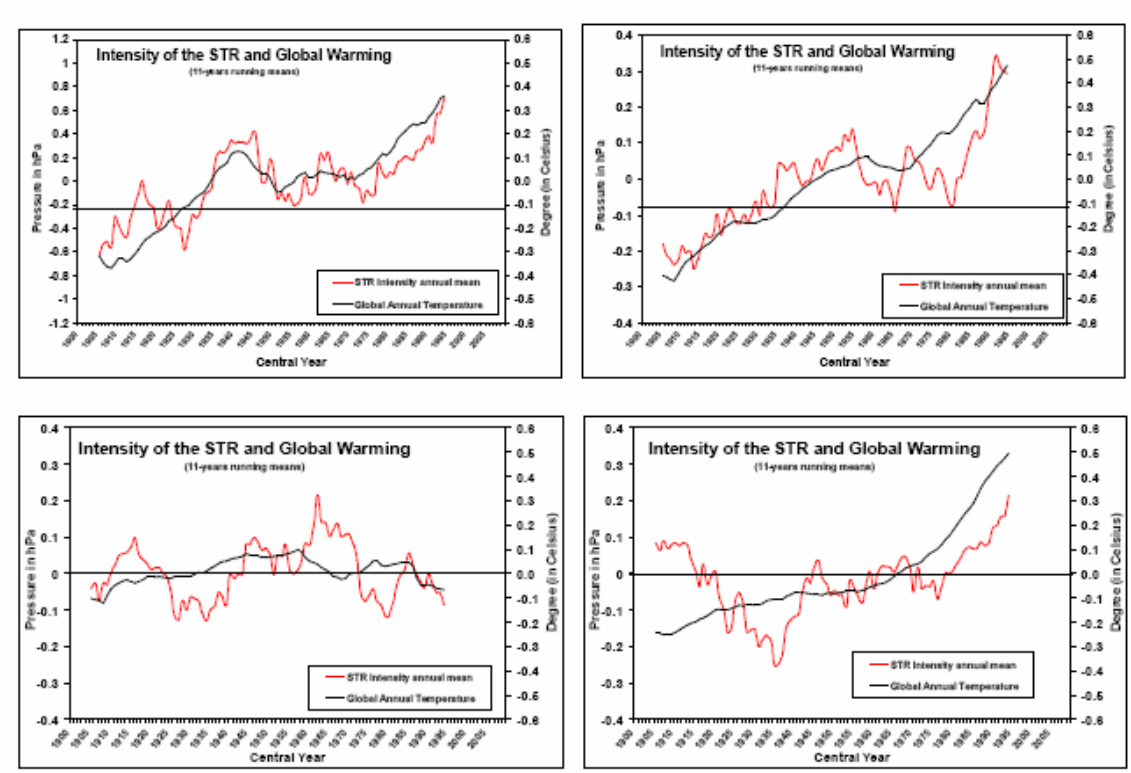

Fig. 51 *11-year running means of anomalies of annual STR intensity (in hPa on the left Y-axis) and global temperature (in ºC on the right Y-axis) calculated from the century long climatology for the observations (top left), the ensemble of CCSM3 simulations with full forcings (top right), natural external forcings only (bottom left) and anthropogenic external forcings only (bottom right).*

For each CCSM3 simulation, 11-year running means were computed for STR intensity, position and global average temperature. Anomalies, expressed relative to the 1900-1999 climatology, are shown as a single average from the 5 members of each of the three ensembles and are compared with the observations (Fig. 51). Running means are used to remove inter-annual variability and to focus on the results at decadal and centennial time-scales. With full forcings (which are expected to provide the most realistic external forcings), the model response is very similar to the observations. The model produces a global warming similar in magnitude to the observations (about 0.9ºC over the century compared to 0.8ºC for the global temperature dataset (Climatic Research Unit, University of East Anglia, UK, Brohan et al. 2006) and a strengthening of the STR. The GW and intensification of the STR appear to occur simultaneously in the model as they do in the observations (Fig. 51). In both the observations

and model simulations, epochs of warming alternate with periods of no significant warming trends. For example, warming occurs from around 1900 to the 1940s and from 1970 to now in the observations. This compares with warming from 1900 to the 1950s and from 1975 to now in the model. Similarly, the STR strengthening is not regular with time and appears to plateau at the time when no significant warming occurred (e.g. around the middle of last century). The covariance of the GW and STR in the CCSM3 simulations reinforced earlier suspicions that the observed relationship did not occur by chance. Instead it appears to be linked to large-scale changes in the climate system dynamics and energetics, most likely involving the transfer of energy from the Equator to higher latitudes through meridional circulations (e.g. the Hadley Cell). The mechanics of these changes in circulation are further discussed in the theoretical modelling section.

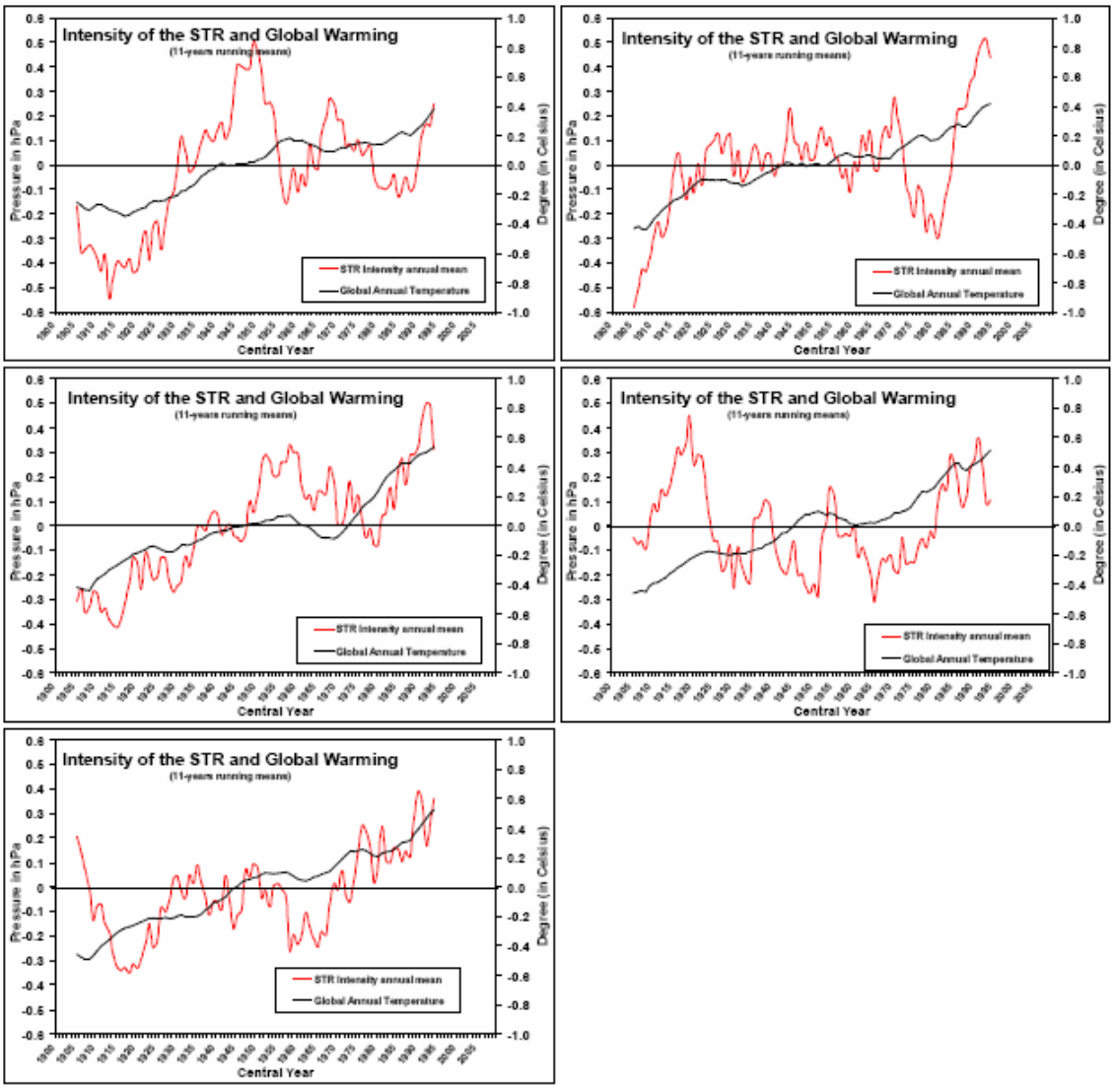

Fig. 52 *As per Fig. 51 but for the five individual simulations forced with full forcings (Note: both Y-axis scales differ from Fig. 50).*

The strengthening of the STR in the ensemble mean (about 0.6 hPa for the full forcings ensemble) is much reduced compared to the observed values (1.2 hPa). Note: the Y-axis scale

for the STR intensity is on the left of the graph (the right Y-axis is for temperature) and, while the right scale is unchanged between graphs, the left scale is amplified by a factor 3 for model results compared to the observations. This result is consistent with earlier findings for MSLP changes in the northern hemisphere (Gillett et al. 2003) and is worth exploring further by looking at individual members of the full forcings ensemble (Fig. 52) to avoid the smoothing issue that arises when comparing an ensemble of simulations with a single realisation for the observations. Individual simulations exhibit much more dramatic rises and falls during the 20th century, typically of the order 1 hPa over a 20 to 40 year period, which is comparable to observed rises of 1 hPa in the 1930s and 1940s and 0.8 hPa since the 1970s. However centennial trends for individual ensemble members are not much larger than for the ensemble mean and are always lower than the observed trend. It is also interesting to compare the temporal relationship between STR intensification and GW in each individual simulation.

Although the match is not as close as with the ensemble mean, which is in part due to more abrupt decadal variability, there are several instances when the model simulations display concomitant periods of sustained warming and STR strengthening. This suggests that part of the close fit between observed GW and STR occurred by chance: i.e. that naturally occurring random variability has reinforced the underlying link between GW and STR driven by anthropogenic forcings.

In addition to the model's ability to reproduce the relationship between observed STR intensification and GW, a second important finding from the model simulations of the 20th century is the role of the various external forcings in simulating realistic changes. The ensemble of simulations with the CCSM3 model forced with natural forcings (solar variability and large volcanic eruptions) alone (Fig. 51 bottom left) does not exhibit either long-term warming or STR strengthening. In these simulations, there is a small warming (about 0.2ºC) up to the 1960s with cooling thereafter and no centennial trends. Similarly, in the absence of sustained period of strong global warming, the STR intensity exhibits sizeable decadal variability (changes of up to 0.5 hPa) but no long-term trends.

Simulations forced with anthropogenic forcings (greenhouse gases, aerosols and stratospheric ozone changes) alone (Fig. 51 bottom right) on the other hand, show a 0.7ºC global warming during the 20th century which accelerates significantly in the last 20 years. In these simulations a strengthening of the STR after the early 1970s occurs, again suggesting that this strengthening is in response to prolonged global warming. However, in the early part of the anthropogenic only simulations a large decrease in STR intensity is observed until the 1930s, which does not show a relationship with the global temperature curve. It is interesting to note that the mid-century maxima (around the 1940s) evident for both observed GW and STR intensity and reproduced (albeit more in the 1950s) in the fully forced ensembles is not present in the anthropogenic only ensemble. This suggests that the mid century maxima in GW and STR can only be accounted for by anthropogenic forcings alone. The implication of this finding for the attribution of the WWII drought which occurred at the time of the maxima in GW and STR will be discussed in the next chapter.

In addition to examining responses in terms of annual means, it is also worth further exploring relationships during May to October when the relationship between STR intensity and south-eastern Australia (SEA) rainfall is the strongest (Chapter 3). Modelled STR intensity and location (Fig. 53 right graphs) are compared with the observations using 21-year running means

(Fig. 53 left graphs). A longer smoothing filter is applied in this instance as the STR movements are noisier on a 6 monthly time period compared to annual means.

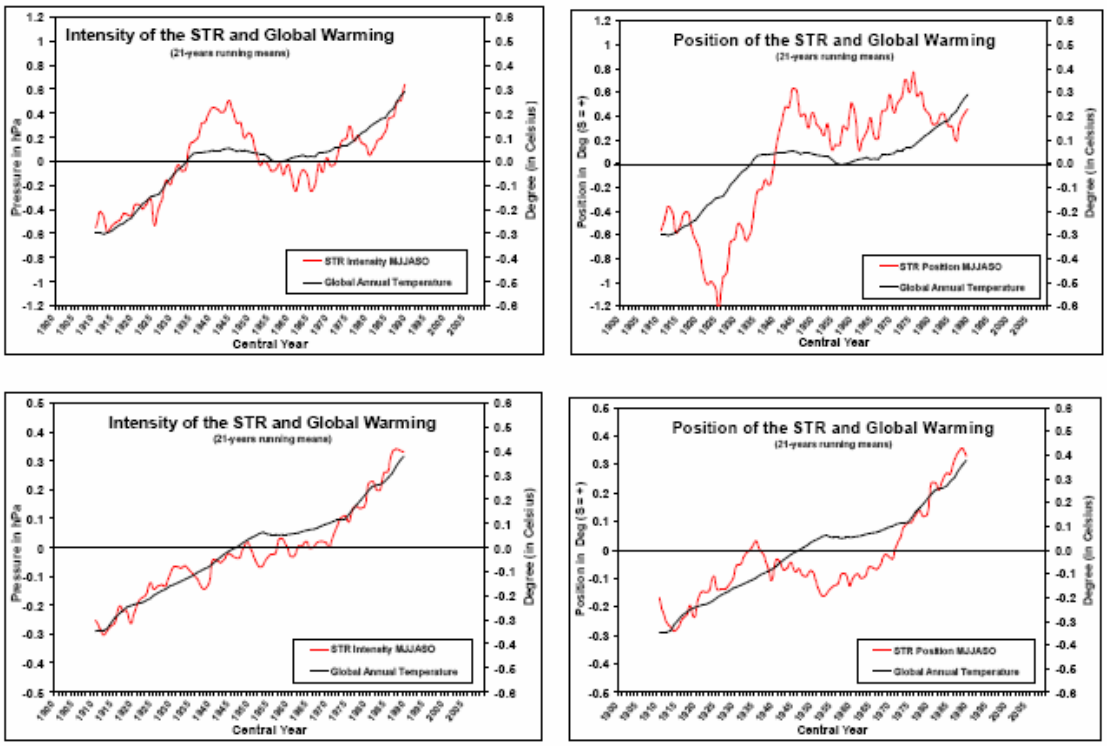

Fig. 53 *21-year running mean of anomalies of STR intensity (left) and position (right) in May-June-July-August-September-October compared with global warming for the observations (top row) and the CCSM3 ensemble forced with full forcings (bottom row).*

The relationship between STR intensity and global annual temperature is very strong in the observations as well as in the CCSM3 simulations. However, as noted earlier, the modelled strengthening is much smaller in magnitude compared to that observed (0.6 hPa instead of 1.2 hPa). The latitudinal shift of the STR is noisy in the observations: there is a large shift south (upward on the graphs) between the 1920s and 1940s at a time of significant GW, but otherwise it appears that multi-decadal variability is position of the STR is unrelated to the global temperature. The movements of the STR in the CCSM3 model are relatively small, but an ongoing positive trend is visible (a shift southward of 0.5° in latitude).

7.3 Centennial trends in CCSM3 STR and global warming

The 15 individual simulations of the 20th century with CCSM3 were used to further investigate the relationship between STR movement and GW. For all simulations, centennial linear trends were calculated for both GW and STR intensity and position (annual and May to October means were computed).

There is a strong relationship between GW and STR intensity and position (Fig. 54): correlations vary between a high of 0.73 (for annual STR position) and a low of 0.54 (for May to October STR position), and all correlations are statistically significant at the 95% level.

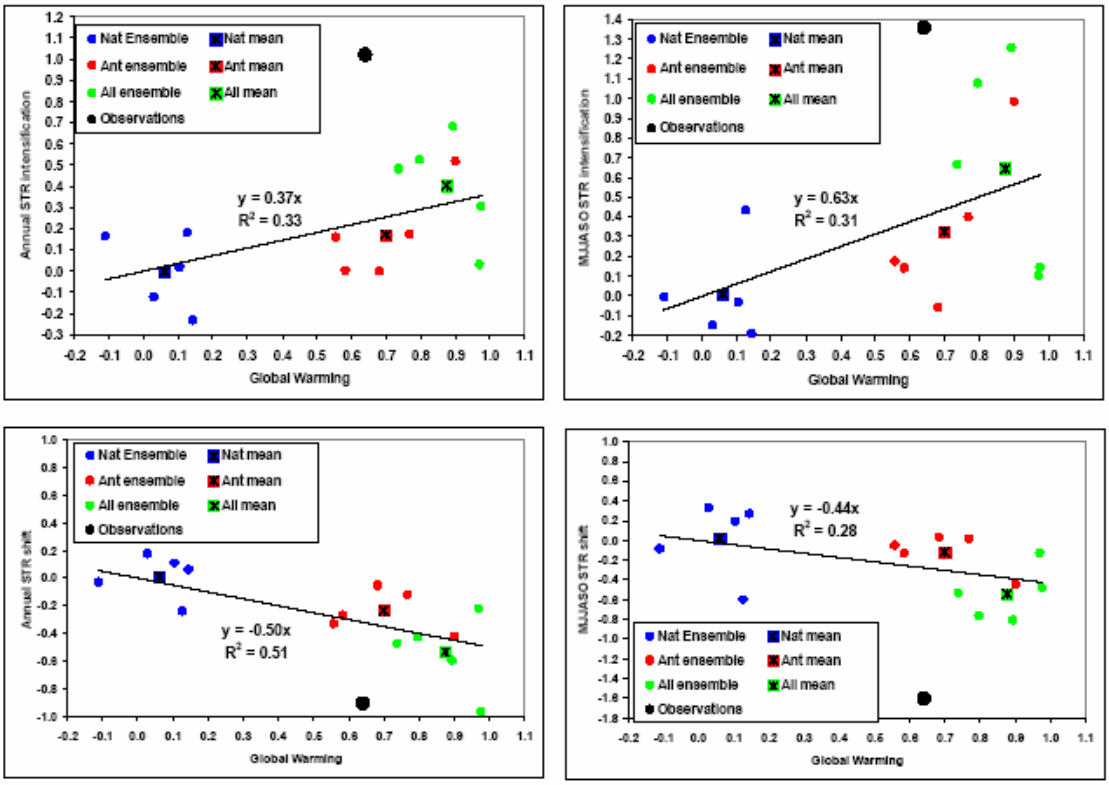

Fig. 54 *Centennial linear trend for each of the 15 CCSM3 simulations of the 20th century for STR intensity (upper) and position (lower) annual mean (left), and May to October mean (right) as a function of the modelled global warming; ensemble means are shown as well as the observations. The lines of best fit to the results are shown.*

The slope of the relationship between GW and STR intensity is 0.63 hPa per degree of warming for the STR in May to October but only 0.37 hPa for the annual mean (Fig. 54, top panels). Shifts in latitude are less seasonal: 0.44º of latitude south per degree of warming for the annual mean and 0.5º for the May to October period (Fig. 54 bottom panels). Individual simulations are clustered according to the forcings applied: almost no warming is associated with natural forcings, a warming comparable to the observed is associated with anthropogenic forcings, and a slightly larger warming is associated with the full forcings. The associated STR response is also seen to be largest with full forcings.

The response computed by taking the ensemble means (shown by coloured squares on the graphs) of any ensemble is always very close to the line of best fit across all members. In all cases, however, the observations (black points) stand out as showing a much larger response of the STR to GW: 1.5 hPa per degree of warming for the intensification (2.2 hPa in May to October) and a shift of 1.5 ºS (2.6 ºS in May to October). With only a single realisation for the observed climate system over the past century, it is not possible to rule out the possibility that these values are large by chance. However, it suggests that the CCSM3 has a tendency to under-represent the response of mid-latitude MSLP around Australia. This is important as it drives the rainfall decline. This result sheds light on earlier findings (Chapter 6) where the direct model rainfall signal for SEA in the CCSM3 simulations with full forcings was relatively small. Once CCSM3 was downscaled (using the Bureau of Meteorology Statistical Downscaling Model

(SDM)), it was found that the rainfall decline was sizeable but still not as large as observed, particularly in autumn. The enhanced signal from the SDM, which nevertheless remains lower than the observed rainfall decline, is due to MSLP being one of the key predictors for the SDM which incorporates much of the STR strengthening signal diagnosed here. Results from Chapter 6 and this analysis are consistent in suggesting that the CCSM3 model forced with full forcings produces a climate change around SEA comparable to what has been observed (in terms of MSLP changes, STR strengthening and rainfall reduction) but with a lesser magnitude.

7.4 Conclusions

The relationship between global warming and STR was investigated using a 15 member ensemble of 20th century simulations with the CCSM3 climate model. Of these 15 members, 5 runs were forced with natural external forcings (e.g. solar variability and volcanoes) only, 5 with external anthropogenic forcings (e.g. greenhouse gases, aerosols and ozone) only, and 5 with both natural and anthropogenic forcings (i.e. "full" forcings). It was found that the observed relationship between the STR intensification and global warming established earlier in Chapter 3 is unlikely to have occurred by chance: i.e. due to internally generated natural variability alone. The fully forced ensemble displays a coherent rise of temperature to observations, and a strengthening of the STR which appears to mimic the time evolution of GW and the STR in the observations. The naturally forced ensemble does not display any sizeable GW trend or STR intensification. However, the simulated strengthening of the STR in the model is weaker than observed, and the match between GW and the STR strengthening is not as strong in individual simulations than with the 5 member ensemble mean.

SUMMARY

Our analysis of the CCSM3 climate model simulations of the 20th century shows that:

- The model has a realistic annual cycle of the STR intensity and position in the vicinity of Australia providing it is diagnosed using a broader longitude band than used for the observations.

- The CCSM3 model produces an intensification of the STR at the end of the 20th century only when anthropogenic forcing or both natural and anthropogenic forcings are used. Otherwise, natural forcings alone does not produce long-term trends in the simulations for either GW or STR intensity.

- The ensemble mean of the model forced with a combination of both anthropogenic and natural external forcings provides the closest match of the three ensembles (natural, anthropogenic and full forcing) to the observations for both GW and STR intensification.

- The relationship between STR-I and GW in the full forced ensemble shows strong similarities with the observed relationship, suggesting that GW drives interdecadal variability and a trend in the STR-I.

- In all simulations, the CCSM3 model exhibits smaller than observed long-term trends in the STR (intensity and position) per degree of warming compared with the observations. This suggests that either the model STR response to GW is too weak or that part of the observed changes in the STR is due to internally generated natural variability.

8 IMPROVED DETECTION OF OBSERVED CLIMATE CHANGE ACROSS SOUTH-EASTERN AUSTRALIA

8.1 Introduction

As part of the SEACI-1 project described in Chapter 2 it was found that the ongoing drought (1997-2006) was not the worst 10 year period on record in terms of annual rainfall. SEA recorded a drier period from 1936 to 1945 (the WWII drought). It was also noted that at the time of the Federation of Australia, there was another very dry period. This is harder to quantify since most BoM gridded rainfall products start in 1900, whereas the Federation drought (from anecdotal and limited observational records) started in the mid-1890s.

Note that a more recent update using data extended to 2009 found that the ongoing drought (1997-2009) across SEA is the largest 13 year rainfall decline in the instrumental record (Timbal 2009), with the reduction in annual rainfall now being more severe than during the WWII drought.

An additional project was undertaken with a view to comparing these two very dry periods (on-going and WWII) in more detail in the light of other findings which have emerged during SEACI – in particular:

- The contribution of rising MSLP, in particular the intensification of the STR and its relationship to GW (Chapter 3);
- The lack of a significant rainfall decline in 20th century climate model simulations forced with natural external forcings and the need for inclusion of anthropogenic forcings in order to explain the ongoing rainfall decline (Chapter 6); and
- The ability of climate models to reproduce the co-evolution of GW and STR-I during the 20th century, and the need to include anthropogenic forcings to generate upward trends in both GW and STR (Chapter 7).

In this project, the evaluation of the ongoing rainfall decline in SEA has been refined by redefining regional climate entities and undertaking a more detailed examination of the spatial and temporal characteristics of the observed drought and comparing it to previous dry periods.

8.2 Re-definition of the climate entities across SEA

During the SEACI period of research it has become increasingly obvious that the entire SEA region consists of different climate entities, which exhibit different responses to remote large-scale modes of variability: ENSO, IOD, the SAM as well as local meteorological forcings (STR intensity and position, the meridional gradient along the eastern coast as measured by the GDI and local SST anomalies).

A first attempt was made to define regions using previous work on rotated EOFs of Australia rainfall (Drosdowsky 1993) in Chapter 2: three regions across the SEA were defined - the SWEA, the SMD and the SEC. These regions were refined further in subsequent chapters.

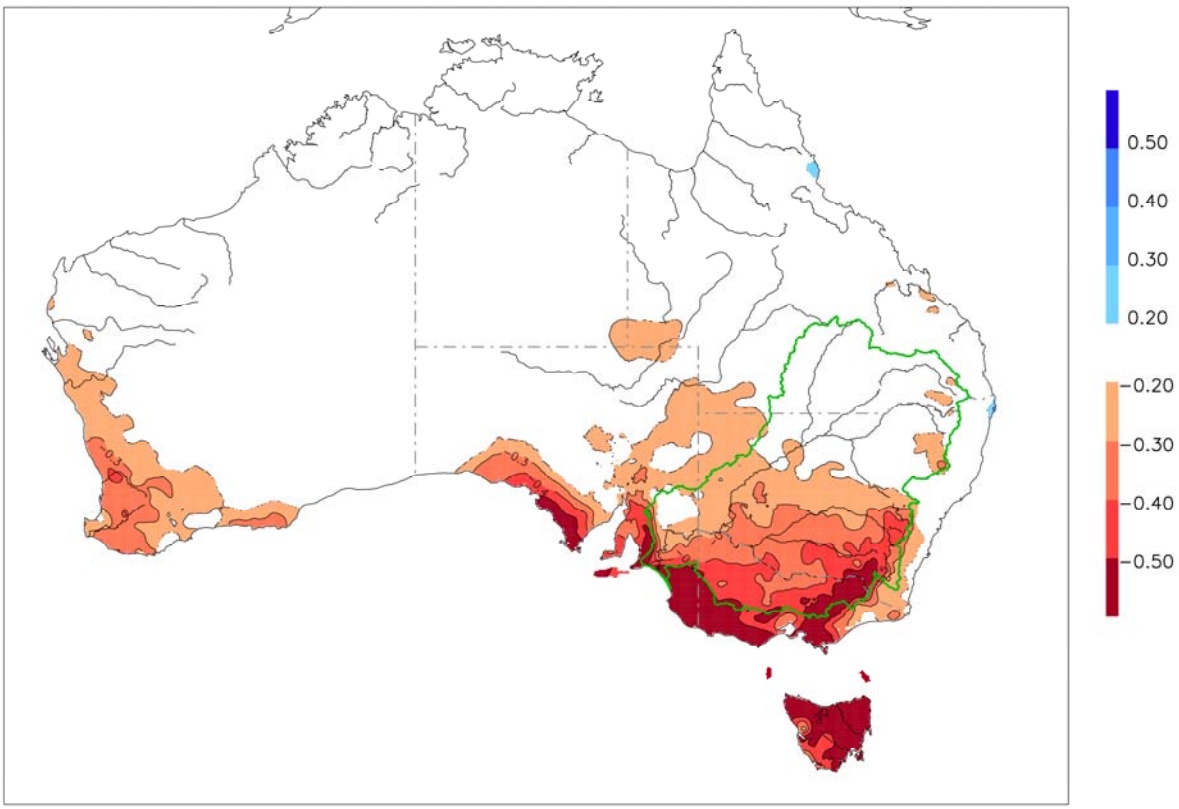

Fig. 55 *Correlations between detrended values of the annual mean of the Sub-Tropical Ridge intensity and rainfall across Australia; correlations significant at the 95% level and above are colour shaded.*

Here we have further refined this approach, using the influence of STR-I on SEA rainfall as a guide. Annual correlations for the relationship between the STR-I and rainfall show the dominant influence of the STR-I across SEA and, in particular, on SWEA (Fig. 55). These correlations were calculated for annual means using detrended values from 1900 to 2008. An analysis of the relationship month by month shows that the correlations peak during May-June-July-August. We will return to this point later (Fig. 60).

Based on these correlations, we defined three distinct regions (Fig. 56):

1. We used the three month period with the largest correlations (MJJ) to define a continuous area in SEA where the STR-I explains more than 20% of the inter-annual correlation (correlations above 0.447). This area is our new definition for SWEA.
2. The NMDB encompasses the rest of the MDB where the influence of the STR-I is less pronounced;
3. The ESB on the eastern side of the GDR where the influence of the STR-I is less marked.

In the rest of this chapter, we will analyse statistics of the recent dry period in each region and to compare the recent drying trend to previous dry periods.

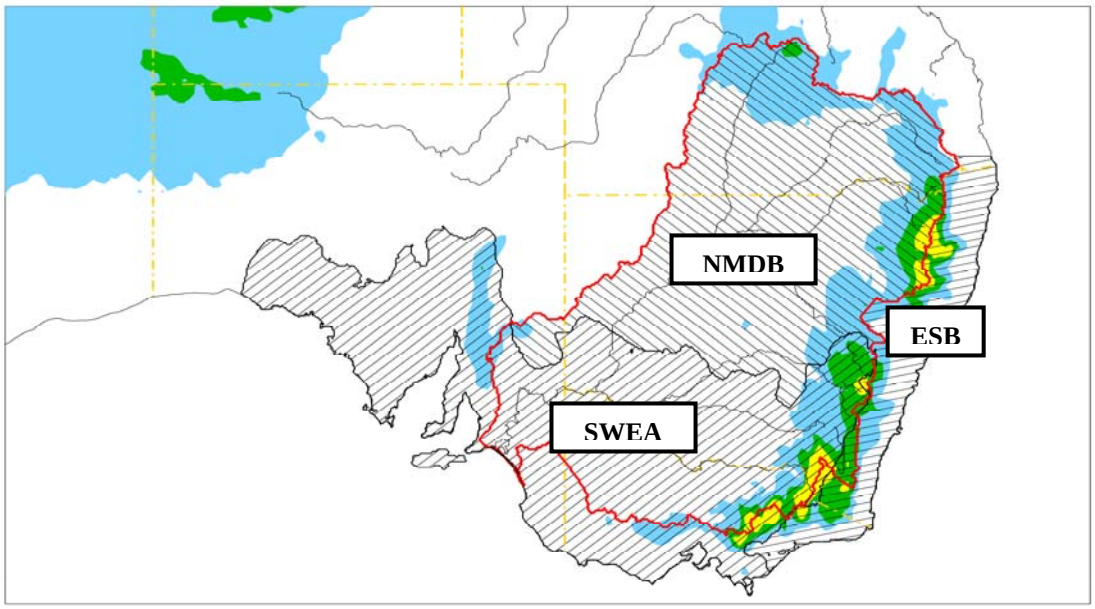

Fig. 56 *The three regions of interest across the SEACI domain are shown with different stipples: the south-west part of Eastern Australia (SWEA), the Northern part of the Murray-Darling Basin (NMDB) and the Eastern Sea-Board.*

8.3 Pattern of rainfall decline during the Federation, WWII and the ongoing droughts

Rainfall deciles from these 3 periods are shown (Fig.57) relative to the 1900-2008 long-term climatology. As stated earlier, the map for the Federation drought (from 1900 to 1908) is not ideal as it should start a few years earlier. Overall, a few points are worth making:

- The current drought is localised to southern Australia and SE Queensland while the rest of the Australian continent is experiencing average to above average rainfall. This contrasts with both previous droughts.
- In the current drought the largest signal is in the SWEA area with impacts decreasing further north. During the WWII drought the impacts were largest in the MDB and during the Federation drought impacts were largest in the ESB;
- The spatial pattern of the current rainfall decline has a very strong similarity with the pattern of the STR-I signature on rainfall across southern Australia (Fig. 55), this is not the case in the two previous drought periods.

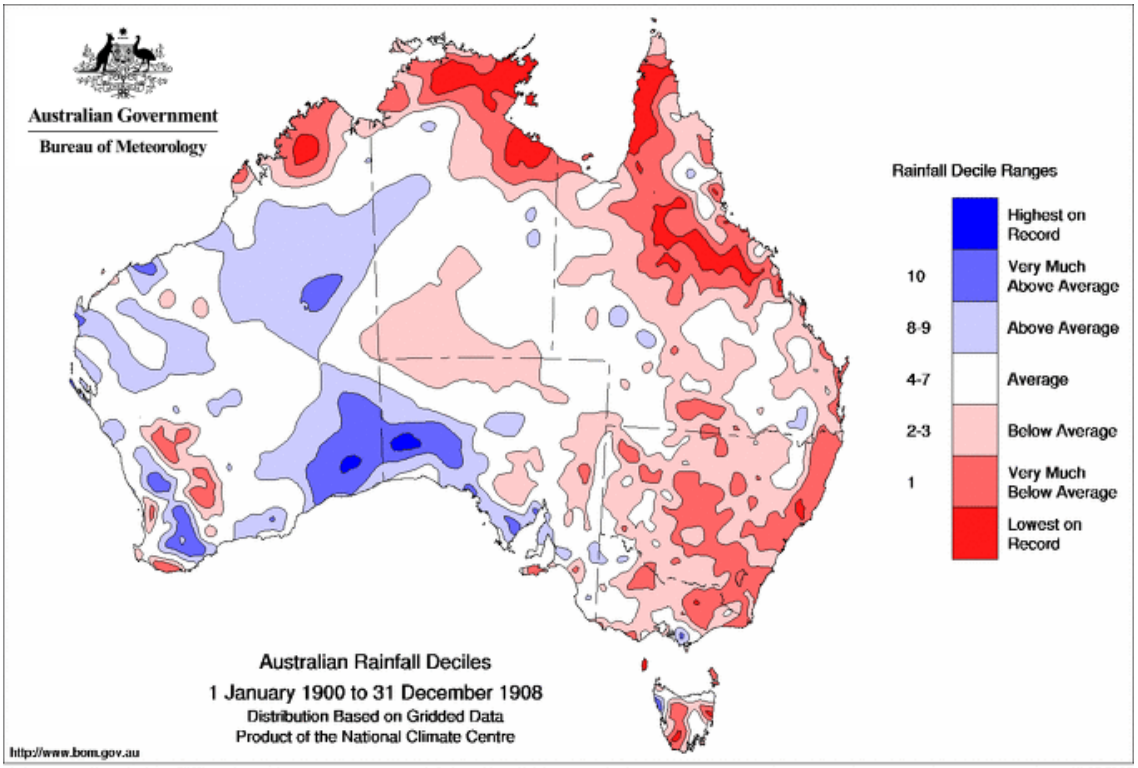
Australian Government
Bureau of Meteorology
Rainfall Decile Ranges
10
8-9
4-7
2-3
1
Highest on Record
Very Much Above Average
Above Average
Average
Below Average
Very Much Below Average
Lowest on Record
Australian Rainfall Deciles
1 January 1900 to 31 December 1908
Distribution Based on Gridded Data
Product of the National Climate Centre
http://www.bom.gov.au
© Commonwealth of Australia 2009, Australian Bureau of Meteorology
ID code: IGiMapOprBarnesRainAust
Issued: 18/06/2009

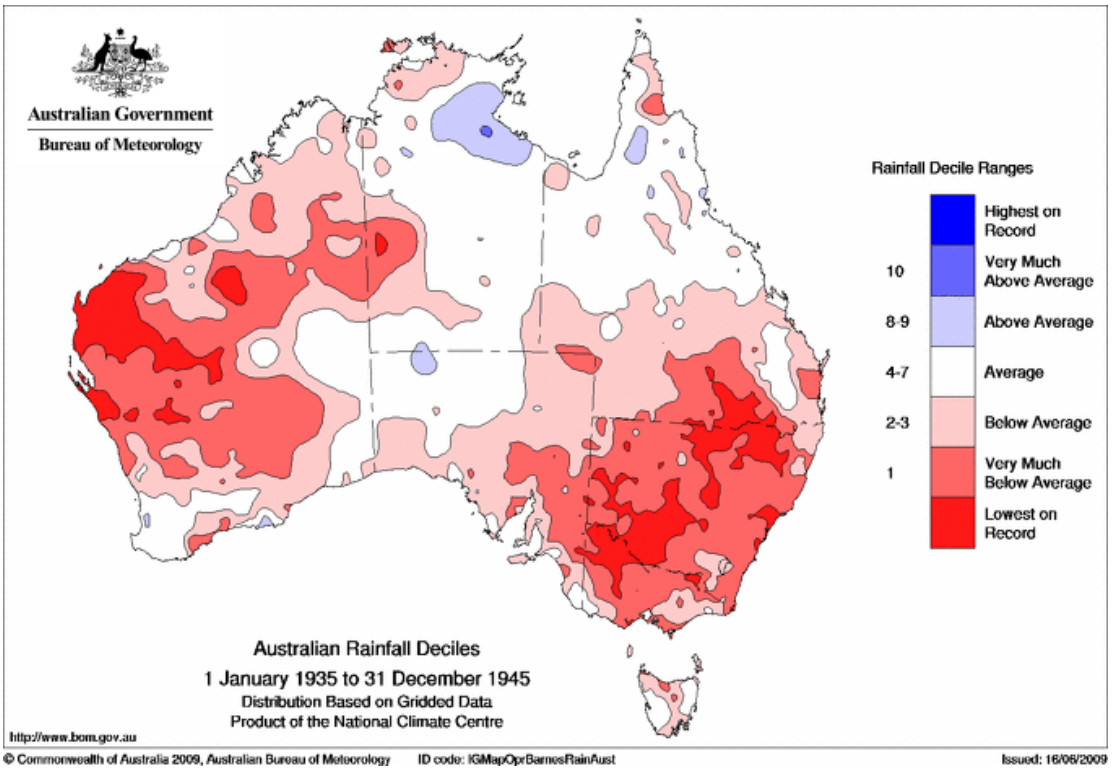
Australian Government
Bureau of Meteorology
Rainfall Decile Ranges
10
8-9
4-7
2-3
1
Highest on Record
Very Much Above Average
Above Average
Average
Below Average
Very Much Below Average
Lowest on Record
Australian Rainfall Deciles
1 January 1935 to 31 December 1945
Distribution Based on Gridded Data
Product of the National Climate Centre
http://www.bom.gov.au
© Commonwealth of Australia 2009, Australian Bureau of Meteorology
ID code: IGiMapOprBarnesRainAust
Issued: 16/06/2009

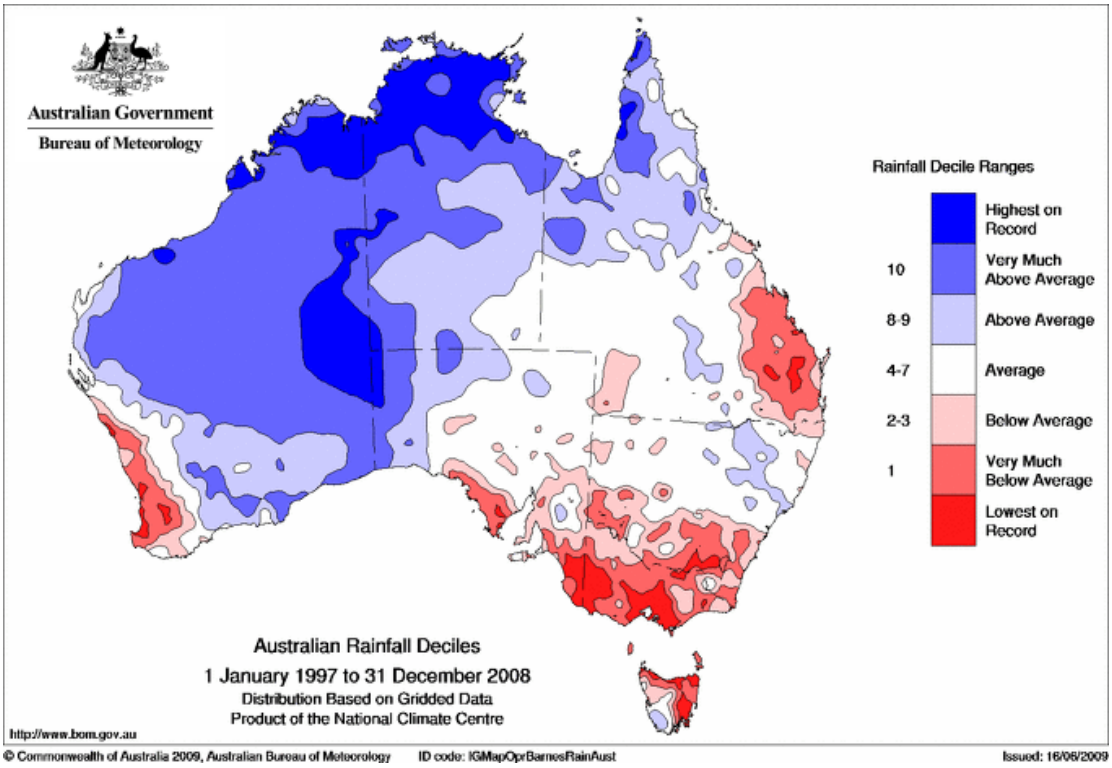

Fig. 57 *Total rainfall deciles across the Australian continent for the 1900-05 period (upper of previous page), 1935-1945 period (lower of previous page) and the 1997-2008 period (above); deciles are expressed using the long-term climatology from 1900 to 2008 (maps courtesy of the National Climate Centre).*

In term of large-scale modes of variability:

- All three periods were marked by a similar number of El Niño events: 1902 and 1905 during the Federation drought; 1940 and 1941 during the WWII drought; and 1997, 2002 and 2006 during the current drought (i.e. 1 more than during the other two droughts);
- All three periods experienced La Niña events: 1903 and 1906; 1938 and 1942; and 1998, 1999, 2000 and 2007 (i.e. 2 more than during the other two droughts);
- There were very few negative IOD events during these decades: 1906 during Federation drought, 1942 during WWII drought and none in the latest period; and
- There were a number of positive IOD events with the numbers of events increasing with time: 1906 only for the earlier period; 1935, 1944 and 1945 during the WWII period; and 1997, 1999, 2004, 2006, 2007 and 2008 for the latest period.

The larger numbers of La Niña events during the most recent period is consistent with the known effect of ENSO across Australia and the latest period being generally wet Australia-wide. The increasing number of positive IOD events is likely to have had an impact on Australian rainfall, peaking in spring. The annual signature of the Saji et al. (1999) Dipole Mode Index (DMI) on rainfall (Fig. 58) shows an impact across most of SEA. However, a close examination of the map compared to the pattern of current rainfall decline (Fig. 57 lower) shows a number of differences:

- No impact of the IOD on the SWWA which is also affected by a rainfall decline since 1997;

- The largest impact of the IOD in SEA is inland of the GDR, while the largest rainfall decline since 1997 is in the SWEA;
- A strong impact of the IOD on rainfall along the GDR in New South Wales up to Queensland. This area has not seen a rainfall decline since 1997.

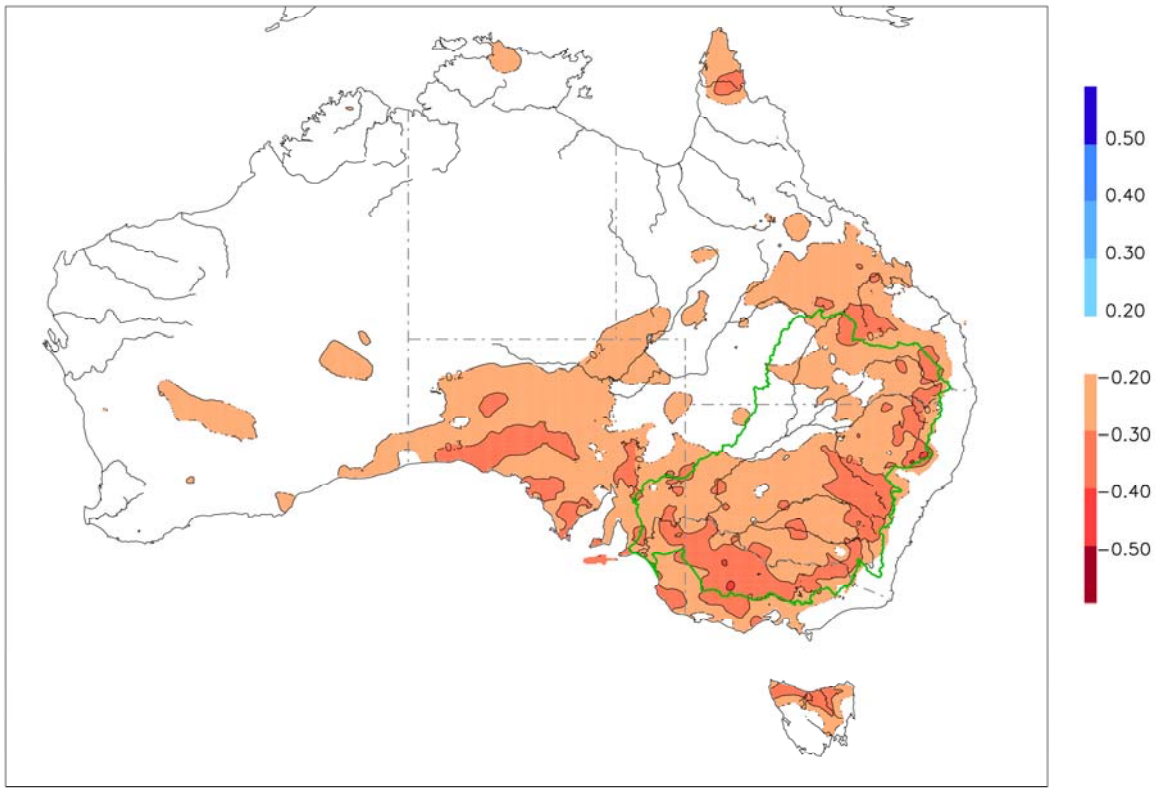

Fig. 58 *Detrended correlations between detrended annual values of the Indian Ocean Dipole and rainfall across Australia; correlations significant at the 95% level and above are colour shaded.*

A similar comparison between the maps of the STR-I impact on Australian rainfall (Fig. 55) and the current decline (Fig. 57, lower) does not show these discrepancies. Beyond this simple visual comparison, the joint contribution of the STR intensification and SST anomalies in the tropics will be investigated further.

8.4 Seasonality of the WWII and current droughts

Due to data limitations in the late 19th century, we will focus on the comparison between the WWII and current droughts in the rest of this chapter. As expected from earlier comments, the characteristics of the rainfall decline across the three climate entities in SEA are very different between the two periods (Table 24).

Table 24 *Rainfall statistics for the 3 climate entities in SEA: long term (1900-2008) mean (annual and seasonal) in mm and anomalies during the WWII dry period and the ongoing drought (as a*

percent of the long-term climatology). Positive anomalies are shown in italics; when anomalies for the recent period are the largest on record, they are shown as bold figures.

		Annual	Autumn	Winter	Spring	Summer
SWEA	1900-2008	456 mm	103 mm	145 mm	120 mm	87 mm
	1935-1945	-10.3%	-13.1%	-7.2%	-18.2%	-1.2%
	1997-2008	**-10.7%**	**-26.5%**	**-12.1%**	-4.2%	*+1.2%*
NMDB	1900-2008	457 mm	105 mm	89 mm	106 mm	157 mm
	1935-1945	-15.4%	-17.2%	-6.3%	-29.1%	-10.1%
	1997-2008	-0.5%	-17.9%	-1.7%	*+15.0%*	*+1.6%*
ESB	1900-2008	954 mm	253 mm	191 mm	210 mm	299 mm
	1935-1945	-12.4%	-11.3%	-15.5%	-11.4%	-12.0%
	1997-2008	-6.3%	-16.7%	-7.0%	*+4.1%*	-1.4%

Similar anomalies (in percentage terms) were observed across all 3 regions during the WWII drought and all seasons were affected (including summer): Autumn and spring anomalies dominate in SWEA and NMDB, while winter anomalies dominate in ESB. The current drought is unprecedented only in SWEA. It is dominated by a strong autumn signature across all three regions. The large size (and common sign) of the anomalies in winter and spring in SWEA alongside the autumn signal explain the record breaking on-going drought. In ESB the current drought has only half the magnitude of the WWII drought (a small negative anomaly in winter is cancelled out by a small positive anomaly in spring), and it is non-existent in terms of annual rainfall anomalies across NMDB: a large spring increase is cancelled out by the autumn decline. Autumn rainfall appears as the only spatial and temporal invariant between the 2 droughts: it is sizeable across all three regions and evident during the two dry periods.

Month by month comparison in the 3 regions of the two periods (Fig. 59) confirms these results. There is a continuum of 8 months from March to October with rainfall deficiencies in SWEA for the current drought. These 8 months include the entire wet season (May to October) over which time 60% of the annual rainfall occurs. This, combined with the spatial extent of the decile 1 rainfall anomalies in the last decade, reinforces the impression that the highest rainfall decline is linked to a weakening of the dominant westerly flow as would be expected from a rainfall deficit whose temporal signature is scattered across the wet autumn/winter/spring months. Indeed, the decile 1 rainfall (Fig. 57, lower) region extends from the south-west across the entire SWEA and covers most of the Murray catchment. Two small pockets show no rainfall decline: the southern part of the Mt Kosciusko National Park (in the lee of the main range) and an area north-east of Adelaide in the lee of the Southern Flinders Ranges. These two small regions are located in the lee of significant orographic features. Orography tends to enhance rainfall on the western slopes and decrease rainfall on the eastern sides in westerly flows, and hence such regions are more likely to receive rainfall from southerly or easterly flows.

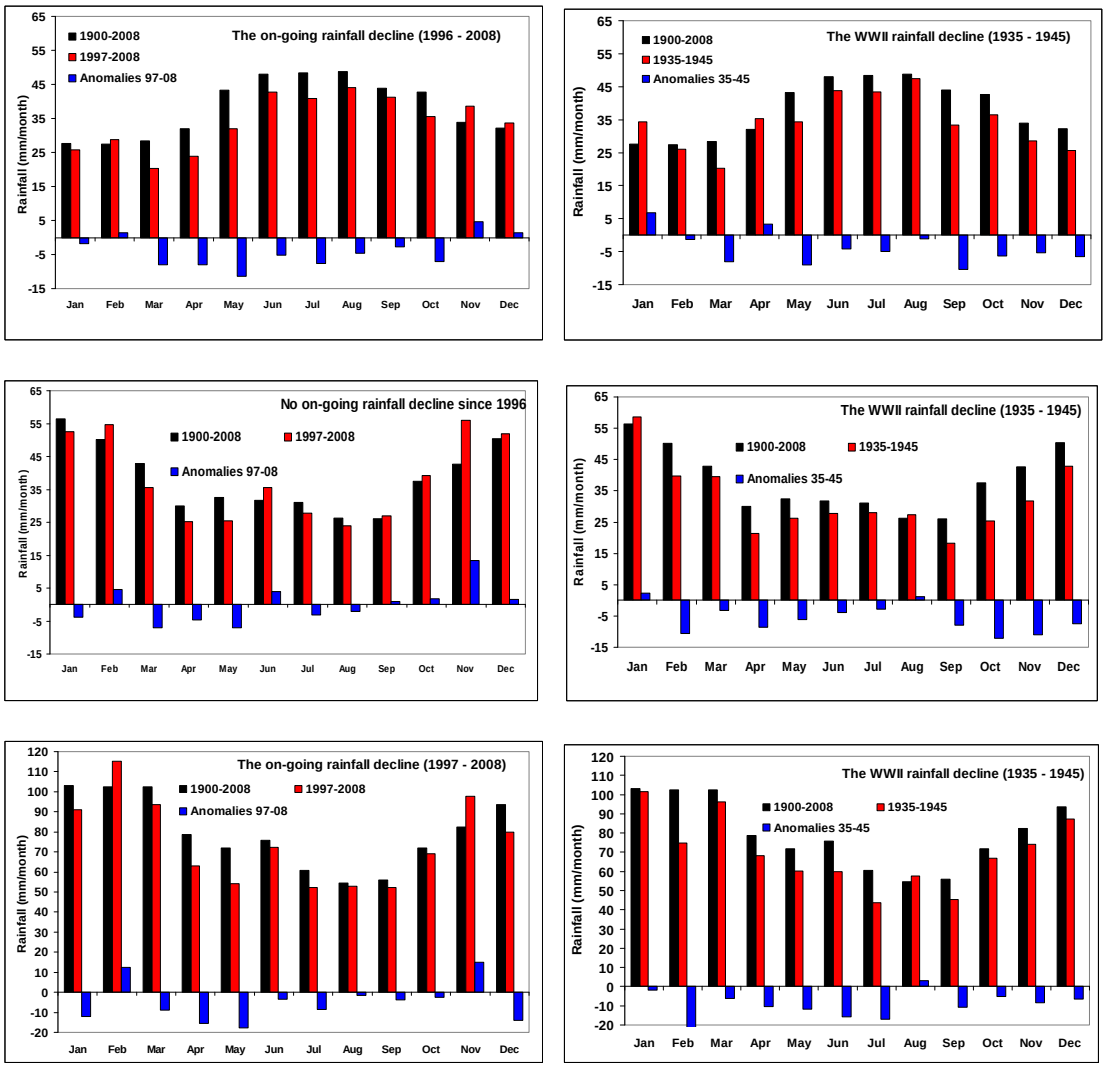

Fig. 59 *Monthly mean rainfall for the long-term climatology (black bars) in SWEA (upper), NMBD (middle) and ESB (lower), for the ongoing drought (red bars in left graphs) and during the World War II drought (red bars in right graphs); changes from the long term climatology are shown as blue bars. [Note: there is no ongoing decline in rainfall in NMBD since 1996].*

8.5 The role of local MSLP indices

The role of the STR-I as well as the possible additional contribution of the position of the ridge (STR-P) and the MSLP gradient along the Eastern coast between the latitude of the STR in summer and the tropical belt of low pressure are worth investigating further. To do so both the Drosdowsky (2005) STR-I and STR-P monthly observed series and the Rakich et al. (2008) monthly GDI are correlated with monthly rainfall across the three regions (Fig. 60). For the ease of comparison the sign of the GDI has been reversed.

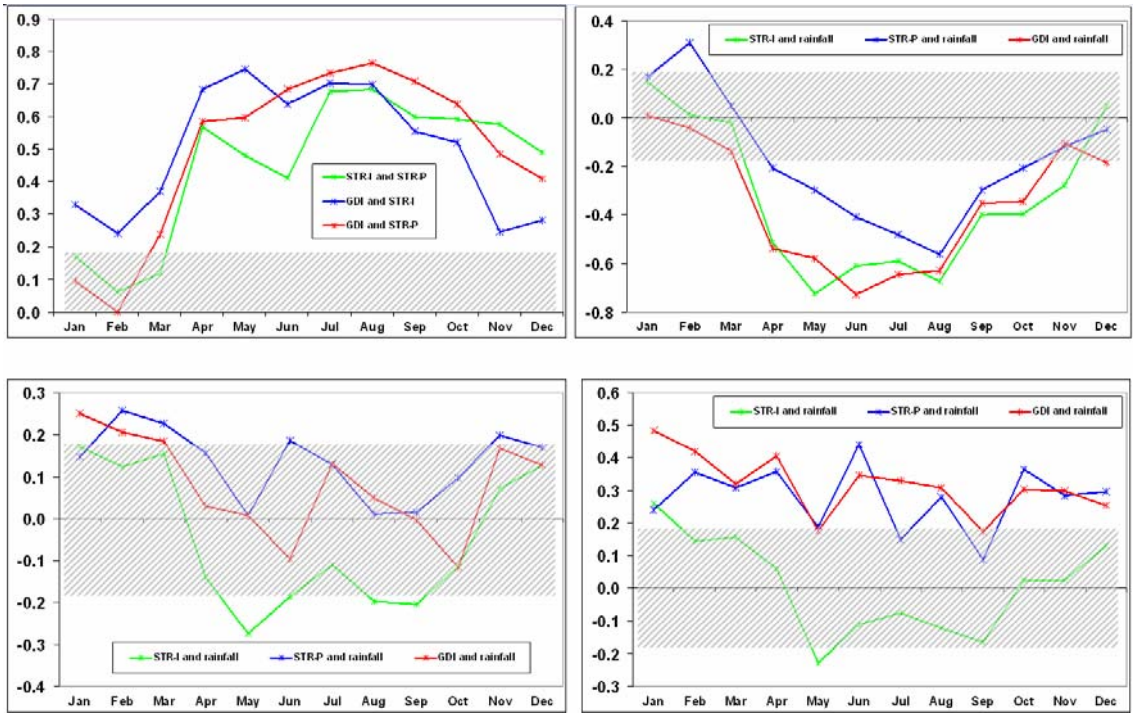

Fig. 60 *Monthly correlations between rainfall in SWEA (top right), NMDB (bottom left) and ESB (Bottom right) and local MSLP indices (STR intensity and position and GDI as well as correlations between the three local MSLP indices (top left). On all graphs, correlations below the 95% statistical significance level are masked by grey stipples.*

In SWEA (top right graph in Fig. 60), all three indices are significantly correlated (at the 95% level) with rainfall for half of the year from April to October. The best correlation for annual rainfall is obtained with STR-I (-0.49) with both the position (-0.23) of the ridge and the GDI (-0.24) contributing less. In NMDB, correlations are low and barely significant in any given month.

Along the ESB, the intensity of the STR does not appear to be relevant. The STR-P and the GDI have a positive impact on rainfall (i.e. a ridge located further south or an enhanced south to north MSLP gradient along the east coast increases rainfall). The GDI has the strongest (0.31) impact on annual rainfall against 0.21 for the STR-P. This discussion and associated results illustrate that relationships between rainfall and local MSLP are not straightforward and evolve both spatially and temporally.

As one would expect, these three MSLP-based regional indices are not independent. They are positively and significantly correlated almost all year around (top left graph in Fig. 60). Nevertheless, the joint contribution of STR-I and STR-P anomalies during the two dry epochs (WWII and ongoing) is worth exploring further, in particular for SWEA. Annual cycles of the STR-I/STR-P during the two dry periods show anomalies compared to the long-term mean (Fig. 61) consistent with the rainfall anomalies in SWEA (Table 24): anomalies are larger in both magnitude and position in the recent period in April to July, while during WWII drought they were larger in August to October.

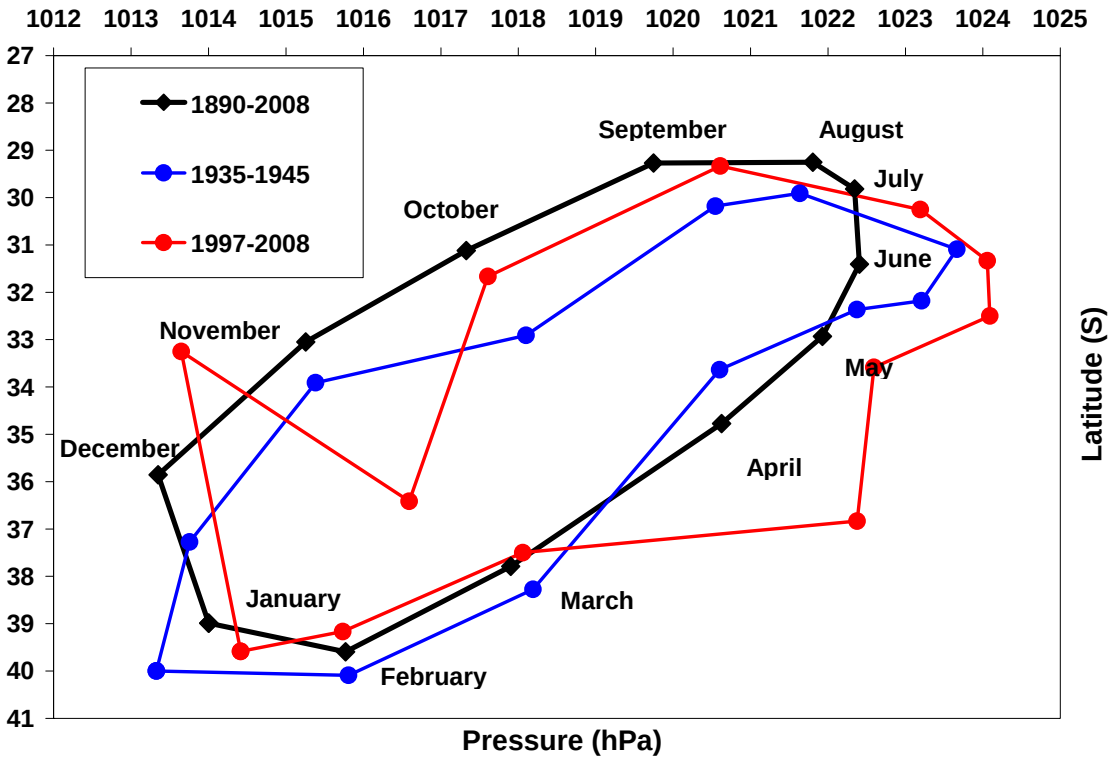

Fig. 61 *Annual cycle of monthly mean sub-tropical ridge position and intensity from the long-term climatology (black curve) and for the two dry periods: WWII drought (blue curve) and current (red curve).*

Using the linear relationships between the STR-P and STR-I, we computed STR-related monthly rainfall anomalies for the two dry periods in SWEA and compared them with observed values, using the following multiple linear regression model:

$$Rain_{anomaly} = a \times STR\_I_{anomaly} + b \times STR\_P_{anomaly} + c$$

with *a*, *b* and *c*, 3 parameters fitted to the observed values for each month. This model was used 3 times:

1. with $b=0$, to evaluate the role of the STR intensification alone;
2. with $a=0$, to evaluate the role of the shift south of the STR alone; and
3. with neither *a* or *b* equal to 0, to evaluate the joint effects of the STR intensification and shift south while taking into account the interdependence between these two variables.

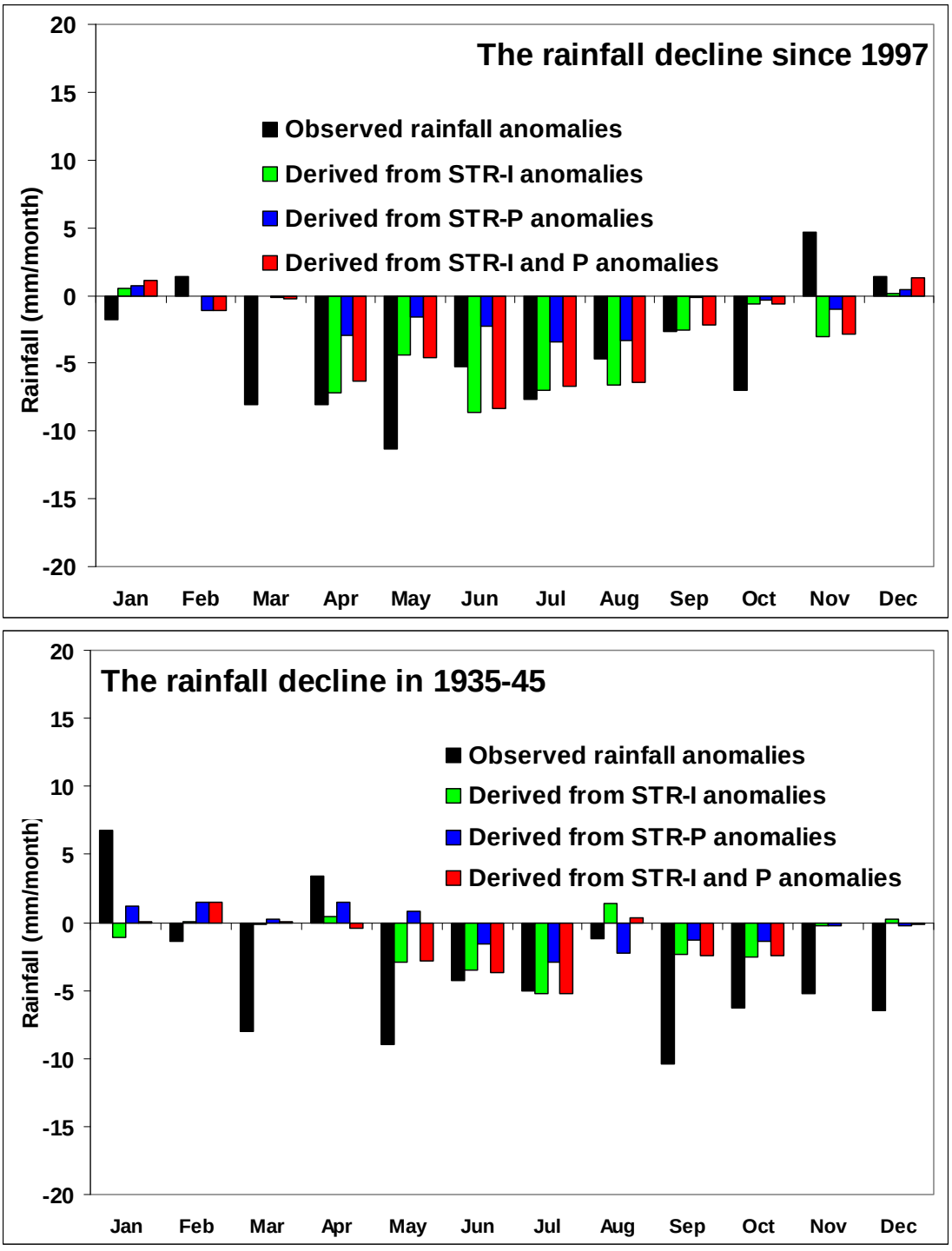

Fig. 62 *Monthly rainfall anomalies for the ongoing drought (upper graph) and the WWII drought (lower graph) as observed and reconstructed using the linear relationship between rainfall and the sub-tropical ridge intensity (STR-I in green), position (STR-P in blue) and both intensity and position combined (in red).*

For the current period the largest reconstructed anomalies were obtained with the STR-I, with rainfall anomalies being equal to 80% of the observed decline. The percentage decreases when both STR-I and STR-P are considered to 75.5%. In the recent period, the anomalies in STR-P alone generate rainfall anomalies equivalent to 30% of the observed decline. Month by month

anomalies (Fig. 62) compare quite well with the observations, especially with STR-I alone, although the reconstructed anomalies are smaller than observed in autumn (in particular in March when no rainfall decline was anticipated based on the STR-I) and larger than observed in the rest of the wet season (winter and spring).

During the WWII drought, the effects of the STR changes are less successful in explaining the rainfall decline, with reconstructed rainfall anomalies equal to 32% of the observed decline with both STR-I and STR-P, 34% with STR-I alone and 10% with STR-P alone. Reconstructed anomalies are very accurate in winter but grossly underestimate autumn and spring months.

In most months and in both periods, despite the sizeable effect of STR-P on rainfall when considered in isolation, it does not appear to have an additional effect when combined with STR-I, in explaining the rainfall decline. The intensification of the STR is overwhelmingly sufficient to explain the part of the rainfall decline attributable to changes in the STR. This is most likely due to the high correlation (around 0.6) between STR-I and STR-P from April to November. The possibility that the shift in position has an additive but non-linear effect compared to the strengthening of the ridge cannot be ruled out completely, as the statistics used here are relatively simple and rely on linearity assumptions. More advanced non-linear statistics (such as the Classification and Regression Tree (CART) technique described in the next chapter) are needed to extend this analysis.

8.6 The role of tropical SSTs

A large number of tropical SST indices were computed using the HadSST2 dataset (Rayner et al. 2006) interpolated on 2.5º by 2.5º grid, from 1900 to 2008:

- The Saji et al. (1999) DMI, the Nicholls (1989) IOD, the Timbal and Murphy (2007) NWS index; in addition, values updated to 2007 for the IOD composite from Meyers et al. (2007) were used;

- The Niño4 SST index, the Ashok et al. (2007) El Niño Modoki Index (EMI) and, in addition, values updated to 2007 for the ENSO composite from Meyers et al. (2007) were used;

- An additional index was created to maximise the influence of tropical SST on SWEA rainfall based on observed correlations (called tropical SST: Fig. 63). This tri-polar index (TPI) is the difference between SST north of Australia in the Eastern Indian Ocean and across the Indonesian maritime continent (0ºS -20ºS and 90ºE to 140ºE on the Equator shifted to 110ºE to 160ºE at 20ºS) minus the average of two SSTs boxes: a square further west in the Indian Ocean (10ºN to 20ºS and 55ºE to 90ºE) and a box in the Pacific Ocean (15ºN to 15ºS and 150ºE to 140ºW at the northern boundary and 180ºE to 140ºW at the southern boundary).

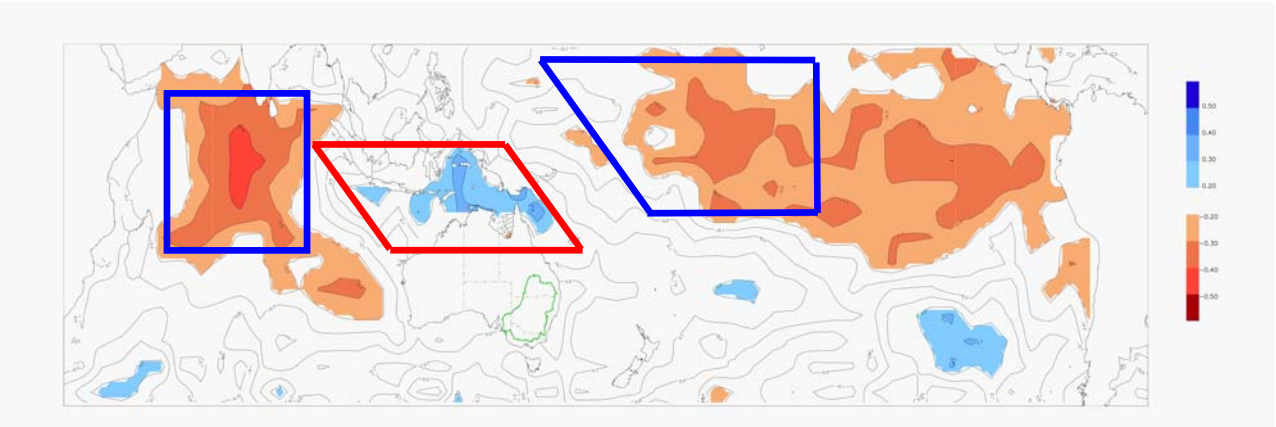

Fig. 63 *Map of the annual correlation of SSTs with SWEA rainfall (correlation significant at the 95% level are shaded). The boxes used to define the tropical tri-polar SST index are shown: the index is the difference between SSTs in the central red box minus the average of the SSTs within the two blue boxes.*

The last index has the advantage of combining SSTs with a negative relationship with SWEA rainfall in both oceanic basins and contrasting them with SSTs with a positive relationship with SWEA rainfall across a large sector north of Australia. The same logic was used by Nicholls (1989) to define an IOD index. The idea is extended here across both oceanic basins. It is therefore expected to provide the strongest relationship with SEA rainfall.

This index provides a broader perspective on the role of tropical SST on SEA rainfall. In particular it captures the enhanced effect of the ENSO signal on SEA rainfall when ENSO has a signature further west (El-Modoki type of ENSO) and the amplification which occurs when ENSO anomalies are transmitted through the maritime continent into the Indian Ocean. This amplification is particularly important when an IOD event occurs. It implicitly takes the view that inter-annual variability between the two oceans is linked although it will also show a signal if only one of the two oceans shows an event (either ENSO or IOD).

It has the disadvantage of not focusing on a particular part of the tropical oceanic dynamic (in contrast to IOD or ENSO indices). But, it has the potential to be very pertinent on inter-annual timescales and possibly on long timescales (such as the decade long dry periods analysed here). It is also important that this index is made of differences of tropical SSTs and, hence, it is unlikely that its first order trend will simply be a regional measure of global warming as is the case with single box indices such as Nino4 or NWS indices or for that matter the IOD which despite being a dipole has been shown to be primarily a reflection of the global warming across the Indian Ocean (Dommenget 2010). We will return to this point in Chapter 10. Instead, it measures the shift of warm waters and associated convection (these shifts could be due to global warming or unlinked naturally occurring variability) in the tropics which we know (based on observed correlations) have the potential to impact on SWEA rainfall.

Monthly correlations with all these indices were computed (Fig. 64) with rainfall in SWEA and a SWEA rainfall residual once the relationship between the STR-I and SWEA was removed. The sign was reversed for NWS and the TPI to ensure consistency of sign between all the indices.

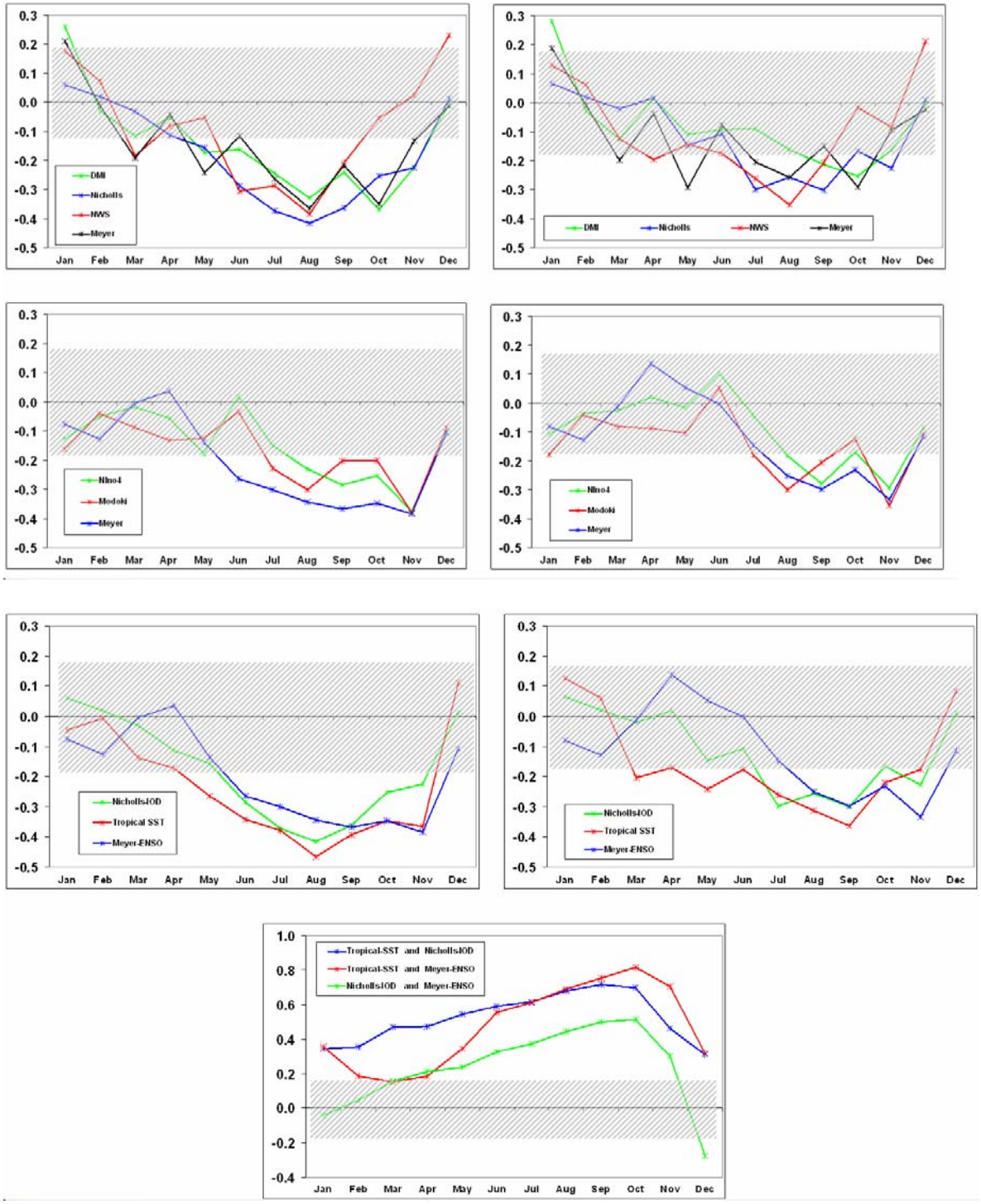

Fig. 64 *Monthly correlations between tropical indices for the Indian Ocean (top row), Pacific Ocean (second row), the best three tropical indices (third row, see text for details) and rainfall in SWEA (left column) and SWEA rainfall residual with the STR-I influence removed (right column); correlations between the three most relevant tropical indices (bottom graph). On all graphs, correlations below the 95% statistical significance level are masked by grey stipples.*

Well known features, such as the predominant influence of the IOD and ENSO in winter and spring are clearly visible. This is also the case for our TPI. All tropical indices have no significant relationship with SWEA rainfall from November to March. Three indices appear to be particularly important: the Nicholls (1989) IOD, the Meyers et al. (2007) ENSO composite and the TPI we introduced earlier (summarised in the third row of graphs in Fig. 64). These three indices are significantly correlated in most months outside summer (last graph in Fig. 64).

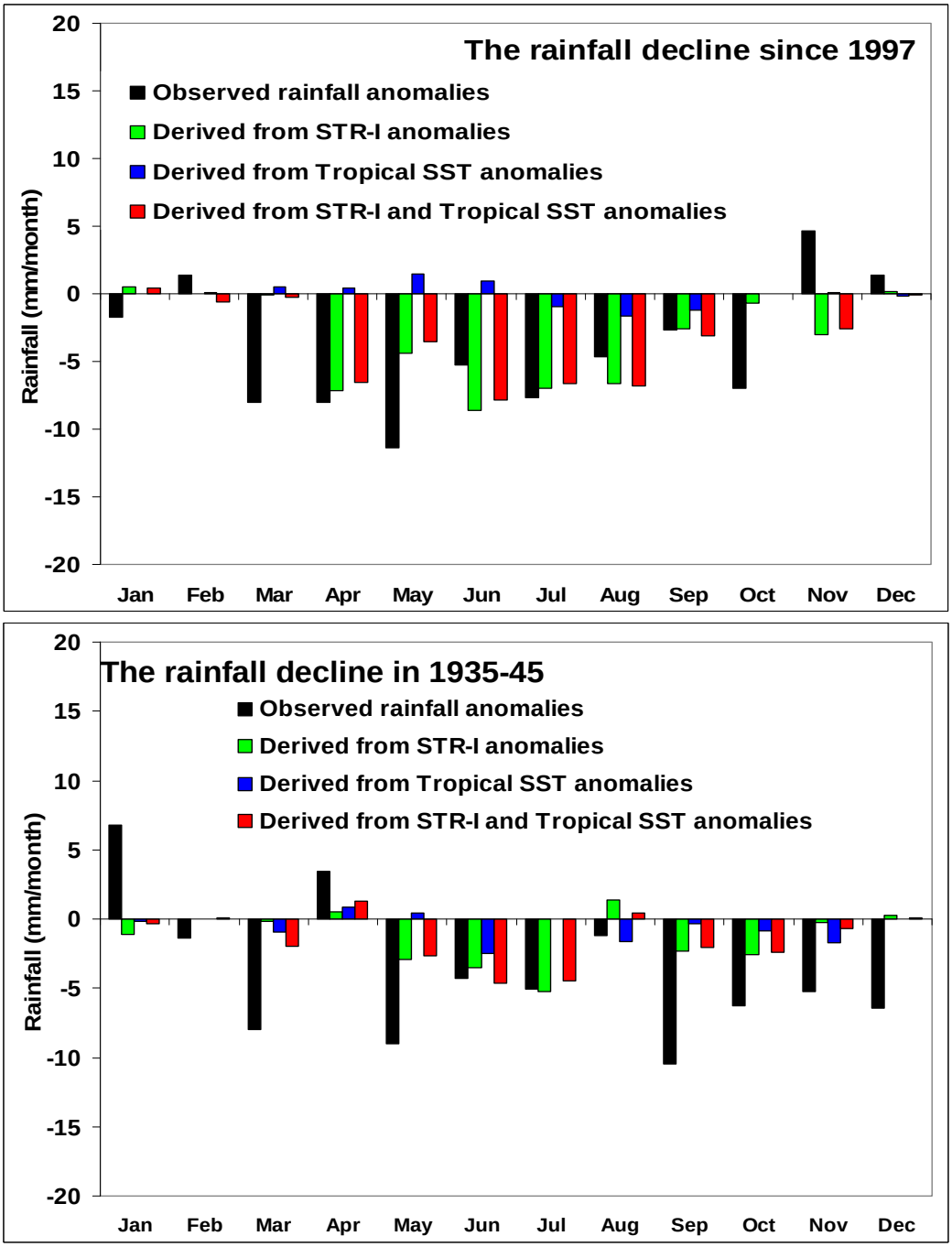

Fig. 65 *As per Fig. 62 but for the sub-tropical ridge intensity (STR-I in green), and the tropical SST index (in blue) and both the combination of both (in red).*

In general, the relationships are weaker with the rainfall residual (after the influence of the STR-I has been removed), suggesting that part of the influence of tropical SST on SWEA rainfall is operating through circulation changes already captured by the STR-I. Overall, many correlations remain sizeable and significant, especially during winter and spring. The relationship with the TPI remains significant: the correlation for the annual means drops from -0.53 to -0.32. As expected since it was purposely built, the TPI has the highest correlation with SWEA rainfall, although, correlations are similar to the other indices once the relationship with the STR-I is removed.

We will now see if tropical SSTs help to explain the SWEA rainfall decline over and above the sizeable contribution from the STR intensification. This is evaluated using the same linear methodology described earlier, but this time STR-I and the TPI are considered (Fig. 65). For the current drought, warming tropical SSTs have had no contribution overall to our rainfall since 1997. The effect on the annual rainfall is close to zero (+0.9%). In other words, the warming of the tropics and its spatial pattern, as captured by the TPI has had little impact on the rainfall decline in SWEA over and above the STR-I influence. In fact, the SWEA rainfall decline has been a little less than the STR intensification on its own would have produced: rainfall reconstructed anomalies are only 77% of the observed once the tropical SST is considered compared to 80% with the STR-I alone.

That small but positive TPI influence (the difference between green and red bars in the graphs) is seen during the autumn and early winter months. The individual contributions from the TPI (blue bars) are positive during all these months (from March to June), thus confirming that tropical SST plays no part at the time of the year when the rainfall decline is the largest (recall that two thirds of SWEA rainfall decline occurred in these 4 months). A negative but small contribution is noticeable in late winter to spring. It is worth noting that, in general, the joint contribution of the STR-I and the TPI is not simply the sum of the two individual contributions, thus confirming that part of the influence of tropical SST occurs though the STR intensification.

In contrast to the apparently minor role of tropical SSTs during the current prolonged drought, during WWII drought, tropical SSTs added a small negative contribution to the dry decade: the size of the reconstructed rainfall anomalies increases from 34% (when only the STR-I is considered) to 37% when both the STR-I and the TPI are considered. The TPI influence on its own (shown by the blue bars) is larger: a decline equivalent to 15% of the observed values. When both effects are combined (as noted for the recent period, it is not simply the sum of the two effects), the rainfall anomalies during the winter months are well accounted for, but this is not the case for large monthly anomalies in autumn and in spring, the seasons with the largest rainfall decline during WWII drought (Table 24).

The influence of the tropical SST index on rainfall in the very southern part of the Australian continent is likely to involve moisture advection across the continent from the wet tropics. The last set of results (which show that tropical SSTs only played a role during the WWII dry period) is consistent with the Australia-wide rainfall anomalies shown earlier (Fig. 57).

8.7 Conclusions

The analysis presented in this chapter has confirmed earlier results. The on-going rainfall decline is largely due to a strengthening of the STR. It has been shown that the shift in position of the STR has had little additional effect. It has also been demonstrated that tropical SSTs (including in the Indian Ocean) do not seem to be the cause of the ongoing decline. Tropical SSTs have made the rainfall decline slightly less severe in early winter while contributing slightly to the spring rainfall decline. This does not preclude the fact that, on inter-annual time-scales, some individual years or seasons can be singled out and a tropical teleconnection established: e.g. the very low rainfall during the 2006 El Niño year, or the enhanced spring rainfall decline since 2006 which is related to three positive IOD events in 2006, 2007 and 2008. These last 3 events are significant contributors to the worsening of the rainfall decline across SEA since 2006 (Timbal 2009).

The current drought can be linked to global warming through the strengthening of the STR which is, in turn, attributable to anthropogenic forcings (as detailed in the previous chapter). The WWII drought can be considered to be the first dry decade in SEA that is partially due to 20th century global warming through the intensification of the STR. Although linked to the STR intensification, the WWII drought should not be linked to anthropogenic forcings: the limited role of anthropogenic forcings and the importance of natural external forcings in this early century warming were discussed in the previous Chapter.

Between the 1900s and 1940s, the planet warmed by about the same amount (0.4ºC) as between the 1970s and now. However, the results presented here show that only around a third of the rainfall decline during the WWII drought can be explained by global warming though STR intensification, while tropical SST patterns at that time played a role, and most likely contributed to the dryness being Australia-wide during that earlier period.

This contrasts with the current drought in which around 80% of the current rainfall decline is accounted for by the intensification of the STR and with tropical SSTs playing a very minor mitigating role.

SUMMARY

- The current drought in southern Australia has occurred in conjunction with above average rainfall over much of the continent further north. This is in contrast with the WWII drought during which most of the continent experienced below average rainfall.

- The spatial pattern of the current drought has a very strong similarity with the pattern of the STR-I signature on rainfall across southern Australia. This is not the case in the WWII or Federation droughts.

- The spatial and temporal signatures of the current drought further indicate that the rainfall decline is linked to a weakening of the dominant westerly atmospheric flow.

- For the current drought, 80% of the observed decline in SWEA can be attributed to a strengthening of the STR. The apparent shift south of the ridge in certain seasons does not appear to have had an additional effect on SWEA rainfall.

- During the WWII drought, up to one third of the rainfall decline can be attributed to the strengthening of the ridge at that time.

- During the current drought, tropical SSTs have not contributed to the rainfall decline since 1997. If anything, tropical SSTs provided a minor mitigating effect.

- During the WWII drought, tropical SSTs and a strengthening of the ridge were largely responsible for the decline in rainfall. The contribution of tropical SSTs in the very southern part of the Australian continent (SWEA) now (non-existent) and during WWII (important) is consistent with the Australia-wide rainfall anomalies during both periods: i.e. a continent that was generally dry during the WWII drought versus a continent that is currently dominated by wet anomalies.

- While the current drought can be linked to global warming through the strengthening of the STR as a result of anthropogenic forcings, the WWII dry decade can be seen as the first dry decade in SEA that could be considered partially due to 20th century global warming through the intensification of the STR but not necessarily to anthropogenic forcings.

9 IMPACT OF OBSERVED CLIMATE CHANGE ON THE HYDROLOGICAL CYCLE

9.1 Introduction

The AWAP gridded hydrometeorological dataset (Raupach et al. 2009) was developed to monitor the terrestrial water balance of Australia. Measurements and model predictions were combined using model-data fusion methods. Funded jointly by CSIRO Marine and Atmospheric Research (CMAR), the BoM and the Bureau of Rural Science (BRS), AWAP establishes soil moisture and water fluxes that contribute to soil moisture from 1900 to the present on a 5km grid across the Australian continent.

Gridded meteorological data, such as precipitation, temperature and solar influx, force the model. Both upper and lower layer soil moisture are model outputs (where the upper and lower layers are typically 0.2 m and 1 m deep, respectively, depending on soil type). Soil moisture levels are determined by tracking a water balance in which the important water fluxes are precipitation, transpiration, soil evaporation, surface runoff and drainage. Of these, precipitation is an input and the other four are variables predicted by the model because they depend on soil moisture itself.

Transpiration is defined as the lesser of energy-limited and water-limited transpiration rates. The energy-limited transpiration rate is defined by the Priestley-Taylor rate attenuated by the vegetation cover fraction. The water-limited transpiration rate in each soil later is specified using a rate parameter which controls the decay of water extraction by roots from a drying soil under water-limited transpiration and full vegetation cover. Soil evaporation is the product of an upper-limit value (Priestley-Taylor evaporation), the relative water content in the upper soil layer and the fraction of bare soil. These two parameters combine to give total evapotranspiration (FWE).

Surface runoff is given by a step function - all precipitation runs off when the upper-layer soil is saturated and there is no runoff otherwise. Leaching or drainage downward out of each soil layer is given by the product of saturated hydraulic conductivity and a power of the relative water content in each layer. Surface runoff and leaching combine into total runoff, or local discharge of water from the soil column (FWDis).

In this chapter, upper and lower soil moistures, total evaporation and total runoff are investigated and compared with rainfall, the most important atmospheric forcing.

9.2 The influence of the sub-tropical ridge on the water balance

As part of the analysis of the observed changes in the climate of SEA, it was found that more than 60% of the rainfall decline occurred in autumn (Chapter 2). The annual rainfall decline for the initial period analysed (1997-2006) was large but not unprecedented. However this large

rainfall decline combined with the absence of wet years, the very large decline in autumn rainfall and higher temperatures, was record breaking for reductions in water availability (i.e. streamflows) across SEA (Murphy and Timbal 2008).

Subsequently (Chapters 2 and 3), an analysis of the large-scale modes of variability known to influence the Australian climate (e.g. ENSO, the IOD and the SAM) showed that they were unlikely to have contributed significantly to the rainfall decline across SEA due to its strong autumn signature. Rather, it was found that the MSLP increase during the late 20th century which has been observed above southern Australia (Timbal and Hope 2008), which is a manifestation of the intensification of the STR, was linked to 80% of the total rainfall decline across SWEA (Chapter 8).

Recently, the rainfall decline across SEA has worsened and become the largest long-term rainfall deficit in the instrumental record (Timbal 2009); its signature is predominant across SWEA, a critical area for the generation of runoff in SEA (Chapter 8).

In the analysis presented in this chapter, the Drosdowsky (2005) STR-I index is used and its impact on the various moisture variables available from AWAP is evaluated. Correlation coefficients between the STR-I and monthly means of AWAP variables for the period from 1900 to 2007 are computed and averaged for 3 monthly periods. These coefficients are shown below for rainfall (Fig. 66), surface and deep soil moisture (Figs. 67 and 68), total evaporation (Fig. 69) and total runoff (Fig. 70).

At first order, there is a strong consistency in the pattern of the influence of the STR-I on all related moisture variables, with negative correlations at certain times of the year (generally from about April through November) apparent across SEA for rainfall, upper and lower soil moisture, evaporation and runoff. Beyond this expected overall consistency between hydrological variables, differences in spatial patterns and seasonality are worth exploring further:

- There is no lag effect between the influence of the STR-I on rainfall and upper soil moisture. The negative correlation with the STR-I starts in autumn (MAM), is maximum in early winter (MJJ) and decreases toward late spring (OND);

- This is mostly the case for total evaporation as well, but differences in the spatial extent of the influence of the STR-I on rainfall versus evaporation suggests that, while the relationship is very similar inland of the GDR (i.e. suggesting that evaporation is primarily moisture limited), it is not so on the GDR and along the coast, where the relationship between evaporation and the STR-I is negligible, suggesting that daily maximum temperature (which is positively related to the STR-I) is a more important factor;

- Lower soil moisture and runoff show lower correlations with STR-I compared with the other variables. This is particularly noticeable in the early part of the wet season (April-June), but less so in the latter part of the wet season (July to November). This reflects the fact that in the earlier part of the wet season, a greater proportion of any rainfall will go into wetting up the soil moisture store;

- The difference in the relationship with the STR-I between the forcing (rainfall) and the response (deep soil moisture and runoff) creates a lag effect in term of importance of the STR-I for these two variables compared with rainfall: the largest correlation between the

STR-I and deep soil moisture is observed in spring (ASO/SON) while for runoff it is fairly similar during the entire wet season (April to November); and

- The spatial extent of the area of significant correlation between STR-I and deep soil moisture and runoff is smaller than for the area significantly correlated with rainfall, evaporation and upper soil moisture. The area of significant correlation between STR-I and deep soil moisture and runoff covers most of SWEA and extend north and east along the GDR thus covering the important catchment areas for the Murray river.

Beside the consistency of the impact of STR-I on all important surface water balance variables available from the AWAP, the lag effect on deep soil moisture and runoff is consistent with the general understanding of the rainfall relationship with deep soil moisture and runoff.

This analysis using AWAP data supports the suggestion made earlier in SEACI-1 that autumn rainfall decline amplified impact on streamflow (Murphy and Timbal 2008) through the linkage back to the primary driver of the rainfall decline (the STR-I). AWAP provides a suitable tool to investigate the possible lag effect between the rainfall decline (predominantly in autumn) and the impact on total runoff which is largest in winter and spring.

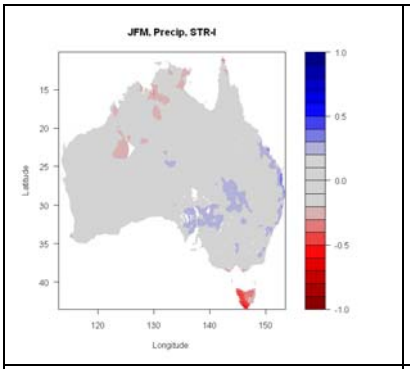	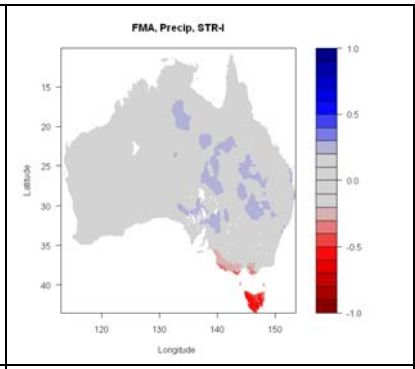	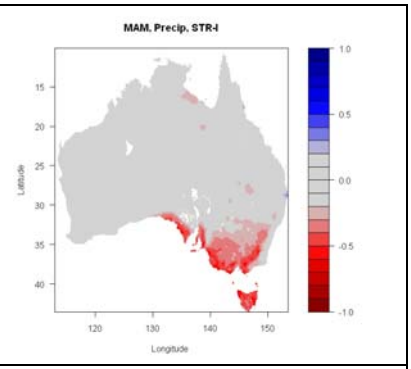
JFM	**FMA**	**MAM**

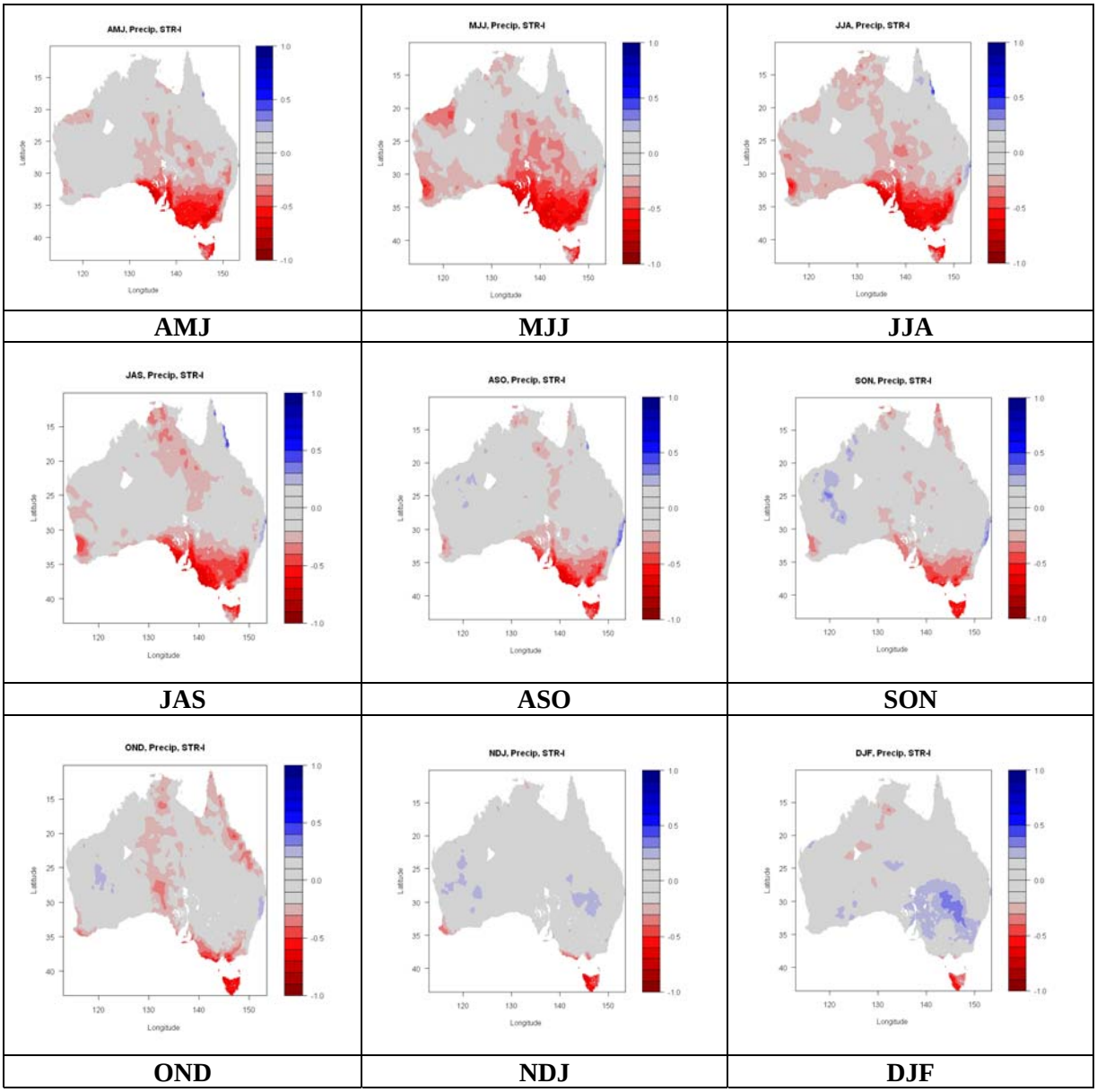

Fig. 66 *Month by month, 3-month average correlations between the sub-tropical ridge intensity and rainfall across Australia, based on observations from 1900 to 2007; only correlations significant above the 95% level are shown.*

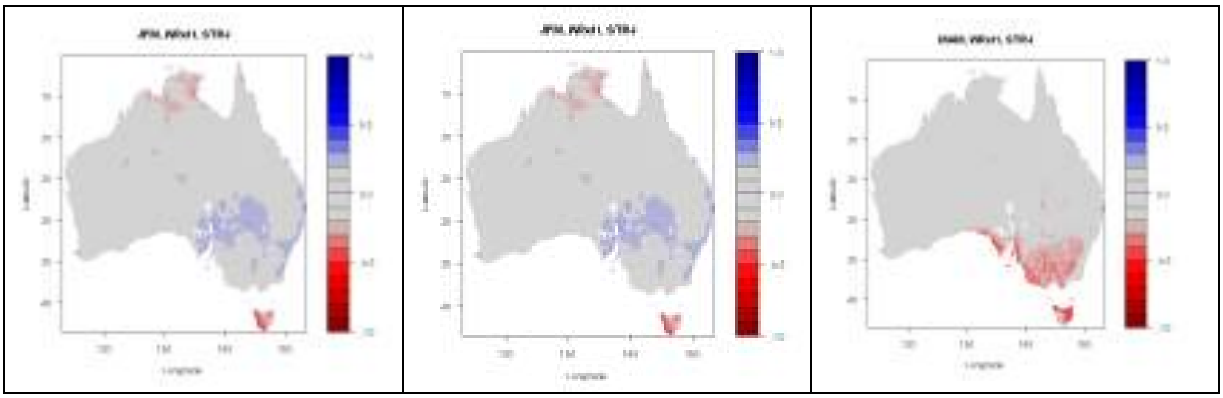

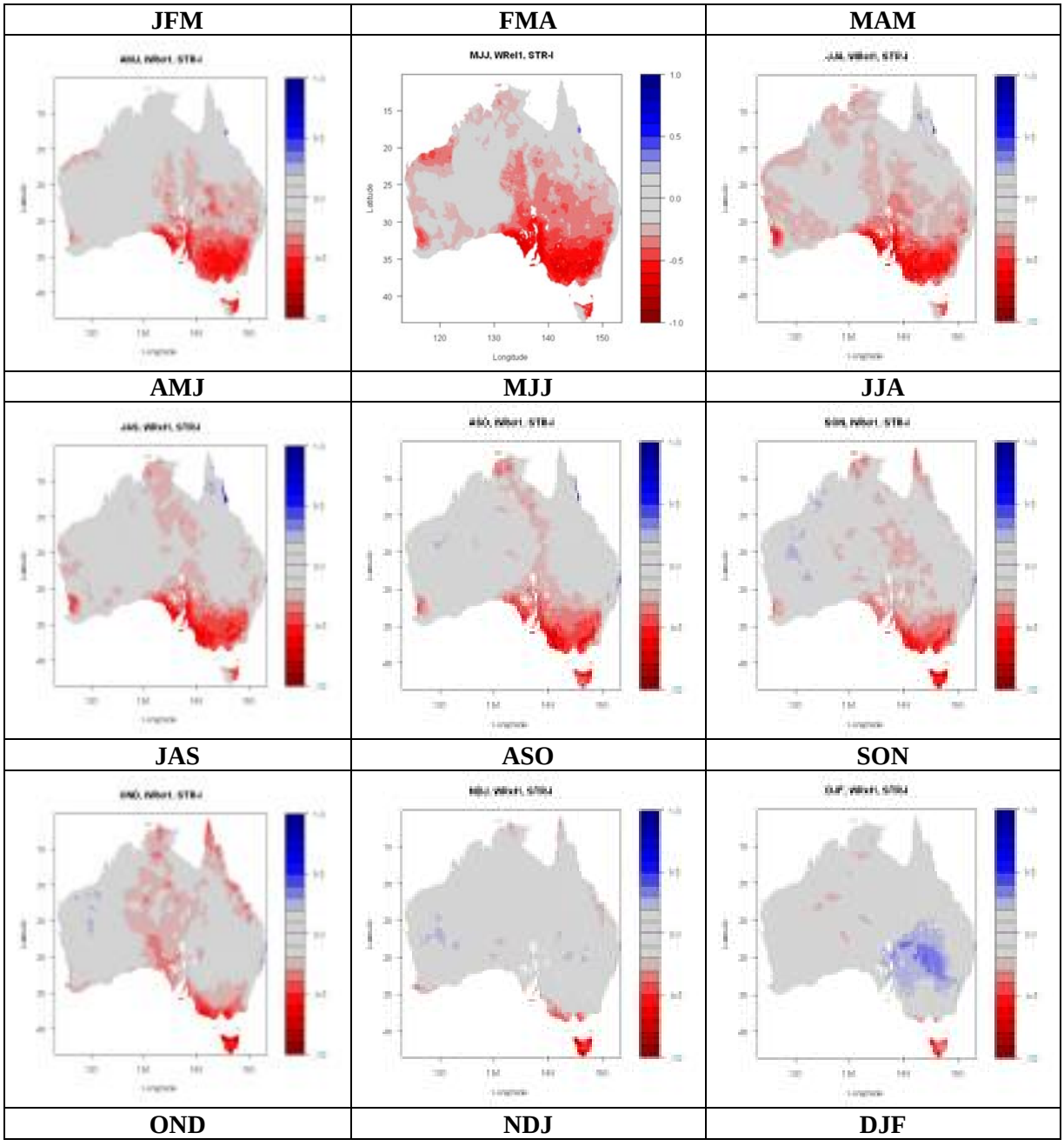

Fig. 67 *As per Fig. 66 but for upper soil moisture (20cm deep).*

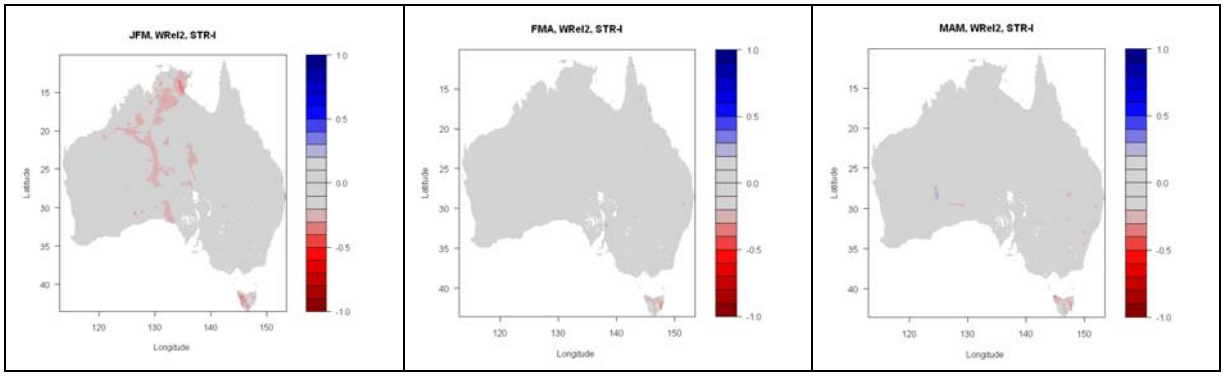

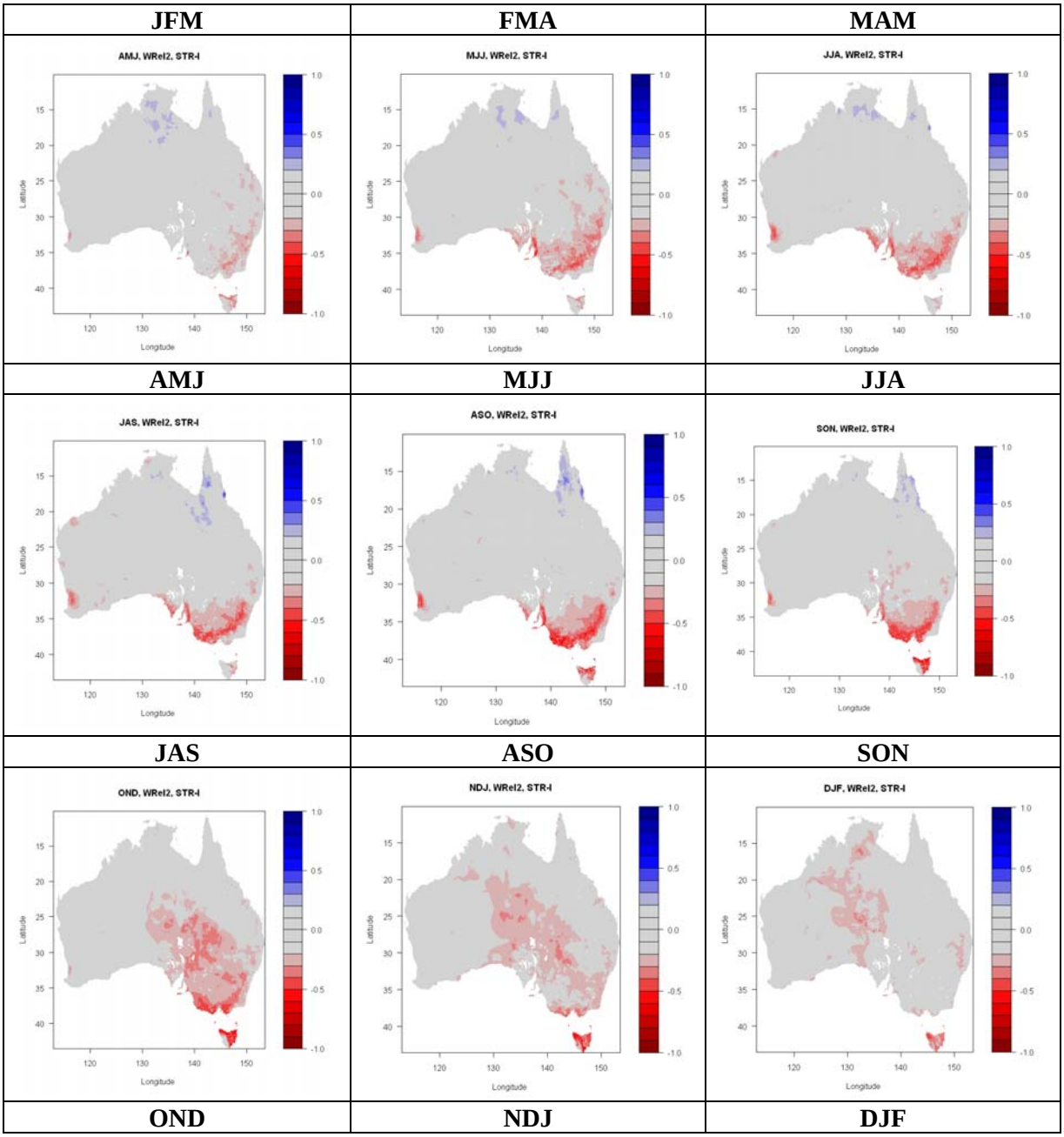

Fig. 68 *As per Fig. 66 but for lower soil moisture (0.2 to 1.5 m deep).*

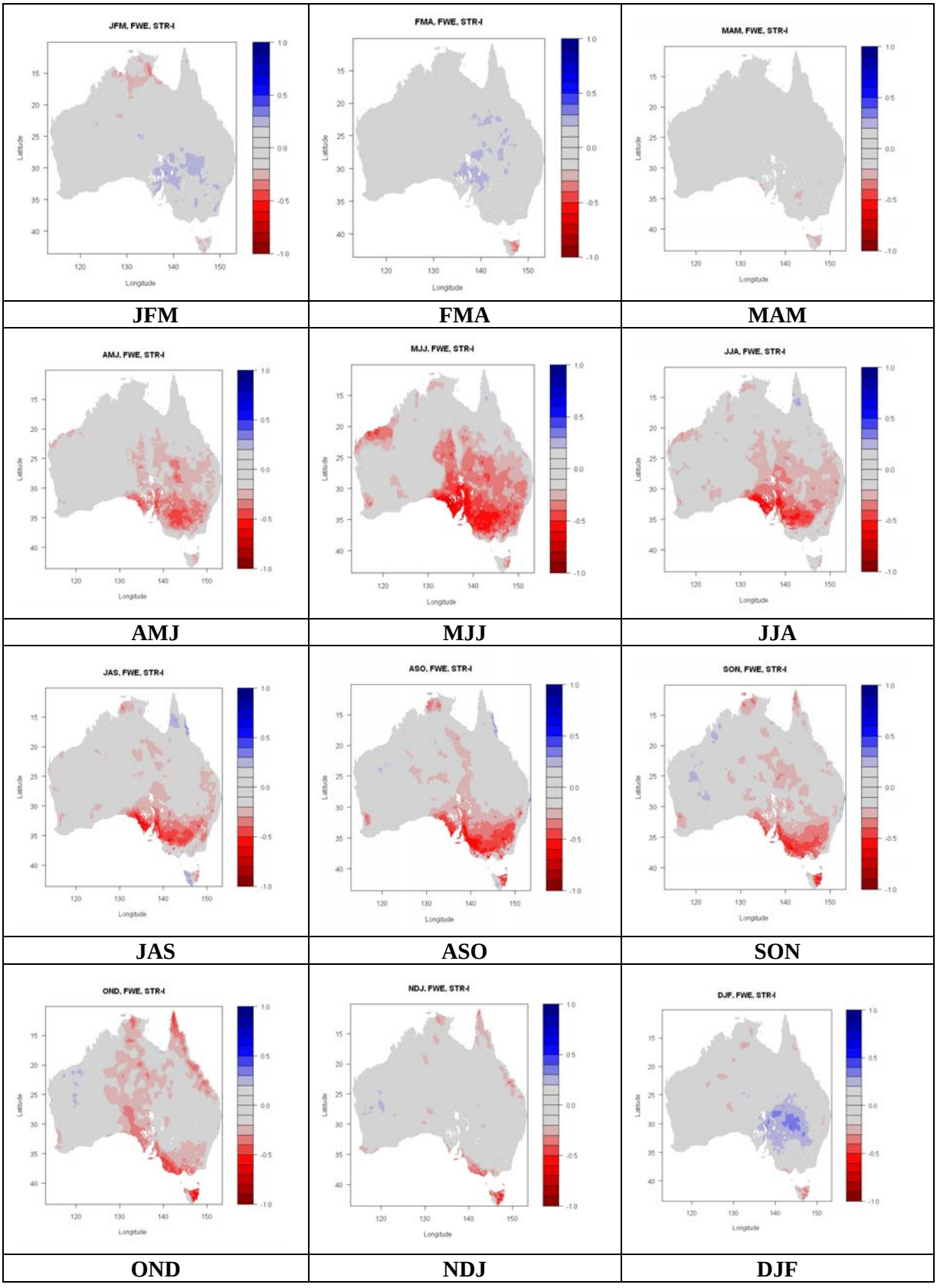

Fig. 69 *As per Fig. 66 but for total evaporation.*

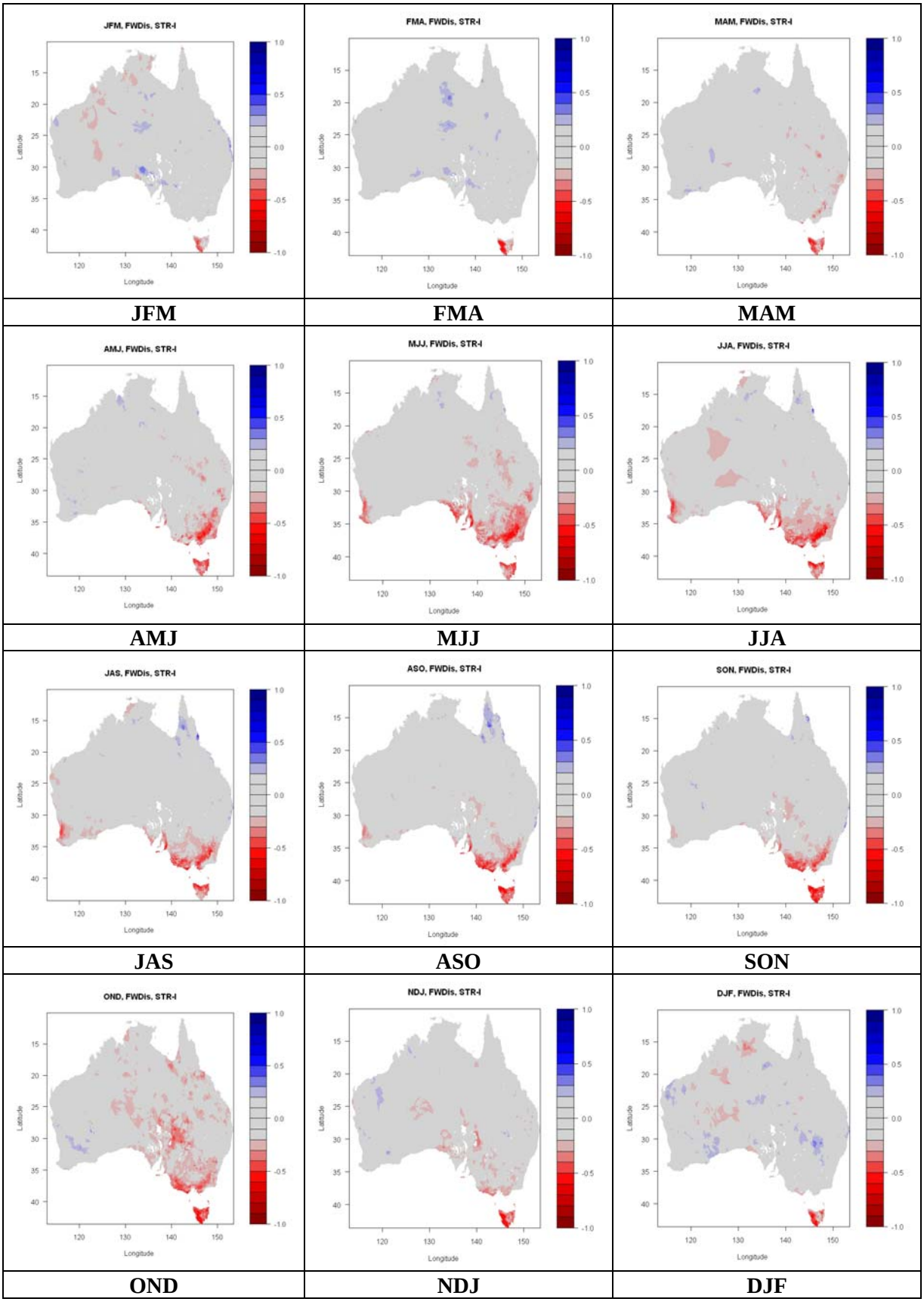

Fig. 70 *As per Fig. 66 but for total runoff.*

9.3 Lagged correlations between large-scale modes of variability and water balance components

In this sub-section, lagged correlations between 3 climate indices and lower soil moisture (Figs 71 and 72) and total runoff (Figs 73 and 74), the two AWAP surface water balance variables that earlier showed a lag effect (a larger correlations with the STR-I at lag of at least one month), are reported for winter and spring. Zero, 3 month and 6 month lag correlations are computed (with AWAP variables lagging behind the climate indices).

A large number of climate indices are used; here we are focusing on three essential indices:

1. the Niño4 (160°E-150°W, 5°N-5°S) SST anomalies (as the ENSO indices most relevant for SEA rainfall) (N4);
2. the Saji et al. (1999) Indian Ocean DMI; and
3. the Drosdowsky (2005) STR-I index.

Although it was shown earlier that ENSO and the IOD have not contributed to the rainfall decline in autumn, it is interesting to compare the lag effect of these three indices on those AWAP variables which show a tendency to display a lag effect.

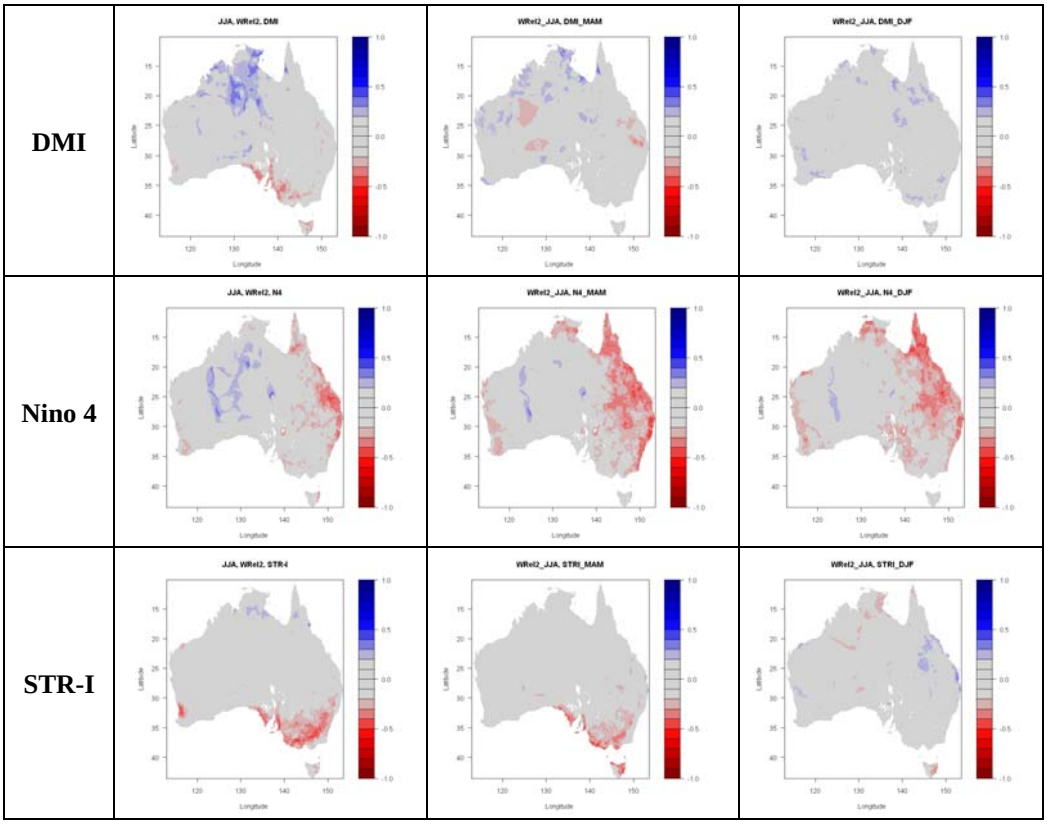

Fig. 71 *Seasonal correlations between various large-scale indices (Nino 4 SST anomalies, the Indian Ocean Dipole Index and the sub-tropical ridge intensity) at lag 0 (left column), at 3-month lag (middle column) and at 6 month lag (right column) for winter lower soil moisture (0.2 to 1.5m deep).*

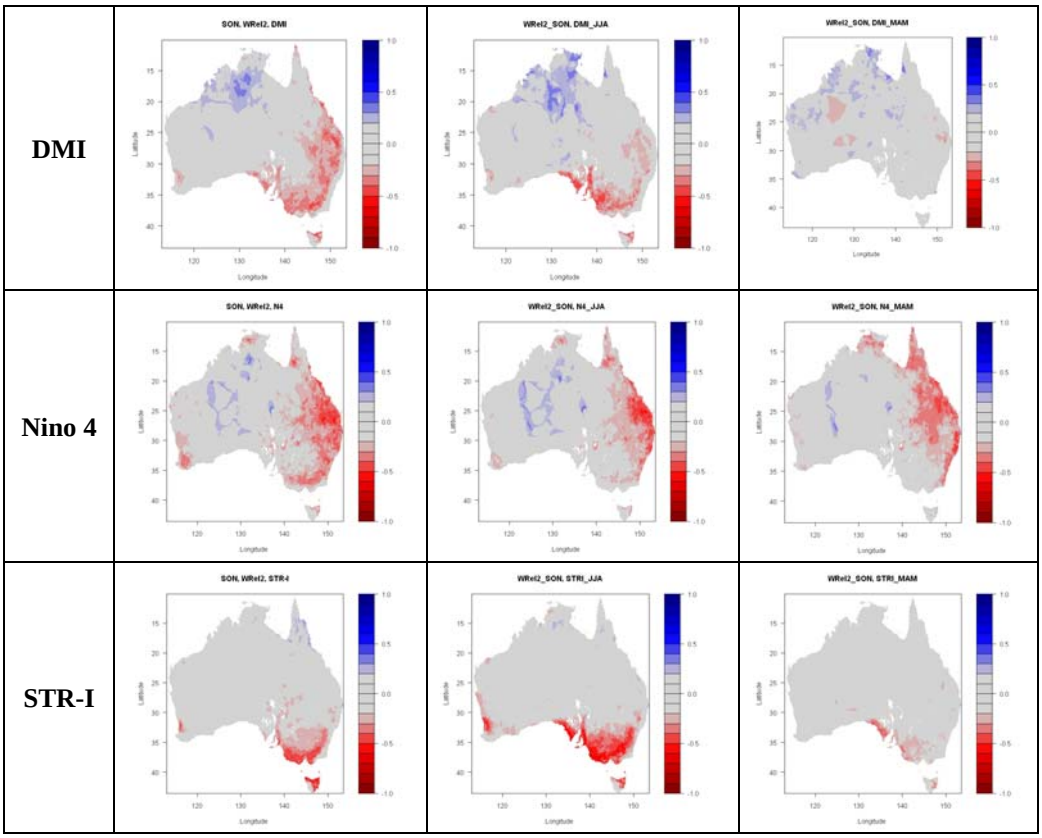

Fig. 72 *As per Fig. 71 but for Spring.*

The main points to note regarding these correlations for winter (Figs 71 and 73) (comparing simultaneous and 3-month lag correlations) are:

- 3-month lag correlations between both N4 and STR-I (3 months ahead) and lower soil moisture are significant but in different parts of SEA: along the ESB and NMDB for N4 and in SWEA for STR-I;
- The lag correlations are lower than the simultaneous correlations for the STR-I but higher for N4;
- The DMI has no significant lag correlations anywhere across SEA, which is consistent with the fact that IOD events do not form until winter and do not therefore have a relationship with rainfall in MAM;
- The above findings for lower soil moisture are equally valid for total runoff.

In the case of the spring correlations (Figs 72 and 74):

- Of the 3 climatic indices, the DMI has the largest simultaneous correlations with lower soil moisture across Australia consistently. This is consistent with the known influence of the IOD across Australia and the fact that it peaks in spring.
- With total runoff, results are mostly similar. The three large-scale indices have in general lower correlations than with lower soil moisture. One difference is that the STR-I appears more important at lag 0 than the DMI in some parts of the SEA, in particular in southern Victoria;

- The most significant relationship at a 3 month lag is with the STR-I ahead of the relationship with the DMI;
- The lag correlations between STR-I and deep soil moisture are larger than the simultaneous correlation (this is also the case for total runoff);
- 3-month lag correlations with N4 are decreased across SEA towards the ESB, while simultaneous correlations are significant across a large part of SEA including the GDR;
- 6-month lag correlations are in most instances insignificant across most of SEA with the exception of N4 along the ESB and STR-I in small pockets along the coast in SWEA.

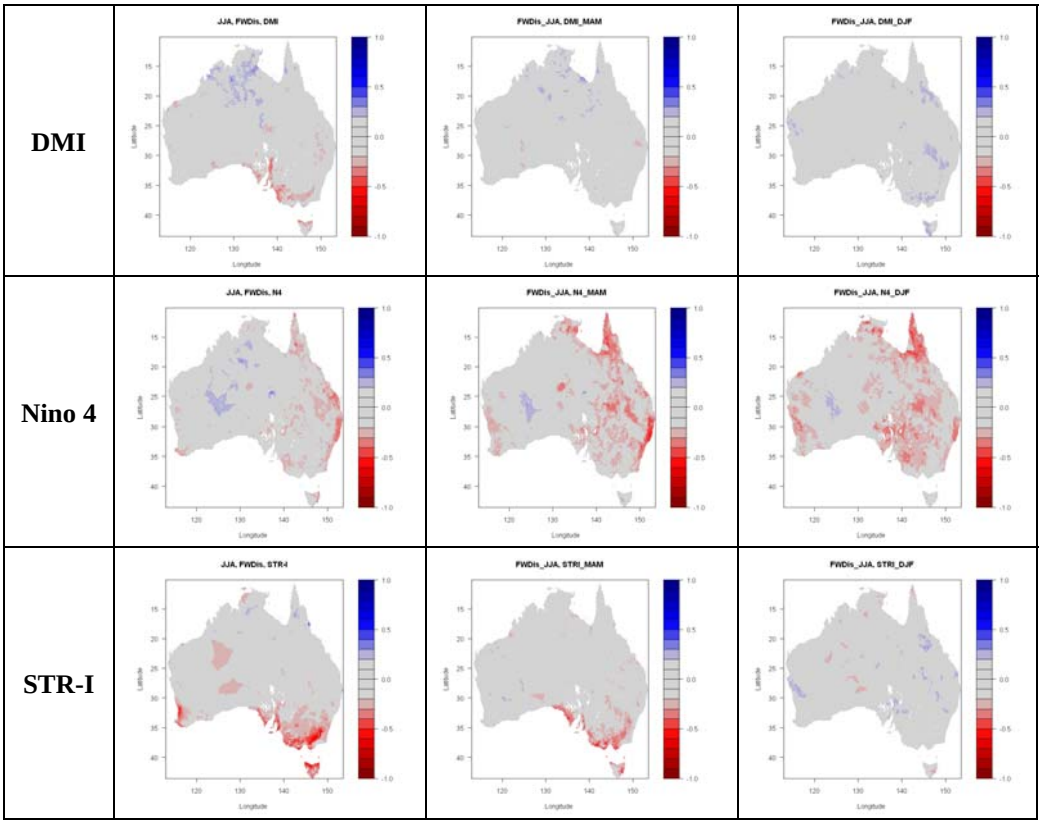

Fig. 73 *As per Fig. 71 but for runoff and discharge.*

This analysis confirms the earlier results that deep soil moisture and total runoff in winter and spring are strongly affected by the STR-I in the previous season. This reflects the strong influence of the STR-I on the rainfall in those earlier seasons (i.e. at lag zero). That lag mechanism is particularly evident in spring when the simultaneous impact of the STR-I on rainfall starts to be reduced but the lag effect between STR-I and deep soil moisture and runoff results is significant. During the last decade, the STR intensification has been larger in JJA than in SON (Chapter 8). This might have contributed to a reduction of streamflows in spring, a season where rainfall reduction is small (Timbal 2009). This together with an absence of very wet year could potentially account for a large part of the additional hydrological amplification observed in the recent decline in streamflows compared to previous droughts (Potter et al. 2010).

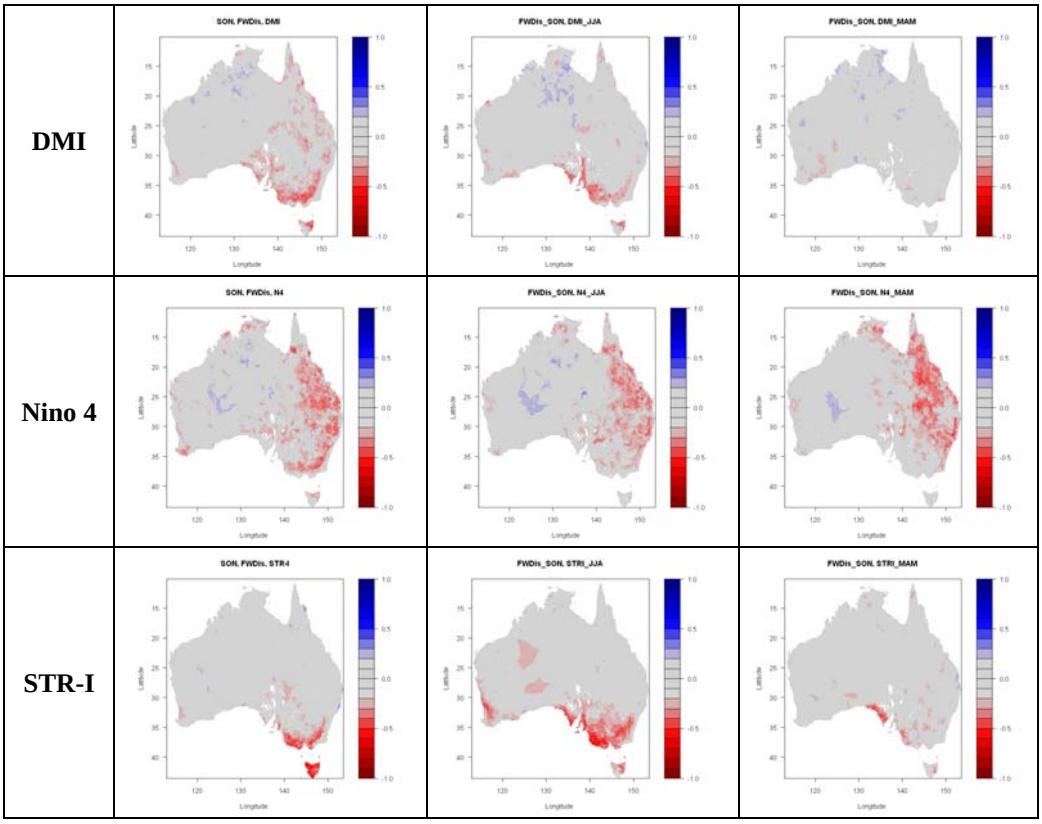

Fig. 74 *As per Fig. 72 but for runoff and discharge.*

This early analysis using the AWAP does not permit a definitive answer. Future analysis will need to investigate how the amplification factor between rainfall and runoff has changed seasonally and annually while the autumn rainfall decline has been happening. In particular, future analyses need to look at how those changes in patterns in rainfall (as a result of changes in STR-I) have affected the other moisture variables and relationships between rainfall and the other moisture variables on a seasonal and annual basis.

9.4 Future prospects

The results obtained in this chapter provide a better understanding of how ongoing climate change affects the entire water balance across SEA. While these early results are very encouraging, further research using AWAP products during SEACI-2 will help advance our understanding further.

A particular focus will be to use more advanced statistics to better understand the influence of large-scale modes of variability and their interactions. Correlation, regression and principal components analysis as used here, have been the cornerstone of climatic research. Such methodologies, however, make assumptions about linearity that may not be always valid. Developments in nonlinear statistics have made the exploration of nonlinear processes possible and, in particular, it is planned to use Classification and Regression Trees (CART). This is a relatively new and powerful regression-based technique that is capable of accounting for nonlinear effects and has many possibilities. Such analysis is particularly informative when

there are multiple predictors and when the relationship between variables is nonlinear, as is most likely the case between remote climate teleconnections (e.g. ENSO or the IOD) and regional drivers influencing the local rainfall (e.g. the STR). Statistical relationships between variables are the basis for the decision rules that are used to split the data into increasingly homogenous groups. CART has been used to successfully predict fire season severity from atmospheric circulation anomalies. Decision trees were grown that classified, and thus predicted, fire season severity based on MSLP in a key region between Tasmania and New Zealand, giving a valuable insight into the prediction of fire season severity in SEA (Bessell 2006; Edwards 2002).

There is considerable potential in the use of this methodology for examining the internal associations between large-scale modes of climate and the associations between the drivers and SEA climate variables. CART allows examination of multiple nonlinear interactions between drivers that affect climate and hydrology. Decision rules based on the state of the major large-scale drivers of climate will be developed to see how their phases are associated with climatic and hydrological variables in SEA.

Linear statistics indicated that the position of the STR generally had no additional effect to that of intensity alone in predicting rainfall (Chapter 8). This finding is somewhat surprising and worth investigating further using more advanced statistical tools such as the CART methodology.

In a second step, the combined influence of the STR and the remote teleconnections will be studied. CART will allow us to determine which drivers have the largest influence on SEA climate and the inter-relationships between the drivers. The combined effect of the large-scale drivers on climate variables such as rainfall and temperature can then be determined and compared with the relationships between the large-scale drivers and hydrological variables, to ascertain if there is a stronger relationship between hydrological variables and large-scale modes of climate than with climate variables and the remote drivers.

SUMMARY

Using the AWAP variables, it was possible to show that:

- There is a strong consistency in the pattern of the STR-I influence on all related moisture variables for the period – i.e. on rainfall, upper and lower soil moisture, total evaporation, and total runoff from around March to October;

- The influence of the STR on rainfall, upper soil moisture and total evaporation is simultaneous. In contrast, both lower soil moisture and runoff show lower correlations with the STR-I in the early part of the wet season (May-June-July), with correlations peaking in the latter part of the wet season (August-September-October);

- The spatial extent of the area having significant correlations between STR-I and deep soil moisture and total runoff is much reduced compared to the area where there are significant correlations between these variables and rainfall, but covers most of the important catchment areas in SEA;

- In contrast to other large-scale influences (ENSO and IOD), the STR intensification is the only variable which exhibits higher lag correlations compared to the simultaneous correlations, in particular with deep soil moisture and runoff; and

- The lag correlation between the STR-I and deep soil moisture and runoff in winter and spring is consistent with the hydrological understanding of the relationship between rainfall and lower soil moisture and run-off but offers a possible additional effect to contribute to the amplification of the rainfall decline in term of impacts on streamflow as the STR intensification is more pronounced in the early part of winter.

10 UPDATE ON THE DETECTION OF ONGOING CLIMATE CHANGES TO THE END OF 2009

During the course of Phases 1 and 1P of SEACI, several sets of data from the Bureau of Meteorology (BoM) were used to monitor and explore the rainfall decline and other aspects of the climate of SEA. Station data used mostly in relation to the application of the BoM SDM (Chapters 4, 5 and 6) are detailed in the Appendix. Gridded rainfall data were used to determine the various regional averages used in the different projects for SEA, SWEA, NMDB, ESB and others (Chapter 2, 3 and 8). Newly formed and improved gridded rainfall became available as part of the Australia Water Availability Project (AWAP) during SEACI-1 and analyses were increasingly performed using this new product (e.g. Chapter 9).

After replacing the operational BoM gridded rainfall (Jones and Weymouth 1997) with the superior AWAP gridded rainfall (Jones et al. 2009), it became obvious that, although the two products are in good general agreement, sizeable differences can be observed across SEA in specific locations. These differences are more pronounced for areas with poor historical data coverage and, in particular, at high elevations. The lack of data combined with the coarse resolution of the previous gridded rainfall in the earliest dataset lead to an overestimation of rainfall across SEA for the early part of the 20th century.

It is therefore of interest to update some of the early graphs and tables produced using the former operational data (Jones and Weymouth 1997) with the new AWAP product (Jones et al. 2009). This has the added benefit of making earlier results more consistent with those presented in Chapter 9 and provides an opportunity to update all the results to the end of 2009.

10.1 The magnitude of the rainfall deficit

Analysis of the AWAP up to the end of 2009 indicates that the ongoing rainfall decline is worse than any previous period in the historical record (Fig. 75). If years up to and including 2006 are instead used, the 10-year anomaly (517 mm) was not as low as the lowest on record (1936-1945) (Table 25). The period of below average rainfall has continued and now extends to 13 years. The 1997-2009 anomalies are now far worse than the previous driest 13-years in the historical record (1933-1945). The current deficit of -11.4%, compared to the entire historical record from 1900 to 2009, is 45% worse than in 1933-1945 when the decline was -7.8% (Table 26).

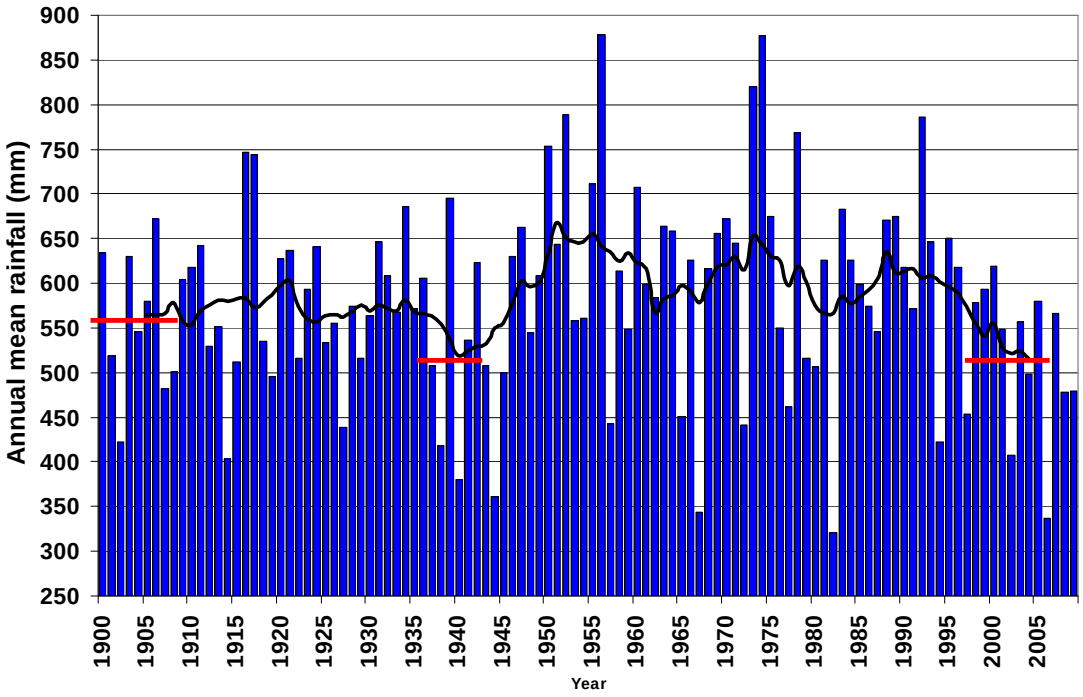

Fig. 75 *Mean annual rainfall over the south-eastern Australia region (mainland south of 33.5°S, east of 135.5°E) from 1900 to 2009. Also shown are the 13-year mean for 1997-2009, the 10-year means for 1900-1909 and 1936-1945 (thick, short horizontal lines), and the 11-year running mean (solid black). [This is an update of Fig. 7 of this report].*

Table 25 *Mean and standard deviation (σ) of annual and autumn rainfall and annual maximum and minimum temperature over SEA from 1997-2006, as well as for the 1961-1990 mean and two previous ten-year dry spells: 1900-1909 and 1936-1945. Values in bold indicate mean differences from the 1961-1990 reference period which are statistically significant at the 5% level according to a Student's t-test. [This is an update of Table 2 in Murphy and Timbal (2008)].*

	1997-2006		1900-1909		1936-1945		1961-1990	
	Mean	σ	Mean	σ	Mean	σ	Mean	σ
Annual Rainfall (mm)	**517.0**	91.5	559.1	78.6	**513.7**	107.7	602.4	121.6
Autumn Rainfall (mm)	**100.0**	33.4	143.7	56.3	**120.4**	37.1	150.8	50.9
Maximum Temp. (°C)	**20.4**	0.27	---	---	19.7	0.47	19.9	0.48
Minimum Temp. (°C)	8.4	0.31	---	---	**7.7**	0.42	8.3	0.42

Table 26 *Means of annual, autumn, winter and spring rainfall (in mm) over SEA for the ongoing drought (last 13 years 1997-2009) and the previous lowest 13-year period on record (1933-1945) and the corresponding percentage of the long-term (1900-2009) mean, using the AWAP gridded rainfall.*

	1997 - 2009		1933 - 1945		1900-2009
	Mean	Percent	Mean	Percent	Mean
Annual	514.9	-11.4%	535.5	-7.8%	580.8
Autumn	101.4	-25.3%	121.0	-10.8%	135.7
Winter	157.7	-9.4%	159.7	-8.3%	174.1
Spring	144.3	-5.0%	137.3	-9.6%	151.9

10.2 The seasonality of the rainfall deficit

In terms of seasonality, the overall picture is largely unchanged: the autumn rainfall decline in the ongoing drought remains clearly visible. It is worth noting that although the annual rainfall deficit has increased in the last 3 years, this is not the case for the autumn decline which is slightly less (Table 26 versus Table 25) and hence it is driven by a winter and spring decline which continue to worsen.

It is now well established that the ongoing rainfall decline in SEA is affecting the entire cool seasons: autumn, winter and spring. As already noted by Timbal (2009), the rainfall decline started in autumn and this is even more predominant if anomalies are considered further back than 1997, e.g. since 1988 (Fig. 76). But the winter decline is now significant and larger than the corresponding season during the WWII drought (Table 26). The decline in spring while not being as severe as during the WWII drought for the entire 1997-2009 period (Table 26), has also declined recently. In fact, the rainfall decline in the last 4 years is actually largest in spring (Fig. 76).

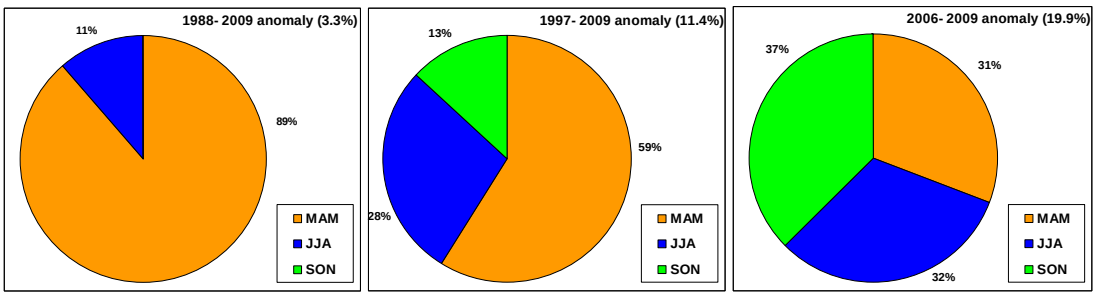

Fig. 76 *Contribution of autumn, winter and spring to the overall rainfall decline for three different periods: since 1988 (left), since 1997 (middle) and since 2006 (right). In all graphs, summer anomalies are omitted and percentages are based on the 3 seasons displayed. The annual rainfall anomalies (shown in the top right of each graph) include all four seasons and are calculated from the long-term 1900-2009 mean. [This is an update of Fig. 3 from Timbal (2009)].*

While the monitoring of the ongoing rainfall deficit has focused on the step change since 1997, as shown in Fig. 76 the seasonal rainfall declines have started at different times. In the 11-year running means (Fig. 77), the decline started after a period when rainfall was well above the long-term average, in the 1960s, 1970s and 1980s depending on the seasons. The recent decline in annual rainfall can be traced back to the early 1990s; the commencement of the larger autumn deficit can be traced back to the 1970s.

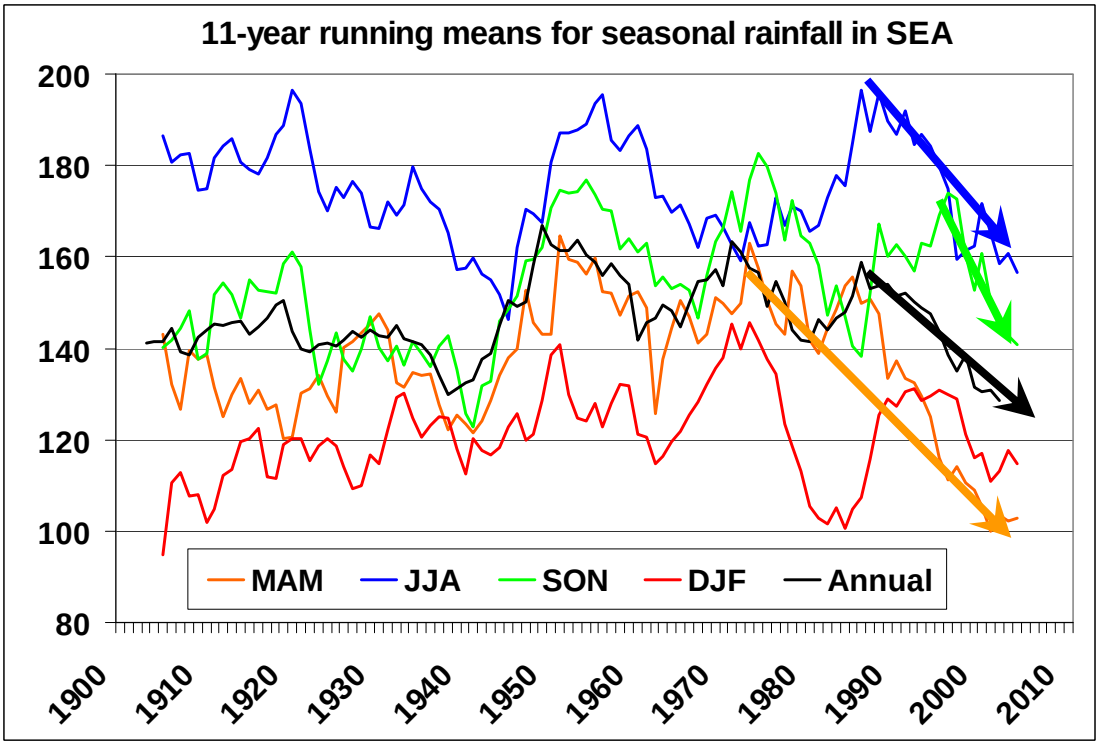

Fig. 77 *11-year running mean seasonal SEA rainfall (the annual mean is divided by 4 to be comparable to the four calendar seasons). The recent annual, autumn, winter and spring declines are indicated by coloured arrows.*

This period since the 1970s corresponds to the period when both global warming and STR-I started to rise again after a 20 to 30-year period of near stability (Fig. 14 in Chapter 3 and Fig. 51 in Chapter 7). In autumn, there has been a steady decline for nearly 40 years which has reached levels below any past historical record. In winter and spring, where decadal (spring) to multi-decadal (winter) variability is very noticeable, the recent declines since the early 1990s in winter and the turn of the 21st century in spring are not outside the range of past variability, in terms of duration and rate of decline.

On a month by month basis, there is a continuum of months showing a rainfall decline from March to October (Fig. 78). This graph updates Fig. 4 from Murphy and Timbal (2008) and Fig. 2A from Timbal (2009). *[NB: An additional difference from the Murphy and Timbal (2008) plot is that the reference period is no longer the WMO recommended 1961-1990 period but the entire record available from 1900 to 2009]*. The only month showing an anomaly of a different sign between Fig. 4 in Murphy and Timbal (2008) and Fig. 77 is June.

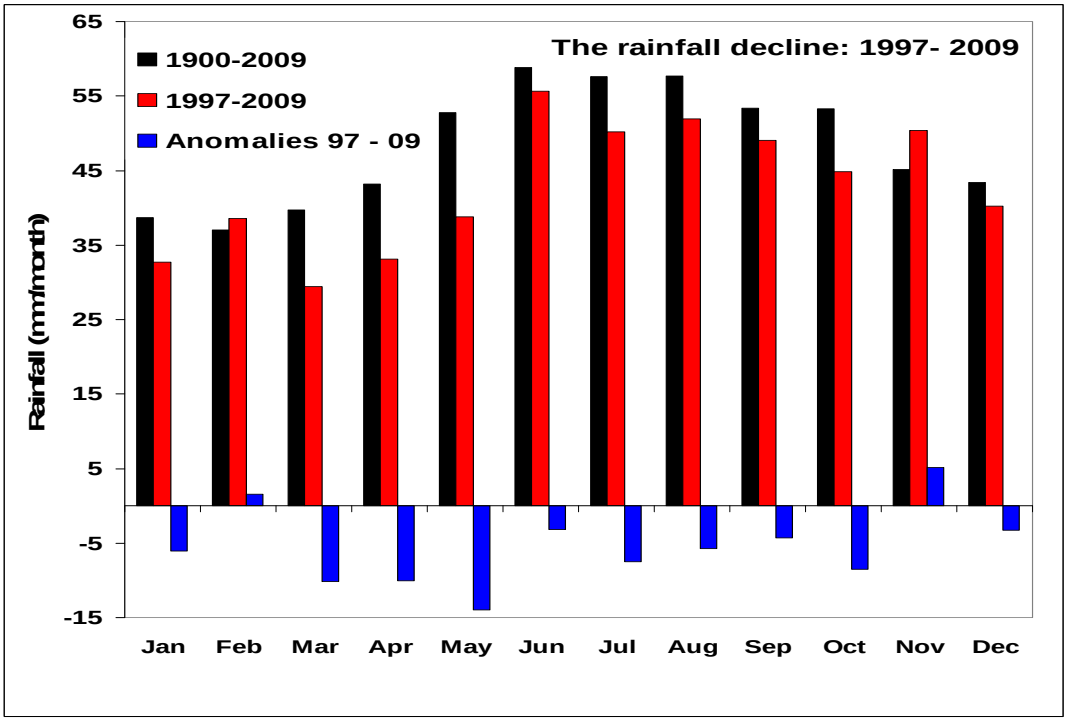

Fig. 78 *Monthly mean SEA rainfall for 1900-2009 (black bars), 1997-2009 (red bars) and the change from the earlier period to the later (blue bars) in mm per month.*

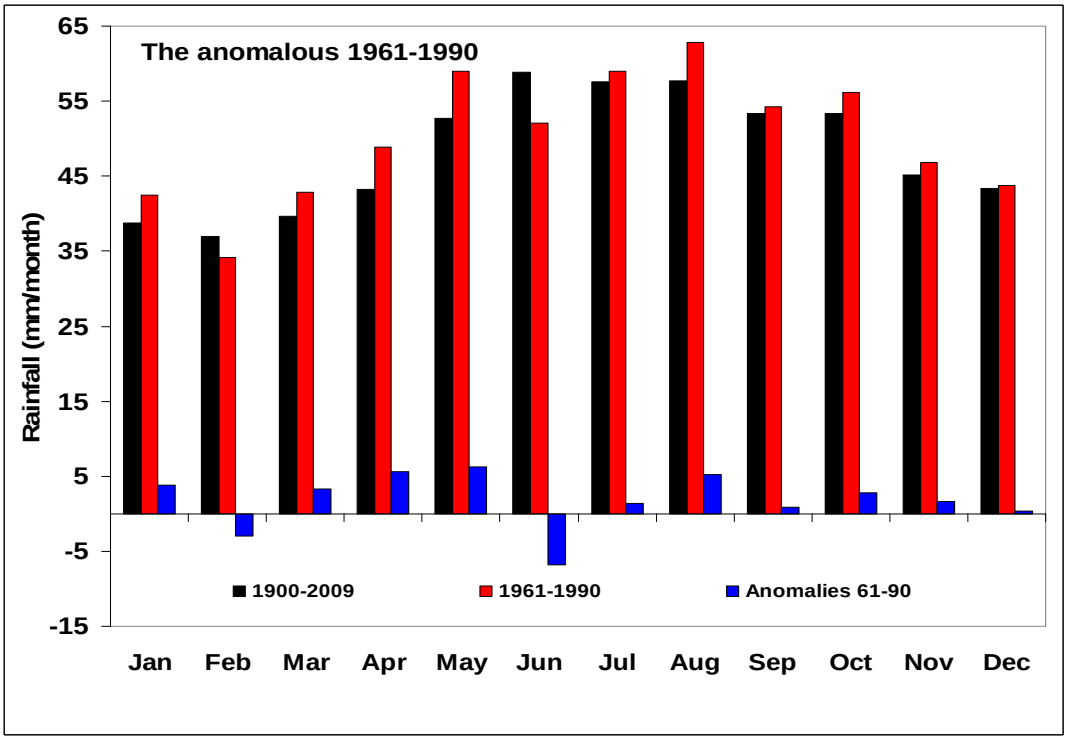

Fig. 79 *Monthly mean SEA rainfall for 1900-2009 (black bars), 1961-1990 (red bars) and the change from the earlier period to the later (blue bars) in mm per month.*

The fact that June exhibits a decline since 1997 as in every other month from March to October is due to the change of reference period. Indeed, it was decided not to use 1961-1990 as the reference period for SEA since it is an anomalously wet period compared to the entire historical record (Fig. 79).

Interestingly, June during 1961-1990 stands as the only month during the cool period of the year where rainfall was not above the long-term average (1900 to 2009). This behaviour explains why in Murphy and Timbal (2008) the month of June stands out: it is partly because the decline in June in 1997 is the smallest of all the months from March to October (Fig. 77) and partly because it was anomalously dry during the wet 1961-1990 period (Fig. 78). In SEA, June is historically the wettest month of the year; in addition it appears to be less variable on decadal time-scales. It is nevertheless experiencing a deficiency in relation to the long term climatology.

10.3 The relationship between rainfall and temperature

As noted in Chapter 2, the ongoing rainfall deficit is happening at a time when the earth is significantly warmer than during the previous dry periods such as the WWII drought. The mean temperature difference between the periods 1997-2006 and 1936-1945 is about 0.7°C across SEA (Table 25). This rate of warming is about twice faster than the rate of GW (Fig. 14 in chapter 3).

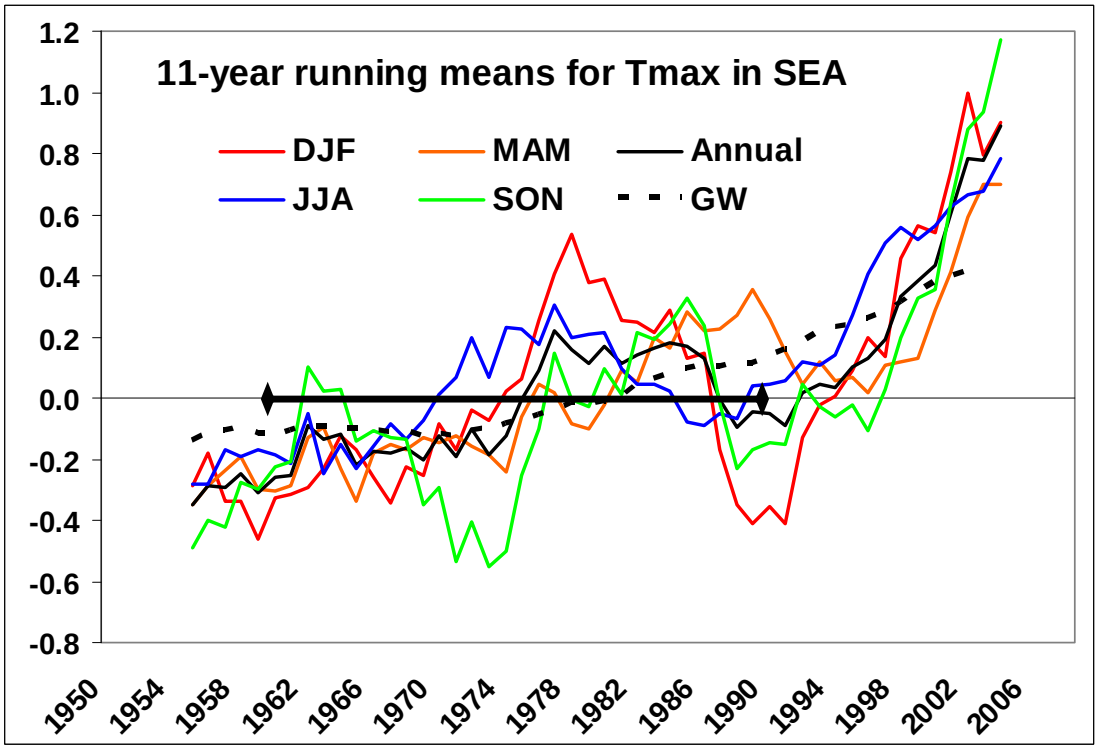

Fig. 80 *11-year running mean of annual and seasonal SEA daily maximum temperature from 1950 to 2009. The global warming of the planet is shown (thick dash line). Anomalies are calculated from the 1961-90 reference period, shown with a black line on the X-axis.*

Here, both T_{max} (Fig. 80) and T_{min} (Fig. 81) averaged across SEA are compared with the global warming of the planet. It is well known that rainfall has a negative relationship with the diurnal temperature range (DTR), being the difference between the daily maximum and minimum temperature across Australia (Power et al. 1998). Indeed, it is apparent that while T_{max} has been warming twice as fast across SEA than for the planet as a whole, T_{min} across SEA has been warming much slower than the GW rate. Trends in both T_{max} and T_{min} contributed to an increase in the DTR across SEA as expected from the rainfall reduction. The warming of T_{max} is particularly spectacular since the early 1990s (using 11-year running means) being up to 0.9°C in 20 years for the annual mean. It is worth noting that this is the case for every season. This was expected in autumn, winter and spring where rainfall has declined. However, the rise is largest (+1.3°) in summer, a season where rainfall has not declined overall. Therefore, the very strong summer warming for daily maximum temperature above the rate of GW is likely to be due to other factors than concurrent changes in both DTR and rainfall. This has not been explored yet.

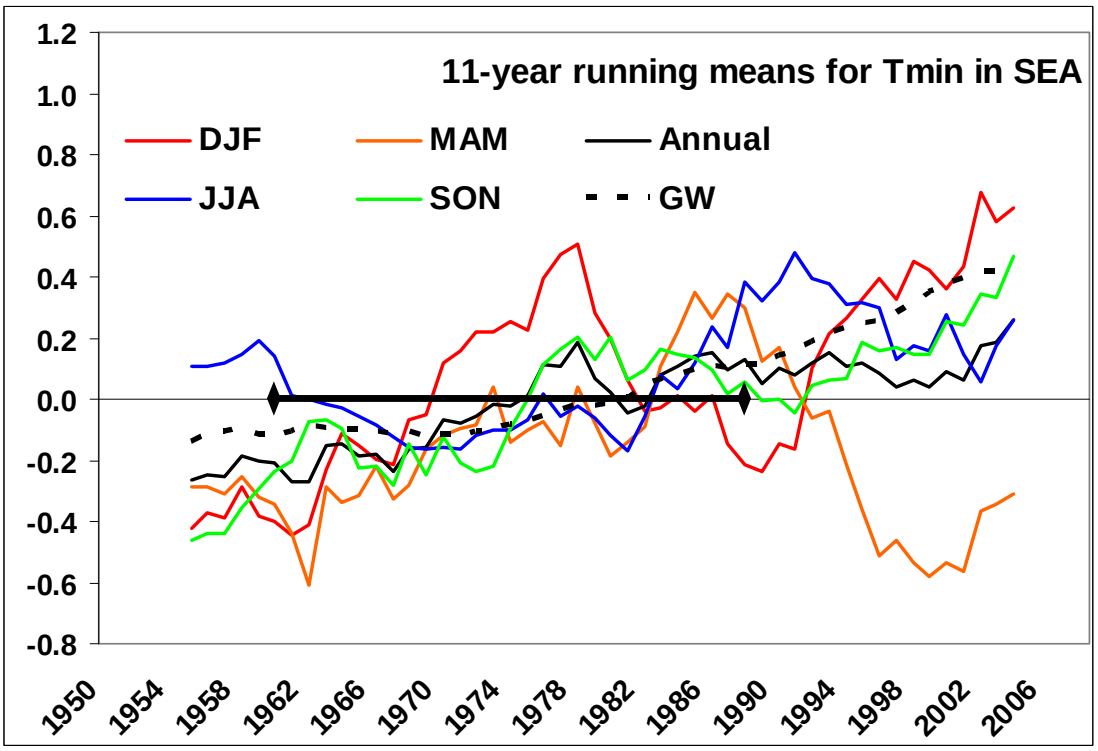

Fig. 81 *As Fig. 80 but for daily minimum temperatures.*

In contrast, daily minimum temperature has not been warming as fast across SEA as the mean GW of the planet, at least since the early 1980s. Autumn, the season where the rainfall decline has been the largest, is particularly noticeable since it has cooled off by up to 0.8°C over the last 20 years. The reduction of T_{min} in autumn and the absence of a trend in spring across SEA are consistent with the slight increase in frost occurrences in those two seasons noted in certain parts of SEA (Chapter 5).

10.4 The baseline issue

Two of the six scientific questions posed at the start of SEACI-1 (see Chapter 1) deal with the issue of what is the current *climate baseline*. This is a difficult issue which we will try to address here.

From a climatological perspective, it is often convenient to use a set period to define the "current" climate. The recommendation of the WMO is to use the 30-year period from 1961 to 1990. As a world standard, it has the advantage of providing a consistent basis for the comparison of results from various sources. More recently, the IPCC 4th assessment (Solomon et al. 2007) in general uses the last 20 years of the 20th century: 1980 to 1999 as a reference period.

For temperature, while the warming is gradual and natural variability less important, both periods could be used as a reasonable reference and basis for the evaluation of anomalies for future projections. However, for SEA, based on the discussions in the previous section, temperatures for the last 20 years have been affected by the ongoing rainfall deficiency. Using the last 20-years as per the IPCC 4th assessment would therefore build in the chosen baseline natural variability that will not necessarily persist. This would be an argument for using the WMO 1961-1990 reference period in order to avoid the additional effect of the current rainfall deficiency on temperature, unless users are convinced that the additional rainfall effect is here to stay over their period of interest; then the IPCC reference period is acceptable. The sizeable difference (at least for T_{max}) between the two periods must be noted.

When it comes to rainfall, using the WMO reference period for SEA is highly problematic. The 1961-1990 rainfall climatology for this period is very high (mean of 602.4mm, which is 3.7% above the long-term 1900-2009 climatology). Hence this benchmark is a poor representation of the long-term climatology and provides an inflated view of what the current baseline is for rainfall. A fall back position would be to use the longest possible instrumental record from 1900 to 2009 as the baseline in order to reduce as much as possible the impact that naturally occurring variability would have if any shorter period is chosen. However, the choice used is a matter for discussions with users as the choice made may well differ depending on the applications. A more conservative choice may be justifiable in particular cases.

Based on the results of the relationship between global temperature and rainfall via the STR-I, presented in this report, it might be worth investigating the possibility of using a climatology based on previous periods of warming and STR intensification during the existing instrumental record. To define such epochs it is best to use long-term averaging such as 21-year running means. This was done for global temperature and linearly detrended global temperature (using the linear trend from the entire 20th century from 1900 to 1999, Fig. 82A). All anomalies are normalised using the mean and standard deviation calculated on the full 20th century. Similar calculations were performed for the STR-I (Fig. 82B), SEA rainfall (Fig. 83A), a SAM index (Fig. 83B), a measure of ENSO (Fig. 83C) and finally for two additional indices the IOD (Fig. 84A) and an index of the Pacific Decadal Oscillation (PDO) (Zhang et al. 1997) (Fig. 84B). The SAM index was calculated using observed MSLP across the three continents of the southern hemisphere and an estimation of the MSLP in Antarctica during the first half of the 20th century (before measurements of MSLP became regular) using a mass balance argument (Visbeck 2009). The ENSO measure is a simple count of the number of El Niño events minus the number

of La Niña events per 30-year period (Power and Smith 2007); the same idea was applied to IOD events (Cai et al. 2009). The PDO was sourced from the University of Washington and based on Mantua et al. (1997) methodology, despite being 11-year running means of an EOF loading, a 21-year smoothing was also applied.

In each graph, the solid black line Y-axis is on the left and is kept constant between graphs (two different scales are used depending on whether the raw or linearly detrended global temperature are shown), while for the dashed line (Fig. 82A) or blue lines (all other graphs), the Y-axis is on the right and is chosen for each graph in order to match the amplitude of the solid black curve. The choice between raw or detrended global temperature for all the graphs is based on the closer match to the index shown. For rainfall in SEA (Fig. 83A), values are reversed since it is an inverse relationship with detrended global warming.

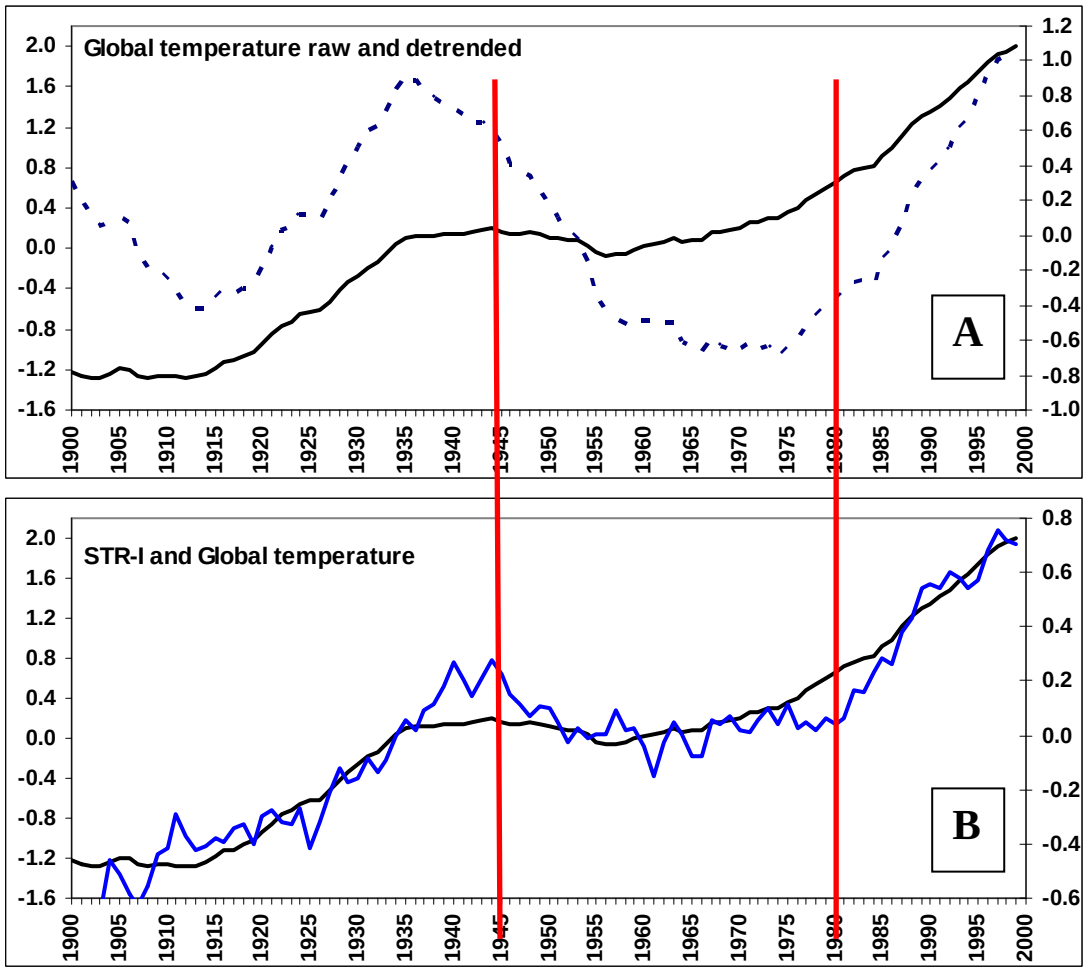

Fig. 82 *21-year running means of (a) global temperature (raw: solid line and linearly detrended: dashed line), (b) STR-I (blue) and global temperature. All curves are normalised anomalies calculated using the 20th century as the reference period; for the solid black curve, the Y-axis is on the left, while for the other curves the Y-axis is on the right. The red vertical lines separate epochs based on the STR behaviour (1900-1944 and 1980-now); see text for details.*

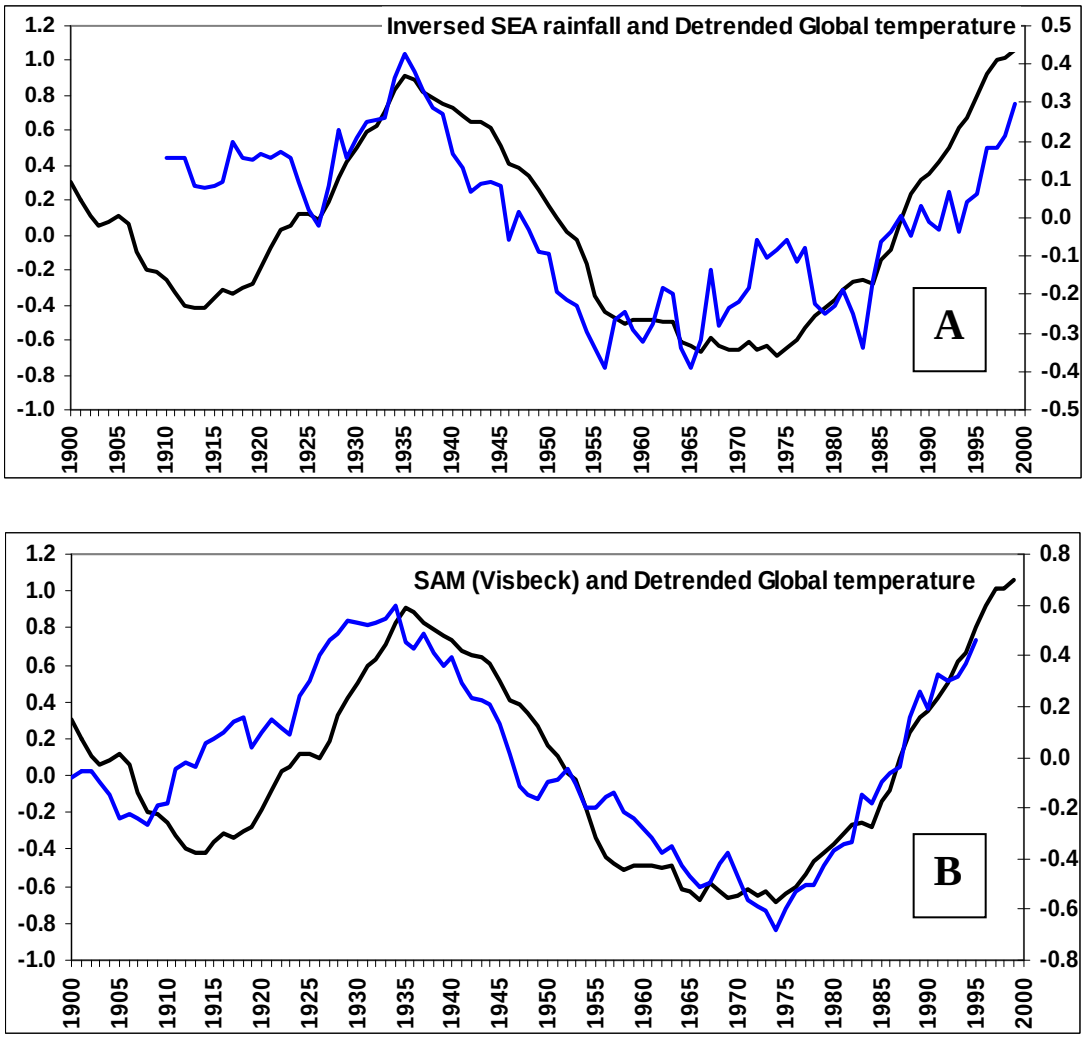

Fig. 83 *Continuation of Fig. 82 for (a) SEA rainfall multiplied by -1 and global temperature linearly detrended (b) an index of the SAM and detrended global temperature.*

The plot shows that the STR intensification matches closely the GW during the 20th century as discussed earlier (Chapter 3 and 8). In addition, the similarities between the SEA rainfall and the rate of warming (or detrended global temperature) is an interesting feature of the plots in Fig. 83A). It points to the possibility that, despite the STR intensification responding to the absolute warming, the rainfall response might be more related to the rate of warming. This possibility remains to be clarified as part of the SEACI-2 program. It is also worth noting that a key mode of variability which is known to have a negative influence on SEA rainfall during winter, the SAM also appears to evolve in phase with epochs of acceleration and deceleration of the GW (Fig. 83B).

This simple comparison suggests that many aspects of the climate system may be related on inter-decadal time scales with either global warming or the rate of global warming (i.e. the detrended global temperature series outlines epoch of acceleration and deceleration of the global warming).

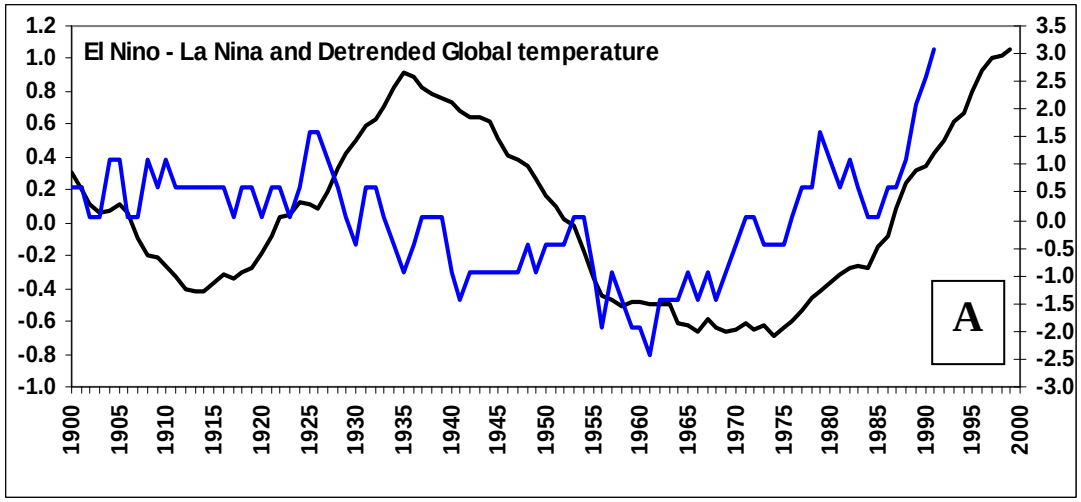

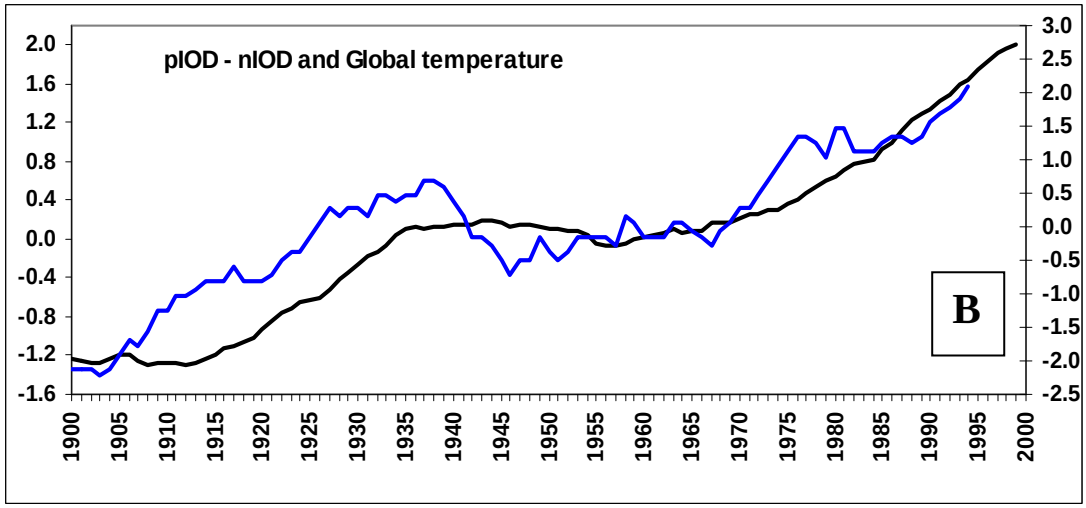

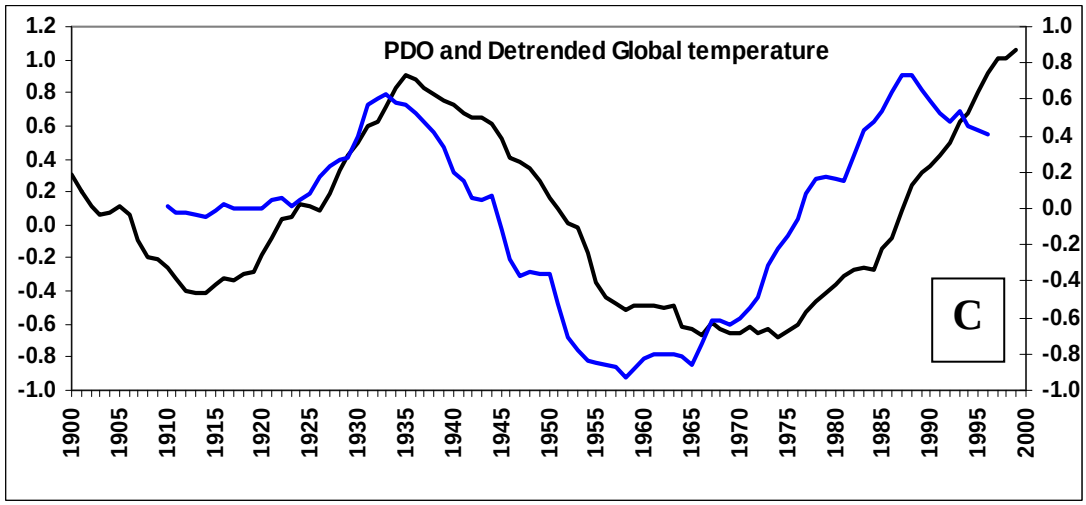

Fig. 84 *Continuation of Fig. 83 for (a) a count of El Nino minus La Nina events per 30 years and detrended global temperature, (b) a similar count of positive vs. negative IOD events per 30 years and raw global temperature and (c) the PDO and detrended global temperature.*

Apart from atmospheric variables (such as STR, SEA rainfall and SAM), the relationship between GW or the speed of GW and SST based indices is also worth investigating, in particular for SST-based indices which capture modes of variability influencing SEA rainfall.

Amongst the indices chosen, the ENSO index does not appear to match either raw (not shown) or detrended global warming (Fig. 84A). This is notable since the lack of certainty about the likely behaviour of ENSO in response to global warming has been outlined in the latest IPCC report (Solomon et al. 2007).

Contrary to the count of ENSO events, the count of IOD events appears well correlated with the GW (Fig. 84B). That result is consistent with studies describing the IOD not as a dipole but an Indian Ocean wide mode of variability (Dommenget 2007 and 2010) which based on our analysis is closely related to global warming.

Finally, the 21-year running mean of the PDO was also compared to the rate of global warming and found to relate well (Fig. 84C). That suggests that the phase of PDO may well be driven by the acceleration and deceleration of the GW and how this projects onto the main mode of variability in the Pacific: the ENSO phenomenon.

Based on these observations of coherent behaviour in the climate system, three epochs can be defined based on the global temperature and STR-I series. The first epoch from 1900 to 1944 corresponds to a period of global warming and STR intensification. The second epoch from 1945 to 1979 corresponds to a period of "relaxation" when the system had a stable global temperature and no intensification of the STR. Global temperatures started to rise earlier than 1980 but did not supersede the previous 1940s maxima until the mid 1970s, and the STR did not start intensifying until the late 1970s. The third period extends from 1980 to now.

Having identified epochs where several low-pass filtered indicators of the climate dynamics appear related; it appears meaningful to combine the first and third epochs when both warming and STR intensification are apparent. This can be seen as an alternative to using a short recent period as a baseline, where the unexplained natural variability is likely to be large. It is relevant for a current climate baseline for SEA rainfall as it uses the two epochs with similar properties as far the global climate system is concerned. The month by month climatology for the two defined global warming epochs is compared to that for the entire record in Fig. 85; anomalies are calculated from that baseline period and can be compared to the same anomalies calculated from the entire period (Fig. 78). However, at this point in time, further research is needed to establish if this is a sound approach.

Overall differences are small; the warming periods tend to have lower rainfall than the entire climatology in all months apart from June; the largest differences occur during the warmer months from October to May, with the exception of December. Overall, anomalies are not too different, but autumn anomalies are reduced and winter anomalies are unchanged. This leads to smaller differences in month by month anomalies amongst all the deficit months from March to October. Positive anomalies in summer are now larger.

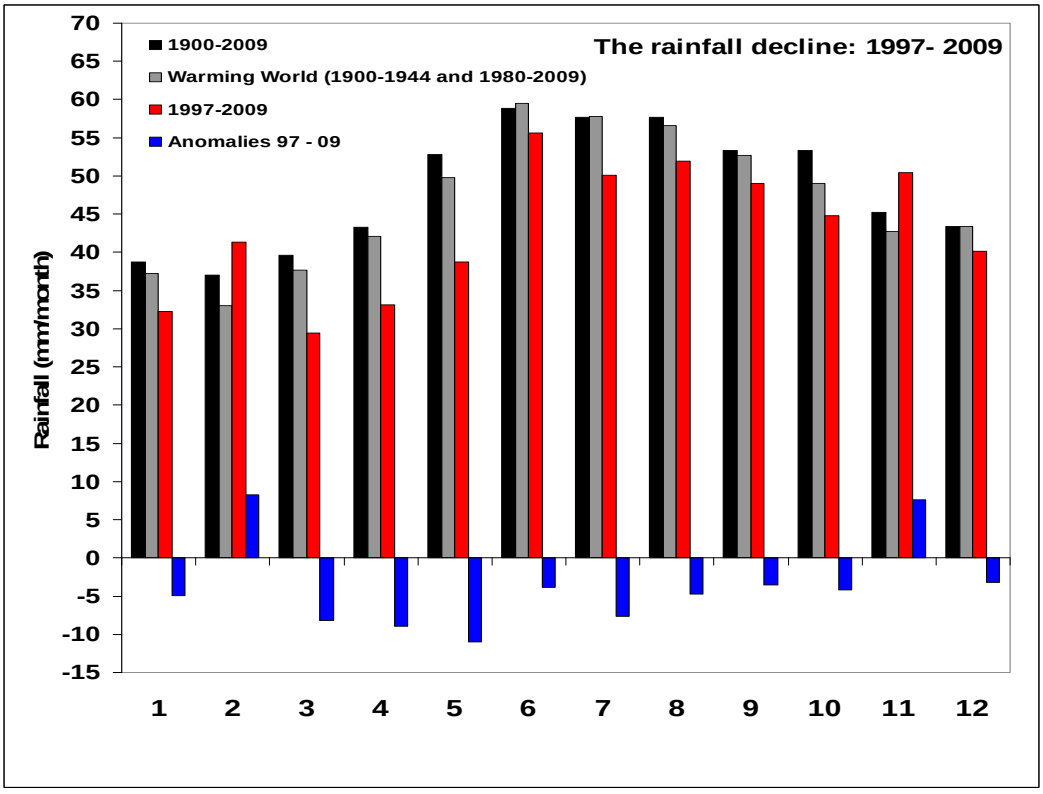

Fig. 85 *Monthly mean south-eastern Australia rainfall for period 1900-2009 (black bars), the warming world period (1900-1944 and 1980-2009: grey bars), 1997-2009 (red bars) and the change from the current (1997-2009) period relative to the warming world period (blue bars) in mm per month.*

Table 27 *Means of annual, autumn, winter and spring rainfall (in mm) over SEA for the ongoing drought (last 13 years 1997-2009) and the previous lowest 13 years period on record (1933-1945) in absolute values and in percentage of the warming world reference period (1900-1944 and 1980-2009). The percentages for the warming world climatology are relative to the long-term (1900-2009) mean. All results are based on the AWAP gridded rainfall.*

	1997 - 09		**1933 - 45**		**Warming World** 1900-1944 & 1980-2009	
	Mean	Percent	Mean	Percent	Mean	Percent
Annual	514.9	-8.0%	535.5	-4.5%	561.5	-3.3%
Autumn	101.4	-20.7%	121.0	-6.3%	129.5	-4.5%
Winter	157.7	-9.3%	159.7	-8.1%	173.9	-0.1%
Spring	144.3	-0.1%	137.3	-7.1%	144.4	-4.9%

Table 27 summarises the characteristics of both the WWII and current droughts using the *"warming period"* climatology that we have just described. Both periods remain anomalously dry, but the WWII drought has a smaller magnitude (-4.5%). All 3 seasons: autumn, winter and spring contribute equally and are partially offset by a positive anomaly in summer (not shown). The ongoing drought is still sizeable relative to this alternative choice of climatology with a magnitude that is twice as large as the WWII drought anomalies. It is heavily dominated by autumn and then winter, the spring anomaly is not present.

SUMMARY

Using the recently released AWAP rainfall in place of the other gridded data set used in previous chapters, and updating the record to 2009, we showed that:

- The on-going rainfall deficiency by the end of 2009, which was already approaching record level in 2006, with three additional below average rainfall years is unprecedented by a large margin. The duration (13 years) and severity of the ongoing rainfall deficiency is remarkable; the annual rainfall deficiency of -11.4% for 1997-2009 is 45% worse than the previous driest 13 years in the historical record (1933-1945 for which the deficit was -7.8%).

- The ongoing rainfall deficiency is still dominated by the autumn signal (a decline of -25.3% in autumn, which accounts for 52% of the total decline). However, the continuation and intensification of the rainfall deficit during the last three years is due to a combination of both the winter rainfall decline becoming sizeable (now the largest on record) and the emergence of a spring rainfall decline in the latter part of the period (since 2000). These growing rainfall declines in winter and spring reinforce the autumn decline and have lead to a very large (-20%) annual decline over the last four years.

- While the origin of below average annual rainfall can be traced back to 1997, rainfall in SEA had in fact started to decline earlier, albeit from the very high values of the relatively wet 1950s to 1990s. Seasonal declines can be traced back to the early 1970s for autumn, the 1990s for winter and the beginning of the 21st century for spring. The earlier the seasonal decline, the larger is the contribution of this season to the current (1997-2009) annual rainfall deficiency.

- Regional warming across SEA has been affected by both the ongoing global warming and the additional contribution of the rainfall deficiency. The two factors combined gave rise to a very large 1°C increase in the last 20 years for maximum day-time temperatures. These two factors have opposing influences on minimum night-time temperatures, leading overall to a decline of T_{min} in the worse drought affected season: autumn.

- Choosing a baseline free of climate variability from which future projections of climate for the next decade can be compared to remains a difficult area. Several options were investigated in this chapter.

11 CONCLUSIONS AND FUTURE PERSPECTIVES

In this chapter we will use the results presented in previous chapters to answer the original six questions formulated at the beginning of the program (Chapter 1). In a few instances, additional evidence emerging from other published research relevant to our conclusions is used. However, no attempt has been made to reconcile all the existing research on this issue; this is a hotly debated area with only little emerging as a consensus (Sherwood 2009). Some evidence presented here contradicts results published elsewhere; it is important to keep that in mind. No attempt is being made in these conclusions to reconcile conflicting findings and, hence, this is not a summary or a consensus position of the entire research conducted in Australia on the SEA rainfall decline; rather, what is presented represents the conclusions arising from this body of work.

11.1 How has climate changed?

Rainfall has been below the long term average since 1997 across SEA (defined as continental Australia south of 33.5°S and east of 135.5°E). It is now the largest rainfall deficiency for SEA (-11.4%) in the historical record dating back to 1900. The deficit has now been ongoing for 13 years. This duration has made the current period remarkable as it is now 3.6% lower (or 45% more severe) than during the previous driest 13 years period on record: 1933-1945 (-7.8%).

The current rainfall decline is dominated by a 25.3% reduction in autumn rainfall which accounts for 52% of the total reduction. Rainfall has declined in every calendar month from March to October, including the usually wettest period (May to October). Since 1997, winter rainfall has been 9.4% below the long-term average while spring rainfall is down 5.0%.

The winter and spring rainfall deficits emerged more recently and have exacerbated the pre-existing autumn rainfall deficit that first emerged in early 1970s. Over the last 4 years (2006 to 2009), the annual total rainfall deficit is much larger (-20.1%) compared with the longer 1997-2009 period. This recent decline is comprised of declines in spring (37%), winter (29%) and autumn (28%). In all three seasons, rainfall had started declining before it dropped below the long-term average from a high rainfall period from the 1960s to the 1980s. Annual rainfall totals first started to decline in the early 1990s, for autumn it can be traced back to the early 1970s, and it started much later for the other seasons (1990s for winter and 2000s for spring). The earlier the start of the decline, the larger is the contribution of the season to the annual rainfall deficit since 1997. Only in the case of autumn is the lengthy decline of rainfall record breaking. The winter-spring declines, at this point in time, are not outside the range of past decadal variability.

Across SEA, 9 out the 10 years of the 21st century (i.e. 2001-2009 inclusive) were below the 20th century (1900-1999) average climatology. The last time SEA experienced rainfall above the 20th century average was in 2000. In simple terms, the probability of observing a sequence of 9 consecutive below average years (2001 to 2009) by chance is less than 0.5% assuming that the series has no auto-correlation. In contrast to the previous long term drought in 1936-1945

(WWII drought), the ongoing drought does not consist of severe dry years mixed with wet years but rather it is a run of below average years with small inter-annual variability.

Spatially, the ongoing rainfall deficit is more pronounced in SWEA extending further inland along significant orography. For SEA, this is approximately the area where winter rainfall dominates. The area of sizeable rainfall deficit has extended over time further north where summer rainfall tends to be dominant. For the ongoing period, areas of rainfall deficits are predominant only across southern Australia while the rest of the continent is experiencing above average rainfall, in particular in most tropical regions. In comparison, during the WWII drought, the entire Australian continent was affected.

SEA has also experienced significant warming during most of the last 50 years; for daily mean temperature this is overall consistent with global warming. The last 20 years have seen an additional signal congruent with the rainfall decline: an increase of the diurnal temperature range. As a result, maximum day-time temperatures have risen across SEA by close to 1°C in the last 20 years. In contrast, minimum night-time temperatures have not risen during the last 20 years and have even declined (by up to 0.8°C) in autumn, the season with the largest rainfall decline. This decline in T_{min} is consistent with the observation of increased frost occurrences in some parts of SEA.

There has also been a noted amplification of the rainfall decline in terms of the hydrological response across SEA. Major rivers and dams have received inflows well below long-term average and the decline in magnitude is larger than the two to three time elasticity factor reported in the literature (Chiew 2006). No clear attribution of this hydrological amplification has emerged from the work reported here. However, additional studies were undertaken as part of SEACI where the three likely causes identified here were quantified (Potter and Chiew 2009). In addition to the rainfall decline which explains more than half of the hydrological response, the other three factors were found to be roughly equivalent and ranked in the following order: 1) the importance of the autumn rainfall decline, autumn being a key season when the soil profile wets up prior to winter rains (an additional 5.4%); 2) the very low inter-annual variability within the ongoing decline and lack of markedly above average years, which will also have contributed to the drying out of the soil profile (an additional 5.3%); and 3) the temperature increase (very large for T_{max} as noted earlier), which is likely to have increased evaporation and contributed to a further reduction in soil moisture (an additional 3.1%). Potter and Chiew (2009) also noted that they could not account for the entire hydrological amplification and that was possibly due to interaction between the 3 factors. It is worth noting that the study was performed on a small basin compared to the entire SEACI domain but nevertheless it provides valuable insight into the very large hydrological response observed in the on-going rainfall decline.

11.2 What are the major drivers affecting historical and current climate?

Major drivers affecting SEA rainfall can be separated into remote and local drivers. The main remote drivers affecting inter-annual variability of SEA climate are tropical modes of

variability: the ENSO in the Pacific Ocean and the IOD in the Indian Ocean; both modes of variability have an impact on SSTs directly north of Australia which relate strongly to SEA rainfall. Tropical modes of variability influence SEA rainfall from winter through to summer with the strongest influence being in spring. There is no significant relationship between ENSO / IOD and SEA rainfall in autumn; therefore, the influence, if any, of these modes of variability on the rainfall decline will be limited to winter and spring, provided an increase in frequency of positive events (El Niño and positive IOD) did occur. In fact, it was shown that combining the influence of ENSO and the IOD into a single index of SST, overall tropical modes of variability contributed to make the winter rainfall decline smaller than it would have been anticipated based on the STR intensification.

The SAM which is the most significant mode of high-latitude variability in the southern hemisphere also has a strong influence on SEA rainfall. The nature of this influence changes with the season. Positive values of SAM indicate a southwards shift of the mid latitude storm-track and this is associated with higher rainfall across SEA in summer and decreased rainfall in winter. In autumn, the SAM rainfall relationship flips between these two influences and hence SAM has no net effect on autumn rainfall.

Local MSLP relates well with SEA rainfall across most of year (with higher pressures leading to reduced rainfall) with the notable exception of summer. The relationship is best captured using the intensity of the belt of high pressures which dominates over SEA during winter: the STR. The intensity of the STR relates very well with rainfall from April to November and the correlation peaks in early winter (MJJ). The strength of the relationship is strongest in SWEA, the area where the rainfall decline has been detected as having the most significant departure from the historical record. Although both the intensification of the STR and its shift south limit the ability of rain bearing systems travelling as part of the storm-track south of Australia to provide rainfall across SEA, overall, the relationship with the STR-I dominates all year around compared to the relationship between SEA rainfall and the position of the STR (STR-P).

Finally, it was noted that SSTs in the neighbourhood of SEA, in particular in the Tasman Sea, have a positive relationship with SEA rainfall. This area has warmed at a very rapid pace in the last 50 years; however, as the relationship is positive (e.g. warmer SSTs are indicative of higher rainfall) it is unlikely to be the cause of the observed rainfall decline. It seems that SST in this region is responding to the same drivers as the rainfall, rather than SST in the region driving the rainfall changes.

11.3 What are the relationships between the drivers operating at different timescales and have these relationships changed over time?

The relationships between tropical modes of variability and SEA rainfall are evident during 1997-2009. Noted El Niño and positive IOD years have resulted in lower rainfall, while La Niña years have resulted in years of rainfall above (2000) or very close to (2007) the long-term average since 1997. However, it was found that although tropical modes of variability were a key contributor to the previous most severe rainfall deficit in the historical record (the WWII drought from 1936 to 1945), this was not the case in the ongoing decline, where tropical modes

of variability have not contributed to the annual rainfall deficiency, with only a small contribution in spring. This result was obtained using an analysis of a tri-pole index (TPI) describing variability in SSTs across the tropical waters which are known to influence the rainfall in SEA, with the index encompassing the effects of both ENSO and IOD variability. This noted difference in the role of tropical modes of variability is consistent with the fact that, during the WWII drought, the rainfall decline was a broad feature across most of the Australian continent while currently it is limited to a smaller region mostly across southern Australia which does not match the broad area of influence of tropical modes of variability across the entire Australian continent. The relationship between remote tropical modes of variability and SEA rainfall is mostly independent from the STR-I control on SEA rainfall as shown by partial correlations.

The SAM rainfall relationship is mostly felt through changes in the local MSLP. Since the late 1950s the SAM index has been trending upward in summer, autumn and early winter but not in spring. Upward trends in SAM index can be translated in a rise of MSLP above SEA: in May-June-July (MJJ) up to 30% of the MSLP increase can be traced back to SAM trends. As a consequence, it is tempting to relate part of the rainfall decline to the increase in SAM; however, this can only be true for the months where SAM has both a negative relationship with SWEA rainfall (from May to October) and the SAM index has trended upward (from December to May). Therefore, SAM is likely to have played a role in the rainfall decline only in the early part of winter around the month of May. The SAM index has trended upwards in the rest of winter (June and July) during the 1960s and 1970s but not since the 1980s. Interestingly, winter rainfall across SEA did decline in the 1960s and 1970s but it recovered in the 1980s before declining again in the last 20 years.

The main control of MSLP over southern Australia is the STR-I. The intensity of the STR has been rising since the 1970s and this can be translated into a sizeable rainfall decline (about 80% of the total observed decline). Furthermore, the annual cycle of the STR-I related rainfall decline is spread across the same seasons as the observed decline (autumn-winter-spring), although the STR-I – rainfall relationship underestimates the observed autumn decline while overestimating it in winter and spring. It was found that although the shift in STR-P in itself could explain a sizeable rainfall decline (up to 30% of the observed values), using simple linear statistics, the southward shift of the STR did not appear to have any effect *in addition* to the strengthening of the STR. This results is surprising since the largest shift south is observed in autumn at the time of the largest rainfall decline and will need to be investigated again using non-linear statistics.

The STR intensification over the 20th century actually occurred in two marked epochs: from 1900 to 1944 and from 1980 to now. There was no upward trend for an extended period from 1945 to 1980. This intensification of the STR in these two epochs has been observed to match the long-term trends in global warming during the 20th century. It was noted that the WWII drought from 1936-1945 occurred following a prolonged (30 years plus) period of global warming and STR intensification, at a time when STR-I reached values which were not surpassed until the mid 1980s. The high value of the STR-I during 1936-1945 can be translated into a rainfall deficit equal to 30% of the observed deficit. This suggests that a part of the WWII drought can be attributed to the global warming experienced up to that time, through the STR-I mechanism. This is a smaller estimated contribution for STR-I than in the case of the current drought (80%). This finding is consistent with the fact that the WWII drought was not

limited to the area of influence of the STR-I, and also the importance (noted earlier) of tropical modes of variability in contributing to the rainfall decline during that decade. In other words, while the WWII drought was primarily driven by naturally occurring modes of variability (in particular in the tropics), it was made worse by the STR strengthening which, in turn is linked to the observed global warming during the first half of the 20th century.

11.4 What are the causes of the dry conditions affecting parts of the study area over the last decade, and what is the prognosis?

The biggest contributor to the ongoing rainfall decline appears to be the strengthening of the STR (which accounts for a rainfall decline up to 80% of that observed) which, in turn, is linked to the uninterrupted 30+ years of global warming since the 1970s. The global warming - STR-I relationship observed during the 20th century is unlikely to have occurred by chance since it has been reproduced in simulations of the 20th century by CCSM3, a state-of-the-art fully coupled climate model developed and run by the National Center for Atmospheric Research (NCAR, USA). This model was forced with different external forcings and hence exhibits different behaviours during the 20th century, shedding light on the STR-I - global warming relationship. In some simulations, on secular time scales, no global warming were observed and no strengthening of the STR, while in other simulations, both global warming and STR-I increased. The different behaviour was traced back to the external forcings: only when anthropogenic forcings were added to natural forcings did the model reproduce a strengthening of the STR alongside a global warming of the system. The ability of the model to reproduce the STR-I - GW relationship when both are tracking upward offers a strong suggestion that the observed changes did not occur by chance.

In addition, the mean response from the naturally forced ensemble pointed toward significant rainfall increases in autumn, winter and spring across SEA and therefore does not match the observations. Of particular interest is the fact that the observed rainfall decline in autumn is outside the uncertainty range (at least in parts of the SEACI domain) computed from the naturally forced ensemble. However, it is worth noting that, if a larger ensemble was available or more climate models had been examined, that may not be the case. In contrast to the ensemble forced with natural external forcings alone, the two ensembles forced with anthropogenic forcings alone, and combined with natural forcings, point toward rainfall declines in the last 20 years: large in autumn, small in spring and very small in winter. The largest rainfall decline is obtained from the ensemble combing both natural and anthropogenic external forcings (rather than anthropogenic alone). The modelled rainfall declines are in general smaller than the largest observed declines being about 50% of the observed autumn decline, but they are comparable to observed values in other seasons. These results suggest that, from this modelling perspective, while the autumn rainfall decline across SWEA would not have been possible in the absence of anthropogenic forcings, it remains an extreme outcome in response to the anthropogenic forcings.

Finally, it is worth noting that the downscaling of CCSM3 provides a more definitive attribution of the ongoing surface warming across SEA (for both T_{max} and T_{min}) as the most recent trends in temperature are outside the 90% range of uncertainty obtained from the naturally forced

ensemble. In contrast, the fully forced ensemble extended to 2008 using the A2 scenario matches the observed temperature trends very well.

Using the CCSM3 model, it was noted that results are more accurate when the BoM SDM is used to enhance the signal (climate trend) over the background noise (natural variability) in this detection and attribution study. When DMOs from CCSM3 were used for local variables (rainfall, temperature) averaged across SEA, only small, and not statistically significant, differences were observed. This is consistent with the IPCC statement about the difficulties of attributing observed regional rainfall trends to external forcings (Solomon et al. 2007, p714): "Responses to external forcing in regional precipitation trends are expected to exhibit low signal-to-noise ratios and are likely to exhibit strong spatial variations because of the dependence of precipitation on atmospheric circulation and on geographic factors such as orography." The need to employ additional regionalisation tools such as SDMs can clearly be seen in the case of the SEA rainfall decline.

When it comes to a future prognosis, it is important to remember that even from a broad-scale perspective, while the model produced a global warming comparable to the observed one, it reproduced only 30 to 50% of the observed STR intensification. Two hypothesis can be formulated which together or separately can explain this discrepancy: 1) part of the observed STR strengthening is not in response to global warming and, rather, is a form of unforced natural variability; or/and 2) the climate model used (CCSM3), while responding to the external forcing on a global scale with the same magnitude as that which has been observed, underestimates the observed changes in atmospheric circulations in the vicinity of the southern part of the Australian continent.

These two hypotheses have very different implications for future prognosis. If the observed discrepancy is mostly due to the role of natural variability, than it is most likely that the part of the STR intensification due to natural variability will recede in the decades ahead. Based on the work presented here, this will have a positive impact on rainfall in the near future. This plausible future scenario for the decade ahead is consistent with the current suite of climate model projections (based on the CMIP3 database): a future rainfall decline but of a lesser magnitude that what has been experienced in the recent past.

On the contrary, if this discrepancy is primarily due to the underestimation of the circulation changes by the CCSM3 model (a contributor to the CMIP3 database used for future projections in the IPCC-AR4), it opens up the possibility that this model also underestimates future changes in regional circulations and, hence, future rainfall projections. Assuming that the CCSM3 model is representative of the current suite of GCMs, it may raise doubts about the ability of current GCMs to produce realistic estimates of the magnitude of a future drying. The importance of determining the likelihood of both hypotheses, with appropriate precision, is a key driver of the research agenda in Phase 2 of SEACI.

A further aspect worth mentioning in this discussion comes from the relationship between findings in Theme 1 (understanding of the current climate) and Theme 2 (future projections) in SEACI-1. GCMs show a very large range of future rainfall projections across SEA; however, they are most consistent in the southern part of the domain corresponding to the SWEA defined

here. It suggests that where the intensification of the STR is the predominant influencing feature, GCMs tend to agree about a drier future. On the other hand, where the STR-I influence decreases and the influence of tropical modes of variability (ENSO and IOD) increases, the GCMs are less in agreement. This hints to a greater consistency amongst models for mid-latitude surface pressure increases than for future behaviours of tropical modes of variability. Again, the role of these various forcings of the regional rainfall in future projections will be investigated further in SEACI-2.

11.5 What is the current climate baseline?

Broadly speaking, a baseline climate is a characterisation of the "typical" climate of a region or particular locality over a particular period. How a "baseline" climate is defined depends on the application for which it will be used.

The current climate baseline (1961 to 1990) as defined by the WMO appears inadequate for rainfall in SEA as it corresponds to one of the wettest periods of the 20th century. A fall-back position would be to use the longest possible instrumental record from 1900 to 2009 as the baseline in order to reduce as much as possible the impact that naturally occurring variability would have if any shorter period is chosen.

However, there is a case for using the last 10-15 years as a baseline because of the evidence regarding the nature and causes of the ongoing deficiency and the possibility that it is a shift toward a new climate regime. The last 13 years can be seen as anomalous in terms of the long-term record, but the probability of encountering a similar dry decade in future is increasing. But choosing the most recent 10, 13 or 20-year as the reference period is a risky proposal since it remains likely that a sizeable part of the rainfall anomalies on such a short period is due to unexplained natural variability; unexplained as opposed to explainable modes of natural variability such as ENSO, IOD or SAM, which are discussed in this report and cannot explain the recent anomalies. The reason why unexplained natural variability remains a possibility is that, thus far, the externally forced model simulations analysed do not reproduce the full magnitude of the rainfall (and other observed surface variable) changes. Therefore alongside the possibility that the model is not sensitive enough to the forcings, there is also the possibility that the model is sensitive enough but part of the observed signal is not in response to anthropogenic forcings.

An alternative to using a short recent period has been investigated. It makes use of the relationship between global warming and the STR intensification and can be defined as warming world climatology: from 1900 to 1944 and from 1980 to now. Although differences are not large, using this reference period provides a longer period (75 years) which therefore encapsulates a large part of the natural variability on inter-annual and decadal time-scales while, in essence, removing most of the very wet period from the 1950s to the 1970s. These high rainfall years occurred during a period of stagnant global warming which is unlikely to be repeated soon. Based on the evidence presented earlier, the absence of global warming at that time was likely to have been the cause of the above average rainfall. It is therefore possible to provide an alternative for hydrological applications which require a well defined climate baseline.

It is worth noting that from the IPCC perspective, future projections of climate change are generally expressed as percentage changes relative to a 1980-1999 reference period. However, it is unclear how much of the observed changes discussed in this document are reproduced in the current suite of GCM simulations at the end of the 20th century. Any assessment of GCM performance needs to be done in light of the findings presented here. As well as regional rainfall, the important regional changes such as the intensification of the STR need to be assessed; in addition the seasonality of the changes (across autumn, winter and spring) needs to be investigated. This work is required before the important question of what is the appropriate current baseline for future projections can be answered. Again, this will be a major focus of research in SEACI-2.

Finally, while the above discussion focuses on defining a climate baseline for rainfall, to some extent it is also valid for temperature. Temperatures across SEA exhibit smaller natural variability than rainfall; however, it was shown that both daily extremes T_{max} and T_{min} are responding to the rainfall anomalies. Therefore, while using the 1980-1999 benchmark to calculate future anomalies from is convenient and ensures consistency with the larger body of the science (as reported in the IPCC), it is important to remember that across this period, SEA temperatures have had noticeable trends, partly in response to the ongoing rainfall decline.

11.6 What criteria should be used to determine whether shifts in the baseline have occurred, or are likely to occur?

This is a difficult question to answer from a climate perspective. SEA rainfall series does display break points or shifts such as in 1945 towards wet conditions and in 1997 towards dry conditions. However, while these changes are important from the impacts point of view, they are not necessarily statistically significant, either because the changes are relatively small (this is often the case for temperature although the recent increase of T_{max} is statistically highly significant) or because although the changes are large, natural variability is also large (which is the case for rainfall). Besides a consideration of statistical significance, these observed shifts may not be physically meaningful and can represent the inter-play of long-term trends and inter-annual to decadal variability.

On the contrary, criteria based on the impact variables (streamflow, crop yield) might be more suitable for determining shifts in the baseline, as they tend to integrate several climate variables (e.g. the combined impacts of temperature and rainfall). From that perspective, it is likely that the ongoing rainfall decline marks a shift toward a regime of lower streamflows due to the amplified hydrological response to changed rainfall patterns (lower interannual variability and changes in seasonality) together with increasing temperatures. Similarly it is possible that, using appropriate measures of agricultural outputs, a significant shift may be detectable. This latter approach, which was not examined here, is likely to be more fruitful in answering this particular question.

11.7 Future perspectives: the roadmap for Theme 1 in SEACI-2

Following on from the above summary of how the original scientific questions have been answered thus far in Phase 1 of SEACI, research plans agreed upon as part of the second phase of SEACI (SEACI-2) are briefly discussed and their relevance in addressing recognised gaps in the existing knowledge is spelled out. SEACI-1 has laid the foundation for the possibility of attributing the rainfall decline and other observed changes across SEA to anthropogenic forcings by targeting the triangulation detection-understanding-attribution (Fig. 86). Work proposed in SEACI-2 will be aimed at continuing to monitor ongoing changes and their characteristics while targeting scientific gaps identified during SEACI-1.

In terms of detection, additional research will be conducted to lengthen the available historical rainfall record across SEA. Although it is unlikely that the gridded product used here (AWAP) can be extended back in time, it might be possible, using a small network of long records, to infer what rainfall across SEA was at the time of the Federation drought (which started in the mid 1890s and therefore is poorly captured with the existing gridded product which commences in 1900, as discussed in chapter 8). An extension of the record back in time towards the mid 19th century may provide the opportunity to further test the observed relationship between global warming, STR-I and SEA rainfall across earlier epochs (prior to 1900) which are similar to the 1950s to 1980s when the planet was not warming. In addition, this proposed extension of the historical record may provide an opportunity to re-evaluate the issue of the apparent shift in the current climate baseline from a rainfall deficiency perspective.

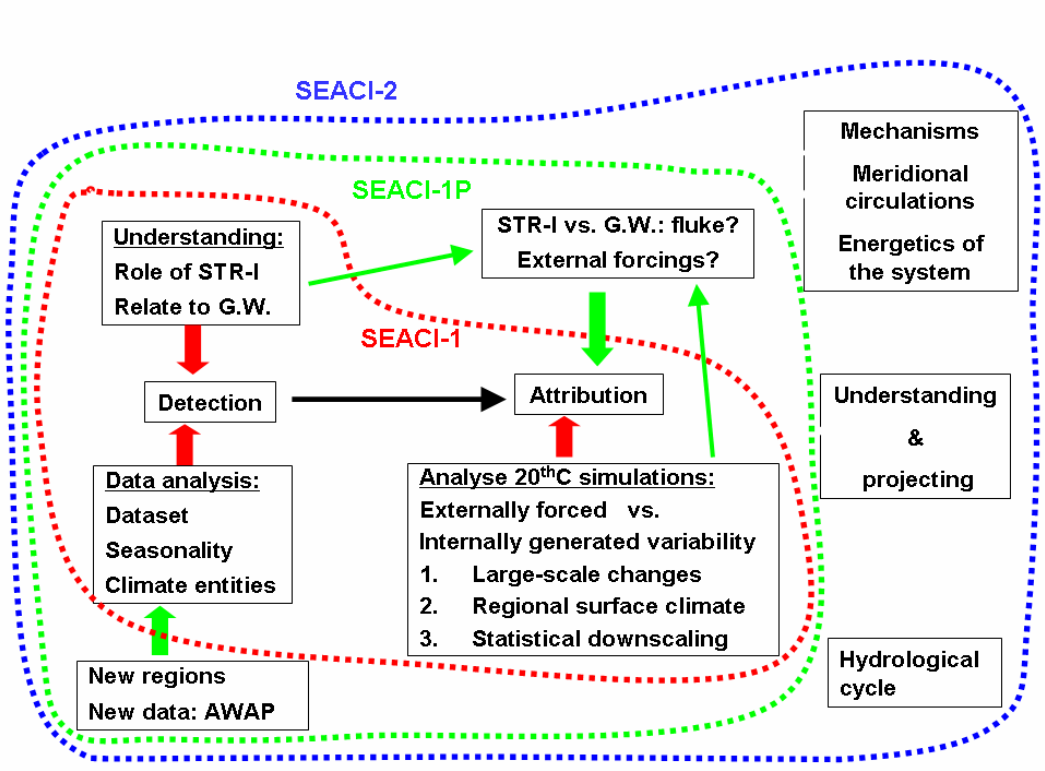

Fig. 86 *Progression of the science within SEACI Theme 1 across, Phase 1, 1P and Phase 2.*

The SEA hydrological cycle, in particular the relationships between rainfall, soil moisture and streamflow will be investigated further. The AWAP provides a model estimate for soil moisture (Raupach et al. 2009) which is a useful step between rainfall and streamflows. It will allow an evaluation of the contribution that increasing temperature has on soil moisture alongside the rainfall deficiency and provide additional insight into the evaluation of the role of temperature following the work done on inflow (Potter and Chiew 2009). Furthermore, the relationship between soil moisture and streamflow can also be investigated to provide some insight about how this relationship has evolved with time. This analysis might help to draw out additional effects due to land changes on streamflows. Overall, this is likely to progress our understanding of the amplification of the hydrological response across SEA and its changing nature with time.

The interactions between various large-scale forcings thus far have been investigated using linear statistics. That was noted as a possible limitation for some results discussed earlier (i.e. Chapter 8 on the relative roles of the STR-I and STR-P and other tropical influences). It is intended to further investigate these interactions using non-linear statistics (e.g. CART methods).

In terms of understanding, a large emphasis in SEACI-2 will be put on further investigation of the mechanisms linking global temperature and STR-I. The existence of the belt of high pressures across the sub-tropics is a consequence of the meridional transport of energy in the climate system by the Hadley Cell (HC). But before the meridional circulation is investigated, it is intended to analyse the STR relation to the zonal circulation in the Tropics, primarily the Walker Circulation (WC), and its variability (i.e. ENSO). In addition, using a gridded database, it will be worthwhile to investigate the global nature across the southern hemisphere of the mid-latitude pressure increase observed at Australian longitudes. The zonal nature of the signal, its projection onto long-wave patterns, and the role of the continental surface in influencing the zonal distribution are all worth investigating.

In addition to the surface response, the observed strengthening of the STR and its small shift south in position needs to be reconciled with existing observations and an understanding of the movements of the HC. There appears to be a consensus (based on several upper air data: tropospheric jets, tropopause height, Out-going Long wave Radiation (OLR), total Ozone column, stream function) regarding a broadening of the HC (Seidel et al. 2007), consistent with the theoretical understanding of the effect of global warming on this circulation (Held 2000). This needs to be reconciled with the very small (and indeed statistically non-significant) shift of the STR-P at the surface around the Australian continent.

In addition, there appears to be a lack of consensus on the intensity of the HC in response to global warming. While Held and Soden (2006) have argued that the entire tropical circulation will weaken, it is not obvious if that is only the case for the zonal circulation or for the meridional circulation as well. Previous studies have argued that the meridional transport of energy should increase in response to global warming (Oort and Yienger 1996); this was confirmed using a simple modelling approach as part of SEACI-1 (Timbal and Smith 2009). Other directions appear particularly relevant for SEA and worth exploring further such as the response of the mid-latitude circulation. The mid-latitude storm track, which is the main driver of energy from the mid-latitudes to higher latitudes captured by the Ferrel Cell (FC), is likely to contract poleward in a warmer climate (Lim and Simmonds 2008). The implications of both the

FC and HC changes for the STR changes, and associated rainfall changes, need to be investigated.

Finally, as observed earlier, it appears that while the STR-I is responding to the absolute global warming, SEA rainfall relates better to the rate of GW. In the light of this observation, the possibility that the gradient of SSTs is more important than their absolute values is worth pursuing. This would have consequences for the future prognosis discussed earlier. In this context, the role of continental surfaces which play a role in the intensity of the HC (Cook 2003), and have been observed to warm faster than the oceans (Solomon et al. 2007), may contribute to the changes in intensity of the HC globally and, more importantly, at the longitude of important land masses such as Australia.

During SEACI-2, it is also proposed to use the findings of SEACI-1 regarding the causes of the ongoing rainfall decline presented here to evaluate future projections of climate change. Of particular interest is the evolution of the STR in the simulations of the 20th and 21st centuries. What role do STR movements play in the simulation of SEA rainfall in the climate models now and in the future? Do they provide an avenue for evaluating the reliability of the model projections?

REFERENCES

Allan, R. and Ansell T. 2006: A new globally complete monthly historical gridded Mean Sea level Pressure dataset (HadSLP2): 1850-2004, *J. Climate,* **19**: 5816-42.

Ashok, K., Behera, S., Rao, S., Weng H. and Yamagata, T. 2007: EL Niño Modoki and its possible teleconnections, *J. Geo. Res.*, **112**, DOI: 10.1029/2006JC003798.

Bessell, R. 2006: In *The Fenner School of Environment and Society*, Vol. Bachelor of Science (Hons), the Australian National University, Canberra.

Brohan, P., Kennedy, J.J., Harris, I., Tett, S.F.B. and Jones, P.D. 2006: Uncertainty estimates in regional and global observed temperature changes: a new dataset from 1850. *J. Geo. Res.,* **111**, D12106, DOI: 10.1029/2005JD006548.

Cai, W., Cowan, T. and Sullivan, A. 2009: Recent unprecedented skewness towards positive Indian Ocean Dipole occurrences and its impact on Australian rainfall, *Geophys. Res. Let.*, **36**, L11705, DOI: 10.1029/2009GL037604.

Chiew, F.H.S. 2006: Estimation of rainfall elasticity of streamflow in Australia, *Hydrological Sciences,* **51(4)**, 613-25.

Collins, W.D. and Co-authors, 2006: The Community Climate System Model version 3 (CCSM3), *J. Climate*, **19,** 2122–43.

Cook, K.H. 2003: Role of the continents in driving the Hadley Cells, *J. of Atmos. Sci.*, **60**, 957-76.

Dommenget, D. 2007: Evaluating EOF modes against a stochastic null hypothesis, *Clim. Dyn.,* **28**: 517-31.

Dommenget, D. 2010: An objective analysis of the observed spatial structure of the tropical Indian Ocean SST variability, *Clim. Dyn.,* DOI 10.1007/s00382-010-0787-1.

Drosdowsky, W. 1993: An Analysis of Australian seasonal rainfall anomalies: 1950-1987. I: Spatial Patterns, *Int. J. Climatology*, **13**, 1-30.

Drosdowsky, W. and Chambers, L.E. 2001: Near global sea surface temperature anomalies as predictors of Australian seasonal rainfall. *J. Climate*, **14**, 1677-87.

Drosdowsky, W. 2005: The latitude of the subtropical ridge over eastern Australia: the L index revisited, *Int. J. Climatol,* **25**, 1291-9.

Edwards, K. 2002: In *Fenner School of Environment and Society*, Vol. Bachelor of Science (Hons), the Australian National University, Canberra.

Gillette, N.P., Zwiers, F.W., Weaver A.J. and. Stott, P.A. 2003: Detection of human influence on sea-level pressure, *Nature*, **422**, 292-4.

Held, I.M. 2000: The general circulation of the atmosphere, paper presented at 2000 Woods Hole Oceanographic Institute Geophysical Fluid Dynamics Program, Woods Hole Oceanographic Institute, Woods Hole, Massachusetts, available on-line at http://www.gfdl.noaa.gov/cms-filesystem-action/user_files/ih/lectures/woods_hole.pdf.

Held, I.M. and Soden, B.J. 2006: Robust Responses of the Hydrological Cycle to Global Warming, *J. Climate,* **19**, 5686-99.

Hendon, H.H., Thompson, D.W.J. and Wheeler, M.C. 2007: Australian rainfall and surface temperature variations associated with the Southern Annular Mode, *J. Climate,* **20**, 2452-67.

Hope, P., Timbal B. and Fawcett, R. 2009: Associations between rainfall variability in the southwest and southeast of Australia and their evolution through time, *Int. J. Climatol.*, DOI: 10.1002/joc.1964.

Houghton, J.T., Ding, Y., Griggs, D.J., Noguer, M., van der Linden, P.J. and Xiaosu, D. (eds.), 2001: "Climate Change 2001: The Scientific Basis", contribution of Working Group I to the Third Assessment Report of the Intergovernmental Panel on Climate Change, Cambridge University Press, Cambridge, United Kingdom, 944 pp.

Huth, R. 2005: Downscaling of humidity variables: a search for suitable predictors and predictands, *Int. J. Climatol.*, **25**, 243-50.

Jones, D.A. and Weymouth, G. 1997: An Australian monthly rainfall dataset, *Technical Report 70*. Bureau of Meteorology: Melbourne, Australia, 19pp.

Jones, D.A., Wang, W. and Fawcett, R. 2009: High quality spatial climate data sets for Australia, *Aust. Met. Mag.*, submitted.

Jovanovic, B., Jones, D.A. and D. Collins, 2008: A high quality monthly pan-evaporation dataset for Australia, *Climatic Change*, **87**, 517-35.

Lavery, B., Kariko, A. and N. Nicholls, 1992: A historical rainfall data set for Australia, *Aust. Met. Mag*, **40**, 33-9.

Lavery, B., Joung, G. and Nicholls, N. 1997: An extended high-quality historical rainfall dataset for Australia, *Aust. Met. Mag*, **46**, 27-38.

Lim, E.-P. and Simmonds, I. 2008: Effect of tropospheric temperature change on the zonal mean circulation and SH winter extratropical cyclones, *Clim. Dyn,* DOI:10.1007/s00382-008-0444-0.

Lucas, C. 2006: A high quality humidity database for Australia. Abstracts for 17th Australia New Zealand Climate Forum, Canberra, September 2006, p 35.

Mantua, N.J., Hare, S.R., Zhang, Y., Wallace, J.M. and Francis, R.C. 1997: A Pacific interdecadal climate oscillation with impacts on salmon production, *Bulletin of the American Meteorological Society*, **78**, 1069-79.

Marshall, G. J. 2003: Trends in the Southern Annular Mode from observations and reanalyses, *J. Climate,* **16**: 4134-43.

Meehl, G.A., Washington, W.M., Santer, B.D., Collins, W.D., Arblaster, J.M., Hu, A., Lawrence, D., Teng, H., Buja, L. E. and Strand, W. G. 2006: Climate change projections for twenty-first century and climate change commitment in the CCSM3, *J. Climate*, **19**, 2597– 616.

Meyers, G., McIntosh, P., Pigot L. and Pook, M. 2007: The years of El Niño, La Niña and interactions with the tropical Indian Ocean, *J. Climate*, **20**, 2872-80.

Miller, R.L., Schmidt, G.A. and Shindell, D.T. 2006: Forced annular variations in the 20th century Intergovernmental Panel on Climate Change Fourth Assessment Report models, *J. Geophys. Res.,* **111**, D18101, DOI:10.1029/2005JD006323.

Murphy, B. and Timbal, B. 2008: A review of recent climate variability and climate change in south-eastern Australia, *Int. J Climatol*, **28(7)**, 859-79.

National Climate Centre, 2005: An exceptionally warm April and dry start to 2005. *Special Climate Statement*, **5**, April 2005.

Nicholls N. 1989, Sea surface temperatures and Australian winter rainfall, *J. Climate*, **2**, 965-73.

Oort, A.H. and J.J. Yienger, 1996: Observed Interannual Variability in the Hadley Circulation and Its Connection to ENSO, *J. Climate*, **9**, 2751–67.

Potter, N.J. and Chiew, F.H.S. 2009: Statistical characterisation and attribution of recent rainfall and runoff in the Murray-Darling Basin, *Proceedings from the 18th IMACS/MOSDIM Conference,* Cairns Australia, 2812-8.

Potter, N.J., Chiew F.H.S. and Frost, A.J. 2010: An assessment of the severity of recent reductions in rainfall and runoff in the Murray-Darling Basin, *J. of Hydrology,* **381**, 52-64.

Power, S., Tseitkin, F., Torok, S., Lavery, B., Dahni, R. and McAvaney, B. 1998: Australian temperature, Australian rainfall and the Southern Oscillation, 1910-1992: coherent variability and recent changes, *Aust. Met. Mag*., **47**, 85-101.

Power, S., Haylock, M., Colman, R. and Wang, X. 2006: The predictability of interdecadal changes in ENSO activity and ENSO teleconnections, *J. Climate*, ***19***, 4755-71.

Power, S.B. and Smith, I.N. 2007: Weakening of the Walker Circulation and apparent dominance of El Niño both reach record levels – but has ENSO really changed? *Geophys. Res. Let*., **34**, L18702, DOI: 10.1029/2007GL030854.

Rakich, C., Holbrook N. and Timbal, B. 2008: A pressure gradient metric capturing planetary-scale influences on eastern Australian rainfall, *Geophys. Res. Let.,* **35**, L08713, DOI: 10.1029/2007GL03297.

Raupach, M.R., Briggs P.R., Haverd, V., King, E.A., Paget, M. and Trudinger, C.M. 2009: Australian Water Availability Project, CSIRO Marine and Atmospheric Research Component: Final Report for Phase 3. *CAWCR research report, **13***, 62 pp.

Rayner, N., Brohan, P., Parker, D., Folland, C., Kennedy, J., Vanicek, M., Ansell T. and Tett, S. 2006: Improved analyses of changes and uncertainties in sea surface temperature measured *in situ* since the mid-Nineteenth Century: The HadSST2 Dataset, ***J. Climate***, **19**, 446-68.

Saji N.H., Goswami, B.N., Vinayachandran P.N. and Yamagata, T. 1999: A dipole mode in the tropical Indian Ocean, *Nature,* **401,** 360–3.

Seidel, D.J., Fu, G., Randel R.J. and Reichler, T.J. 2007: Widening of the tropical belt in a changing climate, *Nature*, doi:10.1038/ngeo.2007.38.

Sherwood, S.C. and 30 other workshop participants, 2009: Southeast Australian Rainfall Workshop - Summary. *Bulletin of the Australian Meteorological and Oceanographic Society*, 2009, in press. Available on-line at:
http://web.science.unsw.edu.au/~stevensherwood/SEA_two_pager_v4.pdf.

Smith, T.M. and Reynolds, R.W. 2004: Improved Extended Reconstruction of SST (1854-1997), *J. Climate*, **17**: 2466-77.

Solomon S., Qin, D., Manning, M., Chen, Z., Marquis, M., Averyt, K., Tignor, M. and Miller H.M. (eds.), 2007: "Climate Change 2007: The Physical Science Basis", contribution of Working Group I to the Fourth Assessment Report of the Intergovernmental Panel on Climate Change, Cambridge University Press, Cambridge, United Kingdom and New York, NY, USA, 996 pp.

Timbal B. and McAvaney, B.J. 2001: An Analogue based method to downscale surface air temperature: Application for Australia, *Clim. Dyn*, **17,** 947-63.

Timbal B., Dufour A. and McAvaney, B.J. 2003: An estimate of climate change for Western France using a statistical downscaling technique, *Clim. Dyn,* **17**, 947-63.

Timbal B. 2004: South West Australia past and future rainfall trends, *Clim. Res.,* **26(3)**, 233-49.

Timbal, B. and Arblaster, J. 2006: Land covers change as an additional forcing to explain the rainfall decline in the South West of Australia, *Geo. Res. Let.*, 33, L07717, DOI: 10.1029/2005GL025361.

Timbal, B., Arblaster, J. and Power, S. 2006: Attribution of the late 20th century rainfall decline in Southwest Australia, *J Climate*, **19(10),** 2046–62.

Timbal B. and Murphy, B. 2007: Observed climate change in South-East of Australia and its relation to large-scale modes of variability, *BMRC Res. Let.,* **6**, 6-11.

Timbal, B. and Hope, P. 2008: Observed early winter Mean Seal Level Pressure changes above southern Australia: a comparison of existing datasets, *CAWCR res. Let,* **1**, 1-7.

Timbal, B. and Jones, D. 2008: Future projections of winter rainfall in southeast Australia using a statistical downscaling technique, *Climatic Change,* **86**, 165-87.

Timbal, B., Li, Z. and Fernandez, E. 2008: The Bureau of meteorology Statistical Downscaling Model Graphical User Interface: user manual and software documentation, *CAWCR research report*, **4**, pp 95.

Timbal, B. 2009: The continuing decline in South-East Australian rainfall – Update to May 2009, *CAWCR Res. Let.*, **2**, 8pp.

Timbal, B., Fernandez E. and Li, Z. 2009: Generalization of a statistical downscaling model to provide local climate change projections for Australia, *Env. Mod. & Software,* **24**, 341-58.

Timbal, B. and Smith, I. 2009: Assessing the relationship between the Hadley Circulation and position and intensity of the sub-tropical ridge in the Australian region", South-Eastern Australian Climate Initiative (SEACI), final report for project **1.1.1P**, 24 pp.

Trewin, B.C. 2001: *Extreme temperature events in Australia*, PhD Thesis, School of Earth Sciences, University of Melbourne, Australia.

Trewin, B.C. 2006: An exceptionally dry decade in parts of southern and eastern Australia October 1996 - September 2006. *Special Climate Statement* **No. 9**, Australian National Climate Centre, 9 pp.

Visbeck, M. 2009: A station-based Southern Annular Mode index from 1884 to 2005. *J. Climate*, **22**, 940-50.

Von Storch, H. 1999: On the Use of "Inflation" in Statistical Downscaling, *J. Climate*, **12,** 3505–6.

Zhang, Y., Wallace J.M. and Battisti, D.S. 1997: ENSO-like interdecadal variability: 1900-93, *J. Climate*, **10**, 1004-20.

APPENDIX

List of rainfall stations

Location	Station Id	Lon. (E)	Lat. (S)	Start Date	End Date	Quality
addington	89106	143.67	-37.42	1991	Open	1
adelaide (clapham)	23075	138.60	-35.00	1954	Open	1
adelaide airport	23034	138.52	-34.95	1955	Open	1
adelong post office	72000	148.06	-35.31	1883	Open	1
ainslie tyson st	70000	149.14	-35.26	1935	Open	1
airlie	43023	148.41	-26.80	1934	Open	3
alawoona (schells well)	25018	140.50	-34.79	1908	Open	1
andrews (geralka)	21069	138.58	-33.62	1957	Open	1
angellala downs homestead	44001	147.03	-26.02	1911	Open	3
angledool (angledool station)	48168	147.90	-29.12	1886	Open	1
annuello	76000	142.78	-34.85	1925	Open	1
apoinga (wilivere)	21121	138.93	-33.96	1957	Open	1
appila	19001	138.43	-33.05	1874	Open	HQ
ardrossan	22000	137.92	-34.42	1880	Open	HQ
arnobay	18001	136.57	-33.91	1908	Open	HQ
arthurville (cramond)	65000	148.75	-32.50	1888	Open	1
ashford (springvale)	54045	151.29	-29.34	1958	Open	1
ashley (the prairies)	53040	149.94	-29.05	1928	Open	3
attunga (garthowen)	55000	150.86	-30.91	1903	Open	3
attunga (the pines)	55120	150.79	-30.93	1958	Open	1
augathella post office	44002	146.59	-25.80	1889	Open	1
australia_plains	24501	139.17	-34.10	1891	Open	HQ
ballarat aerodrome	89002	143.79	-37.51	1908	Open	1
balranald (rsl)	49002	143.56	-34.64	1879	Open	1
bannaby (hillasmount)	70002	150.00	-34.43	1945	Open	1
barcaldine	36007	145.29	-23.55	1887	Open	HQ
barraba	54003	150.61	-30.38	1893	Open	HQ
barraba (neranghi)	54023	150.81	-30.29	1908	Open	1
barrackdale	43058	148.73	-27.53	1955	Open	3
bathurst	63005	149.56	-33.43	1909	Open	HQ
bawnduggie	42075	150.84	-26.16	1947	Open	3
baynton	88073	144.69	-37.13	1953	Open	1
bayrick	44168	146.03	-25.46	1904	Open	1
beales reservoir	87011	144.03	-37.54	1881	Open	1
beaufort	89005	143.36	-37.45	1883	Open	HQ
beaumaris	86146	145.03	-37.98	1955	Open	1
beechal	44004	144.74	-27.14	1873	Open	1
beechworth	82001	146.71	-36.37	1876	Open	HQ
belah park	42002	150.28	-27.21	1913	Open	3
bell store	41005	151.45	-26.93	1910	Open	1
benalla (shadforth street)	82002	145.97	-36.55	1882	Open	1
bendemeer (charles st)	55004	151.15	-30.89	1879	Open	1

bendemeer (glenclair)	55109	151.11	-30.80	1958	Open	1
berriwillock	77005	142.99	-35.64	1898	Open	1
bettowynd	69006	149.78	-35.72	1897	Open	HQ
biala (alvison)	70111	149.25	-34.56	1938	Open	3
bierbank	44007	145.07	-26.78	1888	Open	3
bingara	54004	150.57	-29.87	1879	Open	HQ
birchip	77008	142.85	-35.93	1910	Open	HQ
birchip (marlbed)	77028	142.87	-35.80	1905	Open	1
birdsville	38002	139.35	-25.90	1898	Open	HQ
black mountain	84044	148.27	-37.01	1920	Open	1
black springs (swatchfield)	63080	149.71	-33.89	1937	Open	1
blackville post office	55006	150.24	-31.64	1879	Open	1
blanchetown (wyn-moor)	24523	139.78	-34.42	1899	Open	1
bollon mary st	44010	147.48	-28.03	1885	Open	1
bombala (cambalong)	70013	149.11	-36.89	1920	Open	1
booleroo centre	19006	138.35	-32.88	1883	Open	1
booligal (belmont)	75007	144.91	-33.84	1890	Open	1
booligal (toms lake)	49118	144.77	-33.71	1935	Open	1
boorara	44012	144.38	-28.66	1885	Open	1
boorhaman	82006	146.28	-36.22	1908	Open	1
booroorban (ramsay)	75056	144.74	-34.94	1923	Open	1
boort (gredgwin)	77016	143.61	-35.97	1917	Open	1
boree creek (richmond st)	74014	146.61	-35.11	1924	Open	1
bower	24504	139.35	-34.12	1900	Open	1
branxholme (bassett)	90010	141.77	-37.86	1883	Open	1
branxton	61014	151.42	-32.64	1863	Open	HQ
breeza (the park)	55065	150.54	-31.17	1914	Open	1
brewarrina hospital	48015	146.87	-29.96	1872	Open	1
brinkworth (bungaree)	21010	138.56	-33.75	1860	Open	1
broken hill (langawirra)	46015	142.14	-31.45	1887	Open	1
broken hill (topar)	47037	141.99	-31.89	1896	Open	1
broken hill (waterbag)	46117	142.33	-31.48	1946	Open	3
buchan (post office)	84005	148.17	-37.50	1883	Open	1
bukalong station	70009	149.20	-36.80	1857	Open	1
bullengarook east (seskinore)	87075	144.50	-37.50	1951	Open	1
bumbaldry (weowna)	73100	148.44	-33.91	1897	Open	1
bundaleer	41317	151.42	-27.07	1958	Open	1
bundarra (araluen)	54000	150.94	-30.05	1926	Open	1
bungaree (kirks reservoir)	87014	143.93	-37.55	1881	Open	1
bungowannah(roseleigh)	74236	146.76	-36.02	1893	Open	1
burkes flat	81006	143.55	-36.67	1902	Open	1
burra (worlds end)	21086	139.07	-33.84	1898	Open	1
burrinjuck dam	73007	148.60	-35.00	1908	Open	1
cambooya	41011	151.87	-27.71	1909	Open	HQ
campbelltown	88011	143.96	-37.23	1889	Open	1
camperdown (ettrick)	90012	143.25	-38.00	1930	Open	1
canaryisland	80004	143.85	-35.98	1888	Open	HQ
canberra airport	70014	149.20	-35.30	1939	Open	1
caniambo	81007	145.66	-36.46	1903	Open	1
canningdowns	41013	152.07	-28.23	1903	Open	HQ
cape borda comparison	22801	136.59	-35.75	1865	Open	1
cape bridgewater	90013	141.41	-38.32	1905	Open	1

cape otway lighthouse	90015	143.51	-38.86	1861	Open	1
capemoreton	40043	153.47	-27.03	1870	Open	HQ
carawatha	41033	151.99	-28.76	1913	Open	1
carbean	41014	151.63	-28.35	1946	Open	3
carboor	82009	146.54	-36.61	1910	Open	1
carroll	55055	150.46	-30.96	1891	Open	HQ
casino	58063	153.05	-28.88	1879	Open	HQ
casterton (warrock)	90020	141.34	-37.44	1880	Open	1
casterton showgrounds	90135	141.41	-37.59	1956	Open	1
cataract	68016	150.81	-34.27	1904	Open	HQ
cathcart (old post office)	70106	149.39	-36.84	1899	Open	1
caulfield (racecourse)	86018	145.04	-37.88	1887	Open	1
charleville aero	44021	146.26	-26.41	1942	Open	1
cheltenham kingston centre	86020	145.08	-37.96	1914	Open	1
cherry gardens	23709	138.66	-35.06	1899	Open	1
cherry tree hill (kulki)	54057	150.96	-29.52	1958	Open	3
clare (calcannia)	21075	138.61	-33.75	1937	Open	1
clare (hill river)	21025	138.65	-33.83	1882	Open	1
clarencetown	61010	151.78	-32.59	1896	Open	HQ
clear lake	79008	141.87	-36.94	1903	Open	1
clydebank	85020	147.18	-38.04	1883	Open	1
cobar (double gates)	48034	145.48	-31.69	1891	Open	1
cobar (tambua)	48115	145.25	-31.42	1888	Open	3
cockburn (tepco)	20053	140.80	-32.17	1928	Open	1
colbinabbin	81008	144.78	-36.54	1899	Open	1
collarenebri	48031	148.59	-29.55	1898	Open	HQ
collarenebri (bundabarina)	48018	148.40	-29.54	1914	Open	1
collerina (kenebree)	48052	146.52	-29.77	1925	Open	1
comongin north	45004	144.33	-26.50	1900	Open	3
conargo (puckawidgee)	75054	145.21	-35.28	1880	Open	1
conargo (willurah)	75075	145.09	-35.00	1877	Open	1
conargo post office	74192	145.18	-35.30	1895	Open	1
condamine plains	41019	151.29	-27.72	1870	Open	3
coolabah (tara)	48095	146.16	-30.95	1950	Open	1
coolatai (willunga)	54032	150.61	-29.20	1903	Open	3
coolesha	41041	151.73	-28.24	1920	Open	3
cooma (kiaora)	70054	149.06	-36.20	1904	Open	1
coonabarabran (namoi street)	64008	149.27	-31.27	1879	Open	1
coonamble comparison	51010	148.38	-30.98	1878	Open	1
coondambo	16009	135.87	-31.06	1886	Open	HQ
coonooerbridge	80009	143.35	-36.48	1888	Open	HQ
copeton (carinya)	54028	150.92	-29.96	1951	Open	1
coranderrk badger weir	86219	145.56	-37.69	1879	Open	1
corowa airport	74034	146.36	-35.99	1890	Open	1
cowal	40013	152.62	-25.82	1910	Open	HQ
crookwell (gundowringa)	70069	149.57	-34.54	1945	Open	1
cryon (koothney)	52003	148.47	-29.96	1935	Open	1
cudlee creek (millbrook)	23731	138.82	-34.83	1914	Open	1
culcairn bowling club	74188	147.04	-35.67	1912	Open	1
culgoa (post office)	77014	143.10	-35.72	1899	Open	1
cunnamulla	44026	145.68	-28.07	1879	Open	HQ
curlewis	55045	150.03	-31.18	1903	Open	HQ

dalveen	41022	151.97	-28.50	1887	Open	1
darlington point (st paul close	75166	146.00	-34.57	1909	Open	1
dealisland	99001	147.32	-39.48	1871	Open	HQ
deniliquin	74128	144.95	-35.55	1870	Open	HQ
dergholm (dorodong)	90034	141.08	-37.33	1943	Open	1
dergholm (hillgrove)	90033	141.21	-37.36	1899	Open	1
derrinallum (craigmore)	89103	143.22	-37.97	1898	Open	1
dinton vale (berrilee)	54069	151.16	-29.60	1958	Open	3
doctorscreek	41024	151.85	-27.21	1906	Open	HQ
drillham post office	42009	149.98	-26.64	1918	Open	3
drungdrung	79010	142.40	-36.78	1906	Open	HQ
dulacca truck stop	42010	149.76	-26.64	1890	Open	1
dundee (wattle dale)	56094	151.99	-29.55	1958	Open	1
dunedoo post office	64009	149.40	-32.02	1912	Open	1
duri (ashgrove)	55183	150.86	-31.30	1958	Open	1
east sale airport	85072	147.13	-38.12	1943	Open	1
echuca aerodrome	80015	144.76	-36.17	1859	Open	1
ehlma park	41291	150.87	-26.86	1958	Open	1
eldorado	82015	146.52	-36.31	1890	Open	1
elliston	18069	134.89	-33.65	1882	Open	HQ
elong elong (bendeela st)	64010	149.04	-32.11	1926	Open	1
elsmore (danthonia)	56111	151.35	-29.78	1958	Open	1
emmaville (strathbogie)	56029	151.48	-29.46	1872	Open	3
enngonia (shearer street)	48039	145.85	-29.32	1889	Open	1
ensay	84015	147.84	-37.38	1909	Open	1
eromanga - webber st	45006	143.27	-26.67	1905	Open	3
erudina	20005	139.39	-31.48	1911	Open	1
eudunda	24511	139.08	-34.18	1881	Open	HQ
eurobin	83010	146.86	-36.64	1912	Open	1
euston (benington)	49023	142.91	-34.45	1935	Open	1
eversley	79014	143.17	-37.19	1888	Open	1
fairymead	39037	152.36	-24.79	1881	Open	HQ
farina	17024	138.27	-30.07	1879	Open	HQ
fernlee	44034	147.05	-28.27	1890	Open	3
frogmoor	43010	149.11	-27.08	1918	Open	3
gaboisland	84016	149.91	-37.57	1871	Open	HQ
ganmain post office	74044	147.04	-34.79	1899	Open	1
gellibrand river west	90042	143.28	-38.62	1915	Open	1
geurie post office	65018	148.83	-32.40	1910	Open	1
giffard	85033	147.09	-38.42	1906	Open	1
gilgandra (wallumburrawang)	64024	148.96	-31.56	1901	Open	1
gladfield hopefield estate	80017	143.94	-36.04	1889	Open	1
glen innes ag research stn	56013	151.69	-29.70	1910	Open	1
glen innes post office	56011	151.74	-29.74	1881	Open	1
glen morrison (branga plains)	56083	151.55	-31.26	1940	Open	3
glenburn	88028	145.47	-37.38	1936	Open	1
glenmaggie weir	85034	146.80	-37.91	1938	Open	1
glenorie	44038	147.15	-27.02	1929	Open	3
glenroy	41277	151.20	-26.77	1958	Open	1
goode	18033	133.76	-31.97	1909	Open	HQ
goodooga post office	48046	147.45	-29.11	1891	Open	1
goolgowi (moira st)	75025	145.71	-33.98	1930	Open	2

goombie	45007	144.13	-26.11	1925	Open	1
goombungee post office	41037	151.85	-27.31	1909	Open	1
goulburn (pomeroy)	70071	149.50	-34.65	1901	Open	1
goulburn-murray wat. (kerang)	80110	143.93	-35.74	1957	Open	1
gowrie north	55194	150.85	-31.34	1953	Open	1
gowrie south	55190	150.84	-31.37	1958	Open	1
graman (ulupna)	54049	150.90	-29.41	1925	Open	1
gulargambone (emby)	51014	148.04	-31.13	1908	Open	3
gulargambone (yalcogrin st)	51022	148.47	-31.33	1886	Open	1
gulgong post office	62013	149.53	-32.36	1881	Open	1
gumbardo	44040	144.87	-26.11	1885	Open	3
gunnedah pool	55023	150.25	-30.98	1876	Open	1
gunnedah resource centre	55024	150.27	-31.03	1948	Open	1
haden post office	41042	151.88	-27.22	1926	Open	3
hall (lochleigh)	70045	149.06	-35.15	1903	Open	1
hallett (ashrose)	21067	138.82	-33.41	1957	Open	1
hallett (lorraine old greenfields	21024	138.75	-33.46	1898	Open	1
hallett (old canowie)	21062	138.76	-33.30	1884	Open	1
happyvalley	23721	138.56	-35.06	1863	Open	HQ
harden (dunolly)	73012	148.32	-34.75	1941	Open	1
harewood	42078	150.47	-26.92	1937	Open	3
harrisville	40094	152.67	-27.81	1897	Open	HQ
harrogate	23722	139.01	-34.93	1896	Open	1
hatfield (clare)	49008	143.94	-33.40	1873	Open	1
hatfield (the vale)	49047	143.80	-33.69	1924	Open	3
hawker	19017	138.44	-31.88	1882	Open	1
hawker (holowilena)	19018	138.84	-31.88	1868	Open	1
hawker (wilson)	19050	138.34	-31.99	1885	Open	1
hay (miller street)	75031	144.85	-34.52	1877	Open	1
hebel store	44042	147.80	-28.97	1899	Open	1
hermidale tank	51026	146.72	-31.56	1905	Open	1
highlands (glentannar)	88031	145.42	-37.07	1915	Open	1
hillston airport	75032	145.52	-33.49	1881	Open	1
holbrook (glenfalloch)	72019	147.56	-35.66	1909	Open	3
horsham (polkemmet)	79023	142.11	-36.65	1873	Open	1
hoyleton	21026	138.56	-34.04	1878	Open	1
huddleston (willow ponds)	21072	138.32	-33.33	1957	Open	1
hume reservoir	72023	147.03	-36.10	1922	Open	1
huntly	70093	148.98	-35.28	1956	Open	1
ilford (tara)	62029	149.81	-32.98	1928	Open	1
injune post office	43015	148.57	-25.84	1925	Open	1
inverell (glendowne)	54077	151.07	-29.69	1958	Open	3
inverell (wandera)	54078	151.15	-29.68	1958	Open	3
irymple (arlington)	76015	142.15	-34.23	1908	Open	1
ivanhoe (mt manara)	47022	143.94	-32.48	1887	Open	1
ivanhoe downs	44044	147.13	-26.35	1908	Open	3
ivanhoe post office	49019	144.30	-32.90	1884	Open	1
jandowae post office	41050	151.11	-26.78	1898	Open	1
jindivick	85042	145.89	-38.02	1899	Open	1
kandos cement works	62017	149.97	-32.86	1951	Open	1
kaniva	78078	141.24	-36.37	1883	Open	HQ
kanmantoo	23724	139.00	-35.07	1874	Open	1

karoola park	43080	148.74	-27.23	1955	Open	3
katoomba (murri st)	63039	150.31	-33.71	1885	Open	1
keith	25507	140.35	-36.10	1907	Open	HQ
kelvin (carellan)	55274	150.44	-30.78	1909	Open	1
kenilworth	44045	147.43	-27.41	1926	Open	3
kerang	80023	143.92	-35.72	1880	Open	1
kerang (meran downs)	80024	143.80	-35.87	1880	Open	1
kersbrook (mabenjo)	23758	138.87	-34.74	1951	Open	1
kindon	41058	150.74	-28.09	1924	Open	3
kings plains (croye)	54082	151.41	-29.64	1958	Open	1
kingston on murray	24006	140.34	-34.22	1896	Open	1
kingston se (keilira station)	26010	140.16	-36.71	1913	Open	1
kondoolka	16022	134.88	-32.00	1906	Open	HQ
koolunga	21029	138.33	-33.59	1884	Open	1
koorrnong	41242	151.64	-27.02	1958	Open	1
kurrowah	41061	151.20	-27.66	1915	Open	3
kuyura	41310	151.20	-26.89	1958	Open	3
laguna	41062	151.33	-27.81	1938	Open	1
lake bathurst (somerton)	70036	149.65	-35.01	1931	Open	1
lake cargelligo airport	75039	146.37	-33.28	1881	Open	1
lake eildon	88023	145.91	-37.23	1887	Open	1
lake leake (kooeeyong)	26014	140.58	-37.61	1892	Open	1
lake marmal	80029	143.52	-36.15	1881	Open	1
lake victoria storage	47016	141.27	-34.04	1922	Open	1
lakehamilton	18045	135.27	-33.95	1877	Open	HQ
lameroo comparison	25509	140.52	-35.33	1899	Open	1
lang lang	86063	145.57	-38.27	1918	Open	1
langhornecreek	24515	139.03	-35.30	1890	Open	HQ
lauriston reservoir	88037	144.38	-37.25	1948	Open	1
laverton raaf	87031	144.76	-37.86	1941	Open	1
leaghur	77027	143.78	-35.97	1905	Open	1
leeton (bents hill)	74007	146.55	-34.48	1941	Open	2
leeton (yarramundi)	74132	146.26	-34.64	1956	Open	2
legume (new koreelah)	56022	152.35	-28.46	1903	Open	1
leyburn post office	41063	151.59	-28.01	1883	Open	1
lilydale	20012	139.97	-32.96	1899	Open	1
lilydale	86066	145.34	-37.75	1885	Open	1
lindenow	85050	147.46	-37.80	1897	Open	1
little river	87033	144.49	-37.99	1906	Open	1
longwood	23727	138.73	-35.05	1949	Open	1
lovelybanks	87034	144.33	-38.07	1877	Open	HQ
loxton (pyap)	24013	140.49	-34.45	1896	Open	1
maitland (weetulta)	22019	137.59	-34.24	1887	Open	1
mallan (niemur valley)	75020	143.87	-35.16	1877	Open	2
malmsbury reservoir	88042	144.37	-37.20	1872	Open	1
manangatang (daytrap)	76011	142.81	-35.20	1930	Open	1
manangatang (eureka east)	76012	143.00	-35.17	1912	Open	1
manildra (hazeldale)	65022	148.59	-33.16	1888	Open	1
manilla (kimberley)	55328	150.75	-30.86	1950	Open	1
manoora (cooinda)	21076	138.81	-33.93	1957	Open	1
marnhull	41145	151.17	-26.84	1900	Open	3
maroondah weir (Melb. Water)	86070	145.55	-37.64	1892	Open	1

marree	17031	138.06	-29.65	1886	Open	HQ
maryborough	88043	143.73	-37.06	1878	Open	1
maryland	56207	151.99	-28.54	1868	Open	1
mathoura state forest	74069	144.90	-35.81	1949	Open	1
matong (main street)	74071	146.92	-34.77	1938	Open	1
maude (nap nap)	75049	144.17	-34.45	1889	Open	2
melbourne regional office	86071	144.97	-37.81	1908	Open	1
melva	41371	151.68	-28.46	1920	Open	1
menindee post office	47019	142.42	-32.39	1876	Open	1
meningie (mill park)	25529	139.47	-35.81	1958	Open	1
meningie (naranga)	25523	139.56	-35.86	1956	Open	1
meredith	87043	144.15	-37.82	1875	Open	HQ
merrinee	76030	141.76	-34.38	1925	Open	1
merriwagga (charney street)	75044	145.62	-33.82	1930	Open	1
michelago (soglio)	70064	149.16	-35.68	1884	Open	1
miepoll (avondale)	81032	145.51	-36.69	1901	Open	1
mildura airport	76031	142.08	-34.23	1946	Open	1
miles	42023	150.18	-26.66	1885	Open	HQ
mincha	80036	144.10	-35.96	1898	Open	1
minlaton	22009	137.59	-34.77	1880	Open	HQ
mitcham	86074	145.19	-37.82	1936	Open	1
mitchell post office	43020	147.98	-26.49	1884	Open	1
mitta mitta forestry	82068	147.37	-36.53	1953	Open	1
moble	45037	143.93	-26.87	1941	Open	1
mole river (trenayr)	56055	151.62	-29.02	1911	Open	1
molka (lowana)	81033	145.42	-36.64	1901	Open	1
moonbi (bellevue)	55143	151.07	-31.02	1958	Open	1
moorabool reservoir	87045	144.08	-37.52	1912	Open	1
morchard (the rocks)	19025	138.51	-32.77	1916	Open	1
moruya	69018	150.15	-35.91	1876	Open	HQ
moulamein (tchelery)	75062	144.17	-34.81	1886	Open	2
mount barker	23733	138.85	-35.06	1861	Open	1
mount bold reservoir	23734	138.68	-35.12	1938	Open	1
mount gambier aero	26021	140.77	-37.75	1941	Open	1
mount irving	41072	151.60	-27.48	1899	Open	3
moutajup	89022	142.23	-37.65	1899	Open	1
mudgee	62021	149.60	-32.60	1877	Open	HQ
mulga downs	44054	147.12	-28.81	1905	Open	1
mulgadowns	44054	147.12	-28.81	1905	Open	HQ
mullaley (garrawilla)	55018	149.65	-31.17	1884	Open	3
mullaquana	18058	137.36	-33.21	1911	Open	HQ
mungindi (burrenbah)	48020	148.65	-29.04	1896	Open	3
mungindi (cambo cambo)	48022	148.60	-29.08	1895	Open	3
mungindi post office	52020	148.99	-28.98	1887	Open	1
murgon	40152	151.94	-26.24	1910	Open	HQ
murralah	41388	151.33	-28.06	1952	Open	3
murray bridge (tepko)	24533	139.19	-34.97	1892	Open	1
murraybridge	24521	139.27	-35.12	1886	Open	HQ
murringo (windermere)	73051	148.55	-34.21	1888	Open	1
murtoa	79035	142.47	-36.62	1883	Open	1
mutooroo	20017	140.92	-32.45	1887	Open	1
nappa merrie	45012	141.11	-27.60	1908	Open	3

naradhan	75050	146.32	-33.61	1910	Open	HQ
narrabri (mollee)	53026	149.68	-30.26	1926	Open	3
narraport	77030	143.03	-36.01	1887	Open	HQ
natimuk	79036	141.94	-36.74	1907	Open	HQ
natte yallock	81038	143.47	-36.94	1898	Open	1
netherton (the glen)	25515	139.95	-35.52	1915	Open	1
newstead	88048	144.06	-37.11	1897	Open	1
nhill	78031	141.64	-36.33	1897	Open	1
nhill (salisbury (lynbar))	78033	141.77	-36.30	1930	Open	1
nicholson (yendalock)	84025	147.77	-37.85	1905	Open	1
nonning	16032	136.49	-32.52	1903	Open	HQ
normanville	23741	138.32	-35.45	1867	Open	1
northparnda	18049	136.16	-34.12	1906	Open	HQ
nullamanna (belmore)	54073	151.24	-29.64	1958	Open	1
nullawarre (lynlea)	90060	142.75	-38.47	1899	Open	1
nundle (benoni)	55078	151.09	-31.41	1953	Open	3
nyngan (mudall)	51033	147.13	-31.86	1881	Open	1
nyngan airport	51039	147.20	-31.55	1879	Open	1
oakleigh	41108	150.52	-27.38	1911	Open	1
old junee (millbank)	73025	147.56	-34.79	1895	Open	1
old koreelah (mcpherson)	56023	152.42	-28.39	1912	Open	3
omeo comparison	83025	147.60	-37.10	1879	Open	1
omeo shannon vale	83035	147.43	-36.92	1951	Open	1
orange (mclaughlin st)	63066	149.11	-33.27	1889	Open	1
orbost	84030	148.46	-37.69	1884	Open	HQ
orroroo	19032	138.61	-32.74	1868	Open	HQ
orroroo (black rock)	19005	138.69	-32.82	1877	Open	1
orroroo (kylmorn)	19012	138.78	-32.71	1901	Open	1
ourigilla	42034	150.00	-27.17	1931	Open	1
ouyen (post office)	76047	142.32	-35.07	1911	Open	1
padthaway (marcollat)	26017	140.38	-36.50	1950	Open	2
pallamallawa post office	53033	150.14	-29.47	1913	Open	1
parawa (sharon)	23761	138.34	-35.56	1942	Open	1
parkes (macarthur street)	65026	148.16	-33.14	1889	Open	1
patchewollock	77033	142.19	-35.38	1926	Open	1
peakhill	50031	148.19	-32.73	1891	Open	HQ
peebinga	25023	140.91	-34.93	1951	Open	1
pella	77036	141.94	-35.83	1902	Open	HQ
penola	26025	140.84	-37.38	1863	Open	HQ
penshurst (the gums)	90062	142.42	-37.88	1906	Open	1
perola park	44062	146.32	-25.71	1916	Open	3
peterborough (anda-vale)	19014	138.92	-32.80	1902	Open	1
pilliga post office	52023	148.88	-30.35	1883	Open	2
pine ridge (mooki springs)	55037	150.40	-31.51	1886	Open	3
pineside	18065	136.38	-33.87	1910	Open	HQ
pingine	44129	145.00	-26.42	1920	Open	3
pinnaroo	25015	140.91	-35.26	1907	Open	HQ
pittsworth	41082	151.63	-27.72	1887	Open	HQ
pointperpendicular	68034	150.80	-35.09	1900	Open	HQ
pooncarie	47029	142.57	-33.39	1883	Open	HQ
pooncarie (karpa kora station)	47013	143.11	-32.97	1886	Open	1
pooncarie (moorara)	47020	142.39	-33.22	1884	Open	2

pooncarie (tarcoola)	47033	142.57	-33.43	1878	Open	2
port clinton (yararoo)	22022	138.01	-34.14	1869	Open	1
port pirie zinifex comparison	21043	138.01	-33.17	1877	Open	1
portarlington	87053	144.64	-38.12	1885	Open	HQ
preston reservoir	86096	145.00	-37.72	1910	Open	1
purlewaugh (byfield)	64020	149.51	-31.34	1937	Open	1
purnong (claypans)	25002	139.67	-34.83	1927	Open	1
purple_downs	16039	136.89	-30.79	1903	Open	HQ
pykes creek reservoir	87095	144.30	-37.61	1956	Open	1
quambatook (barraport north)	77001	143.65	-35.98	1912	Open	1
quambatook south	77034	143.50	-35.93	1887	Open	1
quambone (sandy camp)	51044	147.75	-30.87	1886	Open	3
quandialla post office	73032	147.79	-34.01	1925	Open	1
quendon	41086	151.40	-26.67	1949	Open	1
quilberry rail siding	44063	145.92	-27.09	1893	Open	3
quilpie airport	45015	144.26	-26.61	1917	Open	1
rainbow (werrap (oak-lea))	77051	141.94	-35.94	1898	Open	1
rand post office	74131	146.58	-35.59	1954	Open	1
redesdale	88051	144.52	-37.02	1903	Open	1
redhill	21045	138.22	-33.54	1878	Open	1
renmark irrigation	24003	140.75	-34.17	1884	Open	1
rhynie (salters springs)	23039	138.63	-34.19	1957	Open	1
riverton	41087	151.49	-29.03	1920	Open	3
robe comparison	26026	139.76	-37.16	1860	Open	1
robertstown	24528	139.08	-33.99	1898	Open	1
rochester	80049	144.71	-36.36	1904	Open	1
rocklands reservoir	79052	141.96	-37.23	1948	Open	1
rosehill	44137	148.03	-27.87	1957	Open	1
rowena (bunna bunna)	52008	149.20	-29.80	1886	Open	3
rumbulara vineyards	41030	151.85	-28.76	1927	Open	1
running stream (brooklyn)	63012	149.88	-33.03	1899	Open	1
rutherglen research	82039	146.51	-36.10	1913	Open	1
rylstone	62026	149.98	-32.81	1885	Open	HQ
scotsburn (mount buninyong)	87046	143.94	-37.67	1856	Open	1
sealake	77039	142.85	-35.50	1910	Open	HQ
seaspray (burong)	85073	147.17	-38.32	1898	Open	1
sedan (sandleton)	24530	139.36	-34.46	1887	Open	1
sedgwick	81086	144.32	-36.86	1954	Open	1
shelbourne	42033	150.18	-26.30	1958	Open	3
sherwood park station	44120	144.86	-25.89	1935	Open	3
snowtown (condowie)	21015	138.29	-33.70	1879	Open	1
sofala old post office	63076	149.69	-33.08	1892	Open	1
somerton (clermont park)	55118	150.70	-30.92	1927	Open	3
somerton (glen burn)	55140	150.71	-31.01	1958	Open	1
south comongin	45003	144.34	-26.90	1884	Open	3
spring ridge (murrumbah)	55039	150.21	-31.38	1922	Open	1
springhurst	82041	146.47	-36.19	1900	Open	1
st arnaud (coonooer bridge)	80009	143.35	-36.48	1887	Open	1
st arnaud (tottington)	79079	143.12	-36.79	1884	Open	1
stanhope	81046	144.98	-36.44	1921	Open	1
strathbogie	82042	145.73	-36.85	1902	Open	1
stuart town (canobla)	62099	149.00	-32.84	1938	Open	1

sunny corner (snow line)	63079	149.90	-33.39	1903	Open	3
surat	43035	149.07	-27.16	1881	Open	1
swan reach	24535	139.60	-34.57	1898	Open	1
swan vale (numeralla)	56128	151.52	-29.83	1958	Open	1
swanreach	24535	139.60	-34.57	1899	Open	HQ
tailem bend (woodlands)	24510	139.52	-35.11	1911	Open	1
tandarra	80053	144.25	-36.43	1887	Open	1
tantanoola	26027	140.46	-37.70	1950	Open	1
tarcowie	19043	138.52	-32.95	1934	Open	1
tawonga	83038	147.13	-36.66	1942	Open	3
taylors flat (callaba)	70082	149.01	-34.28	1926	Open	1
temora research station	73038	147.52	-34.41	1934	Open	1
tenterfield (federation park)	56032	152.02	-29.05	1870	Open	1
tenterfield (mole station)	56052	151.74	-29.10	1950	Open	3
terang (wooriwyrite)	90085	142.99	-38.08	1894	Open	1
texas post office	41100	151.17	-28.85	1897	Open	1
thallon post office	42028	148.87	-28.63	1912	Open	1
thargomindah	45017	143.82	-28.00	1879	Open	HQ
the head	41046	152.42	-28.28	1958	Open	1
thylungra station	45018	143.45	-26.09	1893	Open	3
tibooburra post office	46037	142.01	-29.43	1886	Open	1
tinnenburra	44067	145.55	-28.73	1907	Open	3
tocumwal airport	74106	145.60	-35.81	1897	Open	1
toorourrong	86117	145.15	-37.48	1893	Open	HQ
tootool (bryntirion)	74017	146.97	-35.29	1911	Open	1
toowoomba	41103	151.93	-27.58	1869	Open	1
top plains	41134	152.40	-28.31	1952	Open	1
trangie research station aws	51049	147.95	-31.99	1922	Open	1
truro	24573	139.13	-34.41	1880	Open	1
tuena (wyoming)	63271	149.36	-34.04	1951	Open	1
tuppal (warragoon)	74208	145.20	-35.61	1950	Open	1
turallin	41110	151.20	-27.83	1909	Open	1
tyrendarra (ellangowan)	90038	141.78	-38.16	1902	Open	1
tyrrell downs	77047	142.99	-35.36	1885	Open	1
uni_qld_gatton	40082	152.34	-27.55	1899	Open	HQ
uplands (gibbo river park)	82018	147.69	-36.77	1904	Open	1
uralla (mihi)	56065	151.67	-30.72	1916	Open	1
uralla (salisbury court)	56028	151.51	-30.73	1862	Open	1
urana (butherwah)	74026	146.31	-35.35	1870	Open	1
urana (nowranie)	74087	146.03	-35.33	1892	Open	1
vaughan	88108	144.21	-37.16	1958	Open	1
ventnor (oaklands)	86119	145.18	-38.49	1915	Open	1
victor harbor (rivington grange	23743	138.50	-35.54	1910	Open	1
victoria downs	44070	147.04	-26.38	1906	Open	3
wagga wagga amo	72150	147.46	-35.16	1941	Open	1
wakool	75012	144.60	-35.42	1896	Open	HQ
walcha (craigdarroch)	56077	151.50	-31.07	1953	Open	1
walgett (dungalear)	48036	148.12	-29.66	1881	Open	3
wallaby_creek_weir	88060	145.21	-37.45	1885	Open	HQ
wallangra	54036	150.89	-29.24	1883	Open	HQ
wallaroo	22020	137.63	-33.93	1864	Open	HQ
walpeup research	76064	142.00	-35.12	1939	Open	1

wanaaring (borrona downs)	46002	143.11	-29.77	1938	Open	1
wanaaring (owen downs)	46052	143.38	-29.41	1956	Open	1
wanaaring post office	48079	144.15	-29.70	1884	Open	2
wandsworth (strabanne)	56036	151.52	-30.07	1895	Open	3
wanganella (zara)	75080	144.70	-35.17	1867	Open	1
warburton (o'shannassy MW)	86090	145.79	-37.71	1915	Open	1
warooka	22018	137.40	-34.99	1861	Open	1
warracknabeal (earlstan)	78038	142.24	-36.26	1900	Open	1
warren (mumblebone)	51034	147.69	-31.50	1882	Open	1
warrion	90080	143.53	-38.20	1897	Open	1
wartook reservoir	79046	142.43	-37.09	1890	Open	1
waverley downs	43093	148.54	-26.61	1950	Open	3
wee waa (pendennis)	53034	149.32	-30.12	1890	Open	1
weeaproinah	90083	143.51	-38.64	1901	Open	1
weemelah (crinolyn)	52010	149.12	-29.25	1913	Open	3
weetaliba (weetalabah)	64028	149.58	-31.63	1884	Open	1
wellington (agrowplow)	65034	148.95	-32.56	1881	Open	1
wentworth	47053	141.91	-34.11	1868	Open	HQ
wentworth (willow point)	47045	141.77	-33.33	1933	Open	1
westbrook	41126	151.83	-27.62	1890	Open	3
white cliffs (kayrunnera)	46093	142.54	-30.67	1939	Open	2
white cliffs (monolon)	46019	143.23	-30.20	1940	Open	3
white swan reservoir	89048	143.93	-37.52	1953	Open	1
whitecliffs	46042	143.09	-30.85	1901	Open	HQ
whitfield	83031	146.41	-36.75	1903	Open	1
whitlands (burders lane)	83032	146.32	-36.85	1929	Open	1
whittaker	41182	151.57	-27.17	1958	Open	1
whorouly	82055	146.60	-36.50	1913	Open	1
whynot station	45022	143.90	-26.69	1930	Open	3
whyte-yarcowie (gum park)	21120	138.79	-33.25	1941	Open	1
wickliffe	89033	142.72	-37.69	1880	Open	HQ
wilcannia (reid st)	46043	143.37	-31.56	1879	Open	1
wilcannia (billilla)	47005	143.15	-31.83	1882	Open	1
williamstown (glen gillian)	23756	138.93	-34.66	1951	Open	1
willow tree (parraweena)	55043	150.41	-31.71	1932	Open	3
willow tree (cooinda)	55244	150.57	-31.64	1950	Open	3
willow tree (valais)	55057	150.29	-31.77	1881	Open	1
wilsons reservoir	87067	144.02	-37.52	1896	Open	1
wilsonsprom	85096	146.42	-39.13	1873	Open	HQ
windorah	38024	142.66	-25.42	1891	Open	HQ
winnambool (kulwin)	76069	142.74	-34.95	1922	Open	1
winton	37051	143.04	-22.39	1884	Open	HQ
wirrabara forest	19053	138.22	-33.09	1879	Open	1
wirrega (taunton)	25518	140.57	-36.18	1910	Open	1
wollar (barrigan st)	62032	149.95	-32.36	1901	Open	3
wondalli	41128	150.59	-28.50	1910	Open	3
woodlea	42086	150.41	-27.13	1939	Open	3
woodspring	41391	151.15	-28.36	1954	Open	3
woolbrook (danglemah road)	55136	151.35	-30.97	1958	Open	1
woolgangi	20025	139.52	-33.50	1903	Open	1
woolomin (culwulla)	55189	151.18	-31.34	1958	Open	1
wooragee	82057	146.73	-36.30	1889	Open	1

wyalong post office	73054	147.24	-33.93	1895	Open	1
wyanga (barcoo)	51008	148.15	-32.46	1899	Open	1
wyangala dam	63267	148.95	-33.97	1929	Open	1
wylie creek (aloomba)	56038	152.16	-28.55	1914	Open	1
yacka	21057	138.45	-33.57	1881	Open	1
yamba	58012	153.36	-29.43	1882	Open	HQ
yamburgan	44166	148.40	-28.51	1898	Open	1
yan_yean	86131	145.13	-37.56	1863	Open	HQ
yanac	78043	141.42	-36.11	1898	Open	HQ
yanco glen (corona homestead	46003	141.44	-31.29	1882	Open	1
yangan post office	41120	152.21	-28.19	1912	Open	1
yannergee (dobroyd)	55069	150.02	-31.45	1925	Open	1
yantabulla station	48087	145.00	-29.34	1892	Open	3
yardea	16055	135.52	-32.38	1894	Open	HQ
yarrawalla south	80039	144.06	-36.19	1886	Open	1
yarroweyah	80065	145.55	-35.88	1893	Open	HQ
yass	70028	148.89	-34.74	1899	Open	HQ
yass (linton hostel)	70091	148.91	-34.83	1898	Open	1
yelarbon post office	41122	150.75	-28.57	1923	Open	1
yenda (henry street)	75079	146.19	-34.25	1925	Open	1
yongala	19062	138.75	-33.03	1881	Open	1
yunta (paratoo)	20021	139.40	-32.73	1880	Open	1

In total 585 stations have been selected within the SEACI climatic region. The full list is not provided here but some general information about the data quality. All stations are available on request:

Notes: **There are 95 HQ stations in the SEACI region**

Rainfall high quality dataset was initially put together by B. Lavery et al. (1992, Aust. Met. Mag.)
The dataset has been updated by D. Collins NCC, 2006, available online at:
ftp://ftp.bom.gov.au/anon/home/ncc/www/change/HQdailyR/HQdailyR_info.pdf
A known issue with HQ rainfall station is the existence of unreported accumulations. See:
Viney and Bates, Int. J. of Climatol., 24: 1171–1192 (2004)

Additional stations:

Quality = 1 (395 stations)	These stations have < 5% missing data (since 1996: < 3% & no missing months)
Quality = 2 (15 stations)	These stations are approaching the Q1 thresholds and fill gaps in the coverage
Quality = 3 (80 stations)	These stations meet the Q1 standard (5% and 3%) but have a low percentage (< 20%) of small rainfall events (less than 2mm) This suggests bad observing practices and is a concern for the overall quality at the site

List of temperature stations

Location	Station Id	Lon. (E)	Lat. (S)	Start Date	End Date	Quality	Known quality issue
adelaide	23090	138.62	-34.92	1887	Open	HQ	
adelaide airport	23034	138.52	-34.95	1955	Open	1	Urban affected
amberley	40004	152.71	-27.63	1941	Open	HQ	
ballarat	89002	143.79	-37.51	1908	Open	1	
barcaldine	36007	145.29	-23.55	1957	Open	HQ	
bathurst	63005	149.56	-33.43	1908	Open	HQ	
benalla	82002	145.97	-36.55	1882	Open	1	
birdsville	38002	139.35	-25.90	1957	Open	HQ	
bollon	44010	147.48	-28.03	1885	Open	1	Some missing data
boulia	38003	139.90	-22.91	1949	Open	HQ	
bourke	48013	145.94	-30.09	1957	Open	HQ	
brisbaneap	40223	153.11	-27.42	1949	Open	HQ	
bundaberg	39128	152.32	-24.91	1959	Open	HQ	
cabramurra	72091	148.38	-35.94	1962	Open	HQ	
canberra	70014	149.20	-35.30	1939	Open	HQ	
capeborda	22801	136.59	-35.75	1957	Open	HQ	
capeotway	90015	143.51	-38.86	1957	Open	HQ	
casterton	90135	141.41	-37.59	1956	Open	1	
ceduna	18012	133.71	-32.13	1939	Open	HQ	
charleville	44021	146.26	-26.41	1942	Open	HQ	
cobar	48027	145.83	-31.49	1957	Open	HQ	
coffsharbour	59040	153.12	-30.31	1943	Open	HQ	
condobolin	50052	147.23	-33.07	1965	Open	1	
coonabarabran	64008	149.27	-31.27	1879	Open	1	
cunnamulla	44026	145.68	-28.07	1879	Open	1	Reasonable
dalby	41522	151.26	-27.18	1958	Open	1	
deniliquin	74128	144.95	-35.55	1949	Open	HQ	
dubbo	65012	148.57	-32.21	1957	Open	HQ	
echuca	80015	144.76	-36.16	1957	Open	1	
gaboisland	84016	149.91	-37.57	1957	Open	HQ	
gayndah	39039	151.61	-25.63	1957	Open	HQ	
gunnedah	55024	150.27	-31.03	1959	Open	HQ	
hay	75031	144.85	-34.52	1877	Open	1	
hillston	75032	145.52	-33.49	1881	Open	1	
horsham	79023	142.11	-36.65	1873	Open	1	
inverell	56017	151.11	-29.78	1957	Open	HQ	
jervis	68034	150.80	-35.09	1957	Open	HQ	
kerang	80023	143.92	-35.73	1957	Open	HQ	
lameroo	25509	140.52	-35.33	1899	Open	1	
laverton	87031	144.75	-37.86	1943	Open	HQ	
longreach	36031	144.28	-23.44	1957	Open	HQ	
maitland	22008	137.67	-34.37	1879	Open	1	
marree	17031	138.06	-29.65	1957	Open	HQ	
melbourne	86071	144.97	-37.81	1855	Open	HQ	
mildura	76031	142.08	-34.23	1946	Open	HQ	
miles	42023	150.18	-26.66	1957	Open	HQ	

moree	53048	149.84	-29.48	1879	Open	HQ	
moruya	69018	150.15	-35.91	1921	Open	HQ	
mount barker	23733	138.85	-35.06	1861	Open	1	
mountgambier	26021	140.79	-37.75	1942	Open	HQ	
nhill	78031	141.64	-36.34	1951	Open	HQ	
nowra	68076	150.55	-34.94	1955	Open	HQ	
nuriootpa	23321	139.00	-34.48	1957	Open	HQ	
omeo	83025	147.60	-37.10	1879	Open	1	
oodnadatta	17114	135.44	-27.54	1940	Open	HQ	
orbost	84030	148.46	-37.69	1957	Open	HQ	
ouyen	76047	142.32	-35.07	1911	Open	1	
parkes	65026	148.16	-33.14	1958	Open	1	
port pirie	21043	138.01	-33.17	1877	Open	1	
portlincoln	18070	135.86	-34.72	1957	Open	HQ	
portmacquarie	60026	152.92	-31.44	1921	Open	HQ	
quilpie	45015	144.26	-26.61	1958	Open	1	
richmond_nsw	67105	150.78	-33.60	1939	Open	HQ	
robe	26026	139.76	-37.16	1957	Open	HQ	
rockhampton	39083	150.48	-23.38	1939	Open	HQ	
rutherglen	82039	146.51	-36.11	1957	Open	HQ	
sale	85072	147.13	-38.11	1945	Open	HQ	
scone	61089	150.93	-32.06	1959	Open	HQ	
snowtown	21046	138.21	-33.78	1958	Open	HQ	
stgeorge	43034	148.58	-28.04	1957	Open	HQ	
sydney	66062	151.21	-33.86	1859	Open	HQ	
sydney airport	66037	151.17	-33.94	1939	Open	1	Urban affected site
taralga	70080	149.82	-34.40	1882	Open	1	
tarcoola	16044	134.57	-30.71	1950	Open	HQ	
tewantin	40264	153.04	-26.39	1957	Open	HQ	
thargomindah	45017	143.82	-28.00	1957	Open	HQ	
tibooburra	46037	142.01	-29.44	1921	Open	HQ	
wagga	72150	147.46	-35.16	1942	Open	HQ	
walgett	52088	148.12	-30.04	1957	Open	HQ	
wilcannia	46043	143.37	-31.56	1957	Open	HQ	
williamtown	61078	151.84	-32.79	1942	Open	HQ	
wilsonsprom	85096	146.42	-39.13	1957	Open	HQ	
woomera	16001	136.80	-31.16	1949	Open	HQ	
wyalong	73054	147.24	-33.93	1959	Open	HQ	
yamba	58012	153.36	-29.43	1921	Open	HQ	

Notes: **There are 62 HQ stations in the SEACI region**

Temperature HQ dataset was initially put together by B. Trewin (2001, PhD thesis, Melbourne Uni.) The dataset has been updated by D. Collins NCC, 2006, available online at:

ftp://ftp.bom.gov.au/anon/home/ncc/www/change/HQdailyT/HQdailyT_info.pdf

Additional stations (23)

Quality = 1 for stations with few missing data since 1958 but which fail test for the HQ network

Some locations are the merging of neighbouring sites and hence have homogenisation issues

Additional problems if any are noted for individual station

List of surface humidity stations

Location	Station Id	Lon. (E)	Lat. (S)	Start Date	End Date	Quality	Footnote
adelaide	23000	138.58	-34.93	1957	2003	HQ	
bourke	48239	145.95	-30.04	1957	2003	HQ	F1
canberra	70014	149.20	-35.30	1957	2003	HQ	
ceduna	18206	133.70	-32.13	1957	2003	HQ	
charleville	44021	146.25	-26.42	1957	2003	HQ	
cobar	48027	145.83	-31.49	1957	2003	HQ	
laverton	87031	144.76	-37.86	1957	2003	HQ	
melbourne	86071	144.97	-37.81	1957	2003	HQ	
mildura	76031	142.08	-34.23	1957	2003	HQ	
mountgambier	26021	140.77	-37.75	1957	2003	HQ	
sale	85072	147.13	-38.12	1957	2003	HQ	
wagga	72150	147.46	-35.16	1957	2003	HQ	
woomera	16001	136.81	-31.16	1957	2003	HQ	

Notes:
The Dew point high quality (HQ) dataset was compiled by C. Lucas (2006, ANZ Clim. For., Canberra)
Variables are:
Maximum dew point (dTmax)
Minimum dew point (dTmin)
9am dew point (taken between 9-10am depending on Daylight savings)
9am relative humidity
RH *
* RH is based on non-homogenised 9am temperature
F1: Has a lot of missing data (20%)

List of pan evaporation stations

Location	Station Id	Lon. (E)	Lat. (S)	Start Date	End Date	Quality
adelaide	23090	138.62	-34.92	1975	31/12/2005	1
bathurst_agri	63005	149.56	-33.43	1975	31/12/2005	1
canberra_ap	70014	149.20	-35.30	1975	31/12/2005	HQ
ceduna_amo	18206	133.70	-32.13	1975	31/12/2005	HQ
charleville_aero	44021	146.25	-26.42	1975	31/12/2005	1
cobar_mo	48027	145.83	-31.49	1975	31/12/2005	1
condobolin_agri	50052	147.23	-33.07	1975	31/12/2005	HQ
east_sale_ap	85027	147.13	-38.12	1975	31/12/2005	HQ
gunnedah_scs	55024	150.27	-31.03	1975	31/12/2005	HQ
lake_eildon	88023	145.91	-37.23	1975	31/12/2005	HQ
mildura_ap	76031	142.08	-34.23	1975	31/12/2005	1
moree_aero	53115	149.85	-29.49	1975	31/12/2005	1
mt_gambier_aero	26021	140.77	-37.75	1975	31/12/2005	HQ
nuriootpa_viti	23373	139.01	-34.48	1975	31/12/2005	1
rutherglen_res	82039	146.51	-36.10	1975	31/12/2005	HQ
st_arnaud(tottington)	79079	143.12	-36.79	1975	31/08/2005	1
wagga_wagga_amo	72150	147.46	-35.16	1975	31/12/2005	HQ
woomera_aero	16001	136.81	-31.16	1975	31/12/2005	1
wurdiboluc_res	87126	144.05	-38.28	1975	31/10/2005	1

Notes:

Pan-evaporation high quality (HQ) dataset was put together by B. Jovanovic et al. (2006)

Daily data were generated using monthly homogenisation coefficients

Quality = HQ	no corrections were needed and hence the daily values are of the highest quality
Quality = 1	

List of acronyms

ANU	Australian National University
ASO	August-September-October (later part of the austral cool season)
AWAP	Australian Water Availability Project
BoM	Australian Bureau of Meteorology
BRS	Bureau of Rural Science
CAWCR	Centre for Australian Weather and Climate Research
CCSM3	Community Climate System Model (version 3)
CMAR	CSIRO Marine and Atmospheric Research
CSIRO	Commonwealth Scientific and Industrial Research Organisation
DCC	Department of Climate Change (former name)
DCCEE	Department of Climate Change and Energy Efficiency
DJF	December January February (austral summer)
DMI	Indian Ocean Dipole Mode Index
DMO	Direct Model Output
DSE	Department of Sustainable Environment (Victoria)
DTR	Diurnal Temperature Range (i.e., the difference between T_{max} and T_{min})
ENSO	El Niño Southern Oscillation
EOF	Empirical Orthogonal Function
ESB	Eastern Sea-Board (also called SEC)
GCM	General Circulation Model (as well as Global Climate Model)
GW	Global Warming
GDI	Gayndah-Deniliquin Index
GDR	Great Dividing Range
HQ	High Quality
IOD	Indian Ocean Dipole
IPCC	Intergovernmental Panel on Climate Change
JJA	June-July-August (austral winter)
LWA	Land and Water Australia
MAM	March-April-May (austral autumn)
MDB	Murray-Darling Basin
MDBA	Murray-Darling Basin Authority
MDBC	Murray-Darling Basin Commission (now defunct)
MJJ	May-June-July (early part of the austral cool season)
MSLP	Mean Sea Level Pressure
NCAR	National Center for Atmospheric Research (USA)
NCC	National Climate Centre, Bureau of Meteorology
NCEP	National Centers for Environmental Prediction (USA)
NMDB	Northern Murray-Darling Basin
NNR	NCEP / NCAR reanalyses
NTS	Neighbouring Tasman Sea (geographical box within the Tasman Sea)
NSW	New South Wales
NWS	North-West Shelf (geographical box within the eastern Indian Ocean)
OLR	Out-going Long wave Radiation (in W/m2)
PDO	Pacific Decadal Oscillation
RMSE	Root Mean Square Error
SAM	Southern Annular Mode
SDM	Statistical Downscaling Model (BoM SDM)
SEA	South-Eastern Australia

SEACI	South Eastern Australian Climate Initiative
SEC	South-East Coast (also called ESB)
SMD	Southern Murray-Darling Basin
SON	September-October-November (austral spring)
SRES	Special Report on Emissions Scenarios
SST	Sea Surface Temperature
STR	Sub-Tropical Ridge, intensity (STR-I) and position (STR-P)
SWEA	South-West of Eastern Australia
SWWA	South-West of Western Australia
T_{min}	Minimum daily temperature
T_{max}	Maximum daily temperature
TPI	Tri-polar Index (tropical SST based index)
WWII	Period of low rainfall encompassing the World War 2; generally the period is 1935-1945 unless specified otherwise

The Centre for Australian Weather and Climate Research is a partnership between CSIRO and the Bureau of Meteorology.